CHARACTERIZATION OF VIRAL-VIRAL AND VIRAL-HOST INTERACTIONS THAT CONTRIBUTE TO THE REPLICATION AND PATHOGENESIS OF THE SEVERE ACUTE RESPIRATORY SYNDROME VIRUS (SARS-CoV)

KENG CHOONG TAT

(Master of Science), NTU

A THESIS SUBMITTED

FOR THE DEGREE OF DOCTOR OF PHILOSOPHY

DEPARTMENT OF MICROBIOLOGY

NATIONAL UNIVERSITY OF SINGAPORE

2011

ACKNOWLEDGEMENTS

This work is directed and supervised by Associate Professor Tan Yee-Joo. I would like to give my deepest appreciation to Dr. Tan for her valuable ideas, instructions and guidance on the project. I would also like to thank her for her patience and time to improve my scientific writings as well as in creating opportunities for me to work with collaborators for my scientific development. I would like to acknowledge Professor Hong Wanjin and Associate Professor Victor Yu for their constructive opinions and suggestions on my project, as members of my committee meetings.

I am grateful to our collaborators from the Sweden Karolinska Institute, Dr. Ali Mirazimi and Dr. Sara Akerstrom, for their help and contributions to the project. I am also grateful to our collaborators from the Hong Kong University, Professor Malik Peiris, Dr. Leo Poon and Cythia Leung, for their help and contributions to the project. I would like to extend my thanks to the members of Professor Malik Peiris' lab for their kind hospitality during my 4-month attachment in Hong Kong.

I would like to thank the past and current laboratory members of the collaborative anti-viral research (CAVR) group for their guidance, advice, discussions and support: Dr. Shen Shuo, Dr. Chou Chih Fong, Dr. Bertie Fieldings, Dr. Seeham Khan, Dr. Timothy Tan, Dr. Wee Boon Yu, Dr. Annie Chan, Scottz Lip, Choi Yook Wah, Tham Puay Yoke, Daphne Chan, Janice Oh, Vithia Gunalan and Nur Khairiah Mohd Ismail.

Lastly, I would like to leave my greatest gratitude to my parents and my wife, Mandy, for their understanding, encouragements and support over the past years.

TABLE OF CONTENTS

SUMMARY VII

LIST OF TABLES IX

LIST OF FIGURES X

ABBREVIATIONS XIII

CHAPTER 1: INTRODUCTION

1.1 An overview of SARS-CoV 1

1.1.1 Non-structural proteins (NSPs) 3

1.1.2 Structural proteins 9

1.1.3 Accessory proteins 25

1.2 Zoonotic origins of SARS-CoV

1.2.1 Cross-species transmission of SARS-CoV 31

1.2.2 Molecular evolution and genomic differences of SARS-CoV 34

1.3 Goals of the project 37

CHAPTER 2: MATERIALS AND METHODS

2.1 Mammalian cell lines used in this study 39

2.2 Viruses 39

2.3 Construction of plasmids

2.3.1 Plasmids for expression of viral proteins in mammalian cells 40

2.3.2 Plasmids for expression of viral proteins in *Escherichia coli* 41

2.4 Expression and purification of GST-fusion proteins 42

2.5	Generation of rabbit polyclonal antibodies	43
2.6	Transient expression of SARS-CoV proteins in mammalian cells	43
2.7	SDS-PAGE	44
2.8	Coomassie blue staining	44
2.9	Immunoprecipitation	44
2.10	Western blot analysis	45
2.11	Indirect immunofluorescence microscopy	45
2.12	Radioactive pulse-chase protein labeling	46
2.13	Virus neutralization assay	48
2.14	Generation of monoclonal antibodies	49
2.15	Purification of monoclonal antibodies	50
2.16	Fluorescence activated cell-sorting (FACS) analysis	51
2.17	Cell-cell membrane fusion assay	51
2.18	Generation of escape SARS-CoV	52
2.19	TOPO cloning and sequencing	53
2.20	Pseudovirus luciferase assay	54
2.21	P24 ELISA assay	55
2.22	Culturing of stable cell lines	55
2.23	SARS-CoV infection and titration	56
2.24	Northern blot analysis	56
2.25	Reverse transcription reaction	57
2.26	Microarray analysis	57
2.27	Real-time quantitative PCR	58

CHAPTER 3: NEUTRALIZING ANTIBODIES AGAINST SARS-CoV

3.1 Characterization of rabbit polyclonal antibodies against SARS-CoV S

3.1.1 Generation of rabbit polyclonal antibodies against different regions of S 59

3.1.2 Detection of denatured form of SARS-CoV by Western blotting 60

3.1.3 Detection of the recombinant form of S in transfected cells 61

3.1.4 Detection of the native S in virus-infected cells and cultured Media 64

3.1.5 Maturation of S from EndoH-sensitve to EndoH-resistant form 64

3.1.6 Detection of SARS-CoV S on surfaces of Cos7 cells 67

3.2 A region in S2 can elicit neutralizing activity 68

3.3 Generation of monoclonal antibodies (mAbs) against SΔ10 region 69

3.4 Characterization of monoclonal antibodies

3.4.1 Detection of S by mAbs in SARS-CoV infected cells 70

3.4.2 Mapping of binding sites of monoclonal antibodies 71

3.4.3 *In vitro* neutralization of virus infectivity by mAbs 73

3.5 Understanding the mechanism of neutralization by mAbs

3.5.1 Neutralizing mAbs bind to regions upstream of and within the HR2 domain 74

3.5.2 Inhibition of S-induced cell-cell membrane fusion by mAbs 75

3.6 Discussion 80

CHAPTER 4: FURTHER CHARACTERIZATION OF THE SARS-CoV NEUTRALIZING MONOCLONAL ANTIBODIES

4.1 Sequence comparison of human and animals SARS-CoV S 84

4.2 Cross-neutralization ability of both mAb 1A9 and 1G10 in animal strains S-mediated cellular entry 86

4.3 Generation of escape mutant virus of mAb 1A9 and 1G10 91

4.4 Identifying the mutation(s) on S in the mutant viruses that escaped the inhibition by mAb 1A9 and 1G10 93

4.5 Screening the mutation(s) for positive escape activity 94

4.6 Amino acid residues N1056 and D1128 are important for the mAb 1A9 neutralizing activity 95

4.7 Discussion 97

CHAPTER 5: MECHANISM OF NITRIC OXIDE INHIBITION OF SARS-CoV

5.1 Peroxynitrite has no effect on SARS-CoV replication 100

5.2 Treatment of NO donor leads to a reduction in the palmitoylation of the S protein of SARS-CoV 102

5.3 Nitric oxide reduces the cell-cell fusion activity of S 104

5.4 SARS-CoV S pseudoviruses produced in the presence of nitric oxide is less efficient in viral entry 105

5.5 Discussion 107

CHAPTER 6: CHARACTERIZATION OF THE ORF8 REGION OF THE SARS-CoV

6.1 Characterization of the viral-viral interactions of the ORF8 proteins

6.1.1 Characterization of the polyclonal antibodies to the SARS-CoV unique proteins 8a and 8b 109

6.1.2 Expression of 8a and 8b in SARS-CoV infected Vero E6 cells 111

6.1.3 Interactions of 8a, 8b and 8ab with other SARS-CoV proteins 113

6.2 8b down-regulates the small envelope protein (E) in SARS-CoV infected cells

6.2.1 Over-expression of 8b down-regulates the expression of E protein 115

6.2.2 Expression of 8b did not reduce the transcription of the E gene 117

6.2.3 The 8b protein can bind E in SARS-CoV infected cells 118

6.2.4 Expression of 8b and E are mutually exclusive in SARS-CoV infected cells 119

6.3 Discussion 120

CHAPTER 7: SARS-CoV 8b REDUCES VIRAL REPLICATION BY DOWN-REGULATING E VIA AN UBIQUITIN-INDEPENDENT PROTEASOME PATHWAY

7.1 Inhibition of the protein 8b-mediated rapid degradation of the E protein by proteasome inhibitor 123

7.2 Knockout of lysine residues on 8b does not prevent its polyubiquitination and ability to down-regulate E 124

7.3 Substitution of K64 to R on E increases the protein stability by reducing the polyubiquitination of E 126

7.4 Both lysine residues on E are important for 8b-mediated E degradation 128

7.5 Expression of 8b increases with time in SARS-CoV infected vero E6 cells 129

7.6 8b is a negative modulator of SARS-CoV replication 130

7.7 E is down-regulated in SARS-CoV infected GFP-8b expressing cells 132

7.8 Effects of 8b on the transcription of the host genes 133

7.9 Discussion 136

CHAPTER 8: CONCLUSION AND FUTURE WORK 139

REFERENCES 143

APPENDICES 181

SUMMARY

In this thesis, we identified neutralizing epitopes in the region of the severe acute respiratory coronavirus (SARS-CoV) spike (S) protein encoded by aa residues 1055 to 1192 (SΔ10 protein fragment). To understand the mechanism of SARS-CoV neutralization by the anti-SΔ10 antibodies, a panel of monoclonal antibodies (mAbs) was generated. Epitope mapping revealed that the immuno-dominant region within SΔ10 lies between residues 1091 to 1130 and 1150 to 1192, which are part of the loop region between the heptad repeats 1 (HR1) and heptad repeats 2 (HR2) domains and the N-terminal of the HR2 domain, respectively. The HR1 and HR2 domains have previously been shown to be important for the viral-cell fusion process. Using the cell-cell fusion inhibition and *in vitro* neutralizing assays, the mAbs were shown to neutralize SARS-CoV infection and inhibit cell-cell fusion. Taken together, the results suggest that the mechanism of neutralization of SARS-CoV infection by these mAbs is due to the inhibition of the viral-cell fusion step during viral entry.

As these mAbs target highly conserved regions in the C terminal of S, which is known as the S2 domain, two representative mAbs, 1A9 and 1G10, were selected for evaluation of cross-neutralizing properties. A recent report suggests that the bat SL-CoV Rf1 and Rp3 strains could have undergone a recombination event to yield the civet SARS-CoV SZ3 strain which in turn spills over to human during the SARS epidemic. By use of lentiviral pseudotyped particles carrying S on the surface, both mAbs targeting the N-terminal HR2 domain (mAb 1G10) and the loop region between the HR1 and HR2 domains were shown to cross-neutralize the civet SARS-CoV (SZ3 strain) and bat SL-

CoV (Rf1 and Rp3 strains). In order to gain a better understanding of the mechanism of virus neutralization of mAbs 1G10 and 1A9, escape viruses were generated. From the results, two mutations (N1056K and D1128A) in S of the escape viruses generated using mAb 1A9 showed a synergistic effect on the escape activity in pseudovirus assay. Taken together, the results suggest that a novel conserved region in the loop domain between the HR1 and HR2 domains is important for the SARS-CoV and SL-CoV viral-cell fusion process.

The most obvious genomic difference between the human epidemic SARS-CoV strains and the animal and early human SARS-CoV strains is that the ORF8 acquired a 29-nt deletion, resulting in the coding of two proteins, 8a and 8b, instead of a single 8ab protein. Using over-expression systems and co-immunoprecipitation experiments, the viral-viral interaction profiles of all the three proteins (8a, 8b and 8ab) were found to be different, and more interestingly, 8b was found to down-regulate E in a post-translational manner. Infection studies further showed that 8b is expressed late during infection and has mutually exclusive localization with E in infected cells. Cells stably expressing the GFP-tagged 8b were also shown to down-regulate E and reduce virus replication by approximately 10-folds. In addition, it was demonstrated that the mechanism of down-regulation of E by 8b is via an ubiquitin-independent proteasome pathway. An oligonucleotide microarray analysis also revealed that 8b alters the mRNA levels of several host proteins, suggesting that they may be involved in virus replication. In summary, we have identified an important viral-viral interaction that could have evolved in the human epidemic strains.

LIST OF TABLES

Table 1.1:	Functional characteristics of SARS-CoV NSPs	4
Table 1.2:	Functional characteristics of SARS-CoV structural proteins	21
Table 1.3:	Functional characteristics of SARS-CoV accessory proteins	27
Table 3.1:	Neutralizing test at 200 $TCID_{50}$ per well	69
Table 3.2:	Neutralizing test at 1000 $TCID_{50}$ per well	69
Table 3.3:	Internal deleted positions of the S mutants	72
Table 3.4:	*In vitro* neutralizing activities of mAbs	73
Table 4.1:	Percentage identity of the S protein sequence	85
Table 6.1:	The interactions between SARS-CoV 8a, 8b and 8ab with other viral proteins were determined by co-immunoprecipitation experiments	113
Table 7.1:	Host genes with different mRNA expression in GFP-8b and GFP-8b* cells as identified by microarray analysis	134

LIST OF FIGURES

Figure 1.1:	SARS-CoV Genome Organization	2
Figure 3.1:	Schematic diagram showing the different regions of S encoded by the plasmids used in this study	60
Figure 3.2:	Western blot analysis for the detection of SARS-CoV S	61
Figure 3.3:	Radio-labeled immunoprecipitation	63
Figure 3.4:	Detection of the different forms of S in virus-infected cells and viruses	66
Figure 3.5:	S expressed on the surfaces of transiently transfected Cos7 cells	67
Figure 3.6:	Detection of S by mAbs in virus-infected cells and mapping the binding sites of the mAbs	72
Figure 3.7:	Cluster W multiple sequence alignment of coronavirus S proteins	74
Figure 3.8:	FACS analysis of the surface expression of the S and ACE2 and syncytium formation assay	78
Figure 3.9:	Dose-dependent inhibition of syncytium formation between 293T-SP and CHO-ACE2 cells	79
Figure 4.1:	Protein sequence alignment for binding of mAbs to S of human (HK39849), civet (SZ3) and bats (Rp3 and Rf1) coronaviruses	85
Figure 4.2:	Detection of receptor-modified S of civet and bats strains	86
Figure 4.3:	Setting up of pseudovirus assay for performing neutralization test with mAbs	88
Figure 4.4:	Pseudovirus binding assay	89

Figure 4.5:	Cross-neutralization activity of mAb 1A9 and 1G10	90
Figure 4.6:	Generation of escape SARS-CoV mutants for mAb 1A9 and 1G10	92
Figure 4.7:	Schematic diagram showing S with functional domains and the point mutations found in mAb 1A9 and 1G10 escape viruses	93
Figure 4.8:	Pseudovirus entry assay	94
Figure 4.9:	Analysis of positive SARS-CoV escape mutations of clones selected with mAb 1A9	96
Figure 4.10:	Cluster W multiple sequence alignment of SARS-CoV and SL-CoV S proteins	99
Figure 5.1:	SIN-1 treatment has no anti-viral effect on SARS-CoV infected Vero E6 cells	101
Figure 5.2:	Effect of SNAP on nitration and palmitoylation of the S protein	103
Figure 5.3:	SNAP interferes with cell-cell membrane fusion	104
Figure 5.4:	SARS-CoV S pseudoviruses produced in the presence of SNAP is less efficient in viral entry	106
Figure 6.1:	Expression of SARS-CoV 8a, 8b and 8ab proteins	110
Figure 6.2:	Cellular localizations of 8a and 8b in SARS-CoV infected cells and Vero E6 cells transfected with DNA constructs for expressing 8a, 8b and 8ab	112
Figure 6.3:	Interactions of 8a, 8b and 8ab with other SARS-CoV proteins	114
Figure 6.4:	Effects of 8b on the expression of the small structural protein E	116

Figure 6.5: Effects of 8b protein on the transcription of the E gene determined by Northern blot analysis 117
Figure 6.6: Interaction between E and 8b in SARS-CoV infected cells determined by co-immunoprecipitation experiment 118
Figure 6.7: Expressions of E and 8b in SARS-CoV infected cells determined by indirect immunofluorescence experiments 119
Figure 7.1: Inhibition of protein 8b-mediated rapid degradation of the SARS-CoV E protein by the proteasome inhibitor, MG132 123
Figure 7.2: Lysine knockout mutant of 8b undergoes polyubiquitination and down-regulates E 125
Figure 7.3: Substitution of K64 to R on E increases its stability by reducing its polyubiquitination 127
Figure 7.4: Both lysine residues on E are involved in the 8b-mediated down-regulation of E 128
Figure 7.5: 8b has a higher expression at late-stage infection of Vero E6 cells 129
Figure 7.6: Ectopic 8b expression reduces viral replication in Vero E6 cells 131
Figure 7.7 Expression of E is down-regulated in SARS-CoV infected cells stably expressing GFP-8b 132
Figure 7.8: Effects of 8b on the transcription of host genes 135

ABBREVIATIONS

aa	amino acids
ACE2	angiotensin-converting enzyme 2
BSA	bovine serum albumin
CHO	chinese hamster ovary
CPE	cytopathic effect
DC-SIGN	dendritic cell-specific ICAM-3 grabbing non-integrin
DMEM	Dulbecco modified eagle medium
DNA	deoxyribonucleotide acids
ELISA	enzyme-linked immunosorbent assay
EndoH	endoglycosidase H
ER	endoplasmic reticulum
ERGIC	endoplasmic reticulum-golgi intermediate compartments
FACS	fluorescence activated cell sorting
FITC	fluorescein isothiocyanate-conjugated
GADPH	glyceraldehydes-3-phosphate dehydrogenase
GFP	green fluorescence protein
GST	glutathione S-transferase
HEK	hamster embryonic kidney
HIV	human immunodeficiency virus
HR1	heptad repeats 1
HR2	heptad repeats 2
HRP	horse radish peroxidase
IgG	immunoglobulin G
iNOS	inducible nitric oxide synthase
IP	immunoprecipitation
IPTG	isopropyl-β-D-thiogalactopyranoside
kb	kilo-bases
kDa	kilo-Daltons
LB	Luria-Bertani
mAb	monoclonal antibodies
Met-Cys	methionine-cysteine
MBL	mannose binding lectin
ml	milliliters
MHV	murine hepatitis virus
mRNA	messenger ribonucleotide acids
NAP	N-acetyl-penicillamine
NO	nitric oxide
NSP	non-structural protein
ORF	open reading frame
PBS	phosphate-buffered saline
PMSF	phenylmethylsulfonyl fluoride
qPCR	quantitative polymerase chain reaction
RBD	receptor binding domain
RdRp	RNA-dependent RNA polymerase

RNA	ribonucleotide acids
RT-PCR	reverse transcription-polymerase chain reaction
SARS-CoV	severe acute respiratory syndrome coronavirus
SDS-PAGE	sodium dodecyl sulfate polyacrylamide gel electrophoresis
SL-CoV	severe acute respiratory syndrome-like coronavirus
SNAP	2-S-nitroso-N-acetyl-penicillamine
TCID	tissue culture infectious dose
UPR	unfolded protein response
UV	ultraviolet
VLP	virus-like particle

CHAPTER 1: INTRODUCTION

1.1 An Overview of SARS-CoV

In November 2002, the emergence of an unknown virus that causes atypical pneumonia sends a shock wave around the world, causing major social disruption and having an extensive impact on the healthcare systems and the world economies (Bell, 2004; Caulford, 2003; Lee et al., 2003). The virus spreads from Guangdong province in China to 29 countries world-wide, resulting in 8,098 infections with 774 deaths (Peiris et al., 2004; WHO, 2004; Zhong et al., 2003). The aetiological agent for the pneumonia disorder was identified to be a novel coronavirus termed as severe acute respiratory syndrome coronavirus (SARS-CoV) (Drosten et al., 2003; Fouchier et al., 2003; Ksiazek et al., 2003; Kuiken et al., 2003; Peiris et al., 2003b). SARS-CoV belongs to the *Coronaviruses* genus, in the *Coronaviridae* family of the *Nidovirales* order, in the virus taxonomy. Coronaviruses are divided into 3 subgroups, with group 1 and 2 comprising of mammalian coronaviruses and group 3 comprising of avian coronaviruses (Bradburne, 1970; McIntosh et al., 1969; Woo et al., 2009). Based on sequence comparisons and similarity of the ORF1a region of SARS-CoV to group 2 coronaviruses, it is suggested that SARS-CoV belongs to the group 2b of the genus *Coronaviruses* but was later assigned in a novel group 2c of the same genus (Snijder et al., 2003; Woo et al., 2006).

SARS-CoV is an enveloped, positive-sense, single-stranded RNA virus with a genome size of 29.7 kilobases (kb) encoding for sixteen non-structural proteins (NSPs), four structural proteins and eight accessory proteins (Marra et al., 2003; Rota et al., 2003; Ruan et al., 2003) (Fig. 1.1). SARS-CoV replicates in the cytoplasm of the infected cells.

Using electron microscopy techniques, it was shown that SARS-CoV establishes its replication complexes at the endoplasmic reticulum (ER)-derived membranes (Stertz et al., 2007). Recently, the SARS-CoV replication complexes were found to be supported by a reticulovesicular network of modified reticulum and are membrane-protected, possibly having a role in hiding the viral complexes from the host anti-viral defense mechanism (Knoops et al., 2008; van Hemert et al., 2008). Viral RNA synthesis begins with the transcription of a minus-strand RNA template from the viral genome, followed by the transcription of a genomic messenger ribonucleotide acid (mRNA) and eight sub-genomic mRNAs, and subsequently leading to the expression of the NSPs, the structural proteins and the accessory proteins (Sawicki and Sawicki, 2005a; Sawicki et al., 2007; Thiel et al., 2003).

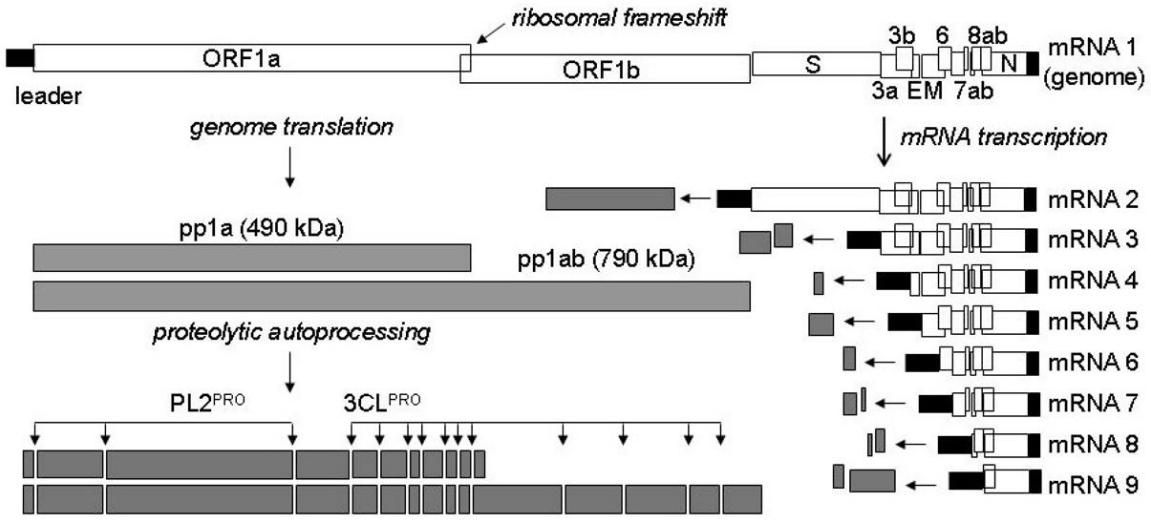

Fig. 1.1: SARS-CoV Genome Organization.
Figure adapted from Plant and Dinman, Front Biosci, 2008.

1.1.1 Non-structural proteins (NSPs)

The expression of the genome of SARS-CoV begins with the translation of gene 1 at the 5' end to two replicase polyproteins, pp1a and pp1ab (Baranov et al., 2005; Dos Ramos et al., 2004). Pp1a is encoded by ORF1a and translation stops at the stop codon resulting in a 490 kilo-Dalton (kDa) polyprotein. A programmed -1 ribosomal frame shift prior to the stop codon of the open reading frame (ORF) 1a directs a fraction of the elongating ribosomes into an alternative reading frame that is -1 relative to the initiating ORF1a for the expression of a 790 kDa polyprotein, pp1ab (Dos Ramos et al., 2004; Plant and Dinman, 2008; Thiel et al., 2003). A slippery site composed of a heptameric sequence and a stimulatory structure such as the mRNA pseudoknot in SARS-CoV is required for the frame shifting event (Brierley et al., 1989; Dos Ramos et al., 2004). Polyproteins pp1a and pp1ab are immediately processed by proteinase activities in the nascent polyproteins into intermediate and mature NSPs and therefore, are not detected during infection (Harcourt et al., 2004). Virally encoded proteinases, the papain-like proteinase (PLP) encoded in NSP3 and the 3C-like proteinase (3CLpro) encoded in NSP5, process pp1a and pp1ab into 16 NSPs (Prentice et al., 2004; Thiel et al., 2003). NSP1 to NSP11 are encoded within pp1a and pp1ab while NSP12 to NSP16 are only encoded within pp1ab (Fig. 1.1). The SARS-CoV NSPs have critical roles in the transcription and replication of the viral genome and extensive studies were carried out to understand their specific roles (See Summary in Table 1.1).

Table 1.1 – Functional characteristics of SARS-CoV NSPs

Protein	Protein properties and effect(s) on viral and/or host replication	Other host cellular effect(s)
NSP1	- Suppression of the host protein synthesis via the inactivation of the translational functions of the 40S ribosomal subunit and by inducing the modification of the 5' region of capped mRNA template to render it translationally incompetent (Connor and Roper, 2007; Kamitani et al., 2009; Kamitani et al., 2006; Narayanan et al., 2008a). - NSP1 mutant that loses its ability to degrade host mRNA induces a large amount of IFN-β during infection, suggesting that the suppression of the host gene expression is vital for the blocking of the host anti-viral response in infected cells (Narayanan et al., 2008a)	- Inhibits the IFN-dependent signaling by decreasing STAT1 phosphorylation, and attenuating NSP1 results in a reduced ability of the virus to replicate in cells with an intact IFN response (Wathelet et al., 2007). - Over-expression of NSP1 dysregulates CCL5, CXCL10 and CCL3 cytokine expression in A549 cells, and CCL5 and CXCL10 cytokine expression in HepG2 cells (Law et al., 2007).
NSP2	- Non-essential for viral replication but its deletion attenuates viral growth and RNA synthesis (Graham et al., 2005).	- Interacts with two host protein complex (prohibitin 1 and prohibitin 2) involved in mitochondrial biogenesis and intracellular signaling, suggesting a role of NSP2 in the disruption of intracellular host signaling during SARS-CoV infections (Cornillez-Ty et al., 2009).
NSP3	- Possesses a papain-like protease (PLP2) domain that carries out the main 3C-like protease activity and was shown to be sufficient to cleave the nsp1/nsp2, nsp2/nsp3 and nsp3/nsp4 sites (Harcourt et al., 2004). - Shares consensus motif LXGG with cellular deubiquitinating (DUB) enzymes and exhibits DUB and deISGylation activities *in vitro* (Barretto et al., 2005; Lindner et al., 2005; Sulea et al., 2005). Crystal structure of PLP2 domain resembles that of cellular DUB enzymes, USP14 and HAUSP (Ratia et al., 2006). - Contains a predicted N-terminal acidic domain that is rich in glutamate (Serrano et al., 2007). - Has an X domain that was predicted to be an ADP-ribose-1" monophosphate (Appr-1"-p) processing enzyme and specifically dephosphorylate Appr-1"-p to ADP-ribose (Putics et al., 2005; Saikatendu et al., 2005). - Has a papain-like non-canonical (PLnc) domain that functions as a replication/transcription scaffolding protein (Imbert et al., 2008).	- Over-expression of NSP3 antagonizes the host interferon response via the inhibition of the NF-κB pathway (Wathelet et al., 2007). - PLP2 domain is a potent IFN antagonist, acting via the blocking of the phosphorylation and activation of IRF3 (Devaraj et al., 2007). - PLP2 domain blocks the NF-κB pathway via the stabilization of the NF-κB inhibitor, IκBα, and ubiquitin-like (UBL) domain is necessary but not sufficient for antagonism of IRF3 function (Frieman et al., 2009). - Novel nuclei acid binding (NAB) domain and SARS-unique domain (SUD) were identified using proteomic analysis (Neuman et al., 2008). - SUD binds RNA G quadruplexes and the G-stretches found on 3'-non-translated regions of host cells mRNA coding for proteins involved in apoptosis and signal transduction (Tan et al., 2007c; Tan et al., 2009).

Table 1.1 - *Continued*

Protein	Protein properties and effect(s) on viral and/or host replication	Other host cellular effect(s)
NSP4	- Involved in the early secretory pathway, which is important for the formation of replication complexes (Oostra et al., 2007b).	- Not known
NSP5	- Functions similar to a 3C-like protease (Anand et al., 2003). - Shares a high degree of structural similarity with other coronavirus 3CLpro and plays a critical role in processing pp1a and pp1ab polyproteins to start the virus replication cycle (Thiel et al., 2003; Ziebuhr et al., 2000). - Exists in equilibrium between the monomeric and dimeric forms but only the dimeric form is active (Fan et al., 2004; Graziano et al., 2006). - Only one active protomer in the dimer is sufficient for the catalytic properties (Chen et al., 2006). - Long-range cooperative interactions also modulate the dimerization of SARS-CoV 3CLpro (Barrila et al., 2006). - Disruption of the dimer interface, using peptides that represent the N-terminus of the protein, results in the inactivation of the 3CLpro (Ding et al., 2005; Wei et al., 2006). - N-terminal residue 1 to 7 (N-finger) is critical for the SARS-CoV 3CLpro dimerization and essential for the formation of an enzymatically active dimer (Chen et al., 2005b; Zheng et al., 2007; Zhong et al., 2008). - Asn28 of SARS-CoV 3CLpro have a critical role in maintaining the structural integrity of the protein's active site and in orientating key residues involved in binding at the dimer interface and substrate catalysis (Barrila et al., 2010). - Arg4, Glu290 and Arg298 were key components in maintaining the dimer form (Chou et al., 2004; Shi et al., 2008a). - Arg4, Ser10, Glu14 and Phe140 on the dimer interface were critical for both the dimer stability and its enzymatic activity (Chen et al., 2008).	- Induces mitochondrial-mediated apoptosis, suggesting that it may contribute to the pathogenesis observed in SARS-CoV infection (Lai et al., 2007).
NSP6	- Not known	- Not known
NSP7	- Possesses a novel and unique sequence and structure to the *Coronaviridae* but the function remains unknown (Peti et al., 2005). - Interacts with NSP8 to forms a hexadecamer structure, which may function as a second, non-canonical RNA-dependent RNA polymerase (RDRP) in SARS-CoV (Imbert et al., 2006; Zhai et al., 2005).	- Not known

Table 1.1 - *Continued*

Protein	Protein properties and effect(s) on viral and/or host replication	Other host cellular effect(s)
NSP8	- Co-localized with NSP2 and NSP3 (Prentice et al., 2004). - Interacts with an accessory protein, ORF6, in a yeast-two hybrid assay (Kumar et al., 2007).	- Not known
NSP9	- Crystal structure revealed that it is a single-stranded RNA-binding protein and possesses a unique RNA-binding subunit (Egloff et al., 2004). - An RNA-binding, dimeric protein that interacts with NSP8 (Sutton et al., 2004). - Disruption of the dimerization of NSP9 by reverse genetics approach demonstrated the non-critical role of NSP9 dimerization for its RNA binding function but was shown to be lethal to the virus (Miknis et al., 2009).	- Not known
NSP10	- Interacts with the two subunits of the cellular RNA polymerase complex, BTF3 and ATF5 (Li et al., 2005c). - Has a novel fold with two zinc-binding motifs and has nuclei acid binding ability, suggesting its possible function as a transcription factor during replication (Joseph et al., 2006; Su et al., 2006). - Has low affinity binding to single and double-stranded RNA and DNA without obvious sequence specificity (Joseph et al., 2006). - Specifically interacts with NSP14 and NSP16 in mammalian-two hybrid system, yeast-two hybrid system and GST pull-down assay (Imbert et al., 2008; Pan et al., 2008). - Is an essential factor to trigger full NSP16 2'-*O*-MTase activity (Bouvet et al., 2010).	- Interacts specifically with NADH 4L subunit and cytochrome oxidase II that may contribute to the extensive cytopathic effect observed in SARS-CoV infection (Li et al., 2005c).
NSP11	- Not known	- Not known
NSP12	- Full-length NSP12 first detected by immuno-blotting using an antibody targeting a fragment of SARS-CoV RdRp, with an observed mass of 106 kDa (Prentice et al., 2004). - Molecular models were developed to predict the critical residues responsible for the RdRp functions (Azzi and Lin, 2004; Xu et al., 2003). - siRNA targeting the SARS-CoV RdRp knock down SARS viral genes in FRhk4 cells, specifically inhibit expression of RDRP in 293 and HeLa cells and significantly reduced the plaque formation of SARS-CoV in Vero E6 cells (He et al., 2003b; Lu et al., 2004). - *In vitro* RdRp activity of NSP12 with primer-dependent activity on poly(A) templates was observed in filter binding polymerase assay (Cheng et al., 2005). - Primer-dependent on both homo- and heteropolymeric templates and its functions were postulated to have a close dependency on the NSP8 primase activity (Imbert et al., 2006; te Velthuis et al., 2010).	- Not known

Table 1.1 - *Continued*

Protein	Protein properties and effect(s) on viral and/or host replication	Other host cellular effect(s)
NSP13	- First predicted as an mRNA cap 1 methyl-transferase by 3D jury system but was later reported to possess a distinct 5' to 3' helicase activity (Tanner et al., 2003; von Grotthuss et al., 2003) . - Possesses both the RNA 5'-triphosphate activity, involved in the formation of the 5' cap structure of viral RNA, and the helicase activity (Ivanov et al., 2004b). - Interacts with a multi-functional cellular protein, DDX5, in a mammalian cell two-hybrid system. siRNA specific for DDX5 that knocked down its expression in FRhK4 cells significantly inhibited SARS-CoV replication, suggesting an important role of DDX5 in the SARS-CoV genome transcription (Chen et al., 2009a).	- Not known
NSP14	- Predicted based on the identification of motifs belonging to the DEDD superfamily of 3' to 5' exonuclease, which includes DNA proof-reading enzymes (Moser et al., 1997; Snijder et al., 2003). - Functional and genetic analysis performed on MHV temperature sensitive mutants mapping to N7-MTase domain of NSP14 and in the (nucleoside-2'-*O*)-methyltransferase (2'-*O*-MTase) of NSP16 indicated that both NSP14 and NSP16 are involved in the positive-strand RNA synthesis by forming replicase-transcriptase complexes (Sawicki et al., 2005b). - Has *in vitro* 3' to 5' exoribonuclease but not exodeoxyribonuclease activity and alanine substitution of the DEDD residues blocks its activity (Minskaia et al., 2006). - Exoribonuclease activity shown to require binding to Mg^{2+} to induce a structural change that is proposed by the authors to be a pre-requisite for NSP14 catalytic activity (Chen et al., 2007c). - Identified as a novel S-adenosyl-L-methionine (Ado-Met)-dependent (guanine-N7)-methyltransferase (N7-MTase), which was proposed to play a role in the formation of CoV mRNA caps (Chen et al., 2009c). - Analysis of viable SARS-CoV mutant viruses containing inactivating substitutions in the NSP14 ExoN DEDD motif I (AADD) showed that the inactivation of ExoN resulted in a 21-fold decrease in replication fidelity compared to wild-type SARS-CoV, suggesting that ExoN is not required for SARS-CoV replication in culture but is required for high-fidelity replication (Eckerle et al., 2010).	- Not known

Table 1.1 - *Continued*

Protein	Protein properties and effect(s) on viral and/or host replication	Other host cellular effect(s)
NSP15	- Predicted to contain a domain called nidoviral uridylate-specific endoribonuclease (NendoU) that is conserved in nidoviruses (Snijder et al., 2003). - Has a preference for cleavage at the 3' end of uridylates of double-stranded RNA (dsRNA) at GU or GUU sequences to produce 2'-3' phosphate ends (Bhardwaj et al., 2006; Ivanov et al., 2004a). - Endoribonuclease activity was found to be dependent on Mn^{2+} but not other divalent metal ions (Bhardwaj et al., 2004; Ivanov et al., 2004a). - Structure analysis using circular dichroism spectroscopy determined NSP15 to exist in solution as monomers and hexamers in equilibrium (Guarino et al., 2005). - Only the hexameric form of this enzyme is active, and the active site is destructed in the monomeric form due to the displacement of two loops in the catalytic domain (Guarino et al., 2005; Joseph et al., 2007). - Crystal structure revealed that the catalytic centre of NSP15 resembles the active site of a nuclease, RNase A (Ricagno et al., 2006). - Similar to RNase A in employing two histidine and one lysine residues for its catalytic action (Bhardwaj et al., 2008).	- Not known
NSP16	- Based on comparative sequence analysis, NSP16 was predicted to encode an AdoMet-dependent mRNA cap 2'-*O*-MTase and is essential for efficient viral replication (Decroly et al., 2008; Snijder et al., 2003; Wang et al., 2008a). - RNA 2'-*O*-MT activity of NSP16 blocks the dsRNA cleavage function of NSP15, indicating a functional interplay between the two NSPs and both the NendoU and 2'-*O*-MT enzymes are shown to be essential for efficient coronavirus RNA synthesis (Almazan et al., 2006).	- Not known

1.1.2 Structural proteins of SARS-CoV

Similar to other coronaviruses, SARS-CoV genome encodes for structural proteins spike (S), envelope (E), membrane (M) and nucleocapsid (N). Nal et al showed the differential maturation and sub-cellular localization of SARS-CoV S, M and E in Baby Hamster Kidney 21 cells that were infected by recombinant Semliki Forest virus expressing the respective proteins (Nal et al., 2005). Highly mannosylated S and M was found to assemble into trimers in the ER prior to acquisition of complex N-glycans in the Golgi while E was not glycosylated and localized to the ER only. S was also detected along the secretory pathway from the ER to the plasma membrane while M predominantly accumulates in the Golgi and partially in ER-Golgi intermediate compartments (ERGIC) trafficking vesicles (Nal et al., 2005). Contrary to the report, Chen et al. demonstrated the glycosylation of recombinant myc-tagged E expressed in Vero E6 cells (Chen et al., 2009b). In addition, the authors reported that E is a double-spanning membrane protein and the two trans-membrane domains are involved in the insertion of the cytoplasmic protein into the ER membrane. These two transmembrane domains also co-localize with M and are required for the interaction of E with M via one of the hydrophilic regions (amino acids (aa) 1 to 10 and aa 60-76).

It was shown that the M and E proteins were sufficient for the efficient formation of virus-like particles (VLPs) using co-infection of recombinant baculoviruses, expressing each of the proteins, in insect cells (Ho et al., 2004; Mortola and Roy, 2004). Contrasting to these reports, Huang et al. described the formation of VLPs using co-expression of M and N in transfected 293 cells (Huang et al., 2004b). The region on N required for interaction with M was found to be between aa 101 to 115, and a minimal

portion of N, aa 301 to 422, is required for pseudoparticle formation when co-expressed with M in human embryonic kidney (HEK)-293 cells (Hatakeyama et al., 2008). It was recently demonstrated that both E and N are required to be co-expressed with M for the efficient production and release of VLPs in transfected Vero E6 cells (Siu et al., 2008). In addition, the authors showed that the native trimeric S glycoprotein can be incorporated into the VLPs when co-expressed with M, N and E. The properties and functional roles of the E, M and N proteins are summarized in Table 1.2. The glycoprotein S will be reviewed in more details in the later paragraphs.

The S protein is a 1255 aa precursor polypeptide that is composed of 23 potential N-linked glycosylation sites (Marra et al., 2003; Rota et al., 2003; Xiao et al., 2003). It was demonstrated that the treatment of Vero E6 with glucosidase inhibitor N-butyl-deoxynojirimycin inhibits the N-glycans processing of SARS-CoV S and protects the cells from the cytopathic effect of the virus (Ritchie et al., 2010). The S protein assembles as trimers on the surface of the coronaviruses to form the characteristic "crown-like" structures (Tripet et al., 2004). S is important for the viral attachment and entry into the host cells (Simmons et al., 2004). The SARS-CoV S is a type-I glycoprotein that consists of the amino-terminal S1 and a carboxyl-terminal S2 subunits. A novel di-basic motif (-KxHxx-COOH) is identified in the cytoplasmic tail of S and it is shown to retain the protein in the ERGIC, contributing to the localization of S near the virus assembly site (Lontok et al., 2004). Further work demonstrated that the KxHxx motif binds to coatomer complex I and plays an important role in the co-localization of S and M in the Golgi compartment, suggesting that KxHxx re-cycles S through the ER-Golgi system for efficient assembly of virions in the ERGIC (McBride et al., 2007).

Li et al. identified a metallopeptidase, angiotensin-converting enzyme 2 (ACE2), as a functional receptor for SARS-CoV (Li et al., 2003b). Further studies by the authors demonstrated that the SARS-CoV binding to rats and murine ACE2 were not as efficient as that to human ACE2, indicating the adaptation of the virus to human receptor (Li et al., 2004a). The receptor binding domain (RBD) has been mapped to amino acid (aa) residues 318 to 510 on the S1 subunit (Babcock et al., 2004; Wong et al., 2004). The RBD binds to ACE2 to trigger a conformational change that allows the heptad repeats 1 (HR1) and heptad repeats 2 (HR2) regions on the S2 subunit to form a six helix bundle to facilitate the insertion of the fusion peptide into the cellular membrane for viral-cell membrane fusion to occur (Liu et al., 2004). A point mutation at residue D454 was shown to abolish the association of the RBD with ACE2 (Wong et al., 2004). In addition, Yi et al. demonstrated that the alanine mutation at residues R441 and R453 abolished entry of pseudovirus carrying the mutant S (Yi et al., 2005). A study using alanine scanning mutagenesis identified ten residues (K390, R426, D429, T431, I455, N473, F483, Q492, Y494 and R495) that significantly reduces binding to ACE2 when mutated (Chakraborti et al., 2005). Further analysis of these mutations with the crystal structure of RBD complexed to ACE2 suggest two hotspots, R426 and N473, which likely contribute to the binding energy (Li et al., 2005a).

It was shown that the infection of the primary human airway epithelia by SARS-CoV positively correlates with the expression and localization of ACE2 and the differentiation state of the cells (Jia et al., 2005). In another study, it was demonstrated that the SARS-CoV infection and the S protein both reduce the expression of ACE2 which resulted in worsened acute lung failure in mice and this induced lung injury can be

attenuated by blocking the rennin-angiotensin pathway, indicating a crucial role of ACE2 in SARS-CoV pathogenesis (Kuba et al., 2005). Further studies revealed that the RBD on S could induce ACE2 internalization in the SARS-CoV susceptible cells (Wang et al., 2008b). More recently, it was demonstrated that the SARS-CoV S induces tumor necrosis factor (TNF)-α-converting enzyme-dependent shedding of the ACE2 ectodomain to facilitate viral entry but also causes tissue damage through TNF-α production (Black et al., 1997; Haga et al., 2008).

Another receptor, CD209L (also known as L-SIGN), has also been identified as a receptor for SARS-CoV by studying the binding of soluble SARS-CoV S with Chinese hamster ovary (CHO) cells that were transduced with a human lung complementary deoxyribonucleotide acids (cDNA) library in vesicular stomatitis virus G pseudovirus (Jeffers et al., 2004). In addition, several groups also identified dendritic cell-specific ICAM-3 grabbing non-integrin (DC-SIGN) as SARS-CoV cellular receptor (Marzi et al., 2004; Yang et al., 2004a). Further studies revealed that the minimal DC-SIGN binding domain on S is residues 324 to 386 and S mutants with N330Q and N357Q mutations showed diminished DC-SIGN-binding capacity (Shih et al., 2006). By using pseudovirus packaged with S, it was shown that an N-linked glycosylation site, N330, is critical for the interaction of S with mannose binding lectin (MBL), which resulted in the blocking of the virus binding to DC-SIGN (Zhou et al., 2010). It was also shown that another lectin, LSECtin, enhances infection driven by the SARS-CoV S, suggesting that LSECtin could be an attachment factor that could function in conjunction with DC-SIGN (Gramberg et al., 2005). Besides identifying the host receptors for SARS-CoV, a close examination of the cysteine residues in the S1 domain of SARS-CoV S also reveal a

significant redox insensitivity, which may contribute to the wide host range of the virus (Lavillette et al., 2006).

By studying various soluble fragments of S expressed from 293T cells for their oligomerization ability, it was demonstrated that the S ectodomain contains the dimerization domain while the trimerization domain may exist in the transmembrane domain in its pre-fusion state (Xiao et al., 2004). Further studies showed that the truncation of the cytoplasmic tail containing the transmembrane domain resulted in a mutant S that is secreted into the medium and has much lower efficiency of trimer formations, suggesting that the transmembrane domain plays an important role in forming and anchoring the S trimers to the virion lipid envelope (Song et al., 2004). A study on the conformational states of the SARS-CoV S ectodomain revealed that low pH induces an irreversible trimerization of S and renders the cleaved S2 insensitive to trypsin digestion (Li et al., 2006). Furthermore, exposure of these S2 trimers to 1 M urea causes most of the protein to form rosettes that possess the final post-fusion conformation. Interestingly, it was found by Arbely et al. that a novel GxxxG motif in the transmembrane domain of SARS-CoV S contributes to the trimerization of the entire spike protein (Arbely et al., 2006). However, a later study demonstrated that the removal of the GxxxG motif does not prevent the trimerization of the mutant S and only moderately affected the entry of the pseudovirus bearing the mutant S (Corver et al., 2007).

Early studies showed that S expressed on the surface of insect cells could be cleaved by exogenous trypsin but not by co-expressed furin, suggesting that the protein is not normally cleaved during infection (Yao et al., 2004). Several other studies supported

this finding showing that the SARS-CoV S was not cleaved (Song et al., 2004; Xiao et al., 2003). However, a later study showed that the cleavage products of S was observed in SARS-CoV infected Vero E6 cells, indicating the presence of proteolytic processing of the S protein in the host cells (Wu et al., 2004a). It was also demonstrated that the S1/S2 cleavage can be enhanced by expression of furin family enzymes (Bergeron et al., 2005). Initial study showed that the introduction of a furin cleavage site at R667, replacing the trysin cleavage site, enhances cell-cell fusion but does not have any effect on the virion entry (Follis et al., 2006). Consistent with this result, Watanabe et al demonstrated that the introduction of a furin-like cleavage sequence in S at aa 798 to 801 resulted in cleavage of the mutant S without trypsin treatment and also induces cell fusion when expressed on cell surfaces (Watanabe et al., 2008). In addition, it was found that the pseudoviruses carrying the cleaved form of mutant S infected cells in the presence of lysosomotropic agents and protease inhibitors but was blocked by heptad repeat peptides, indicating that SARS-CoV with a cleaved form of S is able to enter the cells directly from the cell surface (Watanabe et al., 2008).

Significantly, a study demonstrated that the SARS-CoV could employ two distinct pathways for cell entry, the protease-mediated entry and the endosomal pathway (Matsuyama et al., 2005). The protease-mediated entry, using trypsin, thermolysine and elastase, was shown to be 100 to 1000 fold more efficient than the endosomal pathway. Simmons et al. confirm this finding and in addition, the authors found that the proteolysis mediated by cathepsin L within the endosome was sufficient to activate membrane fusion by SARS-CoV (Simmons et al., 2005). It was also shown that the inhibitors of cathepsin L was found to block the infection of ACE-expressing 293T cells by SARS-CoV and the

expression of exogenously expressed cathepsin L substantially enhanced infection mediated by the SARS-CoV S protein (Huang et al., 2006c; Simmons et al., 2005). Another study confirmed that cathepsin L proteolysis indeed activates the membrane fusion function of the SARS-CoV S protein and mapped the cleavage site to aa residue T678 (Bosch et al., 2008b). The site of trypsin cleavage on SARS-CoV S was identified on residue R667 (Li et al., 2006). It was later shown that the heptad repeat derived peptides block the SARS-CoV entry via the protease-mediated pathway but does not affect entry using the endosomal pathway (Ujike et al., 2008). Interestingly, it was shown that the mutation of R667 and K672 blocked the cleavage of the S protein at the S1/S2 boundary but failed to have any effect on the trypsin-primed membrane fusion, suggesting the presence of a different site for the proteolytic processing of S to activate the virus infectivity (Belouzard et al., 2009). The authors further reported a critical proteolytic cleavage at aa residue R797, which acts in concert with the R667 cleavage to mediate membrane fusion and virus infectivity.

Several other protease were shown to have an effect on the fusion activity and infectivity mediated by the cleaved S. Du et al. reported that the protease factor Xa cleaved the SARS-CoV S and is associated with the viral infectivity (Du et al., 2007). It was recently reported that the aa residue T795 is critical for the elastase-mediated cleavage of SARS-CoV S and altering this site affects both the proteolytic cleavage and fusion activation of the S protein (Belouzard et al., 2010). In addition, it was demonstrated that low pH is not required for triggering membrane fusion mediated by the SARS-CoV S protein (Xiao et al., 2003).

Using bioengineering techniques, it was shown that HR1 and HR2 of SARS-CoV S bind to each other to form a six-helix bundle, also known as the fusion core that is essential for the fusion mechanism of the coronavirus (Zhu et al., 2004). The crystal structures of the pre-fusion core and the fusion core have been solved (Beniac et al., 2006; Deng et al., 2006; Supekar et al., 2004; Xu et al., 2004a). Further biochemical studies revealed that the HR1 and HR2 of SARS-CoV associate in an anti-parallel manner in the very stable α-helical six-bundle structure, and the HR1 can form a stable α-helical coiled coil in the absence of HR2 while the HR2 in isolation formed a weakly stable trimeric coiled coil (Bosch et al., 2004; Ingallinella et al., 2004; Tripet et al., 2004; Xu et al., 2004c). The solution structure of the HR2 domain in the pre-fusion state confirmed that HR2 forms a coiled coil symmetric trimer in the absence of HR1 (Hakansson-McReynolds et al., 2006). In addition, biophysical characterization of the HR2 peptide analogs interaction with the HR regions of the SARS-CoV S reveals the importance of the α-helical structure in the formation of the six-helix bundle (Yan et al., 2006b). It was also shown that the conserved asparagine and glutamine residues on HR1 propagates from two central chloride ions to provide hydrogen-bonding zippers that strongly constrain the HR2 main chain to force it to adopt an extended conformation at either end of the short HR2 α-helix (Duquerroy et al., 2005). The residues that were essential for the interaction was narrowed to residues 902 to 950 on HR1 and residues 1151 to 1184 on HR2 of SARS-CoV S (Tripet et al., 2004; Xu et al., 2004c).

A novel transition state of the fusion complex, represented by an ensemble of unstructured monomers, was also reported to be a required passage from the pre-fusion state to the post-fusion state (McReynolds et al., 2008). The unstructured monomoers

were also shown to be in a dynamic equilibrium with the structured trimer in the pre-fusion state. Further studies of the dynamics of the pre-fusion and transition states of the SARS-CoV S complex reveals that the transition state enables the conformational change of the envelope necessary for the SARS-CoV entry by the efficient sampling of a large area of conformational space (McReynolds et al., 2009).

A hydrophobic stretch of 19 aa residues corresponding to aa 770 to 778 was proposed to function as a fusion peptide of the SARS-CoV S (Sainz et al., 2005a). It was further demonstrated that the putative fusion peptide strongly partitions into membranes containing negatively charged phospholipids to increase the water penetration depth and displayed membrane activity that are modulated by the lipid composition of the membrane, suggesting its involvement in the merging of the viral and target cell membrane by perturbing the membrane phospholipids (Guillen et al., 2008a). Biophysical studies also help to identify a second fusion peptide corresponding to aa 873 to 888 (Guillen et al., 2005, 2008b). Three main membrane-active regions from the S2 subunit were identified to be involved in the SARS-CoV S-mediated membrane fusion process and were shown to participate in the fusion process by acting in a synergistic way (Guillen et al., 2008c; Guillen et al., 2005). The three regions comprise of the two identified fusion peptide domains and a pre-transmembrane domain (aa 1185 to 1202) that is shown to be essential for the enhancement of the viral and cell fusion process (Guillen et al., 2007). In addition, a peptide corresponding to a region in the loop domain of the S2 (aa 1073 to 1095) was also found to play a role in the SARS-CoV S-mediated membrane fusion, suggesting the involvement of this region in the merging of the viral and cell membranes (Guillen et al., 2009).

In another study, residues L803, L804 and F805 were identified to be critical for membrane fusion by functioning as a novel internal fusion peptide for SARS-CoV S after proteolytic cleavage within the S2 domain (Madu et al., 2009a). It was also shown that the conserved domain flanked by cysteines 822 and 833 on the SARS-CoV S is critical for the membrane fusion by forming a loop structure that control the activation of the membrane fusion via its interaction with the other components of the S trimers (Madu et al., 2009b).

Serine-scanning mutagenesis of the C-terminal heptad repeat regions showed that the hydrophobic side-chains within the short helical segment (I1161, I1165, L1168, A1172 and L1175) are critical for cell-cell fusion, suggesting the important role of α-helical packing in promoting S glycoprotein-mediated membrane fusion (Follis et al., 2005). Another mutagenesis study revealed that the amino acid L927, L941, I955 on HR1 domain and I1165 on HR2 domain are important to mediate the membrane fusion while L1179 on the HR2 domain is important for a post-fusion process (Chan et al., 2006b). In addition, alanine substitution were carried out on the tryptophan residues to investigate the importance of the trpytophan-rich region at the pre-transmembrane region, and the results showed that individual substituted mutants have substantial decrease in infectivity of more than 90 percent while global substituted mutants aborogate infectivity suggesting that this region is essential for SARS-CoV infectivity (Lu et al., 2008). A similar study supported this finding, demonstrating that the replacement of all the tryptophan residues in this region with alanines abolish S-mediated entry in a pseudovirus assay (Corver et al., 2009). In addition, the authors showed that the aromatic domain was also crucial for the S-mediated pseudovirus entry and that the positioning of the aromatic domain with

the hydrophobic domain relative to each other is an essential characteristic of the membrane fusion process (Corver et al., 2009).

By circular dichroism analysis, it is shown that the aromatic amino acid rich region within the S2 subunit did not have a propensity for a defined secondary structure and it was shown to strongly partitioned into lipid membrane as well as induced lipid vesicle permeabilization in leakage assays, suggesting that it may function to perturb the target cell membrane during the membrane fusion process (Sainz et al., 2005b). This result is confirmed in another study that demonstrated that the entry of retrovirus pseudoviruses, expressing the aromatic amino acid deletions or substitution, into the human ACE2 (hACE2) expressing HEK-293 cells were greatly reduced (Howard et al., 2008). In addition, S mediated cell-cell fusion were also reduced by 60 to 70 percent in all alanine substituted mutants, suggesting the importance of this conserved juxtamembrane domain in SARS-CoV infection (Howard et al., 2008). By using pseudovirus and cell-cell fusion assay, the transmembrane domain of the SARS-CoV S was also demonstrated to be important for both the fusogenicity and infectivity of the virus (Broer et al., 2006). The authors showed that the replacement of the SARS-CoV S transmembrane domain with that of the VSV-G, that was less stable, resulted in lower fusogenicity and infectivity of the pseudovirus carrying the chimeric S.

A study of the proximal cysteine-rich motif at the carboxyl terminal of S revealed that this region plays an important role in cell-surface expression of S and S-mediated cell-cell fusion (Petit et al., 2005). Further studies showed that the palmitoylation of two of the four clusters of cysteine residues in the cytoplasmic domain are important for the S-mediated cell fusion (Petit et al., 2007). In addition, palmitoylation of SARS-CoV S

was also shown to be required for partitioning into detergent-resistant membranes and for cell-cell fusion (McBride and Machamer, 2010b). Taken together, the data presented demonstrate that the S2 subunit of SARS-CoV S contains multiple essential regions that play important roles for different stage of the viral-cell membrane fusion process.

Several studies were carried out to delineate the effects of S on the host response during SARS-CoV infection. It is found that S specifically modulates the unfolded protein response (UPR) via inducing the transcriptional activation of UPR effectors, GRP78, GRP94 and C/EBP, to facilitate viral replication (Chan et al., 2006a). It was also reported that the first 422 aa of SARS-CoV S is crucial for the induction of cyclooxygenase-2 expression as well as the correct localization of the S protein (Liu et al., 2006a). In addition, it was demonstrated that the over-expression of the S2 domain was shown to induce apoptosis in Vero E6 cells in a time- and dose-dependent manner (Chow et al., 2005). Recently, the SARS-CoV S was shown to trigger ACE2 signaling and upregulates the fibrosis-associated chemokine ligand 2 expressions through the Ras-ERK-AP1 pathway (Chen et al., 2010).

Table 1.2 – Functional characteristics of SARS-CoV structural proteins

Protein	Characterization	Functional role(s)
E	- Well conserved sequence within each coronavirus group (Godet et al., 1992). - Contains a hydrophilic amino and carboxy terminus, with a hydrophobic region in between the two ends (Torres et al., 2007; Wilson et al., 2004). N- and C-terminal ends were commonly found to be exposed to the cytoplasmic side of the membrane but a minor proportion of the protein that were modified by N-linked glycosylation inserted into the membrane only once, exposing only the C-terminus to the luminal side (Yuan et al., 2006c). - Structure study using bioinformatics analysis and circular dichroism (CD) technique reveal that E forms a single transmembrane domain helix and a short β-sheet segment that can form a hydrogen bond with the lipid bilayer (Shen et al., 2003). - Fourier transformed infra-red (FITR) spectroscopy, X-ray reflectivity and molecular modeling showed that E forms an unusual palindromic transmembrane helical hairpin structure that is orientated perpendicular to the dimyristolylated phosphatidylchoine (DMPC) bilayer (Arbely et al., 2004; Khattari et al., 2006). - Contains at least one α-helical transmembrane domain that spans approximately 25 aa residues and the transmembrane domain forms dimer, trimer and two forms of pentamers (Torres et al., 2006). - Site-directed mutagenesis studies revealed the importance of two cysteine residues for the oligomerization of E, and biochemical characterization demonstrated that all the cysteine residues on E is post-translationally modified by palmitoylation (Liao et al., 2006). - Co-localized with NSP3 in infected cells and binds to NSP3 in these cells as well as in cell-free systems via the N-terminal acidic domain on NSP3 (Alvarez et al., 2010).	- Forms ion channel that are more permeable to monovalent cations than to monovalent anions (Wilson et al., 2004). - Oligomerization was shown to have an enhancement effect on the membrane permeability in both bacterial and mammalian cells (Liao et al., 2004; Liao et al., 2006). - Transmembrane domain have improved solubility when flanked with two lysine residues on each end and these terminal lysines induce a kink at the centre of the transmembrane α-helix structure that do not interfere with the ion channel activity, suggesting the presence of inherent conformational plasticity in the transmembrane domain that may be necessary for the ion channel function (Parthasarathy et al., 2008; Torres et al., 2007). - Ion channel activity can be inhibited by amantadine and hexamethylene amiloride (HMA) and viral replication was inhibited by HMA as well (Pervushin et al., 2009; Torres et al., 2007). - Induces apoptosis in transfected Jurkat T cells via its interaction with an anti-apoptotic protein, Bcl-xL, to reduce its anti-apoptotic activity (Yang et al., 2005b). - Mutant virus with the E gene deleted by reverse genetics was able to replicate, although the virus titer was reduced by 20 to 200 fold when compared to the wild-type virus and was attenuated in hACE2 transgenic mouse model and in hamsters (DeDiego et al., 2007; DeDiego et al., 2008; Lamirande et al., 2008).

Table 1.2 - *Continued*

Protein	Characterization	Functional role(s)
M	- A triple-spanning protein that is N-glycosylated at asparagine 4 and is retained in the ERGIC with a steady state accumulation in the Golgi complex (Nal et al., 2005; Oostra et al., 2006; Voss et al., 2006). - Co-localized with S, E and N when co-expressed in cells and the C-terminal is responsible for the binding to N while multiple regions on M interacts with S and E (Hsieh et al., 2008). - Binding domain of M to N is in the region between aa 194 to 205 in the C-terminal region of M (Fang et al., 2005). - Interacts with the S cytoplasmic tail and the M cytoplasmic tail is necessary for retaining S at the Golgi region when the proteins were co-expressed in cells (McBride et al., 2007). - An essential tyrosine residue, Y_{195}, on the M cytoplasmic tail is important for its interaction with S to retain the protein at the Golgi region (McBride and Machamer, 2010a). - Consists of an N-terminal ectodomain, three transmembrane domains and a long cytosolic C-terminus. The N-terminal 134 aa is sufficient for the accumulation of M in the Golgi, recruitment of S to the sites of the virus assembly and budding in the ERGIC. (Voss et al., 2009). - The N-terminal 50 aa are sufficient for the membrane binding, multimerization and Golgi rentention of M in transfected cells and multiple regions on M were involved in the self-assembly and subcellular localization (Tseng et al., 2010).	- Expression of M triggered an accelerated apoptosis in insect cells but did not induce apoptosis in mammalian cells (Lai et al., 2006). - Expression of the cytoplasmic tail of M is sufficient to suppress the expression of NF-kB, TNFα and Cox-2 and M interacts with IKKβ in a co-immunoprecipitation assay, suggesting that M suppresses NF-kB through the direct interaction with IKKβ, resulting in a lower Cox-2 expression. (Fang et al., 2007). - Induces apoptosis in HEK293T cells and transgenic Drosophila via the modulation of the cellular Akt pro-survival pathway and mitochondrial cytochrome c release (Chan et al., 2007). - Associates with RIG-1, TBK1, IKKε and TRAF3, sequestering them in the membrane-associated cytoplasmic compartments to prevent the formation of TRAF3-TANK-TBK1/IKKε complex, resulting in the inhibition of TBK1/IKKε-dependent activation of IRF3/IRF7 transcription factors and subsequently inhibiting gene transcription of type I interferons (Siu et al., 2009). - Inhibits interferon synthesis via the inhibition of IRF3 and NFkB (Kopecky-Bromberg et al., 2007).

Table 1.2 - *Continued*

Protein	Characterization	Functional role(s)
N	- Detected in the alveolar epithelium and macrophages in lung atopsies of SARS patients (Nicholls et al., 2006). - Distributed in the cytoplasm in both transfected and infected cells (Rowland et al., 2005; Surjit et al., 2005; You et al., 2005). - Nucleolar localization was observed in some infected cells and N was shown to have the Pat4, Pat7 and the bi-partite type nuclear localization signal (NLS) and predicted a CRM-1 dependent nuclear export signal (You et al., 2005). - N-terminal contains NLS1 (aa 38 to 44) that localizes to the nucleus while the C-terminal contains NLS2 (aa 257 to 265) and NLS3 (aa 369 to 390) that localizes to the cytoplasm and nucleolus, indicating that N may function as a shuttle protein between the cytoplasm, nucleolous and the nucleus (Timani et al., 2005). - Efficiently phosphorylated by cyclin-CDK complex, active only in the nucleus, and associates with 14-3-3 protein in a phospho-specific manner, indicating the presence of N in the nucleus (Surjit and Lal, 2008). - Molecular modeling and comparison of coronavirus nucleolar retention signals suggest that N may interact with cellular proteins to traffic them to and from the nucleolus and cytoplasm (Reed et al., 2006). - Modified by acetylation and sumoylation (Krokhin et al., 2003; Li et al., 2005b). - Interacts with a ubiquitin conjugating enzyme of the sumoylation system, Hubc9 (Fan et al., 2006). - Sumoylation played a key role in the modulation of the homo-oligomerization, nucleolar translocation and cell-cycle de-regulatory property of the N protein (Li et al., 2005b). - Phosphorylation observed when 293T cells were infected with adenovirus that expresses SARS-CoV N (Zakhartchouk et al., 2005). - Phosphorylated by mitogen activated protein kinase (MAPK), cyclin-dependent kinase (CDK), glycogen synthase kinase 3 (GSK3) and casein kinase 2 (CK2) (Surjit et al., 2005).	- A mutant N lacking the sumoylation motif induces cell cycle arrest (Li et al., 2005b). - Inhibits S phase progression via the down-regulation of cyclin E and CDK2 in cells (Surjit et al., 2006). - Interacts with elongation factor 1-alpha (eIF1-α) to induce its aggregation, leading to inhibition of protein translation and cytokinesis by blocking F-actin bundling (Zhou et al., 2008). - Binding activity of several transcription factors involved in the signal transduction pathway of activated protein-1 (AP-1), such as c-fos, ATF-2, CREB-1 and fos B, was found to be enhanced by exogenously expressed N protein using ELISA, thus suggesting the involvement of N in a number of cellular processes (He et al., 2003c). - Activates NF-kB in VeroE6 cells (Liao et al., 2005). - Activates interleukin 6 (IL6) expressions via direct binding to the NF-kB binding element and trans-locating NF-kB from cytosol to nucleus (Zhang et al., 2007b). - Binds directly to the NFkB response element present in the pro-inflammatory factor, cyclo-oxygenase 2 protein (COX2), via aa 136 to 204 to up-regulate the transcriptional level of COX2 protein (Yan et al., 2006a). - Possesses a high affinity for the human cellular heterogenous nuclear ribonucleoprotein A1 (hnRNPA1), with the interaction domain on N mapped to aa 161 to 210, suggesting an involvement in the regulation of the viral RNA synthesis (Luo et al., 2004a; Luo et al., 2004b). - Strongly associates with human cyclophilin A, a protein previously shown to associate with HIV-1 gag and is crucial for HIV-1 infection (Gamble et al., 1996; Luo et al., 2004a).

Table 1.2 - *Continued*

Protein	Characterization	Functional role(s)
N	- Structural analysis showed two independent domains that are connected by a linker region in N (Chang et al., 2006). - Linker region was predicted to undergo phosphorylation and has been reported to interact with M and a human cellular protein, hnRNPA1 (Luo et al., 2005b; Luo et al., 2006; Luo et al., 2005a). - N-terminal associates with several viral 3' un-translated RNA sequence, indicating the RNA binding property of the protein (Huang et al., 2004a). - RNA binding motif on N was mapped to aa 363 to 382 (Luo et al., 2006). - Another RNA binding domain that has a stronger RNA interaction was identified in the C-terminal region (aa 248 to 365) of N and it is suggested that the genomic RNA is packaged in a helical manner by the N protein (Chen et al., 2007a). - Essential for RNA packaging in a SARS-CoV VLPs system and there are two independent RNA binding domains on the protein; aa 1 to 235 at the N terminal and aa 236 to 384 at the C terminal (Hsieh et al., 2005). - Possesses RNA chaperone activity (Zuniga et al., 2007). - Self-associates via the interactions at its C-terminal (Surjit et al., 2004a) as well as via a domain (aa 184 to 196), encompassing a SR-rich motif, to form an oligomer (He et al., 2004a). - SR-rich motif has binding affinity that is specific for only the central region of another N protein, while the C-terminal (aa 283 to 422) binds to the same region on another N protein to form dimer, trimer, tetramer and hexamer and the essential region for oligomerization, that also encompasses the RNA binding motif, was mapped to aa 343 to 402 (Luo et al., 2005b; Luo et al., 2006; Luo et al., 2005a; Yu et al., 2005; Yu et al., 2006). - Confirmed by structural studies that the ribonucleocapsid formation of SARS-CoV is mediated by the molecular actions of the N-terminal domain of N (Saikatendu et al., 2007).	- Interacts with a transmembrane molecule, HAb18G/CD147, to facilitate the invasion of host cells by SARS-CoV (Chen et al., 2005d). - Induces apoptosis in Cos-1 monkey kidney cells via the down-regulation of pro-survival factors, Akt and Bcl2, and the up-regulation of pro-apoptotic factors, caspase-3 and caspase-7 (Surjit et al., 2006; Surjit et al., 2004b). - Activates the mitochondrial death pathway to induce apoptosis (Zhang et al., 2007a). - Blocks apoptosis of SARS-CoV-infected cells via its interaction with Smad3 to impair the Smad3-Smad4 hetero-complex formation (Zhao et al., 2008). - Promotes the transforming growth factor-beta (TGF-β)-induced expression of plasminogen activator inhibitor-1 (PAI-1), a protein that plays a critical role in tissue fibrosis (Zhao et al., 2008).

1.1.3 Accessory proteins of SARS-CoV

All the coronaviruses encode a group of accessory proteins that are shown to be non-essential for virus growth in vitro (Curtis et al., 2002; de Haan et al., 2002; Haijema et al., 2004; Yount et al., 2005). These accessory proteins are virus-specific and have low levels of homology between the different coronaviruses (Lai and Cavanagh, 1997). SARS-CoV genome encodes eight putative accessory proteins that do not show any significant similarity to proteins of known coronaviruses (Snijder et al., 2003). Intensive studies were performed to understand the specific function(s) of each of these proteins. The characterization and functional roles of the proteins encoded by ORF3a, 3b, 6, 7a, 7b and 9b are summarized in Table 1.3. The studies performed on the proteins encoded by ORF8 will be reviewed in more details in the later paragraphs.

Epidemiological studies revealed that the ORF8 of the SARS-CoV isolated from the middle and late phase SARS patients contain a 29-nucleotide deletion that is present in the virus isolated from the animal and the early phase SARS patients (Guan et al., 2003). As a result, the ORF8 of the virus circulating in the middle and late phase patients encodes for a 39 and 84 aa proteins, 8a and 8b, respectively, instead of a single 122 aa protein, 8ab. It was found in a study by Wu et al. that the infection of civets with SARS-CoV without the 29-nucleotide deletion (BJ01) induces a higher average temperature and slightly stronger antibody response than civets infected with SARS-CoV bearing the 29-nucleotide deletion (GZ01), suggesting a role of ORF8 proteins in SARS-CoV pathogenesis (Wu et al., 2005).

Over-expression studies showed that the 8b-EGFP protein is localized to both the nucleus and the cytoplasm of Vero E6 and CHO cells (Law et al., 2006). In SARS-CoV

infected Vero E6 cells, Oostra et al. reported no detection of 8b expression after 8h post-infection (Oostra et al., 2007a). A characterization study of the ORF8 proteins showed that 8b binds to monoubiquitin and polyubiquitin and was degraded rapidly by proteasomes when expressed in mammalian cells (Le et al., 2007). Interestingly, the over-expression of 8b was also shown to induce DNA synthesis (Law et al., 2006). The over-expression of 8a-EGFP in HEK-293T cells showed that the protein is localized to the mitochondrial and perturb the mitochondrial membrane potential to induce apoptosis via a caspase-3 dependent pathway (Chen et al., 2007b). Using stable cell clones expressing 8a for siRNA transfection, the authors also demonstrated that 8a enhances virus replication and cytopathic effect.

In another study, it was demonstrated that 8ab was modified and stabilized by N-linked glycosylation on the N81 residue and the protein can be further modified by ubiquitination (Le et al., 2007). Subsequent studies showed that 8ab possessed a cleavable signal peptide which directs the precursor protein to the ER and mediates its translocation into the lumen, after which the cleaved protein becomes N-glycosylated for assembly of di-sulfide-linked homo-multimeric complexes, which remained stable in the ER (Oostra et al., 2007a; Sung et al., 2009). In addition, 8ab was found to be capable of inducing the proteolysis of activating transcription factor 6, leading to the up-regulation of endogenous ER-resident chaperones expression that are involved in protein folding (Sung et al., 2009). This suggests that 8ab could play a role in SARS-CoV pathogenicity by modulating the UPR.

Table 1.3 – Functional characteristics of SARS-CoV accessory proteins.

Protein	Characterization of protein	Functional role(s) of protein
3a	- Localized to the plasma membrane and peri-nuclear region of infected and transfected cells (Tan et al., 2004a). - An *0*-glycosylated protein containing three trans-membrane domains as well as an N-terminal ecto-domain and a C-terminal endo-domain (Ito et al., 2005; Oostra et al., 2006; Tan et al., 2004a; Yuan et al., 2005a). - Possesses tyrosine-sorting (YxxΦ) and di-acidic motifs, which are important for the protein sorting and trafficking of 3a to the cell surface, where it eventually undergoes endocytosis (Tan et al., 2004a). - Contains binding motifs for caveolin-1, a protein that is important in cell signaling (Cai et al., 2003; Padhan et al., 2007). - Does not share any homology with any known RNA binding protein but specifically interact with the 5'-UTR of its genomic RNA using a 75 aa interaction domain (Sharma et al., 2007). - Associates with structural proteins S, M and E as well as an accessory protein, 7a and was incorporated into the virus particle through its association with S (Tan et al., 2004a; Zeng et al., 2004). - A novel structural protein that assembles into virus-like particles (VLPs) when co-expressed with S, E, M and N (Huang et al., 2006b; Ito et al., 2005; Khan et al., 2007; Shen et al., 2005; Zeng et al., 2004). - Production of VLPs in the absence of 3a expression as well as the ability to generate viable SARS-CoV in deletion mutants lacking 3a suggest that 3a is not essential for SARS-CoV particle assembly in cell culture (Hsieh et al., 2005; Huang et al., 2006a; Mortola and Roy, 2004; Yount et al., 2005). - Some viruses isolated from SARS patients encode only the truncated form(s) of 3a and not the full-length 3a, indicating that the protein is dispensible for virus replication (Tan et al., 2005c). - 3a deletion mutant of SARS-CoV and the silencing of 3a and 3b using siRNA yields a lower progeny of viruses (Akerstrom et al., 2007; Yount et al., 2005).	- Induces apoptosis in VeroE6 cells (Law et al., 2005b). - Activates the mitochondrial death pathway via the p38 MAP kinase activation (Padhan et al., 2008). - Promotes cell death and membrane re-arrangement (Freundt et al., 2010). - Induces G1 phase cell-cycle arrest by reducing cyclin-D3 expression and inhibiting retinoblastoma protein phosphorylation in *in vitro* expression studies (Yuan et al., 2007). - Functions as a potassium ion channel to modulate virus release by forming a homo-tetramer complex via intermolecular disulfide bridges (Lu et al., 2006) and the ion channel activity is required for its pro-apoptotic function (Chan et al., 2009). - Up-regulates the expression and secretion of fibrinogen in human lung epithelial cells, A549 (Tan et al., 2005b). - Expression of 3a in A549 cells activates nuclear factor kappa B (NF-kB) and enhances the activation of NF-kB responsive chemokines, interleukin 8 (IL8) and RANTES (CCL5) (Kanzawa et al., 2006; Law et al., 2005a). - A significant induction of NF-kB dependent promoter activity in SARS-CoV infected 293/ACE2 cells was shown by Narayanan et al. but Frieman et al. and Spiegel et al. reported no significant induction of NF-kB promoter-driven gene expression in 293 cells (Frieman et al., 2008; Narayanan et al., 2008b; Spiegel et al., 2005). - Expression of 3a in murine macrophage cell-line, RAW264.7, enhanced NF-kB activity and differentiation into osteoclast-like cells in the presence of receptor activator of NF-kB ligand (RANKL) and its expression in A549 cells expressing ACE2 up-regulates TNF-alpha, which is known to accelerate osteoclastogenesis (Obitsu et al., 2009). . - Induces down-regulation of type-I interferon alpha receptor (IFNAR1) by increasing its ubiquitination via inducing serine phosphorylation within the subunit 1 degradation motif (Minakshi et al., 2009).

Table 1.3 - *Continued*

Protein	Characterization of protein	Functional role(s) of protein
3b	- Expressed via an internal ribosomal entry mechanism (Snijder et al., 2003). - Detected in SARS-CoV infected cells and the anti-3b antibody was detected in SARS patient's serum (Chan, 2005; Guo, 2004). - Localize to both the nucleolus and mitochondria in expression studies (Yuan, 2005, 2006). - GFP-tagged 3b localize only to nucleolus without evidence of mitochondrial localization (Kopecky-Bromberg et al., 2007).	- Induces growth arrest in G1/G0 phase (Yuan et al., 2005b). - Over-expression of 3b induces both necrosis and apoptosis in VeroE6 cells (Khan et al., 2006). - Inhibits both interferon production and signaling in SARS-CoV infection, via the inhibition of IRF3 (Kopecky-Bromberg et al., 2007).
6	- Bears a minimal transcription regulatory sequence upstream of its gene and its mRNA was detected in SARS-CoV infected Vero cells (Snijder et al., 2003; Thiel et al., 2003). - Expressed in lung and intestinal tissues of SARS patients and in SARS-CoV infected cells (Geng et al., 2005). - HA-tagged ORF6 protein localizes to ER and Golgi apparatus while EGFP-tagged ORF6 protein localizes to the perinuclear region and ER of the transfected cells (Geng et al., 2005; Law et al., 2006; Pewe et al., 2005). - Localize to the ER and Golgi compartments in SARS-CoV infected cells (Frieman et al., 2007) - Co-localizes with LAMP-1, a lysosomal marker, in SARS-CoV infected Vero E6 cells (Kumar et al., 2007). - A virion-associated protein that can be incorporated into the VLPs and is secreted by transfected cells expressing the protein (Huang et al., 2007).	- Stimulates DNA synthesis in CHO and VeroE6 cells (Law et al., 2006). - Converts a sub-lethal infection of rodents by an attenuated murine coronavirus to lethal encephalitis, and enhances virus growth in cell culture (Pewe et al., 2005). - Viral RNA in virus-infected cultures using recombinant MHV expressing ORF6 protein were five to eight times higher compared to wild-type MHV. Co-immunoprecipitate with viral RNA and co-localized with cytoplasmic vesicles with replicating viral RNAs (Tangudu et al., 2007). - Interacts with SARS-CoV RdRp, NSP8, in a yeast-two-hybrid screen and co-localization were observed in SARS-CoV infected cells (Kumar et al., 2007). - Mutation of the N-terminal hydrophobic region affects ORF6 protein ability to enhance virus growth (Netland et al., 2007). - The hydrophilic C-terminal region containing the YSEL, a sorting motif for endosome/lysosome internalization interacts with cellular importins (Frieman et al., 2007). - Deletion of this C-terminal region does not interfere with the nuclear import processes but the ORF6 protein can still augment MHV infections and siRNA directed against importin-beta mRNAs did prime cells for enhanced MHV infections (Hussain et al., 2008). - Required for optimal replication of SARS-CoV when cells were infected at low MOI and accelerated disease in transgenic mice expressing the human ACE2 (Zhao et al., 2009). - Over-expression of the ORF6 protein induces apoptosis via a caspase-3 mediated ER stress and JNK-dependent pathway (Ye et al., 2008). - Inhibits both the promoter-binding and activation of IRF3 and nuclear translocation of STAT1 (Kopecky-Bromberg et al., 2007). C-terminal tether karyopherin alpha 2 to the ER/Golgi membrane to disrupt STAT1 nuclear import, thus blocking the expression of STAT1-activated genes required to establish an anti-viral response (Frieman et al., 2007).

Table 1.3 - *Continued*

Protein	Characterization of protein	Functional role(s) of protein
7a	- Localize to the perinuclear region and the ER and intermediate compartments of SARS-CoV infected and transfected Vero E6 cells, and possesses an N-terminal signal peptide, an ER retrivel motif (KRKTE) and a transmembrane helix in the C-terminal tail (Fielding et al., 2004). - Nuclear magnetic resonance (NMR) spectroscopy and the crystal structure of 7a revealed a compact seven-stranded β sandwich fold in the N-terminal ectodomain, similar to the topology found in members of the immunoglobulin (IgG) superfamily (Hanel et al., 2006; Nelson et al., 2005). - High structural similarity to the D1 domains of integrin ligands, ICAM-1 and ICAM-2, suggesting that it can binds to the α_L integrin I domain of LFA-1 (Hanel et al., 2006). - Short cytoplasmic tail and transmembrane domain mediate the trafficking of 7a within the ER and Golgi network (Nelson et al., 2005). - Expression of 7a was detected in SARS-CoV infected Vero E6 cells and lung tissues of SARS patients (Chen et al., 2005c). - A novel structural protein that associates with purified SARS-CoV particles and was incorporated into VLPs by co-expression with S, M, N and E (Huang et al., 2006a). - Interacts with 3a, S, M and E (Fielding et al., 2006; Huang et al., 2006a; Tan et al., 2004a). - Interaction with S and 3a were dispensable for its assembly into the VLPs (Huang et al., 2006a). - Interacts with small glutamine-rich tetratricopeptide repeat-containing protein (SGT) in a yeast-two hybrid screen (Fielding et al., 2006). - Function as an RNA silencing suppressor by reducing the levels of siRNA to suppress both the transgene and virus-induced gene silencing, and has the ability to enhance heterologous replicon activity. (Karjee et al., 2010).	- Treatment with and over-expression of 7a inhibited the growth of Balb/C 3T3 cells (Chen et al., 2005c). - Expression of 7a in HEK293 cells correlates with reduction of mRNA transcription and expression of cyclin D3 level as well as the phosphorylation of retinoblastoma (Rb), thus preventing the progression of the cell cycle at the G0/G1 phase, explaining the ability of 7a to inhibit cell growth. (Yuan et al., 2006b). - Over-expression of 7a induces apoptosis via a caspase-dependent pathway in cell-lines from different organs (Tan et al., 2004b). - Extensive apoptosis observed in the pathological tissues of SARS-CoV patients (Chau et al., 2004; Zhang et al., 2003a). - Induction of apoptosis by 7a may be related to its ability to inhibit cellular translation and activate p38 mitogen-activated protein kinase (Kopecky-Bromberg et al., 2006). - Interacts with different members of the Bcl-2 family of pro-survival proteins and is found to co-localize with Bcl-X_L at the ER and mitochondria (Tan et al., 2007b). - Deletion of gene 7 from SARS-CoV reduces the efficiency of the virus to induce DNA fragmentation, suggesting the contribution of gene 7 products to the virus-induced apoptosis (Schaecher et al., 2007a). - Gene 7 deleted SARS-CoV did not induce early apoptosis markers or activate caspase 3, and it has no effect on virus replication in *in vitro and in vivo* models, suggesting that 7a and/or 7b contribute to but are not solely responsible for the apoptosis observed in SARS-CoV infected cells (Schaecher et al., 2008a; Schaecher et al., 2007a).

Table 1.3 - *Continued*

Protein	Characterization of protein	Functional role(s) of protein
7b	- Transcribed via a non-canonical leaky scanning mechanism from the ORF7b initiation codon that overlaps the ORF7a stop codon in a -1 shifted ORF (Schaecher et al., 2007b; Snijder et al., 2003). - A type III integral membrane protein with a Golgi localization signal and complex retention signal within the transmembrane domain and 7b co-localized with both *cis*- and *trans*-Golgi markers (Schaecher et al., 2008b). - Specific antibodies targeting 7b were detected in the convalescent serum of SARS patients (Guo et al., 2004). - Proposed to be a structural component of the SARS-CoV virion as 7b can associate with intracellular virus particle and is detected in purified virus particles (Schaecher et al., 2007b). - SARS-CoV lacking the ORF7 proteins replicated as well as the wild-type virus in cell lines and mice, indicating that 7a and 7b are not essential for SARS-CoV replication *in vitro* (DeDiego et al., 2008; Sims et al., 2005; Yount et al., 2005). - A 45-nucleotide deletion within the ORF7b acquired by serial passaging of the virus did not affect the virus replication as well (Thiel et al., 2003). - Using $CaCO_2$ and Huh7 cells as well as in golden Syrian hamster models, SARS-CoV carrying an ORF7b deletion had a replicative advantage, increasing the virus titer by 4 to 6 fold and 23 fold, respectively, and the viral RNA in the lungs of the hamsters increases by 94.8 fold. (Pfefferle et al., 2009a).	- Not known
9b	- Translated from a bi-cistronic mRNA9 via a leaky ribosome scanning mechanism (Xu et al., 2009). - Antibodies against the protein have been detected in patients, and its expression was shown in diseased organs and SARS-CoV infected cells (Chan et al., 2005; Moshynskyy et al., 2007; Qiu et al., 2005). - Crystal structure reveals a novel fold that comprise of a dimeric tent-like β structure with an amphipathic surface and a central hydrophobic cavity that binds lipid molecules (Meier et al., 2006). - Exported outside the cell nucleus and localizes to the ER (Moshynskyy et al., 2007). - Amino acid residues 46 to 54 on 9b function as a nuclear export signal and the protein is incorporated into both the VLPs and purified SARS-CoV virions (Xu et al., 2009).	

1.2 Zoonotic origins of SARS-CoV

1.2.1 Cross-species transmission of SARS-CoV

It was postulated that SARS-CoV was spread to humans via zoonotic transmission after several studies showed that more animal food handlers and traders were found to be infected and having a higher prevalence of IgG antibodies against SARS-CoV than individuals from other trades in Guangdong Province, China (Xu et al., 2004d; Yu et al., 2003; Zhong et al., 2003). Majority of these individuals also have asymptomatic infection (He et al., 2003a; Xu et al., 2004d; Yu et al., 2003).

The first investigation into the origin of the SARS-CoV in animals was carried out in Dongmen market located within Shenzhen in Guangdong province (Guan et al., 2003). In this study, eight different species comprising of 6 masked palm civets, 1 raccoon dog, 2 ferret badgers, 3 hog-badgers, 3 beavers, 4 domestic cats, 3 Chinese hares and 2 Chinese muntjac were tested for SARS-CoV nuclei acid of the N gene of the human SARS-CoV using reverse transcription-polymerase chain reaction (RT-PCR) and all the swabs were inoculated into rhesus monkey embryonic kidney cells, FRhK4, for virus isolation. All the masked palm civets and raccoon dogs were tested positive by either RT-PCR or virus isolation and neutralizing antibody to a SARS-CoV isolated from a masked palm civet (SZ16) were found in 3 of the masked palm civets, a raccoon dog and a Chinese ferret badgers. Two more surveillance studies carried out on masked palm civets also showed positive results for the detection of antibodies to SARS-CoV (Hu et al., 2005; Tu et al., 2004). Another 3 research teams showed that the sequences of SARS-CoV S genes in samples of masked palm civets and 4 patients from a sporadic outbreak in December 2003, who have direct or indirect contact with the masked palm civets, were

almost identical (Kan et al., 2005; Liang et al., 2004; Song et al., 2005; Wang et al., 2005a). These studies suggest that SARS-CoV could have spread to the human population via the palm civets in the live market. Experimental studies also showed that palm civets were sensitive to infection by human SARS-CoV and in vivo amplification and secretion of the infected palm civets were significantly more efficient than other animal models such as African green monkeys, cynomolgus macaques, ferrets, cats, mouse and golden Syrian hamsters (Buchholz et al., 2004; Bukreyev et al., 2004; Kuiken et al., 2003; Martina et al., 2003; Roberts et al., 2005; Rowe et al., 2004; Subbarao et al., 2004; Wu et al., 2005).

Although SARS-CoV could be detected in some of the masked palm civets, it was shown that majority of the farmed palm civets in China were tested negative for SARS-CoV (Kan et al., 2005). An independent study in the live animal market in Guangzhou also showed negative results for SARS-CoV or SARS-like coronavirus (SL-CoV) infection in the civets (Wang et al., 2005b). In addition, civet SARS-CoV exhibits a limited genetic diversity and was highly identical to the human SARS-CoV (Lam et al., 2008; Song et al., 2005). This suggests that the although it is possible that SARS-CoV could be transmitted from the masked palm civets to the human population, the palm civets may not be the reservoir for SARS-CoV.

Interestingly, the attention were turned to the bats in 2005 when SL-CoV RNA sequences and anti-SARS nucleocapsid antibodies were reported to be detected in *Rhinolophus* Chinese horseshoe bats without any clinical signs of infection (Lau et al., 2005b; Li et al., 2005d). Bats are long known to serve as reservoirs for a variety of viruses, and all human coronaviruses are postulated to originate from the bats

coronaviruses (Sulkin and Allen, 1974; Vijaykrishna et al., 2007). More studies to search for coronaviruses in bats revealed that these flying mammals harbor a diverse array of SL-CoV and novel coronaviruses that could be related to the existing human coronaviruses (Chu et al., 2008a; Dominguez et al., 2007; Pfefferle et al., 2009b; Poon et al., 2005; Tang et al., 2006; Woo et al., 2006). Sequence analysis revealed that the bats SL-CoV has the 29 nucleotide region in the ORF8 that are present in palm civets and early human phase SARS-CoV strains but absent in the late human phase SARS-CoV strain, indicating a close evolutionary relationship to the viruses that cause the SARS outbreak in 2002 (CSMEC, 2004; Ren et al., 2006). Phylogenetic analysis based on the full sequence of bats SL-CoV revealed a close relationship with the human and civet SARS-CoV but not other coronaviruses in the group 2 (Shi and Hu, 2008b). However, based on the relative distant relationship in the phylogenetic tree, it was suggested that none of the currently sampled SL-CoV in bats are the direct ancestor of the SARS-CoV in humans and civets (Hon et al., 2008). The direct ancestor of the SARS-CoV might be still at large in the bats population. Interestingly, a recent study demonstrated that the civet SARS-CoV SZ3 strain may likely be a recombinant virus arising from the bats SL-CoV Rp3 strain and the bats SL-CoV Rf1 strain (Lau et al., 2010).

1.2.2 Molecular evolution and genomic differences of SARS-CoV

Several laboratories had carried out intensive studies on the genomic differences and molecular evolution to understand the evolutionary path and identify the source of the highly infectious virus. Early studies showed that most human SARS-CoV strain during the epidemic carries a 29-nucleotide (nt) deletion upstream of the N gene domain, when compared to viral strains from SARS patients during the early outbreak and animal sources (CSMEC, 2004; Guan et al., 2003). This deletion resulted in the two proteins, 8a and 8b, instead of a single 8ab protein to be encoded by ORF8. The significance of the ORF8 proteins in viral virulence and pathogenesis remained to be investigated. In addition, SARS-CoV strains carrying 82-nt deletion within the ORF8 region were also isolated from several SARS patients (CSMEC, 2004). Sequence comparison reveals that a similar SARS-like CoV strain carrying the 82-nt deletion was previously isolated from farmed civets in Hubei Province, suggesting that this strain could have originated from the animals (Hu et al., 2003). Interestingly, co-infection of the two virus genotypes, with the 29-nt and 82-nt deletions, was found in the lung biopsy of a patient from the epidemic phase (CSMEC, 2004). In addition, another virus genotype with a 415-nt deletion resulting in the loss of the whole ORF8 region was also isolated from two patients during the late phase of the epidemic (CSMEC, 2004). This is not the only report that shows large genomic deletions in the SARS-CoV strains from the late phase epidemic; SARS-CoV strains with a 386-nt deletion flanking the previously identified 29-nt deletion site were also identified (Chiu et al., 2005). Anti-parallel reverse symmetrical sequences that result in hairpin structures were readily predicted around the deletion sites, which may explain for the high occurrence of deletions within this region (CSMEC, 2004).

RNA viruses were known to have high mutation rates, giving them a survival edge either by increasing viral virulence, escaping host defenses or switching tissue tropism (Brown et al., 2001; Rasschaert et al., 1990; Seo et al., 2002). A high number of single nucleotide variations were identified from sequence comparison of 63 SARS-CoV sequences, resulting in either synonymous or non-synonymous mutations (CSMEC, 2004). The ratio of the rates of non-synonymous to synonymous changes (Ka/Ks) for the S gene showed that positive selection pressure was greatest during the early epidemic and progressively slowed down as the epidemic progress to the late phase (CSMEC, 2004). Genomic sequences analysis showed that the mutation rate for the strains obtained from different regions of the world during the 2003 epidemic was 2.2 to 6.7 x 10^{-6} nt substitution per site per day (Zhao et al., 2004). Analysis on the Singapore strains from the epidemic yields similar results at 5.7 x 10^{-6} nucleotide substitution per site per day (Vega et al., 2004).

It was shown that the putative S1 domain of the bats SL-CoV, containing the RBD, has a low sequence similarity compared to the human and civet SARS-CoV S1 domain (Wong et al., 2004). In addition, Li et al. identified one insertion and three deletion sites in the S1 domain of the bats SL-CoV (Li et al., 2005a). These results suggest that the bats SL-CoV use a different receptor molecule for virus entry. However, the S2 domain of all the SL-CoV has a high sequence identity of 96% to that of SARS-CoV, suggesting a similar fusion mechanism employed by the SL-CoV (Wong et al., 2004). Mutational analysis between the bats SL-CoV, the civets and human SARS-CoV revealed some key mutational hotspots in the NSP3, ORF1a, S, ORF3 and ORF8 region (CSMEC, 2004). The host receptor for coronaviruses has previously been shown to be an

important determinant of host range expansion. For SARS-CoV, ACE2 has been shown to be the functional receptor for infection of the human host, and CD209L is shown to function as a co-receptor (Jeffers et al., 2004; Li et al., 2003b) . Comparison of the S RBD in the civets, early and late-phase human SARS-CoV showed that positive selection was taking place in the civet and early-phase SARS-CoV strains while negative selection was taking place in the late-phase SARS-CoV strains (CSMEC, 2004; Hu et al., 2003). Taken together, the results suggest that there is a high genomic similarity between SARS-CoV and the SL-CoV identified in the civets and bats, thus SARS-CoV most likely is an evolved strain from an ancestor SL-CoV strain that is residing in the bats population.

1.3 Goals of the project

The interactions between viruses and their host cells are complex and multi-faceted. Over the years, much effort had been put into understanding the roles of viral-viral and viral-host interactions in infection. SARS-CoV entry into the cell is driven by the S glycoprotein, which is a class I fusion protein (Bosch et al., 2003). The S protein of coronaviruses is known to be responsible for the induction of host immune responses and virus neutralization by antibodies and therefore, it is one of the major targets for the development of vaccine candidates (Buchholz et al., 2004; Castilla et al., 1997).

In this study, our aim is to identify neutralizing epitopes on S that can be used for the development of a vaccine or a therapeutic agent. Control of potential neutralization escape mutants is also an important area of concern in prophylactic and therapeutic treatment. For the development of an effective immune prophylaxis, a better understanding of the dynamics and evolution of the SARS-CoV is crucial. Thus in the current study, we aimed to develop neutralizing monoclonal antibodies for the generation of escape SARS-CoV that can help us to identify critical residues for the inhibitory activity of the mAbs, which may then allow us to identify novel domains necessary for viral entry as well as to gain a better understanding of the roles of the identified critical residues in the mechanism of coronavirus entry into the host cells. In addition, it was previously shown that nitric oxide (NO) can inhibit the replication cycle of SARS-CoV via the production of inducible NO synthase (iNOS) (Akerstrom et al., 2005). In this project, we aim to investigate the mechanism of inhibition of SARS-CoV replication by NO and to explore the potential application of NO as a therapeutic drug in the treatment of coronavirus infection.

For SARS-CoV, there are eight accessory proteins with no significance sequence homology to viral proteins of other coronaviruses. Although most of these accessory proteins have been shown to be expressed during SARS-CoV infection, it has not yet been established which of them are essential for viral replication and/or pathogenesis. Interestingly, a 29 nucleotide deletion has occurred in ORF8 after the transmission of SARS-CoV from animal to human and as a result, the 8ab protein became two separate proteins (8a and 8b) in the human isolates. The approach adopted by our laboratory is to study the interactions between the structural proteins and the ORF8 proteins and to identify cellular proteins that can contribute to the functions of these viral proteins. Our goal for this project is to provide a better understanding on the contribution of the mutation in ORF8 region to the replication and pathogenesis of SARS-CoV.

CHAPTER 2: MATERIALS AND METHODS

2.1 Mammalian cell lines used in the study

The monkey kidney cell lines Cos7 and Vero E6, Chinese hamster ovary CHO and human embryonic kidney 293T used in this study were purchased from the American Type Culture Collection (ATCC; Manassas, Va.). Cos7 and Vero E6 cells were cultured at 37 °C in a 5 % CO_2 incubator in Dulbecco modified Eagle medium (DMEM; Sigma-Aldrich Inc.) containing 0.1 mg/ml of streptomycin, 100 U/ml of penicillin, and 10 % fetal bovine serum (FBS; HyClone, Logan, Utah). A CHO cell line (CHO-ACE2) stably expressing the receptor, ACE2, for SARS-CoV S was established using the methods described previously (Chou et al., 2006) and grown in complete DMEM containing 0.1 mM $ZnSO_4$.

2.2 Viruses

The strain Sin2774 of SARS-CoV (GenBank accession number AY283798) was isolated from a SARS patient in Singapore General Hospital and was adapted to grow in Vero E6 cells. The strain HK39849 of SARS-CoV (GenBank accession number AY278491) was provided and used in experiments done in the University of Hong Kong. The strain Frankfurt 1 of SARS-CoV (AY291315) was provided and used in experiments in Swedish Institute for Infectious Disease Control. Recombinant vaccinia/T7 virus (vTF7-3) was grown and titrated on Vero E6 cells. Recombinant vaccinia viruses, rVV-L-SP and rVV-L-NP, expressing the S and N proteins of SARS-CoV, respectively, were obtained from Baxter Vaccines and grown in CV-1 cells.

2.3 Construction of plasmids.

2.3.1 Plasmids for expression of viral proteins in mammalian cells.

Viral RNA was extracted from a virus isolate from a Singapore patient (strain SIN2774, GenBank accession number AY283798) was extracted and used for amplification of the S gene by reverse transcription-PCR (RT-PCR) with specific primers. For expression of S under the control of a T7 promoter, the full-length S PCR products were digested with BamHI and StuI and ligated into BamHI/EcoRV-cut pKT0 to construct plasmid pKT-S. pKT0 is a modified form of pING14, in which a T7 RNA polymerase promoter sequence was inserted (Liu et al., 1991). pING14 is modified from pSP64T (Addgene). For characterization of the polyclonal antibodies, specific primers were designed to amplify S from nucleotide positions 21476 to 25171, 25066, 24934, 24415, 24157, and 23866 (Appendix 1). The six RT-PCR products were digested with BamHI and StuI and ligated to BamHI/EcoRV-cut pKT0, giving rise to plasmids pKT-SΔ11, pKT-SΔ12, pKT-SΔ13, pKT-SΔ14, pKT-SΔ15 and pKT-SΔ16, respectively.

For screening of monoclonal antibodies binding sites, specific primers were designed for two-round PCR to amplify S fragments with internal deletions of the S gene from nucleotide positions 3084 to 3150, 3151 to 3210, 3211 to 3270, 3271 to 3330, 3331 to 3390, 3391 to 3450, 3451 to 3510, and 3511 to 3576, respectively (Appendix 1). The eight PCR products were digested with EcoRV and SacI and ligated to EcoRV/SacI-cut pKT-S under the control of a T7 promoter, giving rise to plasmids pKT-SΔ50, pKT-SΔ51, pKT-SΔ52, pKT-SΔ53, pKT-SΔ54, pKT-SΔ55, pKT-SΔ56, and pKT-SΔ57, respectively.

For the construction of pXJ-8a, pXJ-8a-myc, pXJ-8b and pXJ-8b-myc, the ORF 8a and 8b were amplified by PCR using cDNA prepared from SARS-CoV infected cells as templates as previously described (Tan et al., 2004a). In order to construct a plasmid for expressing the 8ab protein found in animal SARS-CoVs, we used the cDNA template described above and sequential PCR to insert the 29-nt. Primers were designed based on the early phase human SARS-CoV isolate, GZ02, which has the 29-nt insertion in ORF8 (GenBank accession number AY390556). All sequences were confirmed by sequencing performed by the core facilities at the Institute of Molecular and Cell Biology, Singapore. The PCR amplicons containing ORF8a, ORF8b and ORF8ab were cloned into the mammalian expression vector pXJ3′HA as previously described (Tan et al., 2004a). In order to create a C terminus myc-tag, PCR methods were used to insert a myc-tag (AEEQKLISEEDLLRKH) into the 3′ of the ORFs. These proteins were tagged at their C termini to avoid interference with their post-translational processing as both 8a and 8ab are predicted to contain one signal peptide at their N termini (http://www.cbs.dtu.dk/services/SignalP). The C-terminal HA tag present in the pXJ3′HAvector is not expressed, as a stop codon was added before the HA tag coding sequences. The PCR amplicons containing E gene or E mutants were cloned into the mammalian expression vector pXJ3′HA as previously described (Tan et al., 2004a) and using specific primers (Appendix 3). All primers used in this study were purchased from Research Biolabs or Proligo, Singapore, and are listed in Appendix 1, 2 and 3.

2.3.2 Plasmids for expression of viral proteins in *Escherichia coli*

Five PCR fragments encoding the SΔ1, SΔ2, SΔ3, SΔ9, and SΔ10 fragments (Fig. 3.1) were obtained with the primers listed in Appendix 1. The PCR products were

digested by BamHI/XhoI and ligated into the BamHI/XhoI-cut pGEX4T1 vector (Amersham Pharmacia Biotech, Uppsala, Sweden) to obtain plasmids pGEX-SΔ1, pGEX-SΔ2, pGEX-SΔ3, pGEX-SΔ9, and pGEX-SΔ10 for the expression of glutathione S-transferase (GST) fusion proteins. The GST tag was located at the N terminus of the fusion protein. The cDNA encoding 8a (16–39aa) and 8b (27–84aa) were obtained by PCR methods (see Appendix 2 for primer sequences) and were cloned into pGEX-4T1 vector (Amersham Biosciences) to obtain plasmid pGEX-8aΔN15 and pGEX-8bΔN26 for the expression of GST-8aΔN15 and GST-8bΔN26 proteins.

2.4 Expression and purification of GST-fusion proteins

Plasmids pGEX-SΔ1, pGEX-SΔ2, pGEX-SΔ3, pGEX-SΔ9, pGEX-SΔ10, pGEX-8aΔN15 and pGEX-8bΔN26 were separately transformed into BL21 (DE3) cells (Stratagene, La Jolla, CA). A single colony from each plate was grown at 37 °C overnight in Luria-Bertani (LB) medium containing 100 μg per milliliters (ml) of ampicillin. Five ml of the resulting cultures was inoculated into 2 liters of LB medium containing 100 μg/ml ampicillin and the cultures were incubated in a shaker at 37 °C until the optical density at 600 nm reached 0.6. Expression of proteins was induced with 1 mM isopropyl-β-D-thiogalactopyranoside (IPTG). Cells were harvested 2 h after induction by centrifugation at 5,000 x *g* for 10 min at 4 °C. The cell pellets obtained were re-suspended in phosphate-buffered saline (PBS) containing 1 mM phenylmethylsulfonyl fluoride (PMSF) and 20 μg/ml of DNaseI and lysed by two passages through a French press. Lysates were centrifuged at 22,000 x *g* for 30 min. For GST fusion proteins SΔ1, SΔ2, SΔ3, SΔ9, and SΔ10, the insoluble proteins in the pellet were washed three times and re-suspended in PBS containing 1 % Triton X-100.

Proteins were separated in 10 % sodium dodecyl sulfate polyacrylamide gel electrophoresis (SDS-PAGE) gels. Gel strips containing GST fusion proteins were cut, and the proteins were eluted with a Mini Trans-Blot cell (Bio-Rad, Hercules, Calif.). The resulting fusion proteins were detected by western blotting with mouse anti-GST antibodies (Santa Cruz Biotechnology, Santa Cruz, Calif.), and their concentrations were estimated by comparison with bovine serum albumin (BSA) standards in a Coomassie brilliant blue R-250 (Bio-Rad)-stained SDS-PAGE gel. For GST-8aΔN15 and GST-8bΔN26, 10% glycerol was added to the purified proteins to prevent aggregation. As for GST-8bΔN26, 2 mM DTT and 1.5% sarkosyl were included in the lysis buffer and after sonication; Triton X-100 was added to a final concentration of 2 % before the protein was purified using GSH-sepharose beads.

2.5 Generation of rabbit polyclonal antibodies

One milligram of each of the purified GST fusion proteins SΔ1, SΔ2, SΔ3, SΔ9, SΔ10, 8aΔN15, 8bΔN26 and E was mixed with an equal volume of complete Freund's adjuvant (Sigma, St. Louis, Mo.) and used for the immunization of New Zealand White rabbits. Two rabbits were used to raise antibodies against each respective antigen. Three weeks after the initial immunization, the rabbits were given booster injections at 2-week intervals. Incomplete Freund's adjuvant (Sigma) was used for subsequent booster injections. Ten milliliters of blood was harvested from the rabbits each time after the 4th, 6th, 8th, 12th, 14th, and 16th injections. All procedures for the use of laboratory animals were done in accordance with the regulations and guidelines of Animal Research Ethics Committee.

2.6 Transient expression of SARS-CoV proteins in mammalian cells

Cells were plated on to 60 mm or 100 mm dish for transient transfection for immunoprecipitation, immunoblotting or radio-labeling experiments. For virus-infected cells, transient transfection was carried out at 1 h post-infection with Effectene transfection reagents (Qiagen, Valencia, Calif.) according to the manufacturer's protocol. For other cells, transient transfection was performed using Lipofectamine 2000 reagent (Invitrogen, Carlsbad, CA) according to manufacturer's protocol. Transient transfection was carried out in DMEM without FBS or penicillin, and the medium was replaced 6 h post-transfection with DMEM containing 10 % FBS, 0.1 mg/ml of streptomycin and 100 U/ml of penicillin.

2.7 SDS-PAGE

SDS-PAGE was performed according to Laemmli's method (Laemmli, 1970). Discontinuous SDS-PAGE with a stacking gel (pH 6.8, 0.125 M Tris-HCl, 0.1 % SDS and 3 % acrylamide) and separating gel (pH 8.8, 0.375 M Tris-HCl, 0.1 % SDS and 10-15 % acrylamide) were conducted in 1X SDS running buffer (25 mM Trizma Base, 250 mM glycine, 0.1 % SDS) at 20 milli-Amperes per gel.

2.8 Coomassie blue staining

Gel were stained in 0.25 % Coomassie Brilliant Blue R-250 (Biorad) staining solution containing 20 % methanol and 10 % acetic acid for 30 min, followed by a few washes using de-staining solution (20 % methanol, 10 % acetic acid) until the background of the gel is fully de-stained.

2.9 Immunoprecipitation (IP)

The cells were harvested at 16 h post-transfection and washed with PBS. Then, the cells were re-suspended in 150 µl of IP buffer (50 mM Tris pH 8, 150 mM NaCl, 0.5 % NP40, 0.5 % deoxycholic acid, 0.005 % SDS) supplemented with 0.5 % Triton X-114 and subjected to sonication for 45 min using an ultrasonic processor (Sonics, Newtown, CT, USA), followed by freeze–thawing for six times. 100 µl of the lysates were diluted with 100 µl of IP buffer and 5 µl of rabbit anti-myc polyclonal antibody (Santa Cruz Biotechnology) were added and the mixture was subjected to end-over-end mixing at 4 °C for 2 h. Protein A-agarose beads (Roche) were then added and the mixing continued for at least 4 h at 4 °C. Beads were washed three times with cold IP buffer and then 20 µl of Laemmli's SDS buffer were added and the samples boiled at 100 °C for 5 min to release the immuno-complexes. Samples were separated on SDS–PAGE and subjected to western blot analysis. In some cases, tricine gels (Biorad) were used instead for better resolution of low molecular weight proteins. Co-immunoprecipitation experiments with SARS-CoV-infected cells were performed in a similar manner.

2.10 Western blot analysis

Cell lysates were prepared with SDS loading buffer under reducing conditions (60 mM Tris-HCl (pH 6.8), 1 % SDS, 20 mM dithiothreitol, 10 % glycerol and 0.02 % bromophenol blue). Proteins were separated in 7.5%, 10 %, 12% or 15% SDS-PAGE gel and transferred to a nitrocellulose membrane. The membranes were blocked in 5 % non-fat milk in PBS with 0.05 % Tween-20 and probed with primary antibodies at 4 °C overnight. The membranes were incubated with horseradish peroxidase-conjugated secondary antibodies (Pierce, Rockford, Ill.) at a dilution of 1:2,000 for 2 h at room

temperature and developed with enhanced chemiluminescence reagent (Pierce). For loading control, membranes were stripped with stripping buffer [2 % SDS, 100 mM β-mercaptoethanol, 62.5 mM Tris-HCl (pH 6.8)] for 30 min at 65 °C and washed extensively with PBS containing Tween-20 before being re-probed with a mouse anti-actin antibody (Sigma) at a dilution of 1:3,000.

2.11 Indirect immunofluorescence microscopy

Vero E6, 293T and Cos7 cells grown on Permanox slide (Nalge Nunc International, Naperville, Ill.) were infected and/or transfected as described above. At 8 h post-transfection, cells were fixed with 4 % paraformaldehyde for 10 min at room temperature and blocked with PBS containing 1 % bovine serum albumin for 30 min. The cells were then incubated with primary antibody for 1.5 h and washed three times before incubated with fluorescein isothiocyanate-conjugated (FITC) secondary antibody (1:200; Santa Cruz Biotechnology) for 1 h. All incubations and washes were performed at room temperature. Slides were mounted with fluorescence mounting medium (Dako Cytomation) and analyzed on an Axio-Vision fluorescence light microscope (Carl Zeiss Vision GmbH, Hallbergmoss, Germany).

2.12 Radioactive pulse-chase protein labeling

Cos7 cells were infected with vaccinia virus vTF7-3 and transfected with pKT-S or plasmids expressing the S C-terminal deletion mutant proteins (pKT-SΔ11, pKT-SΔ12, pKT-SΔ13, pKT-SΔ14, pKTSΔ15, and pKT-SΔ16) as described above. Cells were mock transfected with pKT0 as controls. At 3 h post-transfection, the cells were starved for 30 min with methionine-cysteine (Met-Cys)-free medium before being labeled with [^{35}S]Met-Cys for 1 h and chased with 4 mM cold Met-Cys for 2 h. For the time course

experiment, the chase periods before harvesting the cells were 0, 1/2, 1, 2, 4, and 6 h. For virus-infected Vero E6 cells, cells were infected at a MOI of 5, radiolabeled at 5 h post-infection for 1 h, and chased for 3 h. Cells were lysed with lysis buffer containing 150 mM NaCl, 20 mM Tris (pH 7.5), 1 % NP-40, 5 mM EDTA, 1 mM phenylmethylsulfonyl fluoride and centrifuged at 16,000 x *g* for 10 min.

A portion of the supernatant (300 µl) was incubated for 1/2 h with 5 µl of antiserum, followed by a 1 h incubation with protein A-Sepharose beads (Roche). The beads were washed three times with lysis buffer. Twenty microliters (µl) of 1X SDS loading buffer was added to the beads and boiled for 5 min at 100 °C. For the EndoH treatment, the beads were re-suspended in EndoH buffer provided by the manufacturer and the immunoprecipitated proteins were eluted by boiling for 5 min. Samples were treated with EndoH enzyme (Roche Diagnostics) at 37 °C for 2 h. For the control, samples were treated in the same manner except no enzyme was added. All the samples were separated in a 7.5 % SDS-PAGE gel and visualized by autoradiography.

Vero E6 cells grown in 60 mm dishes were infected with recombinant vaccinia virus carrying the S gene (rVV-L-S), at a MOI of 0.1. For mock-infected cells, a recombinant vaccinia virus carrying the N gene (rVV-L-N) was used. At 1 h post-infection, the cells were treated with 400 µM of SNAP (Sigma, St. Louis, Mo.), 400 µM N-acetyl-penicillamine (NAP; Sigma), 400 µM of SIN-1 (Sigma, St. Louis, Mo) or 400 µM of SIN-1 and 400 µM of MnTBAP (Calbiochem). Treatments were repeated 4 times with 2-h intervals. At 24 h post-infection, cells were labeled with 400 µCi of [^{3}H]-palmitic acid (Perkin Elmer, USA) for 2 h or starved with methionine-cysteine (Met-Cys)-free medium for 30 min before being labeled with 22 µCi of [^{35}S]-methionine-

cysteine for 2 h. The labeled cells were washed 3 times with cold PBS and lysed in 1 ml TES lysis buffer [20 mM Tris–HCl (pH 7.5), 100 mM NaCl, 1 mM EDTA, 1 % Triton X-100 and 2 mM PMSF]. Cell debris was removed from the lysates by centrifugation at 13,000 rpm for 10 min.

Immunoprecipitation was carried out by adding rabbit anti-SΔ10 antibody to the lysates and rotating at 4 °C for 1 h, followed by overnight incubation with protein-A Sepharose beads (Roche Diagnostics). The beads were washed 3 times with lysis buffer and boiled in 20 µl of 2X Laemmli's SDS loading buffer. Samples were separated in a 7.5 % SDS-PAGE gel, fixed for 30 min using fixing solution (10 % acetic acid, 45 % methanol), and treated with Amplify Fluorographic Reagent (Amersham Biosciences) according to protocol. Visualization was done by autoradiography.

2.13 Virus neutralization assay

To determine the neutralizing activities of the rabbit anti-sera, we performed a neutralization assay using a 96-well plate. Vero E6 cells (2×10^4) were grown in 200 µl of medium in each well of the 96-well plates and incubated at 37 °C. Serial dilutions of rabbit sera with the medium in ratios of 1:10 to 1:1,280 were prepared. Diluted rabbit anti-sera (0.1 ml) were mixed with 0.1 ml of SARS-CoV at 200 (or 1,000) 50 % tissue culture infective doses ($TCID_{50}$) for 1 h at 37 °C before being added into the respective wells. At each dilution, antiserum and virus mixtures were added to eight wells. The 96-well plate was incubated in a CO_2 incubator for 4 days to observe the cytopathic effect. The ratios of infected wells to uninfected wells were determined under microscopy.

The titers of the neutralizing antibodies were calculated by the Reed-Muench method (Reed and Muench, 1938) and expressed as $TCID_{50}$ per 0.1 ml. All experiments

were carried out in duplicate. Neutralization assays for monoclonal antibodies were performed in a 96-well plate format. Complement proteins in ascitic fluids were inactivated at 56 °C for 30 min before use. Monoclonal antibodies (mAb) were first diluted 10 times, and then serial two-fold dilutions were prepared in maintenance medium. One set of antibody dilutions was added to cells to detect the toxicity of the ascitic fluids. The diluted antibodies were incubated with 10 $TCID_{50}$ of SARS-CoV in an equal volume of medium for 1 h at 37 °C before being added into the respective wells containing 5 x 10^4 Vero E6 cells per well. At each dilution, the mixtures of antibody and virus were added to four wells and incubated with Vero E6 cells. After 3 days, cytopathic effect (CPE) developed in all the negative controls and the back titration wells. The titers of the neutralizing antibodies were determined by applying the Ka¨rber formula: Negative log of the lowest dilution - [(sum of percentage positive/100) - 0.5] x log interval. All experiments were carried out in triplicate, and the neutralizing titers were expressed as the reciprocal of the highest antibody dilution where the viral CPE in 50 % of the wells was neutralized.

2.14 Generation of monoclonal antibodies

GST-tagged and His-tagged fusion proteins, GST-SΔ10 and SΔ10-His, were expressed in *E. coli* and purified as described above. They were used for immunization of mice and screening of hybridomas secreting S-specific mAbs, respectively. Each of the 6-week-old female BALB/c mice was given primary injection (intra-peritoneal) with 100 μg of the protein GST-SΔ10 emulsified in complete Freund's adjuvant (Sigma-Aldrich Inc.). Two weeks later, each mouse was given one secondary booster injection using the

same amount of antigen mixed with incomplete Freund's adjuvant (Sigma-Aldrich Inc.). Booster injections were administered to each mouse at 1-week intervals three more times.

S-specific antibodies in the serum of immunized mice were tested by Western blot assays prior to hybridoma fusion. The spleen was excised, and hybridoma fusion was performed using the Clonal Cell-HY Complete kit (StemCell Technologies, Canada) according to the manufacturer's instructions. All procedures on the use of laboratory animals were done in accordance with the regulations and guidelines of the National Advisory Committee for Laboratory Animal Research, Singapore. MAbs in supernatants of hybridoma cultures were screened in an enzyme-linked immuno-sorbent assay (ELISA). Briefly, 96-well ELISA plates were coated with the protein SΔ10-His or bovine serum albumin (50 ng/well) in 0.1 M sodium carbonate buffer (pH 9.6) overnight at 4 °C. The plates were blocked with PBS containing 5 % FBS and 0.05 % Tween-20 for 1 h at 37 °C and washed three times with PBS containing 0.05 % Tween-20 and three times with PBS. Supernatants of hybridoma cultures (50 µl/well) were incubated for 1 h at 37 °C. After washing, goat anti-mouse immunoglobulin G (IgG)-horse radish peroxidase (HRP) antibodies (200 µg/ml, Santa Cruz, Calif.) at a dilution of 1:2,500 were added to the ELISA plates, which were then incubated for 1 h at 37 °C. After washing three times with PBS, substrate TMB (Pierce Biotechnology) was added and the reaction was stopped 15 min later by adding an equal volume of 1 M H_2SO_4. Optical density was read at 450 nm. Mouse immune and pre-immune sera were used as positive and negative controls. Samples giving a value of optical density that is equal or greater than 3 standard deviations above the mean value of bovine serum albumin controls were considered positive.

2.15 Purification of monoclonal antibodies

A 1ml HiTrap Protein G HP beads column (GE Healthcare) is pre-washed using 10-20 ml of 20 mM sodium phosphate buffer, pH 7.0 at a constant flow-rate of 1 ml/min using a peristaltic pump. Five milliliters of ascites fluids is mixed with equal volume of 40 mM sodium phosphate buffer and passed through a 0.45 µm filter. The filtered ascites fluids were ran at the same flow-rate through the column. Three washes were performed using the 20mM sodium phosphate buffer. Elution buffer (0.1 M glycine-HCl, pH 2.7) was run through the column at a flow-rate of 1 ml/min and the flow-through was collected in 1.5ml eppendorf tubes containing 20µl of neutralization buffer (1 M Tris-HCl, pH 9.0). The protein concentration in each tube was determined against BSA standards at 0.595 nm using a spectrophotometer.

2.16 Fluorescence activated cell sorting (FACS) analysis.

293T cells infected with rVV-L-SP expressing the S proteins (293T-SP) and stable cell line CHO-ACE2 were first detached with 0.04 % EDTA, washed once with PBS, and incubated with rabbit anti-SΔ10 serum diluted 1:40, mAbs or goat anti-ACE2 IgG primary antibodies (100 µg/ml; Santa Cruz) diluted 1:20 in PBS containing 1 % fetal bovine serum and 0.1 % sodium azide for 1 h at 4 °C. Cells in tubes were placed on a roller to ensure constant mixing under non-permeabilizing conditions. The cells were washed and subsequently incubated with FITC-labeled goat anti-rabbit IgG (200 µg/ml; Santa Cruz), rabbit anti-goat IgG secondary antibodies (200 µg/ml; Santa Cruz), or goat anti-mouse IgG secondary antibodies (200 µg/ml; Santa Cruz) at a 1:20 dilution for 1 h at 4 °C and placed on a roller to ensure constant mixing. Immediately after washing, cells

were measured for FITC fluorescence using a Becton Dickinson FACScan flow cytometer and results were analyzed using Cell-quest Pro software.

2.17 Cell-cell membrane fusion assay.

The 293T cells were transfected with plasmid pEGFP-N1 (Clontech Laboratories Inc, Pala Alto, Calif.), which encodes GFP, using Effectene transfection reagent (Qiagen) according to the manufacturer's instructions. After 24 h, medium was removed and the cells (293T-GFP) were washed twice with room temperature PBS before the infection medium was added. 293T-GFP cells were infected with recombinant vaccinia virus expressing the SARS-CoV spike protein (rVV-L-SP) at an MOI of 0.1. After 1 h of adsorption, the infection medium was removed and subsequently replaced with complete DMEM for 24 h for S expression. Infected 293T-GFP (293T-SP) and CHO-ACE2 were first detached with 0.04 % EDTA, washed once with PBS, and re-suspended in DMEM containing 0.25 mg/ml porcine trypsin (JRH Biosciences Inc.) and 5.6% fetal bovine serum. 293T-SP and CHO-ACE2 cells were mixed at a 1:1 ratio per well (up to 1 X 10^6 cells) in a 12-well plate (Nunc). Syncytium formation was observed 6 h after mixing of cells. Serially diluted rabbit anti-SΔ10 serum (at a dilution factor of 1:40, 1:80, 1:160), pre-immune serum (at a dilution factor of 1:40), or serially diluted mAbs (at dilution factor of 1:40, 1:80, 1:160) were pre-incubated with 293T-SP cells at 37 °C for 10 min. Inhibition of syncytium formation could be observed from 6 h onwards.

Five micrographs were taken randomly in a 10X magnified field of view on an Olympus UV microscope CKX41 equipped with an Olympus Camedia C-5060 digital camera. Syncytium with a size equal to or greater than 10 cells was considered a true fusion, and the average numbers of syncytia were scored. The total number (T) of

possible syncytia without cell-cell membrane fusion inhibition was derived from fusion experiment with non-SARS-CoV-related mouse ascitic fluid (anti-dengue mAb serotype I 6F8-3) or rabbit pre-immune serum. The number (I) of syncytia with inhibition effect was derived from fusion experiments in the presence of specific antibodies of interest. Percentage inhibition of cell-cell membrane fusion was expressed as (T-I)/T.

2.18 Generation of escape SARS-CoV

Using 100 $TCID_{50}$ of SARS-CoV for infection in the presence of different concentrations of mAbs, we tested the supernatant of the infected cells for the extent of reduction of virus titers in a 96-well plate. The concentration of mAbs that can reduce the virus titers by about 4 logarithms (log) is ideal as the selective pressure for the generation of virus escape mutants. Quadriplicate experiments were performed. The concentration for the selection of virus escape mutants for mAb1A9 and mAb1G10 is determined at 0.25mg/ml and 0.1mg/ml respectively. Serial dilution ranging from 10^{-1} to 10^{-8} of SARS-CoV strain HKU-39849 were incubated in the presence of a constant amount of mAb1A9 (0.25mg/ml) and mAb1G10 (0.1mg/ml), for 1 h at 37 °C and 5 % CO_2. The virus-mAb mixture is then incubated with Vero E6 cells in a 96-well plate for 1 h at 37 °C and 5 % CO_2, then the virus-mAb mixture was removed and the cells were washed twice with medium. Finally, the cells were incubated for 2 days in the presence of the above concentration of the respective mAb in 0.5 ml medium. The highest dilution, at which the cells exhibit cytopathic effect, will have the supernatant harvested for further selection. The supernatant, containing potential escape viruses, will be passaged three times in Vero E6 cells at the above mAb selection concentration.

The final virus sample will be added to Vero E6 cells in a 6-well plate and incubated for 1 h at 37 °C and 5 % CO_2, before the wells are overlaid with agarose containing the above mAb selection concentration and incubated for 3-5 days at 37 °C and 5 % CO_2. Individual escape virus plaques were picked using a Pasteur pipette and freeze-thawed once, and amplified in Vero E6 cells. Neutralization test were then performed on all the virus clones to confirm that they can escape the mAb inhibition at the previous neutralizing concentration.

2.19 TOPO cloning and sequencing

Viral RNA of all escape virus clones was isolated using the Viral RNeasy kit (Qiagen) and converted into cDNA by standard RT-PCR. Subsequently, the cDNA was amplified by PCR using specific primers targeting the S gene to generate a long fragment (aa 1 to 1003) and a short fragment (aa 969 to 1255). These gene fragments were cloned into TOPO vectors (Invitrogen) and used for sequencing.

2.20 Pseudovirus luciferase assay

To produce HIV pseudovirus bearing the SARS-CoV S protein, 9 μg of HIV-1 luciferase reporter vector pNL4.3.Luc.R-E- (HIV-luc) and 4.5 μg of SARS-CoV S protein expression plasmid (pXJ3′-S-HA) were co-transfected into 293T cells in a 100-mm dish using Lipofectamine2000 reagent (Invitrogen) following manufacturer's instructions. For the negative control, the cells were transfected with pNL4-3.Luc.R-E- alone. The construction of the plasmids has been described previously (Connor et al., 1995; He et al., 1995; Tan et al., 2004a). The virus-containing medium was harvested after 72 h of incubation, and centrifuged at 2000 rpm for 5 min to remove any cell debris.

Virus in the supernatant was subsequently concentrated through a 20% sucrose cushion for 3 h at 30,000 rpm and 4 °C by using an SW41 rotor, and subsequently re-suspended in DMEM. In order to normalize the amount of pseudovirus used, 10 µl of each sample was used to measure p24 content using a p24 ELISA kit (Perkin Elmer Life Sciences, Boston, MA), according to the manufacturer's protocol. Absorbance readings were made at 492 nm in a plate reader (Tecan) and sample concentrations were determined from a standard graph. Appropriate volumes corresponding to 16 ng of pseudovirus were then used to infect GFP, GFP-8b or CHO-ACE2 stable cell lines (Chou et al., 2006). At 24 hpi, the cells were washed once with PBS. Cells were harvested using 0.5ml trypsin and washed twice using PBS. Cell pellet was lysed using the Promega lysis buffer and luciferase activity was determined using a luciferase assay kit, following manufacturer's instructions (Promega, Madison, WI). Luciferase readings were measured using a Veritus microplate luminometer (Turner Biosystems, CA).

2.21 P24 ELISA assay

HIV pseudovirus bearing the SARS-S protein was produced as described in the pseudovirus entry assay (see above). Virus containing medium was harvested after 24 h of incubation and centrifuged at 3000 rpm for 5 min to remove any cell debris. 10 µl of the medium were diluted 20X using DMEM and used to measure virus concentration using a P24 ELISA kit (Perkin Elmer), according to the manufacturer's protocol. Virus concentration was determined from a standard graph, and 80 ng of virus was used for infection of CHO-ACE2 cells. CHO-ACE2 cells were pre-incubated in DMEM with 1 % BSA at 4 °C for 1 h prior to infection at 4 °C for 2 h. After infection, the cells were washed 4X using PBS with 1 % BSA and harvested in DMEM, freeze-thawed six times

and sonicated for 2 min with 20 sec intervals. Samples were centrifuged at 13,000 rpm to remove any cell debris and 200 μl of supernatant was used to determine P24 content using the P24 ELISA kit. The concentration of bound virus was then determined using the standard graph.

2.22 Culturing of stable cell lines

Vero E6 cells were transfected with 10 μg of pEGFP-8b by electroporation and plated onto a 100 mm dish. Medium containing 2 mg/ml G418 (Invitrogen) was added 24 h post-transfection and cells were cultured for 3 to 5 days. Colonies of cells were picked and transferred into individual wells in a flat-bottomed 96-well plate and cultured for 5 days before transferring into a 24-well plate. After 3 to 5 days, cells were split into two 60 mm dishes for screening and freezing down. Positive clones were re-thawed and grown in a T75 flask for experiments.

2.23 SARS-CoV infection and titration

Vero E6 cells, stably expressing GFP-8b and GFP, grown in 24-well plates were infected with SARS-CoV (Frankfurt strain 1) at M.O.I. of 0.1. At 1 hpi, the cells were washed twice and fresh medium was added. After 24 hpi, the virus supernatant was harvested and titration of progeny virus was carried out on a 96-well plate containing fresh Vero E6 cells as described previously (Akerstrom et al., 2005). At 48 hpi, the amount of virus, determined as the 50 % tissue culture infectious dose ($TCID_{50}$), was calculated from the cytopathic effect induced in cell culture by serial ten-fold dilutions of the harvested virus.

2.24 Northern blot analysis

Total RNA from 293T cells transfected as described above was extracted using the RNeasy mini kit (Qiagen) by following the protocol supplied by the manufacturer. The final RNA pellet was re-suspended in diethyl pyrocarbonate-treated water and quantified by measuring absorbance at 260 nm. 15 µg of total RNA was separated on 1.2 % denaturing agarose-formaldehyde gel (containing ethidium bromide), transferred overnight in 1X saline-sodium citrate (SSC) buffer to nylon membranes Hybond N+ (Amersham Biosciences). The blot was dried at room temperature for 30 min and baked at 80 °C for 30 min. The blot was then pre-hybridized with salmon testes DNA (Sigma) in hybridization buffer containing 6X SSC, 2X Denhardt's Reagent and 0.1 % SDS for 2 h. The E gene cDNA fragment was cloned into the TA cloning vector pCRII-TOPO (Invitrogen) and linearized with Hind III restriction enzyme. Probes were generated from the linearized plasmid using T7 polymerase from the DIG RNA labeling kit (Roche). Hybridization was performed overnight at 68 °C with the DIG-labeled probe in the hybridization buffer.

After hybridization, the blot was washed once for 20 min in 1X SSC buffer with 0.1 % SDS followed by 3 washes, each 30 min, in 0.2× SSC with 0.1 % SDS. All washes were performed at room temperature. The blot was then probed with alkaline phosphatase-conjugated anti-digoxigenin antibody and developed using chemiluminescence substrate CSPD (DIG luminescent detection kit; Roche). This was performed according to the manufacturer's protocol and the results were obtained by autoradiography. RNA ladders from Fermentas Life Sciences (Ontario, Canada) were used for size determination of mRNA.

2.25 Reverse transcription reaction

Total RNA were extracted from cells harvested from 60 mm dishes using the RNAeasy Mini Kit (Qiangen) using the manufacturer's protocol. The concentrations of the RNAs were measured at 260 nm using a Nanodrop spectrophotometer. 5 µg of total RNAs were mixed with 10 µM oligo-dTs or specific primers and 1 µl of RNase inhibitor (40 U/ml), followed by incubation at 65 °C for 10 min. For synthesizing cDNAs, 1 µl of dNTPs (New England Biolabs) and Reverse Transcriptase (Invitrogen) were added to the above mixture and incubated at 42 °C for 1 h.

2.26 Microarray analysis

Human genome-wide gene expression was examined with the GeneChip Human Genome U133 Plus 2.0 Array (Affymetrix Inc., Santa Clara, CA), which is composed of more than 54,000 oligonucleotide probe sets interrogating approximately 47,000 unique transcripts, including 38,500 well-characterized human genes. GeneChip hybridization, data acquisition and analysis were performed according to the standard protocols available from Affymetrix. In brief, total RNAs of the stable cell lines (GFP-8b, GFP-8b* and GFP) were extracted using the RNeasy mini kit (Qiagen, Valencia, CA). Single stranded cDNA was synthesized from 10 µg of total RNA with the SuperScript II Reverse Transciptase (Invitrogen). By using the Affymetrix-defined comparison mathematical algorithms, the difference in mRNA levels between the GFP-8b stable cell line and another GFP-8b stable clone, named as GFP-8b*, was calculated. For genes that showed at least 2-fold higher or lower expression in GFP-8b cells than GFP-8b* cells, real-time quantitative PCR was performed.

2.27 Real-time quantitative PCR

Real-Time PCR was performed from reverse-transcribed cDNA samples of GFP-8b, GFP-8b* and GFP cells. Probes and primers for the 16 genes that were identified to be up-regulated or down-regulated by GFP-8b (Table 1) were obtained from Applied Biosystems. Glyceraldehyde-3-phosphate dehydrogenase (GAPDH) probe and primers were obtained from Applied Biosystems to be used as loading control. Real-time PCR was performed with the ABI 7500 Fast Real-Time PCR system. Quantification of the PCR signals was performed by normalizing the cycle threshold value of each sample in triplicate with the cycle threshold values of the GAPDH reference gene.

CHAPTER 3: NEUTRALIZING ANTIBODIES AGAINST SARS-CoV

3.1 Characterization of rabbit polyclonal antibodies against SARS-CoV S

3.1.1 Generation of rabbit polyclonal antibodies against different regions of S

To determine the regions on SARS-CoV S that can elicit strong neutralizing antibodies, we expressed five fragments of S (SΔ1, SΔ2, SΔ3, SΔ9, and SΔ10) encompassing the entire S ecto-domain in *Escherichia coli* and used the purified antigens to generate polyclonal antibodies (Fig. 3.1). Enzyme cleavage studies have shown that SARS-CoV S is cleaved by trypsin into the S1 and S2 domains at residue R667 while cathepsin L cleaves the S1-S2 junction at residue T678 (Bosch et al., 2008b; Li et al., 2006) (Fig. 3.1).

Of the five fragments of S that we have designed, two fragments spanned the S1 domain (SΔ1 and SΔ3), two fragments spanned the S2 domain (SΔ9 and SΔ10), and one fragment contained a portion of both S1 and S2 domains (SΔ2) (Fig. 3.1). Of note, SΔ3 contains the RBD while SΔ9 and SΔ10 include the HR1 and HR2 regions, respectively. The RBD has been shown to be essential for virus attachment to host cells via its interaction with the ACE2 receptor while the highly conserved HR1 and HR2 domains were shown to be involved in the membrane fusion process (Liu et al., 2004; Wong et al., 2004).

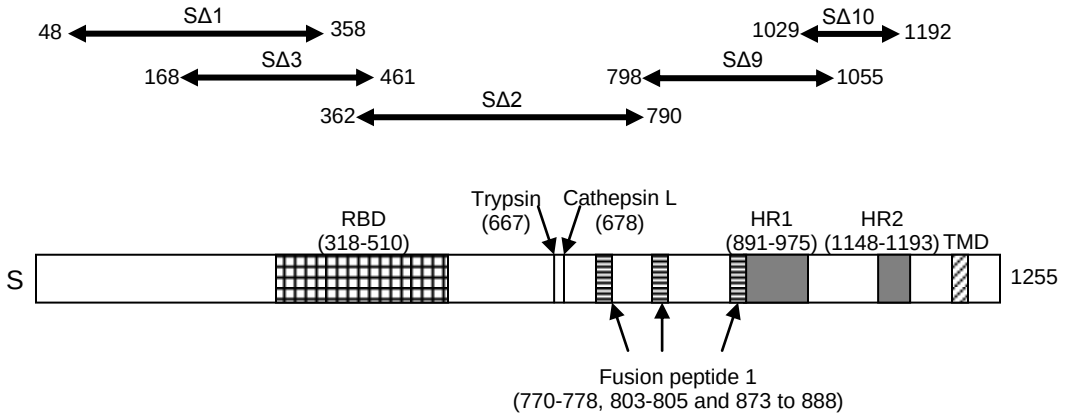

Fig. 3.1: Schematic diagram showing the different regions of S encoded by the plasmids used in this study. Full-length S with the RBD, heptad repeat regions HR1 (aa 891 to 975), HR2 (aa 1148 to 1193) and several important sites are shown. Regions representing the five bacterial-expressed proteins (SΔ1, SΔ2, SΔ3, SΔ9, and SΔ10) used to generate the antibodies are indicated by the arrows on top. The numbers at each end of the arrows represent the positions of the amino acid residues in the S.

3.1.2 Detection of denatured form of SARS-CoV S by Western blotting.

Western blot analysis was used to determine the sensitivity and specificity of the antibodies for full-length S that was expressed in mammalian Cos7 cells. As predicted, anti-S antibodies in the serum of a patient (P6) who has recovered from SARS-CoV infection could detect both the 140 kDa unglycosylated form and the 200 kDa glycosylated form of full-length S expressed in transfected Cos7 cells (Fig. 3.2, lane 1). These are specific bands for S, as they were not detected in mock-transfected cells (Fig. 3.2, lane 2) or when probed using serum from a healthy donor (Fig. 3.2, lanes 13 and 14). We observed similar results with the antibodies that we raised against the five S fusion proteins (Fig. 3.2, lanes 3, 5, 7, 9, and 11). No specific bands were detected in mock-transfected cells (Fig. 3.2, lanes 4, 6, 8, 10, and 12) and by pre-immune sera from the same rabbits (Fig. 3.2, lanes 15 to 24). The results indicate that all the antibodies

generated against the five S fragments could bind specifically to the linearized full-length S under denaturing conditions.

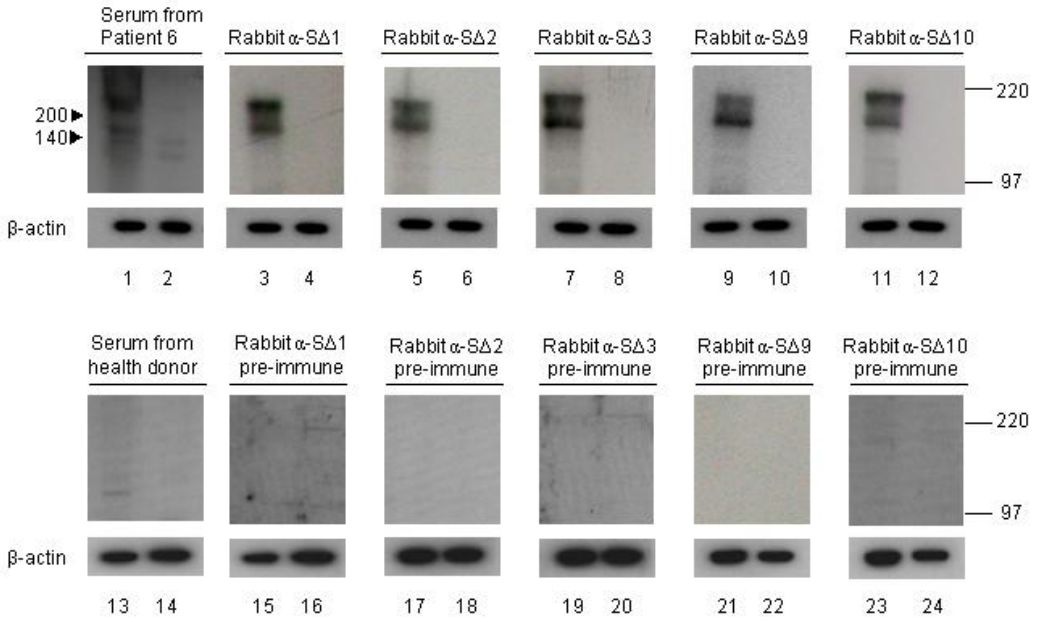

Fig. 3.2: Western blot analysis for the detection of SARS-CoV S. Cos7 cells were transfected with plasmid pKT-S (lanes 1, 3, 5, 7, 9, 11, 13, 15, 17, 19, 21, and 23) or empty vector as a negative control (lanes 2, 4, 6, 8, 10, 12, 14, 16, 18, 20, 22, and 24). Cell lysates were separated in 10% SDS-PAGE gel. Western blotting was performed with the anti-sera, pre-immune sera, and control serum indicated at the top of each gel. Arrowheads (left) indicate molecular masses (in kilodaltons) of specific S proteins. Membranes were re-probed with mouse anti-actin to be used as the loading control. High-range Rainbow molecular weight markers (right; Amersham) were used. α, anti.

3.1.3 Detection of the recombinant form of S in transfected cells

Immuno-precipitation experiments were carried out using the various antibodies to determine the specificity of the antibodies for their respective target regions in the S protein. Lysates of Cos7 cells infected with vTF7-3 vaccinia virus and transfected with plasmids encoding S or S mutant proteins with C-terminal deletions (pKT-SΔ11, pKT-SΔ12, pKT-SΔ13, pKT-SΔ14, pKTSΔ15, and pKT-SΔ16) (Fig. 3.3) were immuno-precipitated with P6 serum and the five generated polyclonal antibodies (Rabbit α-SΔ1,

α-SΔ2, α-SΔ3, α-SΔ9, and α-SΔ10). The SARS-CoV full-length S protein and all the recombinant S proteins with C-terminal deletions were immunoprecipitated by the P6 serum, rabbit α-SΔ1, α-SΔ2 and α-SΔ3 (Fig. 3.3A-C, F). Antibodies targeting SΔ9 only detected full-length S and SΔ11 to SΔ15 proteins but not SΔ16 as it does not comprise of the SΔ9 region (Fig. 3.3D). Antibodies targeting SΔ10 only detected the proteins expressed by pKT-S and pKT-SΔ11 to pKT-SΔ13 (Fig. 3.3E). The regions expressed by pKT-SΔ14 to pKT-SΔ16 do not contain the SΔ10 region and thus, rabbit α-SΔ10 did not detect any bands in these lanes, indicating that these antibodies are highly specific to their target regions.

As expected, the sizes of the S mutants decreased from SΔ11 to SΔ16, as more amino acid residues were removed from the C terminus. Two forms of S (~200 and ~210 kDa) were detected in the lysates of cells transfected with the full-length S construct (Fig. 3.3A-F, lane 1), representing the Endoglycosidase H (EndoH)-sensitive form and the matured EndoH-resistant form of the full-length glycosylated S, respectively (See Fig. 3.4B, lanes 9 and 10). The 140 kDa unglycosylated form of S (Fig. 3.2, lanes 1, 3, 5, 7, 9 and 11) was not detected by immunoprecipitation with any of the antibodies used. The results suggest that either the 140 kDa unglycosylated S protein was not recognized by these antibodies under non-denaturing conditions or it did not accumulate in the pulse-chase experiments. Taken together, the immunoprecipitation results suggest that the protein possesses an epitope(s) which was retained in the non-denaturing conditions that can be recognized by the antibodies raised against all the five fusion proteins.

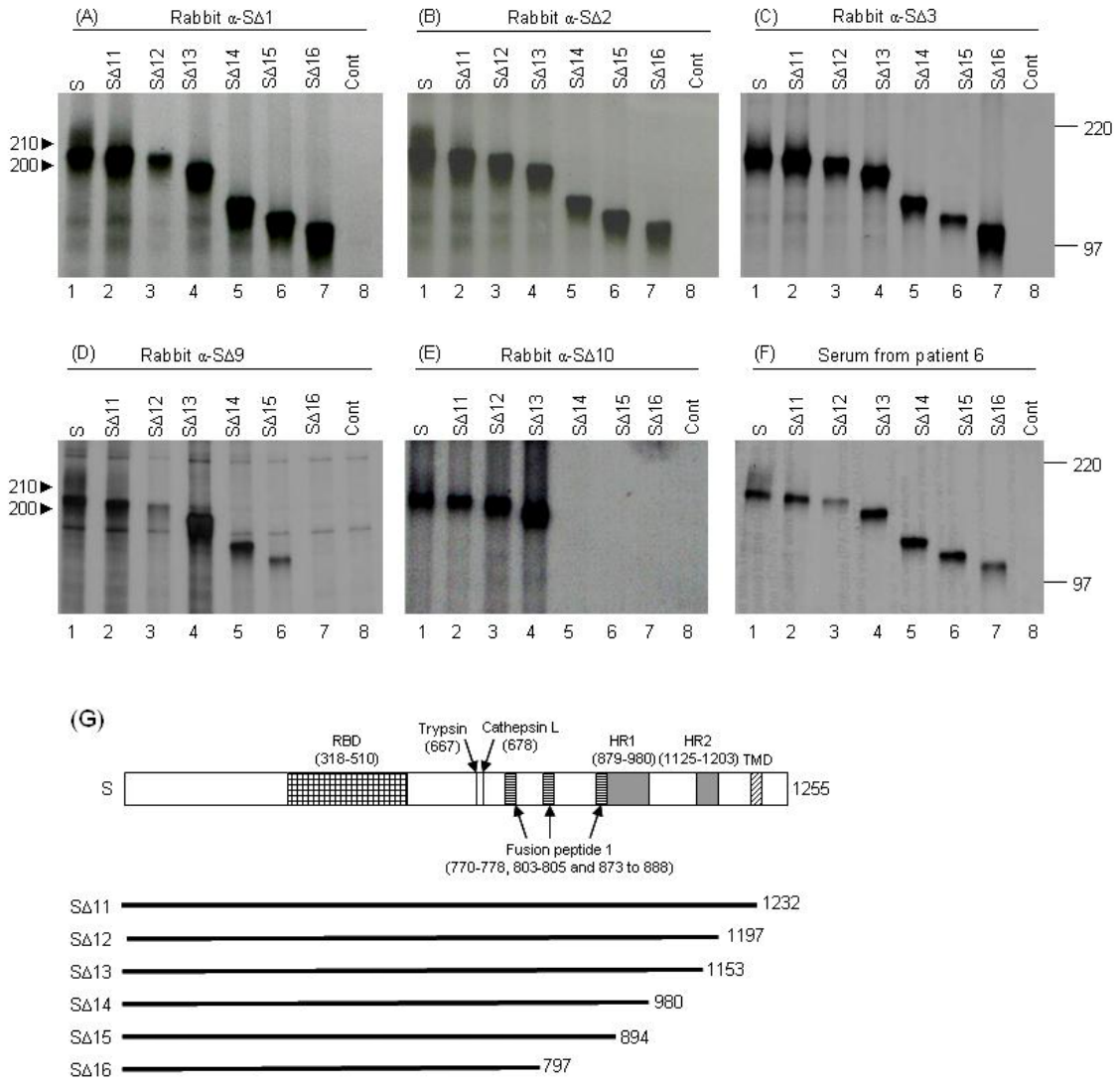

Fig. 3.3: Radio-labeled immunoprecipitation. Cos7 cells were transfected with plasmids expressing full-length S and the C-terminal truncated S proteins, SΔ11, SΔ12, SΔ13, SΔ14, SΔ15, and SΔ16 (lanes 1, 2, 3, 4, 5, 6, and 7) or with a plasmid without an insert as a negative control (lanes 8). ^{35}S-labeled S proteins were immunoprecipitated with the antibodies indicated (top of each autoradiograph) and then separated in 7.5% SDS-PAGE gels. Arrowheads (left), molecular masses (in kilodaltons) of specific S proteins. High range Rainbow molecular weight markers (right; Amersham) were used. α, anti.

3.1.4 Detection of the native S protein in virus-infected cells and cultured media

Using immunoprecipitation, these polyclonal antibodies were further analyzed for their ability to bind native S synthesized in SARS-CoV infected cells that were released as components of the virions into the cultured medium. As shown in Fig. 3.4A, all generated rabbit α-S antibodies can detect S in both cell lysates (top, lanes 2, 6, and 10; bottom, lanes 2 and 6) and media (top, lanes 4, 8, and 12; bottom, lanes 4 and 8). S was not detected in lysates and media of mock-infected cells (lanes 1, 3, 5, 7, 9, and 11) or in infected cells and medium when probed with rabbit pre-immune serum for detection (lane 9-12). S detected in the media had a slightly larger size than S detected in cell lysates, suggesting that the glycosylated S protein had undergone maturation from the 200 kDa to the 210 kDa forms in the cells and that only the fully matured form of S (210 kDa) was assembled into the virion. These results confirmed that all the generated antibodies are specific for the native S in virus-infected cells and virus particles.

3.1.5 Maturation of S from EndoH-sensitive to EndoH-resistant form

Two bands specific for S were observed in the immunoprecipitation experiments (Fig. 3.3A-F, lanes 1). It is hypothesized that the 210 kDa band represents the mature glycosylated S protein while the 200 kDa band is the immature glycosylated S protein. To investigate the maturation of S, we carried out a pulse-chase labeling experiment. Cos7 cells infected with vaccinia virus vTF7-3 and transfected with pKT-S were radio-labeled with [^{35}S] Met-Cys and chased with cold Met-Cys for 0.5, 1, 2, 4, and 6 h, followed by immunoprecipitation with rabbit anti-SΔ10.

The results showed a gradual increase in the amount of 210 kDa protein accompanied by a gradual decrease in the amount of 200 kDa protein (Fig. 3.4B, lanes 1

to 8). The yield of 200 and 210 kDa proteins decreased after chasing for 4 h due to cell death caused by vTF7.3 infection but the ratio of 210 to 200 kDa protein increased. Immunoprecipitation was performed with all the other anti-sera (rabbit α-SΔ1, α-SΔ2, α-SΔ3, and α-SΔ9), and the same results were obtained (data not shown). To provide more evidence to support our findings, an EndoH treatment experiment was carried out to determine whether the bands were sensitive to EndoH. The radio-labeled cell lysates described above were immunoprecipitated with rabbit α-SΔ10 and treated (or mock treated) with EndoH enzyme. Results showed that the 210 kDa protein was EndoH-resistant while the 200 kDa protein was EndoH-sensitive (Fig. 3.4B, lanes 9 and 10). Hence, the results demonstrated the maturation of S from the 200 kDa EndoH-sensitive to the 210 kDa EndoH-resistant forms. Other antibodies (rabbit α-SΔ1, α-SΔ2, α-SΔ3, and α-SΔ9) could also recognize both the immature and mature forms of the S glycoprotein (data not shown).

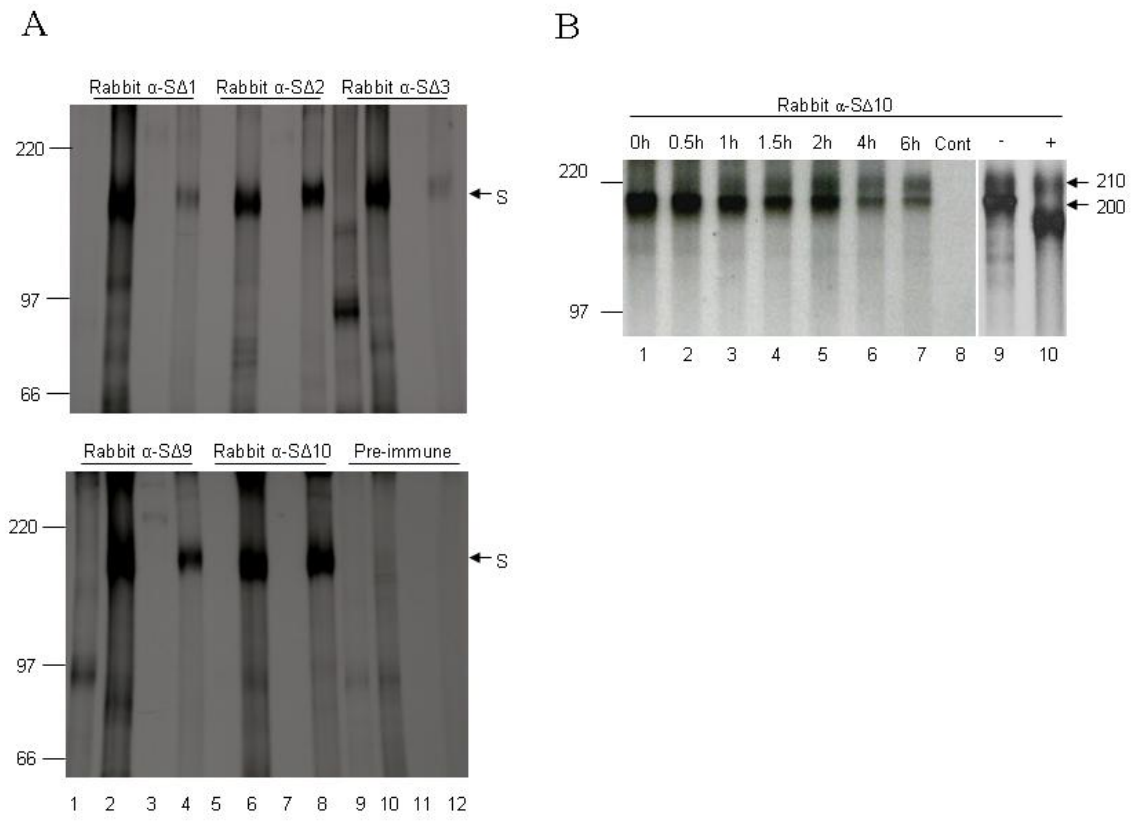

Fig. 3.4: Detection of the different forms of S in virus-infected cells and virions. (A) Immunoprecipitation of S in cell lysate and media of virus-infected Vero E6 cells. Vero E6 cells in 60 mm dishes were infected (lanes 2, 4, 6, 8, 10, and 12) with SARS-CoV at a MOI of 5 or mock infected (lanes 1, 3, 5, 7, 9, and 11). Cells were radio-labeled 5 h post-infection with [^{35}S]Met-Cys for 1 h and chased with medium containing 4 mM Met-Cys for 3 h. Cells (lanes 1, 2, 5, 6, 9, and 10) and media (lanes 3, 4, 7, 8, 11, and 12) were harvested with 1X or 1/5 volume of 5X lysis buffer, respectively. Samples were immunoprecipitated with anti-sera and pre-immune serum as indicated and then separated in 7.5% SDS-PAGE gels. The S-specific bands are indicated on the right. (B) Time-course of S maturation. Cos7 cells transfected with pKT-S were radio-labeled and chased for 0, 0.5, 1, 2, 4, and 6 h (lanes 1, 2, 3, 4, 5, 6, and 7). Cos7 cells transfected with a plasmid without an insert were harvested at 6 h as a negative control (lane 8). All the cell lysates were immunoprecipitated with rabbit α-SΔ10 antibodies and then separated in 7.5% SDS-PAGE gels. In a separate experiment, the immunoprecipitated proteins (6 h post-transfection) were treated (+) with EndoH (lane 10) or untreated (-) as a control (lane 9). The S-specific bands and their molecular masses (in kilodaltons) are indicated on the right. High-range rainbow molecular weight markers (left; Amersham) were used. α, anti.

3.1.6 Detection of SARS-CoV S on surfaces of Cos7 cells

To provide further evidence that the antibodies raised against the five fusion proteins were able to recognize S, we performed indirect immunofluorescence experiments under non-permeabilized conditions. After infection with vTF7-3 vaccinia virus and transfection with pKT-S, sufficient time (8 h post-transfection) was allowed for S to be expressed and transported to the cell surface. Mature S can exist in trimeric or oligomeric forms on the cell surface, and these were clearly detected by any of the antibodies generated against the various S fragments (Fig. 3.5, top row). The results showed that all the antibodies bound to S on the cell surface, suggesting that these antibodies recognize the properly folded mature form of SARS-CoV S.

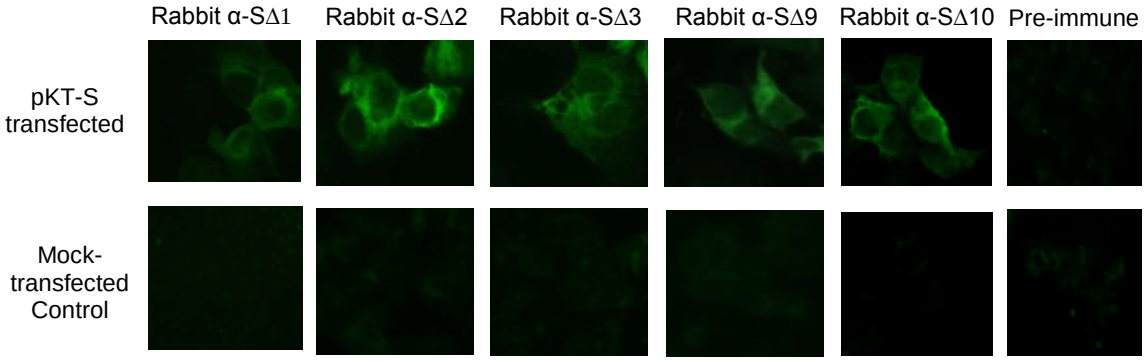

Fig. 3.5: S expressed on the surfaces of transiently transfected Cos7 cells. (Top row) Cos7 cells were transfected with full-length S and visualized under UV light. The green fluorescence represents the S protein expressed on the surfaces of Cos7 cells probed with primary antibodies rabbit anti-SΔ1 (α-SΔ1), α-SΔ2, α-SΔ3, α-SΔ9, and α-SΔ10, followed by fluorescein isothiocyanate-conjugated (FITC) secondary antibodies. (Bottom row) Cos7 cells were mock transfected with the empty vector and probed with the antibodies indicated on the left, as control experiments, and visualized under UV light.

3.2 A region in S2 can elicit neutralizing activity

After confirming that all the antibodies could recognize the native SARS CoV S, we further investigated their neutralizing activities. All anti-sera from rabbits injected with the various bacterial-expressed S protein fragments were tested for their neutralizing activities after each bleed. The bacterial expression system was chosen as it offers a cheap and fast way for large production of vaccines. Results for serum obtained from rabbits injected with bacterial-expressed SΔ1, SΔ2, SΔ3, and SΔ9 were negative. Sera from rabbits injected with SΔ10 but not the pre-immune sera from the same rabbits showed neutralizing activities after the fourth injection. Initial tests using SARS-CoV at 200 $TCID_{50}$/well showed high titers (1:364) of neutralizing antibodies in all the α-SΔ10 sera, beginning with serum bled after the 8^{th} injection (Table 3.1). The 16^{th} injection was the last booster injection and the rabbits were sacrificed at this stage. The neutralizing titer was comparable to, if not higher than, the titers detected in SARS patients. The antibody response in SARS patients at 100 $TCID_{50}$/well ranged between 1:150 to 1:475 over a period of 210 days (Shi et al., 2004).

To ascertain the results above, serum samples taken after the 4th, 6th, 8th, 12th, 14th, and 16th injections of SΔ10 were tested for neutralizing activity using SARS-CoV at 1,000 $TCID_{50}$/well (Table 3.2). Neutralizing activities were found to be as high as 1:189.2 at l,000 $TCID_{50}$/well. This result showed that the SΔ10 fragment expressed in *E. coli* covering amino acid residues 1055 to 1192 can stimulate neutralizing antibodies but not the other fragments covering all other regions of the ecto-domain of S.

It was interesting that SΔ10 (aa 1055 to 1192), which contained the HR2 domain, could elicit a strong neutralizing response but not SΔ9 (aa 798 to 1055), which covered

the HR1 domain. SΔ1, SΔ2, SΔ3, and SΔ9 could possess neutralizing epitopes that are conformation or glycosylation dependent and these epitopes could have been impaired in the bacterial expression system, which explains the lack of neutralizing activity in antibodies raised against these regions.

Table 3.1: Neutralizing test at 200 $TCID_{50}$ per well [a]

No. of injections before bleeding	Neutralizing titers in $TCID_{50}$/ 0.1ml [b] (Average of 2 experiments)
0 (Pre-immune serum)	0
8	70
12	364
14	208
16	256

[a] Neutralizing tests were done in a 96 well plate at 200 $TCID_{50}$ per well.
[b] Neutralizing titers were determined by the Reed-Muench method.

Table 3.2: Neutralizing test at 1000 $TCID_{50}$ per well [a]

No. of injections before bleeding	Neutralizing titers in $TCID_{50}$/ 0.1ml [b] (Average of 2 experiments)
0 (Pre-immune serum)	0
4	30
6	66.8
8	112
12	67.2
14	98
16	189.2

[a] Neutralizing tests were done in a 96 well plate at 1000 $TCID_{50}$ per well.
[b] Neutralizing titers were determined by the Reed-Muench method.

3.3 Generation of monoclonal antibodies (mAbs) against SΔ10 region

To identify linear neutralizing epitopes and characterize functional domains in S bearing the residues 1029 to 1192, mAbs were generated against this region. By using bacterially-expressed S fragment GST-SΔ10 as an antigen, BALB/c mice were immunized and boosted up to four times. Sera were collected one week after each booster injection and tested for the presence of specific antibodies by Western blot analysis. An antibody response was observed after the first booster injection (at a serum dilution of 1:1,000) (data not shown), indicating that the GST-SΔ10 fragment was highly immunogenic in terms of inducing antibodies in mice.

After hybridoma fusion and hypoxyanthine-aminopterin-thymidine selection, culture supernatants of individual clones were screened by ELISA using a C-terminal His-tagged S protein fragment (SΔ10-His) covering the same region of S. This eliminated clones that reacted to GST antigenic determinants. Out of the 125 ELISA-positive hybridomas, 94 were positive in Western blot screening using the full-length S protein prepared in a vaccinia-T7 expression system in Cos7 cells as previously described. These hybridomas were passaged twice and the supernatants were re-tested in Western blot assays. The results showed that 48 out of 94 hybridomas were stably secreting specific monoclonal antibodies. Among them, eight hybridomas which produced a higher concentration of mAbs in their supernatants were sub-cloned and used to generate ascitic fluids which were characterized in neutralizing and membrane fusion blocking assays as described below.

3.4 Characterization of monoclonal antibodies

3.4.1 Detection of S by mAbs in SARS-CoV infected cells

To confirm the binding specificity of mAbs to the S protein, all the monoclonal antibodies generated were used to detect S in virus-infected Vero E6 cells. As shown in Fig. 3.6A, the mAbs could detect the 210 kDa S in infected (lanes 2, 4, 6, and 8) but not mock-infected (lanes 1, 3, 5, and 7) cells. The results demonstrated that the mAbs were specifically binding to S in SARS-CoV infected cells. The mAbs against the SΔ10 region could recognize the full-length S protein synthesized in virus-infected Vero E6 cells which is consistent with previous results obtained using rabbit anti-SΔ10 polyclonal antibodies.

3.4.2 Mapping of binding sites of monoclonal antibodies

To determine the binding sites of the mAbs, eight internal deletion mutant plasmids were constructed, expressed in Cos7 cells, and used to determine the linear binding sites of mAbs by Western blot analysis. Each of these constructs encodes a S mutant protein with a 20 or 22 residue deletion (20 to 22 residues shorter than the full-length S). The positions of the deleted amino acid residues are indicated in Table 3.3. The binding sites of the eight mAbs were mapped, and the results are shown by representative gels in Fig. 3.6B. Both the glycosylated and unglycosylated forms (bottom gel, lanes 1 to 8) of each mutant protein (SΔ50 to SΔ57) were detected using rabbit α-SΔ10 serum. These were S-specific bands, as no bands were detected in mock-transfected cells (lane 9). In contrast, S encoded by one or two mutant constructs were not detected by each of the four types of mAbs. Therefore, these mAbs bound to residues that were deleted in the corresponding internal-deletion mutants.

In summary, we classified the antibodies according to their binding sites as the type I, II, III, and IV mAbs that bound to residues 1091 to 1130, 1111 to 1130, 1151 to 1170, and 1151 to 1192, respectively (Table 3.4). The results showed that residues 1091 to 1192 of the SΔ10 fragment harbor the major antigenic epitopes, but not the residues 1029 to 1090. Antigenic site I (1091 to 1130) overlapped with site II (1111 to 1130), while antigenic site III (1151 to 1170) overlapped with site IV (1151 to 1192) (Fig. 3.7). Despite the overlap, each site may represent an epitope that is distinct from the other. It seems that these antigenic sites were immuno-dominant within the SΔ10 region (residues 1029 to 1192).

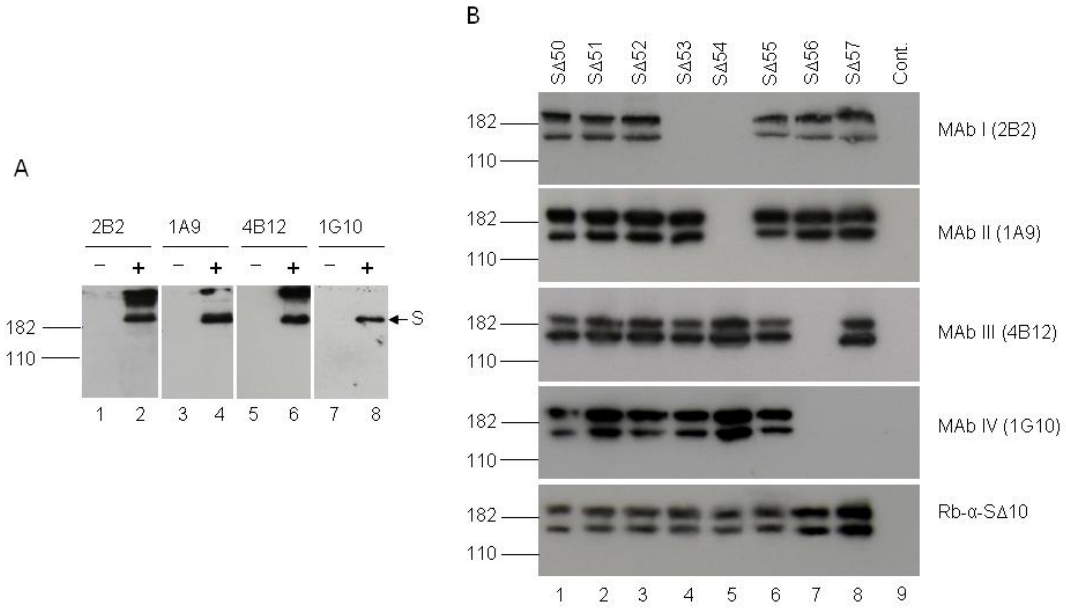

Fig. 3.6: Detection of S by mAbs in virus-infected cells and mapping the binding sites of the mAbs (A) Vero E6 cells were infected with SARS-CoV at an MOI of 1 (lanes 2, 4, 6, and 8) or mock infected (lanes 1, 3, 5, and 7) for 24 h. Cell lysates were separated on 10% SDS-PAGE gels and analyzed in Western blots using mAbs 2B2, 1A9, 4B12, and 1G10. Molecular weight markers are indicated to the left. Position of S is indicated by an arrowhead. (B) The S mutants (lanes 1 to 8, SΔ50 to SΔ57) with an internal 20- or 22-residue deletion were synthesized in a vaccinia-T7 expression system in Cos-7 cells. Cell lysates were separated on 10% SDS-PAGE gels and analyzed in Western blots using type I, II, III, and IV mAbs and polyclonal antibody rabbit α-SΔ10 as indicated to the right of the gels. Mock-transfected cell lysate (lane 9) was used as a negative control (Cont.). Molecular weight markers are indicated to the left.

Table 3.3: Internal deleted positions of the S mutants

Mutant S	Residues deleted
SΔ50	1029-1050
SΔ51	1050-1070
SΔ52	1071-1090
SΔ53	1091-1110
SΔ54	1111-1130
SΔ55	1131-1150
SΔ56	1151-1170
SΔ57	1171-1190

3.4.3 *In vitro* neutralization of virus infectivity by mAbs

Ascitic fluids of the eight mAbs, all of which are of the immunoglobulin isotype 1 (IgG1), were prepared and antibody concentrations of the crude preparations were determined (Table 3.4). The ascitic fluids were diluted 10 times and then two-fold serial dilutions were prepared. Neutralization assays were performed in 96-well plates by incubating equal volumes of diluted antibodies and virus suspension containing 10 $TCID_{50}$/well for 1 h at 37 °C before adding the mixture to confluent Vero E6 cells in the wells. After 3 days, complete cytopathic effect (CPE) was observed in all control wells containing the virus suspension in the absence of antibodies and in wells containing anti-dengue mAb (non-SARS-CoV related) or a non-neutralizing mAb, 7G12-6, which targets amino acid residues 281 to 300 of S. All the ascitic fluids were not toxic to the cells at the starting concentration used. The neutralizing titers were expressed as reciprocal of the final dilution of antibodies required to completely protect cells in 50% of the wells (no CPE observed) from virus infection. As shown in Table 3.4, all four types of mAbs showed neutralizing activity with titers ranging from 24 to 75 at mAb concentrations ranging from 13 to 100 μg/ml.

Table 3.4: *In vitro* neutralizing activities of mAbs

mAb	mAb type	Isotype	Titers	IgG (μg/ml)
2B2	I	IgG1	40	50
2G2	I	IgG1	47	85
1A9	II	IgG1	28	35
1C6	III	IgG1	24	83
1H1	III	IgG1	40	100
6B9	III	IgG1	24	42
4B12	III	IgG1	47	42
1G10	IV	IgG1	75	13
7G12	-	IgG1	0	50
Anti-dengue	-	IgG1	0	50

3.5 Understanding the mechanism of neutralization by mAbs

3.5.1 Neutralizing mAbs bind to regions upstream of and within the HR2 domain

The amino acid sequence of the region (residues 1091 to 1192), which the four types of mAbs target, were aligned with corresponding S regions of other coronaviruses (Fig. 3.7). The HR2 domain of the SARS-CoV S has been predicted to be located within residues 1125 to 1193 or 1144 to 1191 (Bosch et al., 2004; Xu et al., 2004b). Therefore, the upstream region from residues 1091 to 1124 or 1143 is considered to be a part of the spacer region between HR1 and HR2. As shown in Fig. 3.7, type I and II mAbs bound to the spacer region immediately upstream of HR2, residues 1091 to 1131 and 1111 to 1131 respectively. Type III and IV mAbs bind directly to the HR2 domain (residues 1151 to 1192). These results suggest that the HR2 domain and the spacer region immediately upstream of HR2 harbored neutralizing epitopes and therefore, are functionally important domains.

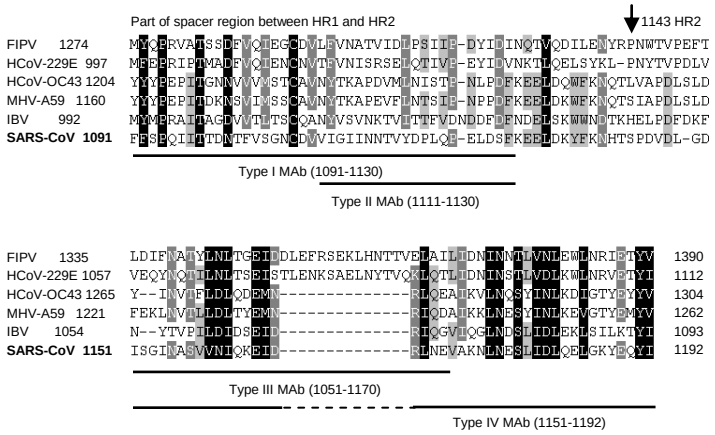

Fig. 3.7: Clustal W multiple sequence alignment of coronavirus S proteins. The S region corresponding to the binding sites of mAbs to SARS-CoV (Singapore strain 2774) is aligned with the group 1 coronaviruses feline infectious peritonitis virus (FIPV) and human coronavirus 229E (HCoV-229E), the group 2 coronaviruses HCoV-OC43 and MHV-59A (mouse hepatitis virus), and the group 3 coronavirus infectious bronchitis virus (IBV) (GenBank accession numbers AY283798, VGIH79, VGIHHC, CAA83661, VGIH59, and M95169, respectively). The shading indicates sequence identity and similarity. The predicted HR2 region and upstream spacer region and binding sequences of type I, II, III, and IV mAbs are shown by arrows and lines.

3.5.2 Inhibition of S-induced cell-cell membrane fusion by mAbs

During virus entry into cells, the HR1 and HR2 domains interact with each other and a subsequent conformational change triggers virus-cell membrane fusion. To test if the antibodies targeting this functional region could interfere with HR1 and HR2 interaction and block membrane fusion, a cell-cell membrane fusion assay was developed. 293T cells infected with recombinant vaccinia virus, rVV-L-SP, expressing S proteins (293T-SP), and CHO-ACE2 cells stably expressing receptor ACE2 were used in this assay.

First, FACS analysis was performed to verify that S and ACE2 were expressed on the cell surface of 293T-SP and CHO-ACE2 cells respectively, under non-permeabilizing conditions. 293T-SP cells were incubated with rabbit α-SΔ10 primary antibodies, and CHO-ACE2 cells were incubated with goat α-ACE2 primary antibodies. The cells were subsequently incubated with FITC-conjugated goat anti-rabbit or rabbit anti-goat IgG secondary antibodies. As shown in Fig. 3.8A (left), FITC fluorescence intensity measured for CHO-ACE2 was higher than that for control cells CHO, indicating expression of ACE2 proteins on the surface of CHO-ACE2 cells. As shown in Fig. 3.8A (right), FITC fluorescence measured for 293T-SP was higher than that for control cells (293T-NP) expressing the N (nucleocapsid) protein of SARS-CoV, indicating expression of S on 293T-SP cells.

To investigate if the epitopes upstream of HR2 (types I and II) and within HR2 (types III and IV) are exposed and accessible to specific antibodies, eight mAbs of interest (1:20) or an unrelated anti-dengue mAb was incubated with 293T-SP cells. The cells were subsequently incubated with FITC-conjugated goat anti-mouse IgG secondary

antibodies, and the interaction between the mAbs and S was measured by FACS analysis. In Fig. 3.8B, a representative histogram for each type of mAb (type I mAb, 2B2; type II mAb, 1A9; type III mAb, 4B12; type IV mAb, 1G10) is shown. Generally, FITC fluorescence intensity measured for each mAb was significantly higher than that for control anti-dengue mAb, suggesting that the four target epitopes on S were exposed and accessible to their specific antibodies.

Next, a cell-cell membrane fusion assay was set up to observe syncytium formation. 293T-SP or 293T-NP cells transfected with pEGFP-N1 (expressing green fluorescent protein [GFP]) was incubated with either target CHO-ACE2 or normal CHO cells. A representation of the morphology of normal cells and cells that have undergone cell-cell fusion is shown in Fig. 3.8C. Syncytium formation (10 or more cells fused together) as a result of the interaction between S and ACE2, expressed on the surfaces of 293T-SP and CHO-ACE2 cells, was displayed in bright field (top row, left), dark field under UV excitation (top row, right), and a combined view (top row, center). In contrast, no syncytium was observed when control cells, 293T-NP, were incubated with CHO-ACE2 (Fig. 3.8C, bottom micrographs). In Fig. 3.8C (bottom micrographs), individual cells were distinguishable with a clear cell boundary in the bright field view (left) and as single spots of green fluorescence in the dark field view (right), in contrast to the lack of cell boundaries and massive bodies of green fluorescence as shown in Fig. 3.8C (top micrographs). 293T-SP cells incubated with normal CHO cells did not yield any syncytia in the fusion experiments (data not shown). Only fusion experiments consisting of 293T-SP cells and CHO-ACE2 cells could form syncytia. These results confirmed that the cell-

cell membrane fusion was induced by S and was dependent on the receptor ACE2 (Li et al., 2003b; Simmons et al., 2004; Sui et al., 2004).

In order to investigate the inhibition of syncytium formation by specific antibodies, all the antibodies were incubated in the cell-cell membrane fusion assay at different dilutions of 1:40, 1:80, and 1:160. Rabbit α-SΔ10 serum and goat α-ACE2 antibody were included as positive controls and rabbit pre-immune serum and anti-dengue mAb were included as negative controls. As shown in Fig. 3.9A, syncytium formation was not observed in the presence of 1:40 diluted rabbit α-SΔ10 serum (top right) or mAb1A9 (bottom right). No syncytium formation was also observed in the presence of goat anti-ACE2 antibody (data not shown). In contrast, as shown in the left panels of Fig. 3.9A, large syncytia were observed in the presence of 1:40 non-inhibiting rabbit pre-immune serum (top left) or anti-dengue mAb (bottom left).

Next, the distribution of the number of nuclei per syncytium was scored. It was found that syncytia formed from 10 or more cells accounted for at least 90 % of all potential syncytia scored (data not shown). Only syncytia with 10 nuclei or more were counted in order to eliminate artifacts scored as a result of cell division or abnormal cell clumping and to avoid difficulty in identifying syncytia of small sizes. The number of syncytia was then scored and the percentage of syncytium formation inhibition at different antibody dilutions is summarized in Fig. 3.9B. At a 1:40 dilution, all the mAbs inhibited more than 50% of syncytia formation. However, syncytia inhibition decreased significantly when each mAb was serially diluted from 1:40 to 1:80 and 1:160. The formation of syncytia was inhibited in a dose-dependent manner, indicating that the mAbs were specific in their syncytia formation blocking activity.

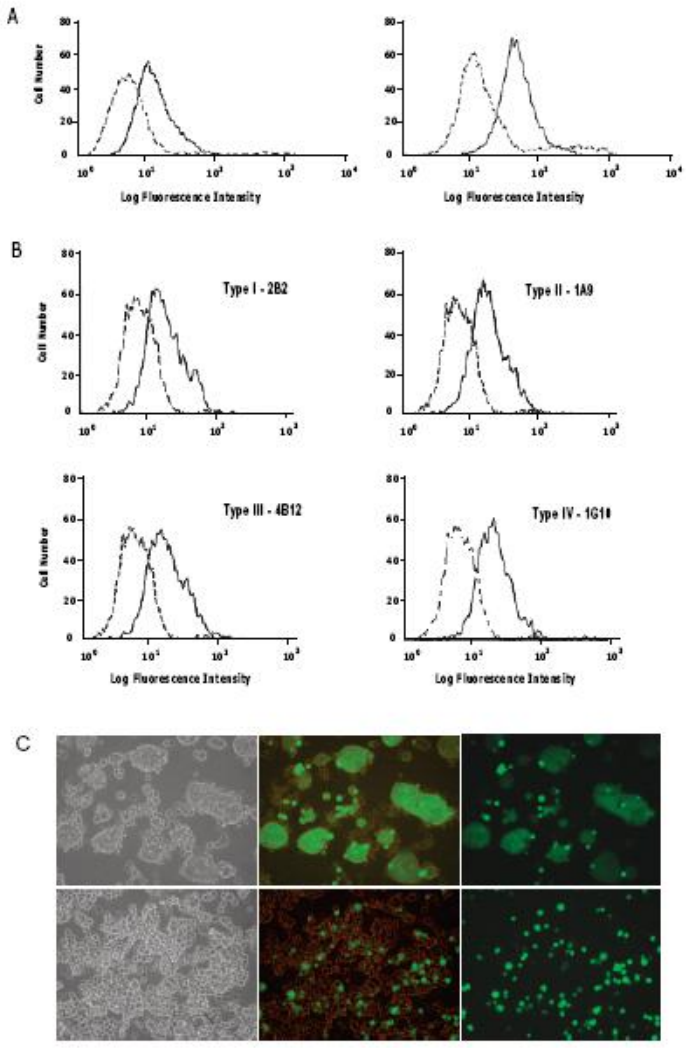

Fig 3.8: FACS analysis of the surface expression of the S and ACE2 and syncytium formation assay. (A) Left, ACE2 surface expression on CHO-ACE2 stable cells (solid line) and negative control CHO cells (dotted line) was probed with goat anti-ACE2 primary and FITC-conjugated anti-goat IgG secondary antibodies. Right, S surface expression (solid line) and N expression (dotted line; negative control) on 293T cells were probed with rabbit α-SΔ10 primary and FITC-conjugated anti-rabbit IgG secondary antibodies. (B) 293T-SP were probed with four representative mAbs of interest and an unrelated anti-dengue MAb, followed by FITC-conjugated anti-mouse IgG secondary antibodies. Top left panel, S was probed with type I mAb 2B2 (solid line) and anti-dengue mAb (dotted line). Top right panel, S was probed with type II mAb 1A9 (solid line) and anti-dengue mAb (dotted line). Bottom left panel, S was probed with type III mAb 4B12 (solid line) and anti-dengue mAb (dotted line). Bottom right panel, S was probed with type IV mAb 1G10 (solid line) and anti-dengue mAb (dotted line). (C) Assay is captured in bright field (left panel), dark field (right panel), and a combination of both (center panel). Top panel, 293T cells expressing S and GFP were mixed with CHO-ACE2 cells expressing ACE2. Bottom panel, 293T cells expressing N and GFP were mixed with CHO-ACE2 cells expressing ACE2 as negative control. Micrographs were taken at a 20X magnification.

A

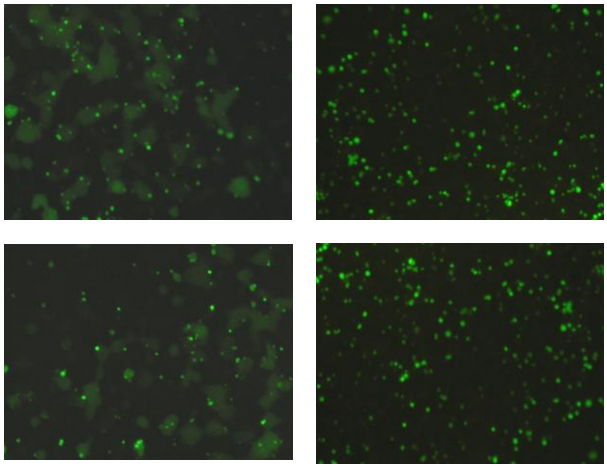

B

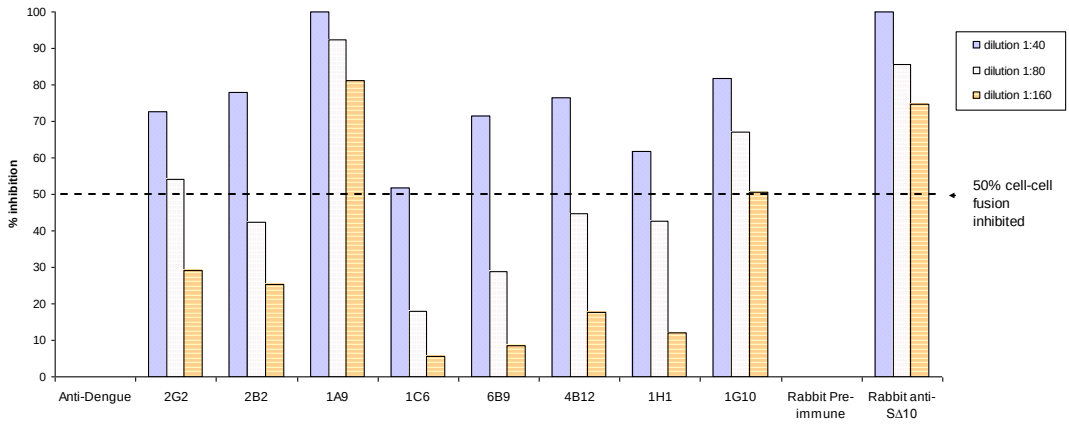

Fig 3.9: Dose-dependent inhibition of syncytium formation between 293T-SP and CHO-ACE2 cells. (A) Top panel, incubation with rabbit pre-immune serum (left) and rabbit α-S10 polyclonal antibody (right) at 1:40 dilution. Bottom panel, incubation with mouse α-dengue ascitic fluid (left) and mouse mAb 1A9 (right) at a 1:40 dilution. Micrographs were taken at a 10X magnification. (B) Percentage of inhibition of syncytium formation between 293T-SP cells and CHO-ACE2 cells, in the presence of antibodies at 1:40 (blue), 1:80 (white), and 1:160 (orange) dilutions, were determined.

3.6 Discussion

The coronavirus S is a major determinant of tissue tropism by mediating binding to cellular receptors and virus-cell membrane fusion. For SARS-CoV, various studies have shown that antibodies targeting S can provide immunity against the virus (Bisht et al., 2004; Buchholz et al., 2004; Bukreyev et al., 2004; Hofmann et al., 2004a; Sui et al., 2004). In this study, we generated rabbit polyclonal antibodies against five S fragments expressed in *Escherichia coli* in order to identify linear neutralizing epitope(s) on S. Interestingly, it was shown that the antibodies can recognize the denatured and recombinant form of S, as well as the native S expressed in SARS-CoV infected cells that was later incorporated into virions detected in the medium (Fig 3.2, 3.3 and 3.4A, respectively). It is likely that the proteins used for immunization maintained a certain degree of conformation or that the antibodies recognize linear and exposed epitope(s) in the native conformation of S. It was also shown that the antibodies could bind to both the EndoH-sensitive (200kDa) and EndoH-resistant (210kDa) forms of S (Fig. 3.4B). Immuno-fluorescence experiment results further confirmed that all the antibodies could recognize the glycosylated mature S expressed on the cell surface (Fig. 3.5).

Neutralization assays showed that antibodies targeting GST-SΔ10 were capable of neutralizing SARS-CoV replication in Vero E6 cells at a titer of 1:364 at 200 $TCID_{50}$ (Table 3.1), which is comparable to the level obtained from convalescent patients (Shi et al., 2004). As shown in Tables 3.1 and 3.2, rabbit α-SΔ10 antibodies showed a steady increase in neutralizing titers with more booster immunizations but none of the antibodies targeting the other four fragments showed neutralizing activity. While it has been shown that the antibodies targeting the RBD have potent neutralizing activity, our antibodies

against the GST-SΔ3 fragment (bearing the RBD) showed no neutralizing activity (Sui et al., 2004). It is possible that the RBD is heavily glycosylated and/or contains rigid tertiary structure under native conditions that is not recognized by the α-SΔ3 antibodies. Hence, our results showed that the region from residues 1055 to 1192, but not residues 48 to 1055, is suitable for the development of vaccines that are peptide-based or based on non-mammalian systems that do not mimic the protein glycosylation and folding processes that occur in mammalian cells.

Interestingly, SΔ10 encompasses the loop region between HR1 and HR2 domain, as well as the N-terminal of the HR2 domain. HR1 (residues 891 to 975) and HR2 (residues 1195 to 1223) have been shown to play crucial roles in forming a six-helix bundle that is essential for the virus-cell membrane fusion process (Gallagher and Buchmeier, 2001). Our results are consistent with several studies that showed that peptides mimicking the HR2 region could block SARS-CoV infection (Bosch et al., 2004; Yuan et al., 2004; Zhu et al., 2004).

To investigate the mechanism of neutralization of SARS-CoV infection by α-SΔ10 antibodies, we generated eight mAbs against this region and mapped their binding sites using S deletion mutants (Fig. 3.6B). The results showed that the antigenic sites recognized by the mAbs could be narrowed down to residues 1091 to 1130 and 1151 to 1192, suggesting that these regions may be immuno-dominant in the humoral immunity against SΔ10. The results also demonstrated the neutralizing activity of the eight mAbs (Table 3.4). However, the titers of the eight mAbs targeting the S2 region were lower than the mAbs that target the RBD of SARS S (Chou et al., 2005; Sui et al., 2004). The results are consistent with previous findings on murine hepatitis virus (MHV) showing

that the neutralizing concentrations of mAbs targeting the S2 region were 3 to 4 orders magnitude lower than those targeting the receptor-binding S1 region (Kubo et al., 1993; Taguchi and Shimazaki, 2000). Nevertheless, α-SΔ10 polyclonal antibodies targeting multiple epitopes do neutralize SARS-CoV infection more efficiently than each of the mAbs, suggesting that the mAbs may act cooperatively or synergistically (ter Meulen et al., 2004; Zwick et al., 2005).

Using a syncytium formation inhibition assay, we showed that all the eight mAbs that could neutralize SARS-CoV infection *in vitro*, could also block syncytium formation in a dose-dependent manner (Fig. 3.9B). The structure of the SARS-CoV S protein was determined and aa 1150-1184 in HR2 were demonstrated to interact with aa 902-947 for the formation of the six-helix bundle, a fusion-competent structure that is observed in all type-I viral fusion proteins (Supekar et al., 2004; Xu et al., 2004b). Interestingly, the type III and IV mAbs which bind to residues 1151-1170 and 1151-1192 respectively on the HR2 domain displayed neutralizing and cell-cell fusion inhibition properties. It is possible that the binding of antibodies to the HR2 domain interfere with the interaction between HR1 and HR2, disrupting the conformational change and hence abolishing the fusion activity. Our results are consistent with other studies demonstrating that peptides mimicking aa 1161-1187 (HR2-18), aa 1153-1189 (CP1), aa 1126-1193 (sHR2-8) and aa 1130-1189 (sHR2-2) of the HR2 domain inhibit the propagation of SARS-CoV (Bosch et al., 2004; Liu et al., 2004; Yuan et al., 2004).

Type I and II mAbs bind to the loop region between the HR1 and HR2 domains and their mechanism of neutralization of SARS-CoV remains unknown. One possible explanation is that the occupancy of the loop region between the HR1 and HR2 domains

interferes with their interaction via steric hindrance, thus abolishing fusion activity. The SARS-CoV S possesses a longer loop region (140 to 170 residues) compared to the fusion proteins of other enveloped viruses (5 to 26 residues) (Bosch et al., 2003). It is postulated that the absence of a spacer region or the very short spacer region between the HR2 and trans-membrane domain is compensated by the presence of a longer loop region between the HR1 and HR2 domains (Ingallinella et al., 2004). This longer loop region may be important in providing the flexibility needed for the trimeric HR1 coiled coil to pack together with the three helices of the HR2 in an anti-parallel manner during the six-helix bundle formation. The loop region that the type I and II mAbs bind is a novel neutralizing domain that may facilitate the development of new entry inhibitors. The identification of novel neutralizing sites may also provide new targets for the development of efficacious vaccines based on peptides mimicking the linear epitope(s).

CHAPTER 4: FURTHER CHARACTERIZATION OF THE SARS-CoV NEUTRALIZING MONOCLONAL ANTIBODIES

4.1 Sequence comparisons of human and animal SARS-CoV S

In recent years, co-ordinated efforts were put into determining the parental strain of SARS-CoV in the animal reservoirs. After much concerted effort, it was reported by Lau et al. that bat SARS-like coronavirus (SL-CoV) Rf1 and Rp3 strains could have undergone a recombination event to achieve the civet SARS-CoV SZ3 strain, which in turn was transferred to humans during the SARS epidemic (Lau et al., 2010). A comparison of the S1 and S2 domains of the three strains (SZ3, Rp3 and Rf1) with the human SARS-CoV strain indicates that the S1 domain is less conserved than the S2 domain (Table 4.1). The S1 domain of the bats Rp3 and Rf1 strains have low sequence identity of only 64.3% and 63.6% when compared to the S1 domain of the human HK39849 strain while the S2 domains have a high sequence identity of 95.8% and 92.7%, respectively.

As mentioned in the previous chapter, the neutralizing mAbs that we have generated target the S2 domain. To investigate the cross-neutralizing ability of the mAbs against the civet and bat strains, we selected two mAbs (mAb 1A9 and 1G10) that target different regions on S. As mentioned earlier, mAb 1A9 targets the loop region between the HR1 and HR2 domains while mAb 1G10 targets the N-terminus of the HR2 domain (Fig. 3.7). Sequence alignment analysis indicates that the binding site of mAb 1A9 is 100% conserved while there are two aa differences in the binding region of mAb 1G10 among the four strains (Fig. 4.1).

Table 4.1: Percentage identity of the S protein sequence

Protein	Amino acid identity to HK39849		
	SZ3	Rp3	Rf1
S1	98.4%	64.3%	63.6%
S2	98.8%	95.8%	92.7%

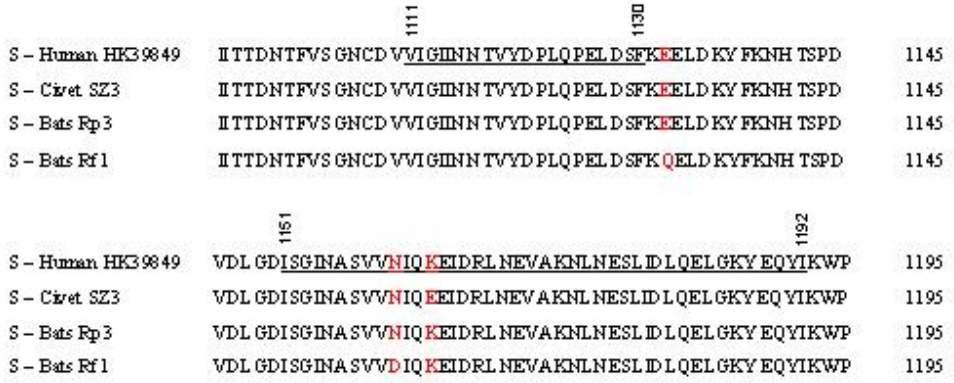

Fig. 4.1: Protein sequence alignment for binding domain of mAbs to S of Human HK39849, Civet SZ3, Bats Rp3 and Rf1 coronaviruses. The differences in the protein sequences are highlighted in red, while the binding sites for mAbs 1A9 (top) and 1G10 (below) are underlined. The number above the amino acid represents the position of the amino acid in the S protein sequence.

4.2 Cross-neutralization ability of both mAb 1A9 and 1G10 in animal strain S-mediated cellular entry

In this study, the receptor-binding domain of S in the bats SL-CoV Rp3 and Rf1 strains and civet SARS-CoV SZ3 strain were replaced with the RBD of S in the human SARS-CoV strain for further investigation using a pseudovirus entry assay. It had been demonstrated by Ren et al. that the bat SL-CoV uses a different receptor for entry and thus, could not infect cells expressing ACE2 receptors. However, the replacement of the receptor binding region on S of these bat SL-CoV can restored their infectivity to cells expressing the human ACE2 receptor in a pseudovirus assay (Ren et al., 2008). Using Western blot analysis, it was shown that receptor-modified S from all three strains were expressed in the transfected 293T cells and could be detected as efficiently as the human SARS-CoV S by both mAb 1A9 and 1G10 (Fig. 4.2).

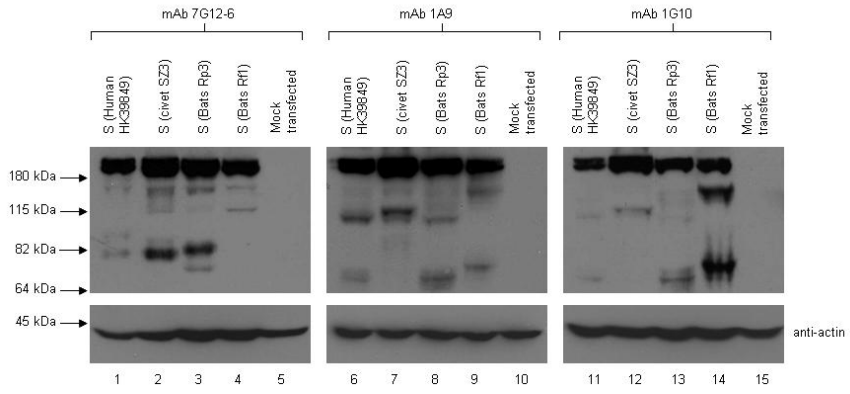

Fig. 4.2: Detection of receptor-modified S of civet and bat strains. 293T cells were transfected with expression plasmid for S(HK39849), S(SZ3), S(Rp3) and S(Rf1) and harvested 24 h post-transfection. The proteins were detected in Western blot using the mAbs indicated at the top of the gel.

To study the efficiency of neutralizing antibodies, peptides and other inhibitors of SARS-CoV without the use of live virus, pseudovirus assays using human immunodeficiency virus (HIV) vectors were commonly used (Chu et al., 2008b; Ni et al., 2005; Yuan et al., 2004). These pseudovirus assays not only eliminate the risk of laboratory outbreaks but also allow for the study of inhibitors for animal SARS-CoV strains that were shown to be difficult to propagate in cell culture.

Here, a viral entry assay was set up by using pseudoviruses packaged with SARS-CoV S and CHO-ACE2 cells. The pseudoviruses in this assay are lentiviral pseudotyped particles encoding a luciferase reporter and expressing the SARS-CoV S on the surface. These pseudoviruses are produced by the co-transfection of 293T cells with plasmids pNL4.3-Luc-R-E- and pXJ3'-S, expressing the lentiviral particles and the SARS-CoV S respectively. The CHO-ACE2 cells express the receptor, ACE2, for S and mediate the entry of the pseudoviruses bearing S into the cells. Luciferase expressed from the pseudoviruses that enters the CHO-ACE2 cells were measured using a luminometer. A negative control experiment with pseudoviruses not packaged with any envelope protein and a positive control experiment with pseudoviruses packaged with the human SARS-CoV S without any mAbs were set up (Figure 4.3A and B, column 1 and 2 respectively). The difference in the luciferase readings between the positive and negative control is set as 100 % viral entry. Different concentrations of the mAbs were tested for its inhibitory effect on the pseudoviruses packaged with S (human strain). The results showed that 150 μg/ml of mAb 1A9 or 1G10 reduced S-mediated pseudovirus entry by more than 50% (Fig. 4.3A and B respectively, column 4).

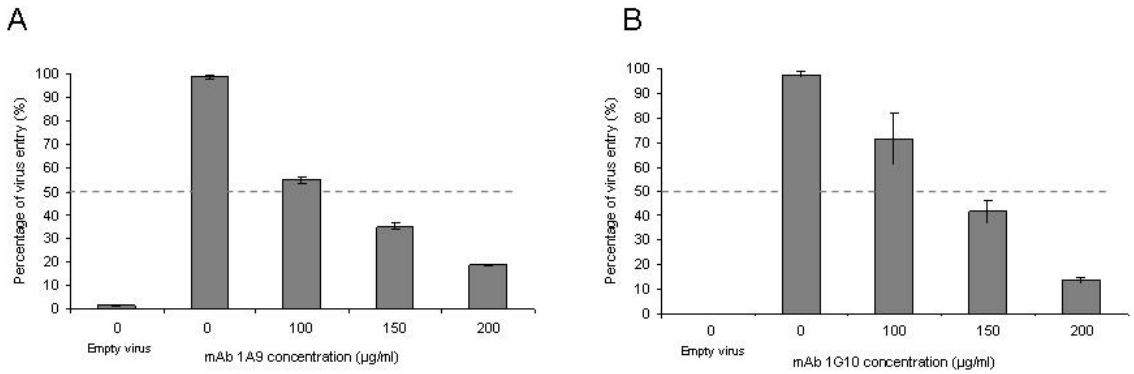

Fig. 4.3: Setting up of pseudovirus assay for performing neutralization test with mAbs. Pseudovirus packaged with S (HK39849 strain) were measured for the efficiency of entry into CHO-ACE2 cells at different mAb 1A9 and 1G10 concentration (100, 150 and 200 μg/ml) in the luciferase assay (A and B, respectively). A negative control experiment with empty virus and a positive control experiment without mAb were also performed.

To investigate whether mAb 1A9 and 1G10 affect the binding of pseudoviruses bearing S to CHO-ACE2 cells, we performed a virus binding assay. This assay was modified from the method previously described using influenza A viruses (Sui et al., 2009). To determine if the mAbs can prevent virus attachment, pseudoviruses bearing S were allowed to attach to CHO-ACE2 cells at 4 °C for 2 h, in the presence of 150 μg/ml of mAb 1A9 or 1G10, before the unbound viruses were washed off. The amount of bound viruses to the cells was determined using a P24 ELISA kit. As shown in Fig. 4.4, the amount of bound viruses in the presence of both mAb 1A9 and 1G10 were not reduced (column 3 and 4, respectively), compared to the control experiment without any mAb (column 2). The result suggests that both mAb 1A9 and 1G10 do not affect the binding of pseudoviruses bearing the SARS-CoV S to CHO-ACE2 cells.

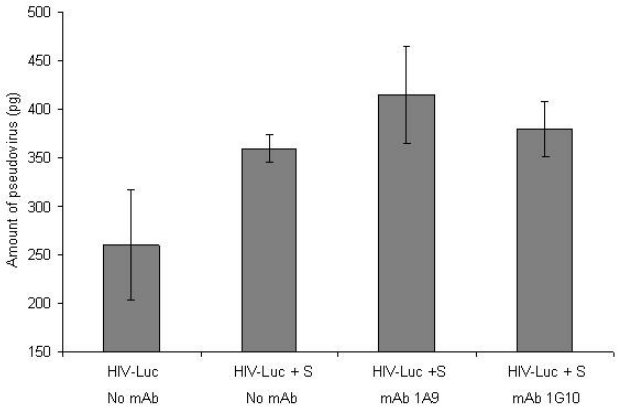

Fig. 4.4: Pseudovirus binding assay. Pseudoviruses packaged with S (HK39849 strain) were generated by co-transfection of pNL4.3-Luc-R.E. and pXJ3'-S expression plasmids in 293T cells. The pseudoviruses in the supernatant were used for infection of CHO-ACE2 cells at 4 °C for 2 h in the absence/presence of mAbs and the amount of virus that were bounded to the cells were determined using a HIV-1 P24 ELISA kit.

Next, the receptor-modified SZ3, Rp3 and Rf1 S were packaged into HIV-1 pseudoviruses and the entry of the pseudoviruses into the CHO-ACE2 cells were shown to be as efficient as the pseudoviruses packaged with the human SARS-CoV S (Fig. 4.5A). In the presence of varying concentrations (100 to 200 μg/ml) of mAb 1A9 and 1G10, the extent of mAb inhibition on the different S-mediated entry was measured. Results indicate that both the mAb 1A9 and 1G10 inhibit the entry of pseudoviruses packaged with human SARS-CoV S as well as the receptor-modified bat and civet SL-CoV S, in a dose-dependent manner (Fig. 4.5B and 4.5C, respectively). These results suggest that both mAb 1A9 and 1G10 have broad neutralizing activities against human and civet SARS-CoV and bat SL-CoV.

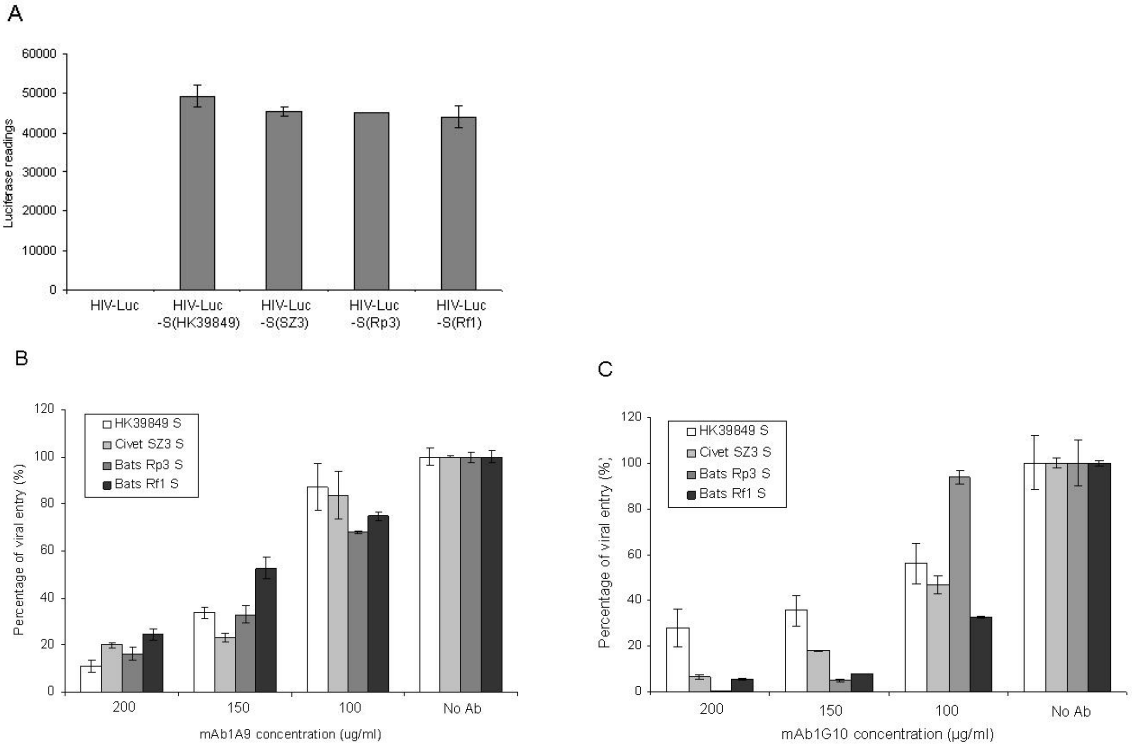

Fig. 4.5: Cross-neutralization activity of mAb 1A9 and 1G10. (A) Pseudovirus packaged with S(HK39849), S(SZ3), S(Rp3) and S(Rf1) were tested for their efficiency of entry in the absence of mAb. (B, C) Pseudovirus packaged with S(HK39849), S(SZ3), S(Rp3) and S(Rf1) were measured for the efficiency of entry into CHO-ACE2 cells in the presence of different mAb 1A9 and 1G10 concentrations, respectively, using a luciferase-based assay.

4.3 Generation of escape mutant virus of mAb 1A9 and 1G10

To further delineate the mechanism of neutralizing activity by mAb1A9 and mAb1G10, SARS-CoV neutralization escape mutants were generated for the two mAbs. The selection concentrations that can reduce the virus titers by more than 3 logarithms were determined as 0.25 mg/ml for mAb 1A9 and 0.1 mg/ml for mAb 1G10 (Fig. 4.6A and 4.6B, respectively). Following 3 passages in VeroE6 cells in the presence of the mAb 1A9 or mAb 1G10 selection concentration, the virus replication titer resumed to the level observed in the wild-type viruses (Fig. 4.6C and 4.6D, respectively). A plaque purification assay was performed and five clones were selected for amplification under the selection mAb concentration.

A neutralization assay was then performed on the HK39849 wild-type viruses and the neutralizing concentration for mAb 1A9 and 1G10 were calculated using the Muench-Reed formulae and determined as 1.5 mg/ml and 0.45 mg/ml, respectively. Following that, all the escape viruses were tested for their ability to escape the mAbs neutralizing concentration. The results showed that all the five escape virus clones for mAb 1A9 were no longer neutralized at the mAb 1A9 neutralizing concentration for the wild-type virus but could still be neutralized by mAb 1G10. Similarly, all the five escape virus clones for mAb 1G10 were not neutralized at the neutralizing concentration of mAb 1G10 but were still neutralized by mAb 1A9. These results indicate that the selected and amplified virus clones from the plaque purification were positive SARS-CoV escape mutants against their respective selection mAbs.

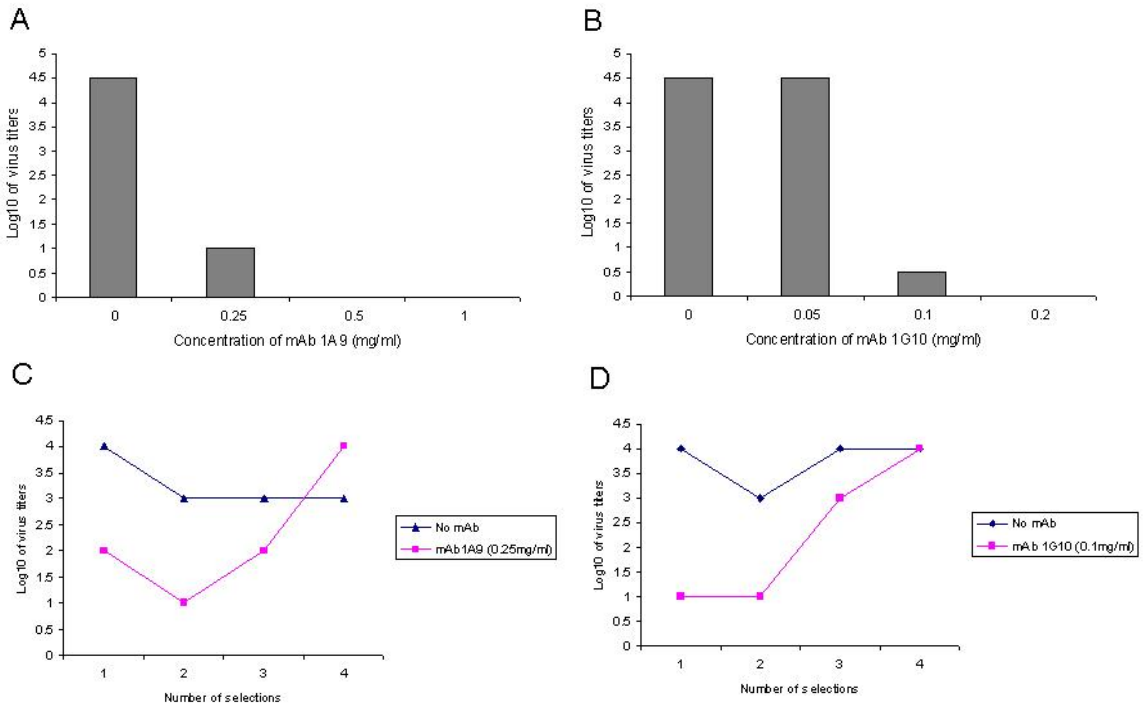

Fig. 4.6: Generation of escape SARS-CoV mutants for mAb 1A9 and 1G10. (A, B) Vero E6 cells were infected with 100 $TCID_{50}$ of SARS-CoV in the prescence of a range of dilutions of the mAb 1A9 and 1G10 respectively, for 1 h at 37 °C and replaced with fresh medium for incubation at 37 °C for two days. The titer of the virus is then determined using a $TCID_{50}$ assay. The mAb concentration that can suppress the virus titer by more than 3 logarithms is ideal as selection concentration. (C, D) Escape viruses were passaged for three rounds in the presence of the selection concentration of mAb 1A9 and 1G10, respectively. Virus titers were measured after each round. Plaque purification was performed when the virus titer recovered to the level of the wild-type virus.

4.4 Identifying the mutation(s) on S in the mutant viruses that escaped the inhibition by mAb 1A9 and 1G10

The viral RNAs were extracted for RT-PCR using S specific primers, and the cDNAs were cloned into TOPO vector for DNA sequencing of the S gene. Three individual mutations (H641Y or T706I and W869L) were identified in the TOPO clones of S from the mAb 1G10 escape virus clones while two individual mutations (N1056K and D1128A) were identified in the TOPO clones of S from the mAb 1A9 escape virus clones (Fig. 4.7). D1128 is found within the binding region of mAb 1A9 while N1056 is located upstream of this binding site. H641, T706 and W869 are not located near the mAb 1G10 binding sites but further upstream of the HR1 domain.

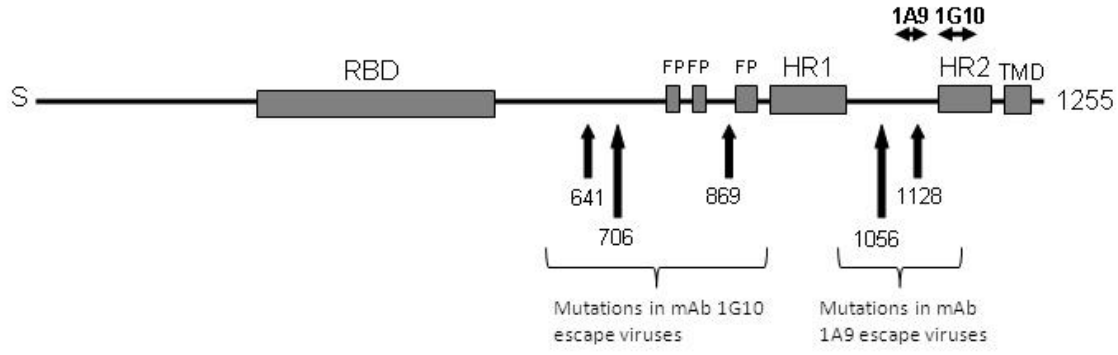

Fig. 4.7: Schematic diagram showing S with the functional domains and the point mutations found in mAb 1A9 and 1G10 escape viruses. The double end arrows represent the binding sites of mAb 1A9 and 1G10. The arrows pointing upwards indicate the position of the mutations that were found to be commonly identified in the TOPO clones of S from the mAb 1A9 and 1G10 escape viruses. RBD, receptor binding domain; FP, fusion peptide; HR1, heptad repeats 1 domain; HR2, heptad repeats 2 domain; TMD, transmembrane domain.

4.5 Screening the mutation(s) for positive escape activity

To verify which of the identified mutations on S contribute to the escape activity of the escape viruses, we screened S mutants bearing individual mutations for their entry activity into CHO-ACE2 cells using a pseudovirus assay. The results from the pseudovirus screening showed that there are only two escape mutations (N1056K and D1128A) that exhibited escape activity (Fig. 4.8). Both the mutations were identified in mAb 1A9 escape viruses. From the luciferase assay result shown in Fig. 4.8A, both mAb 1A9 and 1G10 reduced pseudovirus entry by more than 40% at 150 μg/ml, except for pseudoviruses packaged with S bearing the N1056K or D1128A mutation. The pseudovirus packaged with S bearing the N1056K mutation showed 25% higher luciferase activity while pseudoviruses packaged with S carrying the D1128A mutation showed 30% higher luciferase activity. No escape activity was detected in S bearing mutations identified in the mAb 1G10 escape viruses (Fig. 4.8B). These results showed that only two out of the five identified mutations on S contribute to the escape activity of the viruses against the mAb used for their selection.

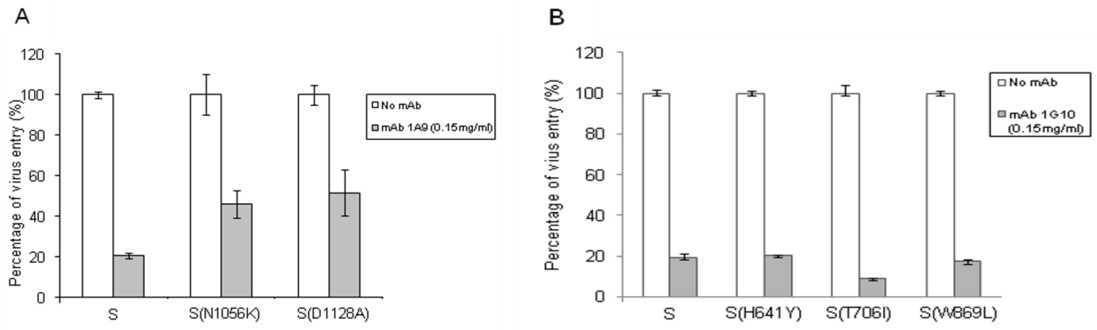

Fig. 4.8: Pseudovirus entry assay. (A) Pseudovirus packaged with wild-type S, S(N1056K), S(D1128A) were measured for the efficiency of entry into CHO-ACE2 cells in the presence of 0.15 mg/ml of mAb 1A9 and 1G10 in the luciferase assay. (B) Pseudovirus packaged with wild-type S, S(H641Y), S(T706I) and S(W869L) were measured for the efficiency of entry into CHO-ACE2 cells in the presence of 0.15 mg/ml of mAb 1A9 and 1G10 in the luciferase assay. A control experiment without antibody was used for normalization (i.e. it is set to 100%).

4.6 Amino acid residues N1056 and D1128 are important for mAb 1A9 neutralizing activity

In order to gain a better understanding of the mechanism underlying the escape activity of the S mutants bearing N1056K and D1128A, further studies on their binding efficiency and escape activity to mAb 1A9 were carried out. An additional S mutant bearing the double mutation (N1056A and D1128A) was cloned to examine if the mutations were synergistic in their escape activity from mAb 1A9. It was demonstrated by Western blot analysis that mAb 1A9 binds to S and S(N1056K) mutant but not as efficiently to S(D1128A) and S(N1056K, D1128A) mutants (Fig. 4.9A), indicating that mAb 1A9 has a lower binding affinity for the denatured form of the S mutants bearing the D1128A mutation. In addition, radiolabelled immuno-precipitations were carried out for S and the S mutants to study their interactions, in the native folded form, with mAb 1A9. The results clearly showed that mAb 1A9 does not bind as well to S bearing the D1128A mutation as compared to its interaction with S and S(N1056K), suggesting that the native folded state of the S mutant bearing D1128A has a conformation that reduces the binding efficiency of mAb 1A9 (Fig. 4.9B). On the other hand, mAb 7G12-6 that binds to the S1 domain can still bind efficiently to the S bearing the D1128A mutation in both Western blot analysis and immunoprecipitation assay.

To confirm specific mAb 1A9 escape activity of the S mutants and investigate the synergy between the two mutations (N1056K and D1128A), we performed a dose-dependent mAb 1A9 inhibition of S-mediated entry using a pseudovirus assay. The results showed that all three S mutants can be inhibited by mAb 1A9 in a dose-dependent manner but the escape activity of S(D1128A) was much higher than S(N1056K) and

S(N1056K, D1128A) showed enhanced escape activity compared to the two single aa substituted mutants (Fig. 4.9C).

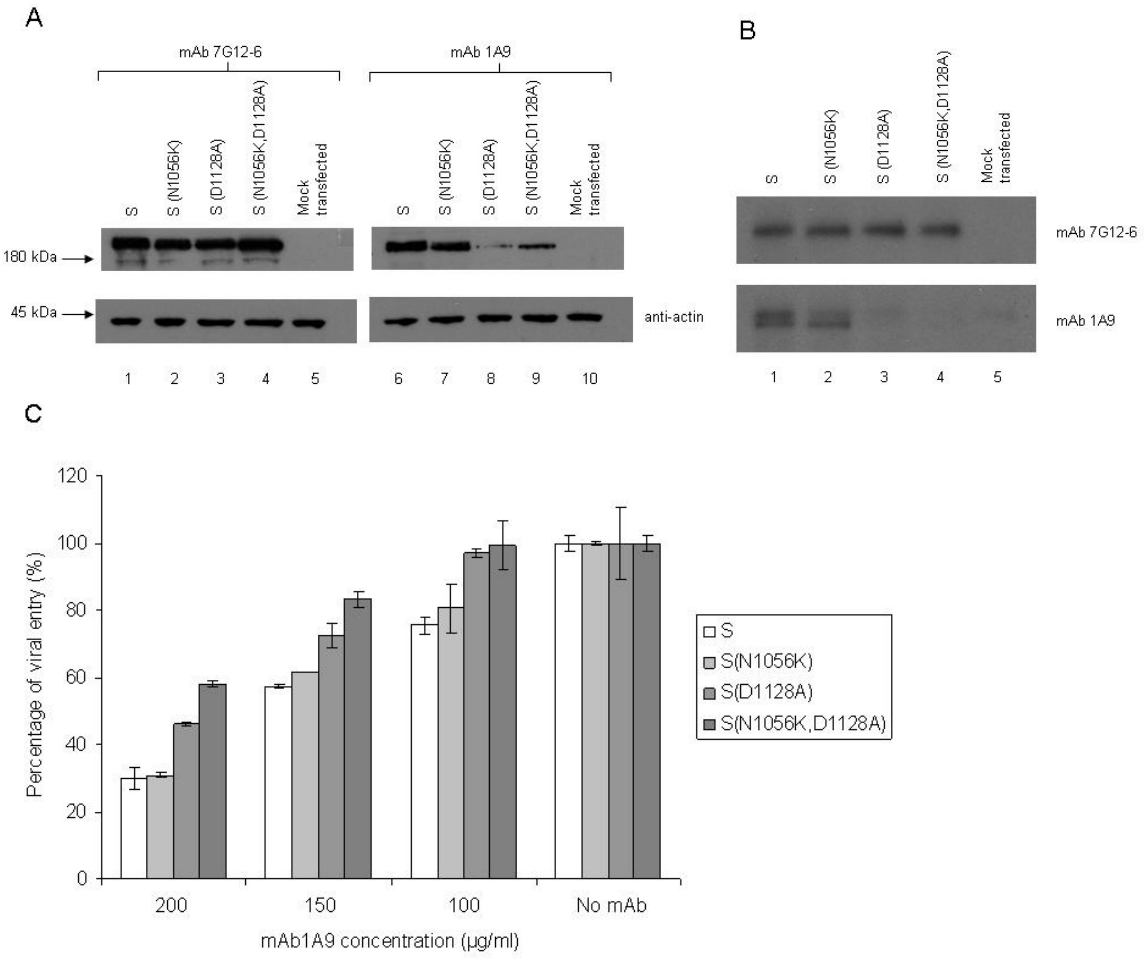

Fig. 4.9: Analysis of positive SARS-CoV escape mutations of clones selected with mAb 1A9. (A) 293T cells were transfected with expression plasmid for S, S(N1056K), S(D1128A), S(N1056K, D1128A) and mock transfected, and detected in Western blot using different mAbs indicated at the top of the blot. (B) 293T cells were transfected with expression plasmid for S, S(N1056K), S(D1128A), S(N1056K, D1128A) and mock transfected, followed by ^{35}[S] radiolabeling and immunoprecipitation using the different antibodies indicated on the right. (C) Pseudovirus packaged with S, S(N1056K), S(D1128A) and S(N1056K, D1128A) were measured for the efficiency of entry into CHO-ACE2 cells at different mAb 1A9 concentration (100, 150 and 200 µg/ml) using a luciferase assay. A control experiment without antibody was also performed.

4.7 Discussion

Only a few studies have been carried out previously to investigate the cross-neutralizing activities of SARS-CoV neutralizing mAbs due to the difficulties of studying the bat SL-CoV, which uses another host molecule as a receptor for entry (Ren et al., 2008). Several research studies that generated neutralizing antibodies against the receptor binding domain of S were also unable to inhibit the bat CoV and early SARS-CoV strains (Rockx et al., 2008; Sui et al., 2005). A comparison between bat SL-CoV S and human SARS-CoV S suggests that the S2 domain is more highly conserved with more than 90% identity while the S1 region has low similarity of slightly more than 60% identity, suggesting a higher possibility for a neutralizing mAb targeting the SARS-CoV S2 region to be able to neutralize the bats SL-CoV (Table 4.1). In the present study, we showed that mAb 1A9 and 1G10, both targeting the S2 domain, can detect receptor-modified civet S (SZ3 strain) and bat S (Rp3 and Rf1 strains) (Fig. 4.2) and exhibit cross-neutralizing activities (Fig. 4.5B and C, respectively).

In order to gain a better understanding of the neutralizing mechanism of mAb 1A9 and 1G10, we generated escape viruses against the mAbs to look for escape strategies employed by the viruses against inhibition by the mAbs. We identified two mutations in the mAb 1A9 escape clones and three mutations in the mAb 1G10 escape clones (Fig. 4.7). The mutations in the mAb 1A9 escape clones were found near or within the binding site of the mAb, suggesting that the mechanism of inhibition could be via the disruption of binding activity between the mAb and S. The mutations found in the mAb 1G10 were located further upstream of the HR1 domain, which may indicate an escape strategy that changes the HR1 conformation to facilitate interaction with the mAb-bound

HR2 domain for fusion to progress. The importance of upstream sequences to HR2 inhibition was recently demonstrated in a MHV study that reported mutations in the HR1 region in viruses that escape from HR2-derived peptide inhibition (Bosch et al., 2008a).

Further analysis of the contribution of these mutations to the escape activity was performed using a pseudovirus assay. Our results suggest that the two mutations identified in mAb 1A9 escape clones were positively contributing to the escape activity of pseudoviruses bearing the S mutants (fig. 4.8). However, the three mutations identified in the mAb 1G10 escape clones did not contribute to any escape activity of the psudoviruses bearing these S mutants (Fig. 4.8). This may indicate that the single mutation was inefficient in the viral escape from mAb1G10. Such mutations may still contribute to low viral escape activity in the infectious virions but the fitness of these viruses may be compromised. This low viral escape activity may not be evidently detected in the pseudovirus assay.

Since the mutations found in mAb 1A9 escape clones were detected to be positively contributing to the escape activity of pseudoviruses, we performed more experiments to understand the escape strategies. As shown in Fig. 4.9A and B, the binding of mAb 1A9 to S(D1128A) and S(N1056K, D1128A) mutants were clearly reduced, suggesting that the mutation D1128A reduces the binding affinity of mAb 1A9 for the virus to escape inhibition by the mAb. However, the mutation N1056K does not reduce the binding activity of mAb 1A9 but could still escape from the mAb inhibition.

To investigate the possibility of the synergism between the two mutations which contribute to escape activity, we performed a dose-dependent neutralization assay of the pseudoviruses bearing the single mutants as well as the double mutant. The results

showed that the pseudoviruses bearing the double mutation exhibited a higher escape activity than any of the two single mutants, suggesting that the N1056K mutation may synergize the mAb 1A9 escape activity of the D1128A mutation (Fig. 4.9C). The mAb 1A9 binding site as well as the amino acids that were shown to be critical for its neutralizing activity (N1056 and D1128) were highly conserved among the human (early, middle and late phases strains), civet (SZ3 and PCC4 strains) and raccoon dog (SZ16 strain) SARS-CoV and bat (Rp3 and Rf1 strains) SL-CoV, suggesting that this region could be further explored for the design of a cross-neutralizing vaccine or therapy (Fig. 4.10).

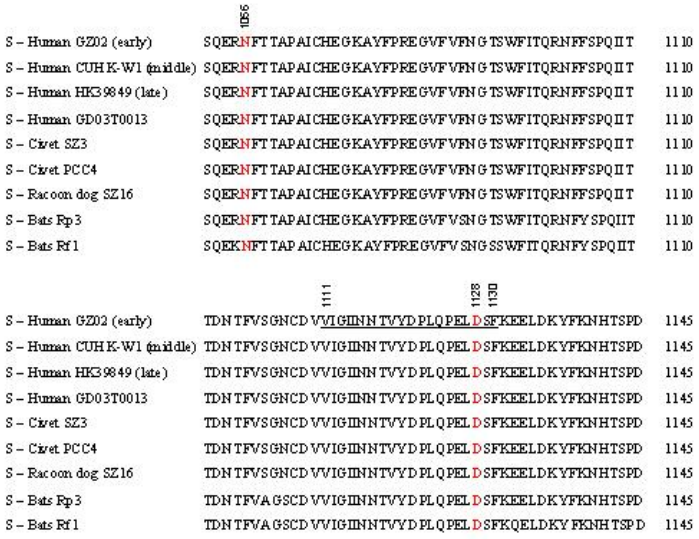

Fig. 4.10: Clustal W multiple sequence alignment of SARS-CoV and SL-CoV S proteins. The S region corresponding to the binding sites of mAb 1A9 to SARS-CoV S is aligned with the early (GZ02), middle (CHUK-W1) and late phases (HK39849) SARS-CoV strains, the civet SARS-CoV (SZ3 and PCC4), the raccoon dog SARS-CoV (SZ16) and the bat SL-CoV (Rf1 and Rp3). The amino acids that contribute to the escape activity to mAb 1A9 (N1056 and D1128) are highlighted in red in the protein sequence, while the binding site for mAb 1A9 is underlined.

CHAPTER 5: MECHANISM OF NITRIC OXIDE INHIBITION OF SARS-CoV

5.1 Peroxynitrite has no effect on SARS-CoV replication (The experiments in this section were performed by our collaborator)

It was previously demonstrated that nitric oxide (NO) treatment of SARS patients has beneficial effect and that NO inhibits SARS-CoV infection in *in-vitro* assays (Akerstrom et al., 2005; Chen et al., 2004b; Cinatl et al., 2003a; Keyaerts et al., 2004a). In this study, we try to understand the mechanism of nitric oxide inhibition of SARS-CoV. It is first demonstrated by our collaborators that peroxynitrite has no effect on SARS-CoV. SIN-1, which produces peroxynitrite, was used in conjunction with a superoxide scavenger, MnTBAP, to determine if peroxynitrite was involved in the inhibition of SARS-CoV replication. SARS-CoV infected Vero E6 cells were treated with different concentrations of SIN-1, and it was observed that no significant inhibition of viral replication occurred (Fig. 5.1A). This suggests that SIN-1 administration had no effect on the replication cycle of SARS-CoV.

Next, SARS-CoV infected Vero E6 cells were treated with different concentrations of MnTBAP together with SIN-1. MnTBAP removes the superoxide, resulting in a reduction in the amount of peroxynitrite and an increase in the amount of free NO. The results in Fig. 5.1B clearly demonstrate that with increasing amount of MnTBAP in presence of SIN-1 (400 μM), there is an inhibition in the production of progeny virus in a concentration-dependent manner. Although a slight reduction on the production of progeny virus was observed when the cells were treated with the highest concentration of MnTBAP used in this study (800 μM, Figure 5.1C), the reduction of

virus replication in cells treated with both SIN-1 and MnTBAP is significantly higher than those treated with MnTBAP alone. This slight reduction might be explained by the fact that the use of the superoxide scavenger resulted in an increase in intracellular free NO, which could then, directly or through an intermediary compound, exert an inhibitory effect.

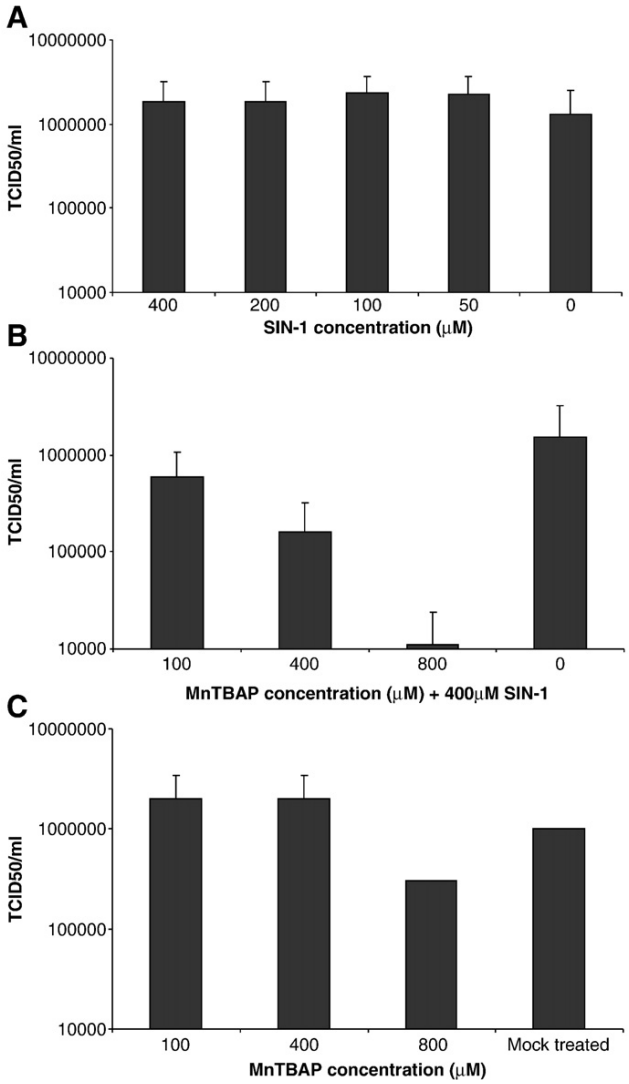

Fig. 5.1: SIN-1 treatment has no anti-viral effect on SARS-CoV infected Vero E6 cells. E6 cells were infected with SARS-CoV at an MOI of 1.0, at 1 hpi cells were treated with different concentrations of SIN-1 and/or MnTBAP. (A) Cells treated with different concentrations of SIN-1. 24 hpi, virus was harvested and titers determined. (B) Cells treated with 400 μM SIN-1 and different concentrations of MnTBAP. Virus was harvested 24 hpi and titers determined. (C) Cells treated with different concentrations of MnTBAP, virus was harvested 24 hpi and titers determined.

5.2 Treatment of NO donor leads to a reduction in the palmitoylation of the S protein of SARS-CoV

In order to determine whether nitric oxide or its derivatives were reacting with the SARS-CoV S protein, Vero E6 cells were infected with recombinant vaccinia virus carrying the S gene (rVV-L-S) and treated with the NO donor, SNAP, or a negative control, NAP. Following immunoprecipitation with nitro-tyrosine affinity sorbent (Cayman), which binds specifically to nitrated proteins, and detection of S by Western blot analysis, it was clearly demonstrated that S had been nitrated after stimulation with SNAP but not with NAP (Figure 5.2A). To determine whether the palmitoylation of S was affected by nitric oxide, cells infected with rVV-L-S were treated with either SNAP or NAP and then labelled with [^{3}H]-palmitic acid. After immunoprecipitation of the S protein with an anti-S rabbit polyclonal antibody, the amount of palmitoylated S protein detected in the SNAP treated cells was found to be greatly reduced when compared to the mock treated or NAP treated ones (Fig. 5.2B). On the other hand, if [^{35}S]-methionine-cysteine labelling was used, there was no difference in the amount of total S protein immunoprecipitated for all three treatments, indicating that SNAP treatment did not affect the expression of S (Fig. 5.2B).

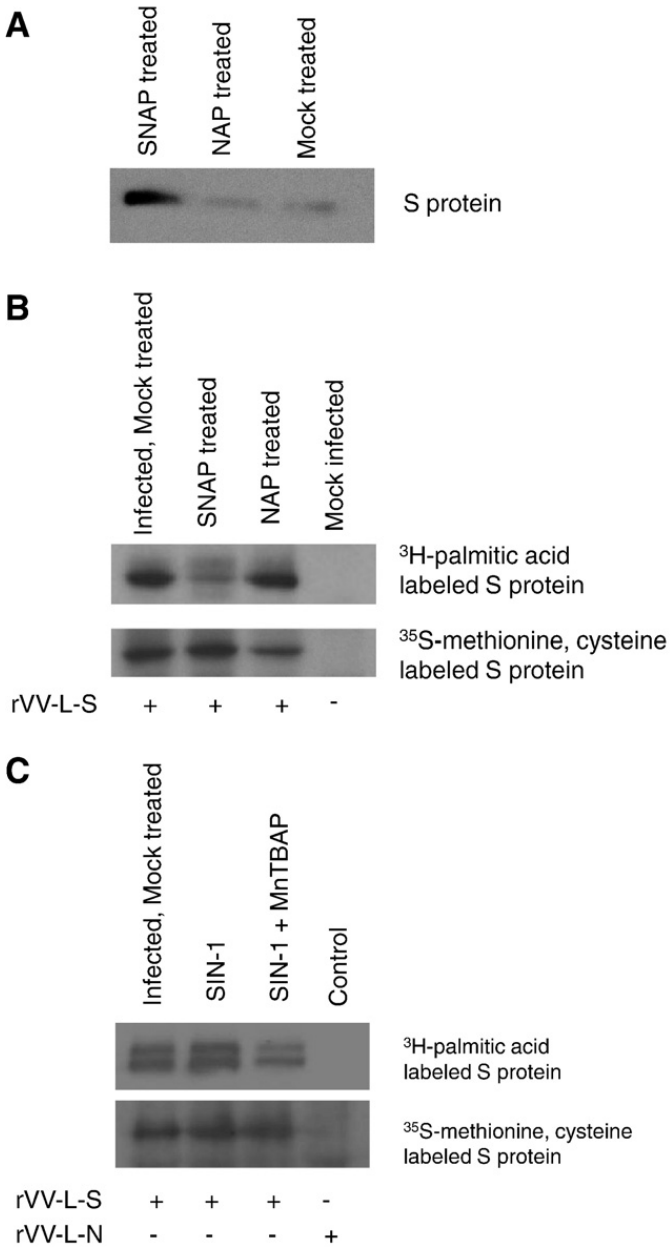

Fig. 5.2: Effect of SNAP on nitration and palmitoylation of S protein. Vero E6 cells were infected with rVV-L-S at an MOI of 0.1. At 1 hpi cells were treated with 400 μM SNAP or NAP. (A) At 24 h post-infection, the cells were lysed and immunoprecipitation was performed with nitro-tyrosine affinity sorbent. Western blot was then performed using rabbit anti-S polyclonal antibody. (B, C) At 24 h post-infection, cells were labeled with 400 μCi of [3H]-palmitic acid for 2 h, or starved with methionine-cysteine (Met-Cys)-free medium for 30 min before being labeled with 22 μCi of [35S]-methionine-cysteine for 2 h. The cells were then lysed and imunoprecipitation was performed with rabbit S polyclonal antibody to detect the amount of radio-labeled S protein.

5.3 Nitric oxide reduces the cell-cell fusion activity of S

An *in vitro* assay was used to examine the effect of nitric oxide on the cell-cell fusion activity of the S protein (Lip et al., 2006). In this case, the S-expressing cells were treated with SNAP or NAP before they were mixed with CHO-ACE2 cells stably expressing the ACE2 receptor. The formation of syncytia was observed 6 hrs later. Cells treated with SNAP showed no fusion (Fig. 5.3B), whereas cell-cell fusion was clearly visible in the NAP (Fig. 5.3C) or mock-treated cells (Fig. 5.3A). As expected, the mock-infected cells showed no fusion as the S protein was not expressed (Fig. 5.3D).

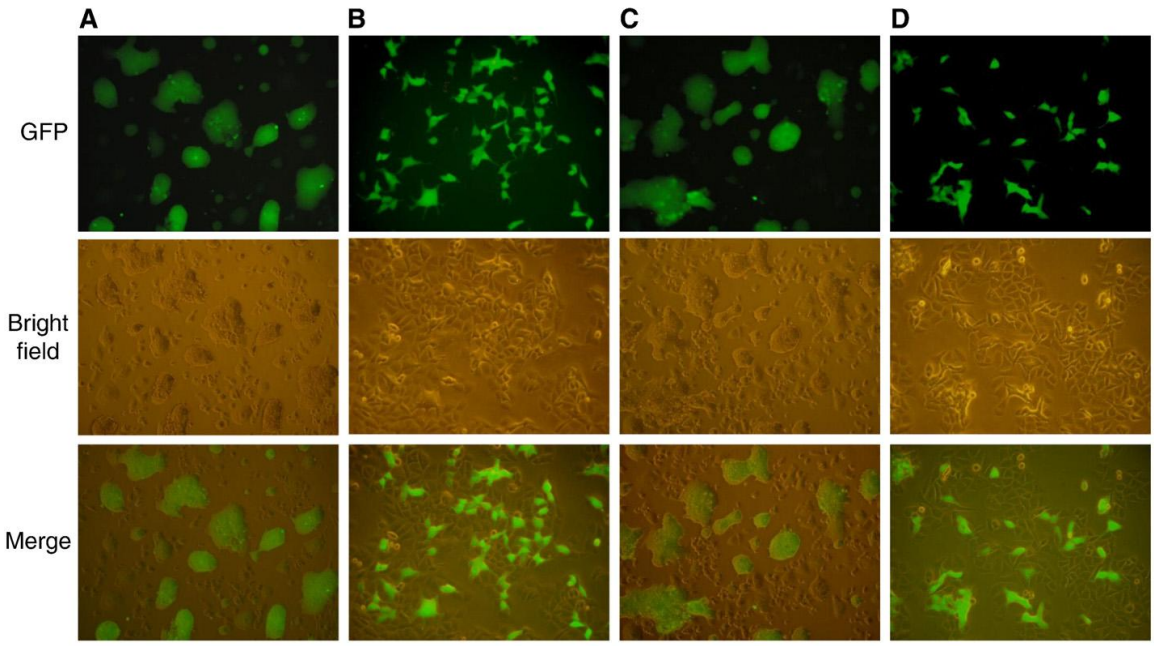

Fig. 5.3: SNAP interferes with cell–cell membrane fusion. A 293T-GFP stable cell line was infected with rVV-L-S and treated with SNAP or NAP 1 h post-infection. At 24 hpi cells were trypsinized and mixed with pre-plated CHO-ACE2 cells. 6 h after mixing the cell lines, syncytium formation was observed. (A) Infected cells, mock-treated (B) Infected cells, treated with 400 μM SNAP (C) Infected cells, treated with 400 μM NAP (D) Mock infected cells.

5.4 SARS-CoV S pseudoviruses produced in the presence of nitric oxide is less efficient in viral entry

In order to investigate the effect of SNAP on the S-mediated entry of SARS CoV into cells, we used the HIV pseudovirus system to produce pseudoviruses with S on the surface as described in chapter 4. Pseudoviruses were produced from untreated cells or cells treated with SNAP (200 μM or 400 μM) or NAP (200 μM or 400 μM). SNAP and NAP treatments did not affect the assembly of S on the pseudoviruses as Western blot analysis showed that similar amounts of S were incorporated into the pseudoviruses (Fig 5.4A). Similar to our previous observation, two forms of S were detected and these correspond to the unglycosylated and glycosylated forms of the protein. The entry of the pseudovirus into CHO-ACE2, which is stably expressing the S receptor ACE2 on the surface of the cells, was reflected by the luciferase activity in the CHO-ACE2 cells at 72h after infection. As shown in Figure 5.4B, the luciferase activity in the cells infected with pseudovirus bearing S was significantly higher than those without S as the latter contained no viral envelope protein and could not enter the CHO-ACE2 cells. The reading from the cells infected with pseudovirus bearing S was normalized to 100% for calculating percentage of infectivity. Treatment with 200 μM and 400 μM of NAP caused appropriately 15% and 25% reduction in infectivity respectively. However, treatment with 200 μM and 400 μM of SNAP resulted in a significantly higher reduction, appropriately 70%, in infectivity. In order to exclude any effect on the binding of S to ACE2, a p24 ELISA kit (Perkin Elmer) was used to determine the concentration of virus bound to cells infected with the pseudoviruses which had been produced in cells either treated with 400 μM SNAP or 400 μM NAP. As shown in Fig. 5.4C, SNAP and NAP

treatment had no significant effect on the concentration of bound virus, indicating that the primary effect of SNAP treatment on the S occur post-binding, possibly during entry.

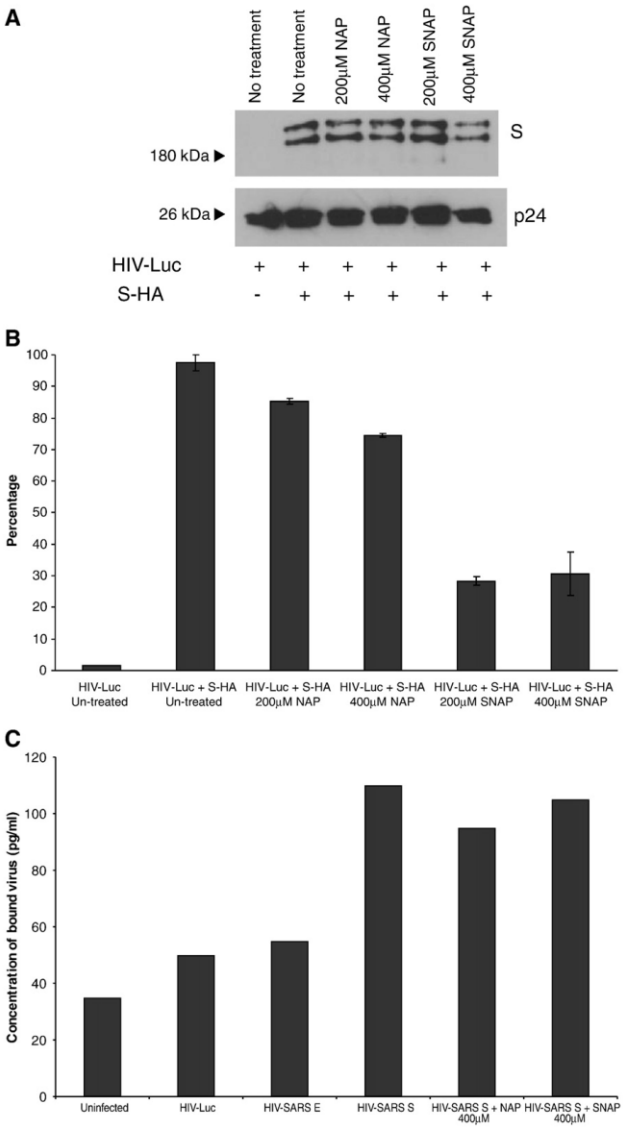

Fig. 5.4: SARS-CoV S pseudoviruses produced in the presence of SNAP is less efficient in viral entry. Pseudoviruses produced under different conditions were purified and concentrated using ultra-centrifugation through a 20% sucrose bed. (A) The presence of S and HIV-1 p24 proteins in the purified viruses were determined by Western blot analysis. (B) Purified viruses were used for the transduction of CHO-ACE2 cells and the degrees of viral entry were determined by measuring the luciferase activities. Percentages of infectivity were computed by normalizing the entry of untreated S-bearing pseudoviruses to 100%. Means and standard deviation from duplicate readings were shown. (C) Nitric oxide or its derivatives do not exert a noticeable effect on the binding of the SARS S protein to ACE2. Cells were infected with pseudotyped virus bearing the S protein, produced under SNAP or NAP treatment. A p24 ELISA kit was used to measure p24 concentration and concentration of bound virus was derived from a standard graph.

5.5 Discussion

It was previously shown by Akerstrom et al. that NO inhibits the replication cycle of SARS-CoV (Akerstrom et al., 2005). In tissues that are stressed or inflamed, both NO and O_2 are elevated. Although SNAP predominantly increases the NO level in the cell, peroxynitrite can also be elevated when NO can react with endogenous O_2. In this study, Our collaborators showed that unlike SNAP, treatment of SARS-CoV infected Vero E6 cells with SIN-1 has no significant effect on the production of progeny virus (Fig. 5.1A), suggesting that peroxynitrite does not inhibit SARS-CoV replication. Moreover, if a superoxide scavenger (MnTBAP) is used to remove the O_2^- and allow more NO to accumulate inside the SIN-1- treated cells, a significant inhibition of the virus replication was observed (Fig. 5.1B). This suggests that it is NO or a derivative of NO that inhibits the virus replication. Further studies were then carried out to understand the mechanism of NO inhibition of SARS-CoV.

Petit et al. have demonstrated that palmitoylation of the SARS-CoV S protein plays a role in S-mediated cell–cell fusion (Petit et al., 2007). By substituting select cysteine clusters at the carboxyl terminus of the S protein for alanines, it was shown that palmitoylation of at least two cysteine clusters at the C-terminus was important in membrane fusion that occurred after binding of the S protein to its cognate ACE2 receptor, critical to the infectivity of SARS-CoV. It has also been previously shown that NO or its derivatives have an effect on the palmitoylation of the rat myelin protein (Bizzozero et al., 2001). In agreement with both of these findings, our results in this work indicate that NO or its derivatives reduce the palmitoylation of the S protein and consequently exerts an effect downstream of the S protein binding to ACE2, which is

shown by the cell–cell fusion assay (Fig 5.2 and 5.3). However, the cell–cell fusion assay does not address the question of whether the under-palmitoylation of the S protein affects its expression, folding or incorporation into the mature virus particle. Hence, we created a HIV pseudovirus which incorporates S into the virus particle. The results showed that SNAP treatment of cells does not affect the expression or incorporation of the S protein but decreases the infectivity of the pseudovirus (Fig 5.4).

In the same study, our collaborators also examined the production of viral RNA by real-time PCR analysis (Akerstrom et al., 2009). The results showed that SNAP pre-treatment and post-treatment of SARS-CoV infected VeroE6 cells resulted in a reduction of the production of positive-stranded RNA as early as 3 h post-infection and the viral RNA levels remained low even after 24 h post-infection. It was also observed that SNAP treatment resulted in a different level of replicase poly-proteins cleavage products and a reduction in the expression of the N protein. These results suggest that NO or its derivatives may alter the substrate specificities of the 3CLpro to interfere with the production of the positive-strand RNA.

In summary, the results presented here suggest that the effect of nitric oxide on the replication of SARS-CoV is at least two-fold: an effect on the production of viral RNA in the early steps of replication and a reduction in the palmitoylation of the S protein later in the replication cycle. What remains to be elucidated is whether both of these effects arise strictly from a direct effect of nitric oxide or its derivatives on viral proteins, or strictly from an effect on host factors which are subverted in the course of infection, or a combination of both.

CHAPTER 6: CHARACTERIZATION OF THE ORF8 REGION OF SARS-CoV

6.1 Characterization of the viral-viral interactions of the ORF8 proteins

6.1.1 Characterization of polyclonal antibodies to the SARS-CoV unique proteins 8a and 8b

As mentioned in Chapter 1.1.3, the ORF8 of SARS-CoV from the middle and late phases acquire a 29-nt deletion compared with virus strains from the early phase and the animal strains, resulting in the coding of two proteins, 8a and 8b, of 39 and 84 aa, respectively, instead of a single 8ab protein (Figs. 6.1A and B). In this study, we characterize these ORF8 proteins and gain a better understanding of their interactions with other structural and accessory proteins of SARS-CoV.

Mouse polyclonal antibodies were raised against bacterially expressed GST-fusion 8a and 8b proteins. To determine the specificity of these antibodies, Western blot analysis was performed to detect 8a, 8b and 8ab expressed in transiently transfected Vero E6 cells. As shown in Fig. 6.1C, mouse anti-8a polyclonal antibody specifically detected 8a and 8ab whereas mouse anti-8b polyclonal antibody detected 8b and 8ab. 8a and 8b migrated close to their predicted molecular weight of 4.5 kDa and 9.6 kDa, respectively, whereas two forms of 8ab, ~14 kDa (major) and ~12 kDa (minor), were detected (Fig. 6.1C). As the predicted molecular weight of 8ab is 13.8 kDa, the minor form is likely to have arisen from cleavage of the full-length protein.

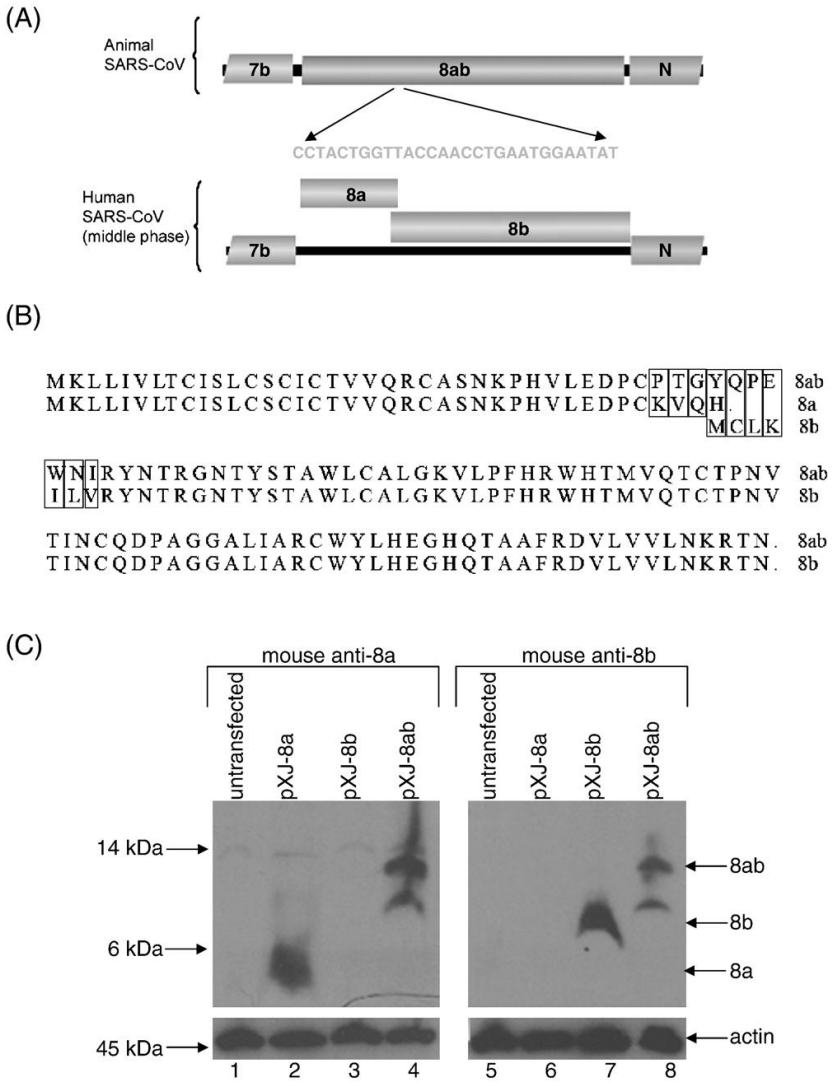

Fig. 6.1: Expressions of SARS-CoV 8a, 8b and 8ab proteins. (A) Schematic diagram showing the genetic differences in the ORF8 region of the SARS-CoV isolated from animals and humans infected during the middle phase of the SARS epidemic in 2003 (modified from Guan et al., 2003). The animal isolates have an extra 29-nucleotides insertion such that the sub-genomic RNA encodes for a single protein, termed 8ab, whereas that of the human isolates (from the middle phase) encodes two proteins, 8a and 8b. Human isolates from early and late phases of the epidemic also have the 29-nucleotides insertion found in the animal SARS-CoV. (B) Alignment of the sequences of 8a, 8b and 8ab proteins used in this study. Mismatches between 8a and 8ab or 8b and 8ab are boxed. The 8ab is reconstructed from a human isolate from the middle phase (SIN2774) by insertion of the 29-nucletoides found in a human isolate from the early phase (GZ02). (C)Western blot analysis was performed to detect 8a, 8b and 8ab proteins expressed in Vero E6 cells using cDNA constructs. The experiments were performed with either mouse anti-8a polyclonal antibody (upper panel, lanes 1–4) or mouse anti-8b polyclonal antibody (upper panel, lanes 5–8). Equal amounts of cells were used in each lane as verified by the level of endogenous actin (bottom panel).

6.1.2 Expression of 8a and 8b in SARS-CoV infected Vero E6 cells

SARS-CoV 2003VA2774, an isolate from a SARS patient in Singapore, was used to infect Vero E6 cells as previously described (Tan et al., 2004a) and anti-8a or anti-8b polyclonal antibodies were used in indirect immunofluorescence experiments to determine the expression of 8a and 8b, respectively, in infected cells (Figs. 6.2A and B). The 8a and 8b proteins were detected in SARS-CoV infected cells and were found to be localized in the cytoplasm. The same antibodies were used to examine the detailed cellular localization of 8a, 8b and 8ab, expressed from DNA constructs, in Vero E6 cells (Figs. 6.2A and B). Whereas 8a and 8b were found in punctuate vesicle-like structures throughout the cytoplasm, 8ab was found to be diffused in the cytoplasm. Hence, there appears to be significant differences in the conformations of 8a and 8ab although 35 out of 39 aa of 8a is present in the 8ab protein (Fig. 6.1B). Similarly, 77 out of 84 aa of 8b is present in 8ab, but the cellular localization of 8b is distinct from 8ab.

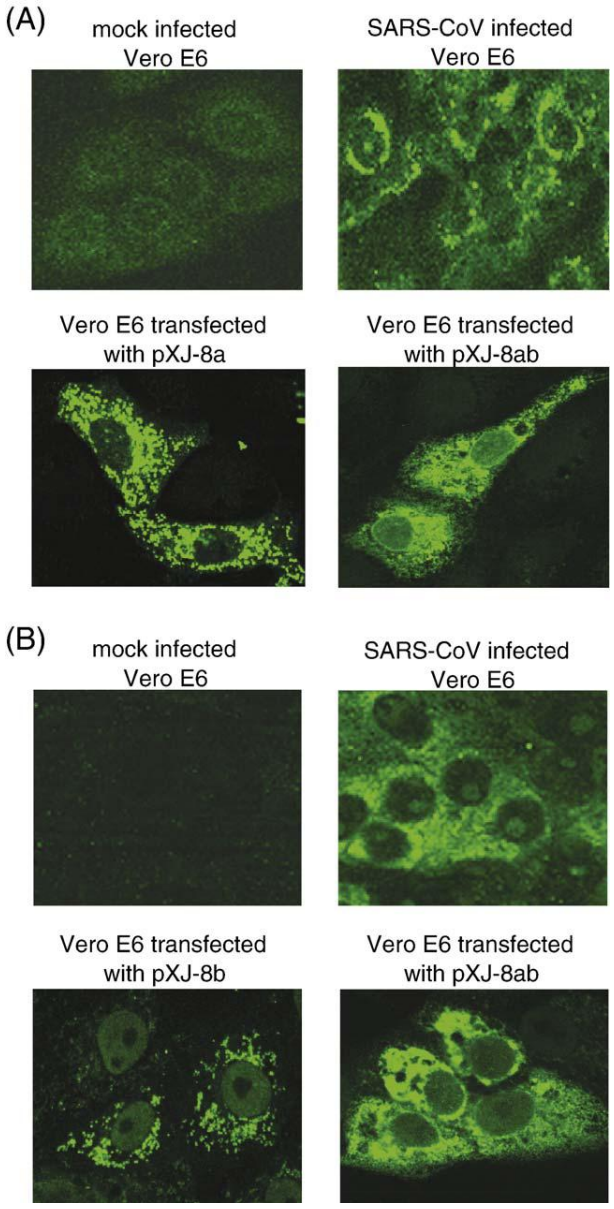

Fig. 6.2: Cellular localizations of 8a and 8b in SARS-CoV-infected cells and Vero E6 cells transfected with DNA constructs for expressing 8a, 8b and 8ab. Specific mouse anti-8a and anti-8b polyclonal antibodies were used in indirect immunofluorescence experiments to determine the expressions of (A) 8a and (B) 8b, respectively. The top two panels showed the specific reactivities of the anti-8a and anti-8b antibodies to proteins expressed in SARS-CoV-infected cells (right panels) as no unspecific staining was observed for the mock-infected cells (left panels). The bottom two panels showed the reactivities of the antibodies to 8a and 8ab (A) or 8b and 8ab (B) expressed in Vero E6 by transfection of cDNA constructs.

6.1.3 Interactions of 8a, 8b and 8ab with other SARS-CoV proteins

In order to further characterize the cellular properties of 8a, 8b and 8ab, co-immunoprecipitation experiments were performed to determine if these proteins can interact with the SARS-CoV structural proteins, S, M, E and N, as well as two SARS-CoV accessory proteins, 3a and 7a, which were previously shown to be expressed in SARS-CoV-infected cells (Fielding et al., 2004; Tan et al., 2004a). All these proteins were not tagged except for M, where the C terminus was fused with a HA tag because of the lack of a suitable antibody for the detection of M. 8a, 8b and 8ab were fused at their C termini with a myc tag so that it is possible to compare the relative expression of the three proteins in this experiment. N-terminal-tagged myc-GST was used as a negative control. The results showed that 8a-myc interacted strongly with S, 8b-myc interacted strongly with M, E, 3a and 7a and 8ab-myc interacted strongly with S, 3a and 7a (Table 6.1 and Fig. 6.3). These results showed that the binding profiles of 8a, 8b and 8ab are clearly distinct, suggesting that the conformations of the 8a and 8b proteins may be quite different from the 8ab protein.

Table 6.1: The interactions between SARS-CoV 8a, 8b and 8ab with other viral proteins were determined by co-immunoprecipitation experiments.

Bait protein [a]	Interacting partners [b]					
	S	E	M	N	3a	7a
8a-myc	Strong	Weak	No	No	No	No
8b-myc	No	Strong	Strong	No	Strong	Strong
8ab-myc	Strong	No	Weak	No	Strong	Strong

[a] These proteins were immunoprecipitated using myc-polyclonal antibody and Protein A agarose.
[b] These proteins were co-expressed with the bait proteins and co-immunoprecipitation experiments were performed to be determined if they could bind the bait proteins.

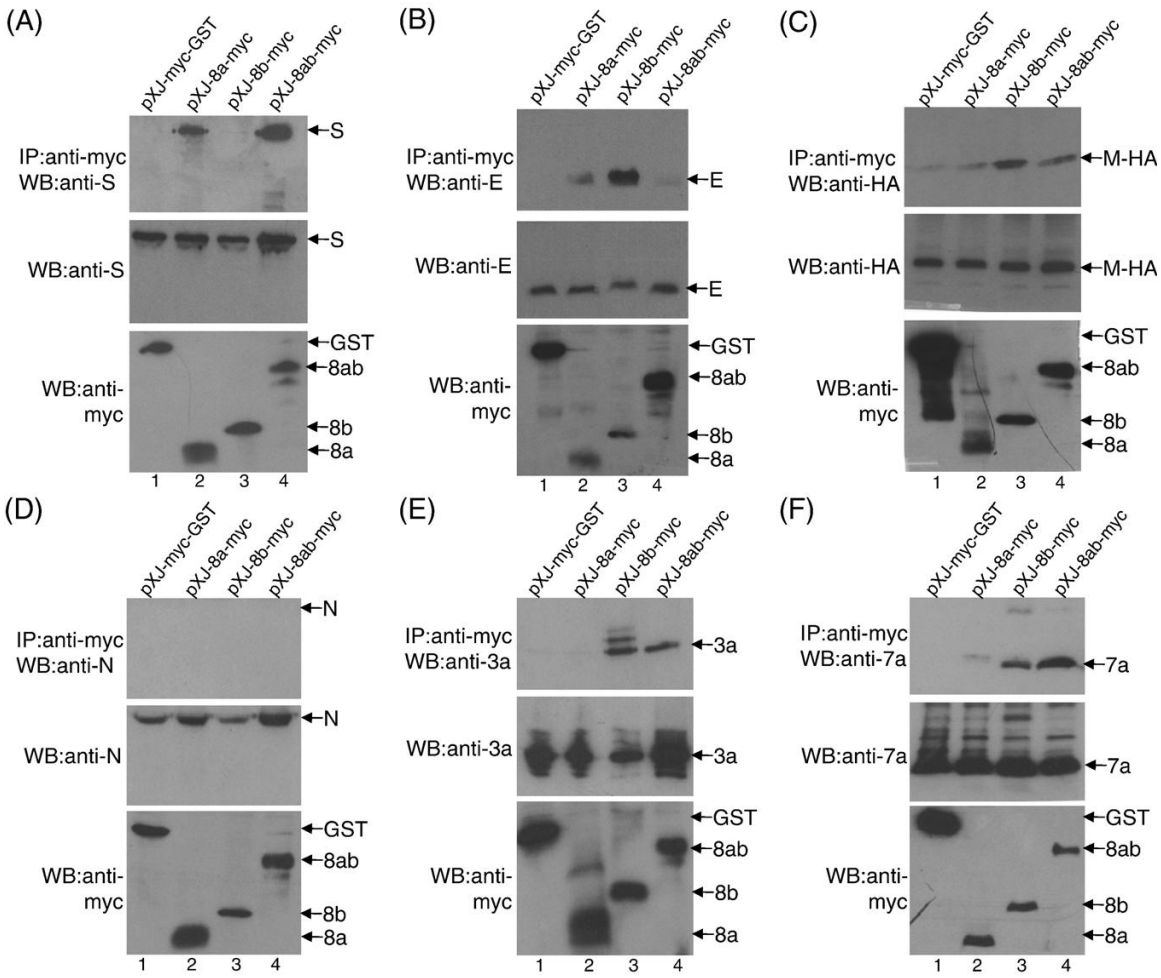

Fig. 6.3: Interactions of 8a, 8b and 8ab with other SARS-CoV proteins. Cell lysates containing myc-GST (lane 1), 8a-myc (lane 2), 8b-myc (lane 3) or 8ab-myc (lane 4) and another SARS-CoV protein (S, E, M-HA, N, 3a or 7a) were immunoprecipitated with an anti-myc polyclonal antibody and protein A-agarose beads. (A) The amounts of S protein co-immunoprecipitated (IP) by the myc-tagged proteins were determined using an anti-S monoclonal antibody (top panel). The amounts of S and myc-tag proteins in the lysates before co-immunoprecipitation were also determined by Western blot (WB) with anti-S and anti-myc monoclonal antibodies, respectively (middle and bottom panels). The same experiments were performed for panels B–F except that different antibodies against the specific viral proteins were used, namely (B) anti-E mouse polyclonal; (C) anti-HA monoclonal (as them protein fused with a HA tag at the C terminus); (D) anti-N mouse polyclonal; (E) anti-3a mouse polyclonal; (F) anti-7a mouse polyclonal.

6.2 8b down-regulates the small envelope protein (E) in SARS-CoV infected cells

6.2.1 Over-expression of 8b down-regulates the expression of E protein

While performing the co-immunoprecipitation experiments, we observed that the expression of E was significantly reduced in the presence of 8b. The co-transfections of pXJ-E and pXJ-8b-myc into 293 T cells were repeated using different amount of the pXJ-8b-myc construct. As shown in Fig. 6.4A, the down-regulation of E expression was specific and dependent on the expression levels of 8b-myc (lane 3 and lanes 5–10). On the contrary, the expressions of E were similar when pXJ-E was co-transfected with control plasmid (pXJ-myc-GST) (lane 1) or pXJ-8a-myc (lane 2) or pXJ-8ab-myc (lane 4). In order to determine if 8b has any effect on the expression of other SARS-CoV proteins, 8b was co-expressed with S (Fig. 6.4B, lane 1) or M-HA (Fig. 6.4B, lane 3) or N (Fig. 6.4B, lane 5) or 3a (Fig. 6.4B, lane 7) or 7a (Fig. 6.4B, lane 9). The results showed that 8b did not have any significant effect on the expression of these other viral proteins examined here. The down-regulation of E expression by 8b was also observed when untagged forms of 8b and E were co-expressed in Vero E6 and 293 T cells (Fig. 6.4C, lanes 1 and 3). Indirect immunofluorescence experiments also showed that E and 8b co-localized partially in Vero E6 cells (Fig. 6.4D).

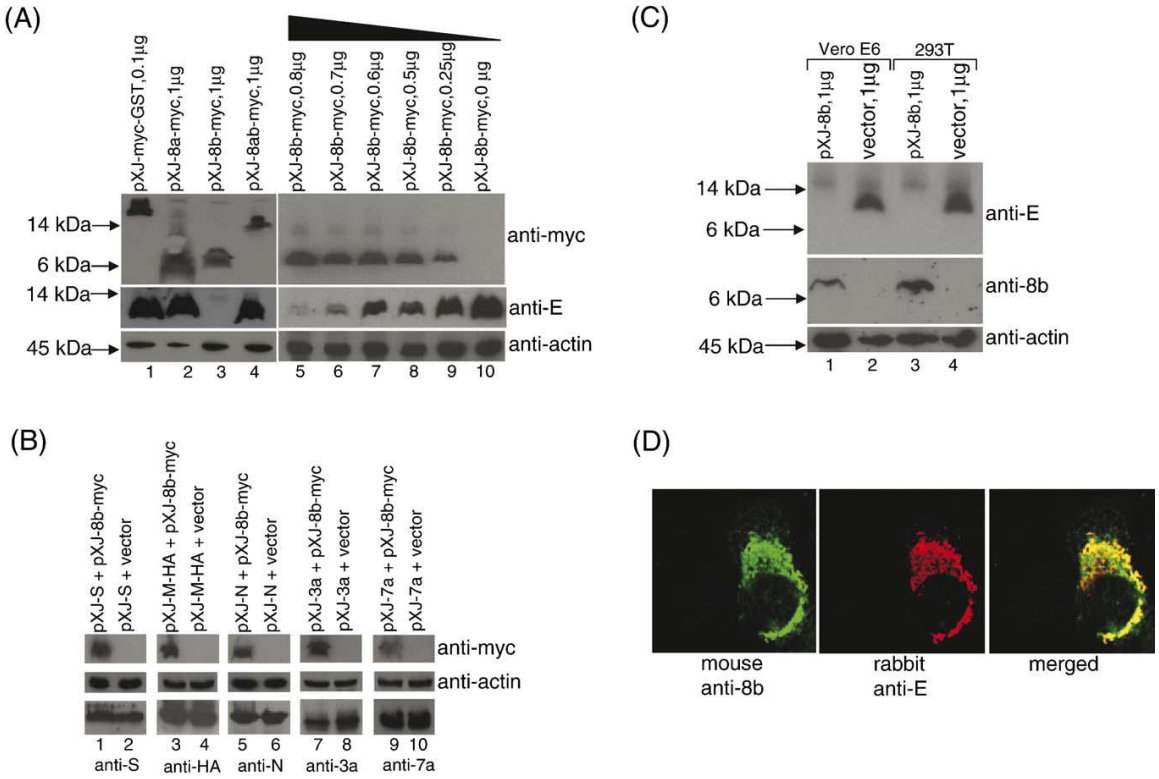

Fig. 6.4: Effects of 8b on the expression of the small structural protein, E. (A) 293T cells were co-transfected with 2 μg of pXJ-E and 0.1 μg of pXJ-myc-GST (lane 1), 1 μg of pXJ-8a-myc (lane 2), pXJ-8b-myc (lane 3), pXJ-8ab-myc (lane 4), or decreasing amount of pXJ-8b-myc (lanes 5–10). Total cell lysates were subjected to Western blot analysis to determine the expression of E (middle panel) and myc-tagged proteins (top panel). Equal amounts of cells were used in each lane as verified by the level of endogenous actin (bottom panel). (B) 293T cells were co-transfected with 1 μg of pXJ-S and 1 μg of either pXJ-8b-myc or empty vector (lanes 1 and 2). Total cell lysates were subjected to Western blot analysis to determine the expression of 8b-myc (top panel) and S (lower panel). Equal amounts of cells were used in each lane as verified by the level of endogenous actin (middle panel). Similar experiments were performed with 1 μg of pXJ-M-HA (lanes 3 and 4), 0.25 μg of pXJ-N (lanes 5 and 6), 0.4 μg of pXJ-3a (lanes 7 and 8) or 0.4 μg of pXJ-7a (lanes 9 and 10). (C) Vero E6 or 293T cells were co-transfected with 2 μg of pXJ-E and 1 μg of pXJ-8b (lanes 1 and 3) or 1 μg of empty vector (lanes 2 and 4). Total cell lysates were subjected to Western blot analysis to determine the expression of E (top panel) and 8b (middle panel). Equal amounts of cells were used in each lane as verified by the level of endogenous actin (bottom panel). (D) Indirect immunofluorescence experiments were performed to determine the cellular localization of 8b and E in Vero E6 cells co-transfected with pXJ-8b and pXJ-E. The expression of 8b is represented by FITC staining (left panel), whereas the expression of E is represented by rhodamine staining (middle panel). The merged images showed that the 8b and E partially co-localized in co-transfected cells (right panel).

6.2.2 Expression of 8b did not reduce the transcription of the E gene

In order to determine if the effect of 8b on the expression of E is due to inhibition of the transcription of the E gene, Northern blot analysis was performed to determine the mRNA level of E in the presence or absence of 8b protein. The results showed that the mRNA level of E was not decreased in 293 T cells co-transfected with pXJ-E and pXJ-8b-myc (Fig. 5, lane 2) when compared to cells transfected with pXJ-E alone (Fig. 6.5, lane 1), but rather there appeared to be an increase in the mRNA level of E in the presence of 8b. This implies that the down-regulation of E protein expression by 8b is not due to a reduction of the transcription of the E gene and is likely to be post-translational. No signal was detected in un-transfected cells (Fig. 6.5, lane 3), showing that the hybridization probe is highly specific for mRNA of E. The experiment was repeated three times and a representative set of data was presented.

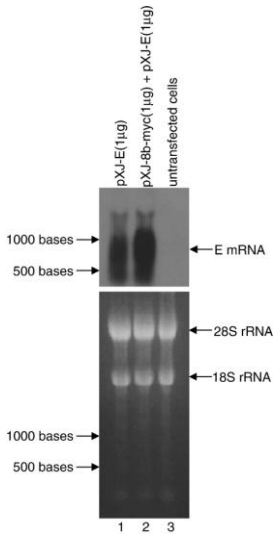

Fig. 6.5: Effects of 8b protein on the transcription of the E gene determined by Northern blot analysis. Equal amount of total RNA (15 µg) isolated from 293T cells transfected with pXJ-E (lane 1), pXJ-8b-myc and pXJ-E (lane 2) cDNA constructs or un-transfected 293T (lane 3) was separated on a denaturing agarose gel and transferred to nylon membrane. The amounts of E mRNA present were determined by hybridization with an E gene-specific probe (top panel). In order to verify that equal amounts of total RNA were loaded in each lane of the agarose gel before transfer, the amounts of 18S and 28S ribosomal RNA were visualized under UV light (bottom panel).

6.2.3 The 8b protein can bind E in SARS-CoV infected cells

Co-immunoprecipitation experiment was also performed to determine the interaction between 8b and E in SARS-CoV infected cells. Lysates from mock-infected or SARS-CoV infected cells were immunoprecipitated using rabbit anti-8b polyclonal antibody (Fig. 6.6, lanes 4 and 6) or an irrelevant antibody (rabbit anti-HA polyclonal antibody, lanes 3 and 5). The results showed that the E protein present in the lysates from SARS-CoV-infected cells could bind specifically to the 8b protein (lane 6). No unspecific binding was observed with the irrelevant antibody (lane 5).

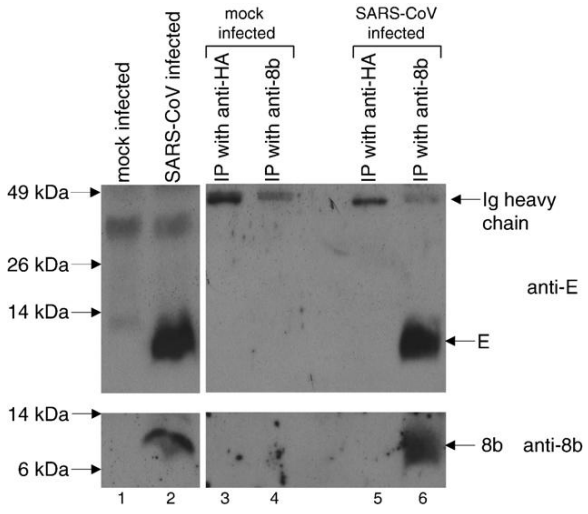

Fig. 6.6: Interaction between E and 8b in SARS-CoV-infected cells determined by co-immunoprecipitation experiment. Lysates from mock-infected or SARS-CoV infected cells were immunoprecipitated using rabbit anti-8b polyclonal antibody (lanes 4 and 6) or an irrelevant antibody (rabbit anti-HA polyclonal antibody, lanes 3 and 5) and protein A-agarose beads. Western blot analyses were then performed to determine the amount of E (upper panel) or 8b (lower panel) present in the lysates before immunoprecipitation (lanes 1 and 2) and the immuno-complexes on the protein A-agarose beads (lanes 3–6).

6.2.4 Expression of 8b and E are mutually exclusive in SARS-CoV infected cells

Indirect immunofluorescence experiments were further performed to determine the localization of E and 8b in SARS-CoV infected cells. Strikingly, cells that were expressing high levels of 8b did not have detectable levels of E (Fig. 6.7). Two representative sets of data were presented and cells expressing high levels of 8b were marked with white asterisks. Hence, it appears that 8b can down-regulate the expression of E during SARS-CoV infection.

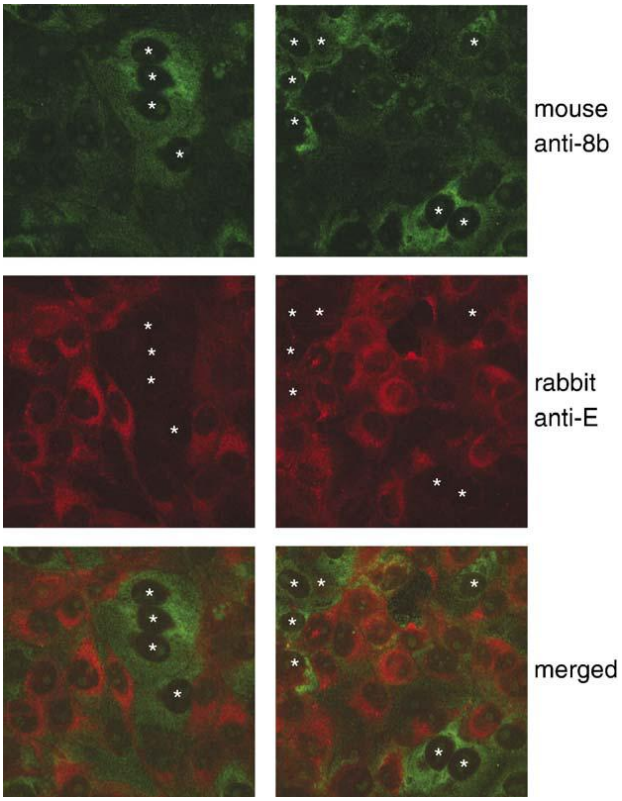

Fig. 6.7: Expressions of E and 8b in SARS-CoV-infected cells determined by indirect immunofluorescence experiments. The expression of 8b was represented by FITC staining (top row), whereas the expression of E was represented by Rhodamine staining (middle row). The merged images showed that the expression of 8b and E were mutually exclusive (bottom row). Two representative sets of data were presented and cells expressing high levels of 8b were marked with white asterisks.

6.3 Discussion

Genomic studies predicted that the reservoirs of SARS-CoV are bats, with the palm civet acting as the amplification media before spilling the virus over to the human population (Cheng et al., 2007; Graham and Baric, 2010; Song et al., 2005; Vijaykrishna et al., 2007). As the virus switched from host to host, genomic changes take place due to the high error rate of the viral RNA-dependent RNA polymerase and absence of a proof-reading mechanism, allowing for the evolution of new strains and selection of the fittest strains (Domingo et al., 1996). During human-to-human transmission in the middle phase of the epidemic, the ORF8 region of the SARS-CoV acquired a 29-nucleotide deletion, resulting in the removal of the 8ab protein and the acquisition of 2 new proteins, 8a and 8b (Guan et al., 2003). Whether this genomic change is a result of the instability of the genome or the acquisition of new functions for host adaptation remains to be addressed.

In this study, we detected the expression of 8a and 8b in Vero E6 cells infected by a human SARS-CoV isolated from the middle phase (SIN2774; GenBank accession number AY283798) and showed that the cellular localizations of 8a and 8b are distinct from 8ab (Fig. 6.2). We used co-immunoprecipitation of over-expressed proteins in mammalian cells to determine the abilities of these proteins to interact with different SARS-CoV proteins and showed that the binding profiles of 8a, 8b and 8ab are different (Fig. 6.3). Although these viral–viral protein interactions need to be verified in infected cells, these observations implied that there are conformational differences between these protein when they are expressed as separate proteins (8a and 8b) and when they are expressed as a single fused protein (8ab).

It has been demonstrated that the palm civets are equally susceptible to the human SARS-CoV isolate BJ01 from the middle phase (with the 29-nt deletion) and the isolate GZ01 from the early phase (Wu et al., 2005). Using reverse genetic methods, Yount and co-workers also reported similar findings in the mouse model (Yount et al., 2005). These results suggested that the 8a, 8b and 8ab proteins are not essential for viral replication or pathogenesis in the mouse and palm civet models. However, we found that the expression of 8b can down-regulate the expression of E in a dose-dependent manner (Fig. 6.4A) and the expression of 8b and E in SARS-CoV-infected cells were mutually exclusive (Fig. 6.7). Interestingly, the expression of E was not affected by either 8a or 8ab (Fig. 6.4A). In addition, Northern blot analysis showed that the mRNA level of E was not decreased in the presence of the 8b protein, suggesting that the effect of 8b on the expression of the E protein is likely to be post-translational (Fig. 6.5).

Although the co-expression of SARS-CoV E and M is sufficient for the assembly of viral-like particles in the baculovirus system (Ho et al., 2004; Mortola and Roy, 2004), it was demonstrated by reverse genetic techniques that the E protein is not essential for the replication of SARS-CoV in Vero E6 cells (DeDiego et al., 2007). However, the deletion of the E gene from SARS-CoV attenuated virus replication significantly both *in vivo* and *in vitro* (DeDiego et al., 2007). In addition, it was reported that over-expression of SARS-CoV E can induce apoptosis in T cells (Yang et al., 2005b); thus, the down-regulation of E may also have an effect on viral pathogenesis.

An interesting question that arises from our observations concerns the regulation of 8b expression during SARS-CoV infection. 8a and 8b are encoded by the bicistronic subgenomic RNA 8 produced in SARS-CoV-infected cells (Marra et al., 2003; Snijder et

al., 2003). Because its translation initiation codon is not the first AUG in the subgenomic RNA, the 8b protein is likely to be expressed via an internal ribosomal entry mechanism or by a leaky ribosomal scanning mode of translation, as have been described for viral proteins encoded by other bicistronic or tricistronic coronaviral mRNAs (Liu and Inglis, 1992; Senanayake and Brian, 1997; Thiel and Siddell, 1994). However, in order for 8b to be expressed via such mechanisms, activation of certain host translational machinery may be necessary (Komar and Hatzoglou, 2005; Stoneley and Willis, 2004). Indeed, we observed that 8b was only expressed in a fraction of the SARS-CoV-infected cells (Fig. 6.7). This means that the effect of 8b on viral replication or pathogenesis is likely to be only modulative as viral replication in those cells that did not express high levels of 8b will be normal. However, this modulating mechanism is not functional in the animal SARS-CoV because 8ab does not appear to have any effect on the expression of E. In future studies, it will be crucial to determine the underlying mechanism regulating the expression of 8b and its temporal expression during the viral replication cycle.

CHAPTER 7: SARS-CoV 8b REDUCES VIRAL REPLICATION BY DOWN-REGULATING E VIA AN UBIQUITIN-INDEPENDENT PROTEOSOME PATHWAY

7.1 Inhibition of the protein 8b-mediated rapid degradation of the E protein by proteasome inhibitor

In Chapter 6, we found that the SARS-CoV E was down-regulated by 8b in a post-translational manner. In this study, we aim to understand the mechanism of down-regulation of E by 8b. First, we explore the possibility of a proteasome-mediated down-regulation of E by 8b. To determine whether proteasome inhibitor, MG132, could inhibit the protein 8b-mediated degradation of the SARS-CoV E, co-expression of protein 8b with E in transfected cells in the presence or absence of the inhibitor was carried out. Analysis of the E expression by Western blot with antibodies to E showed that the addition of MG132 (50 μM) blocked the rapid degradation of SARS-CoV E (Fig. 7.1, top panel). However, addition of 50 μM MG132 did not significantly affect the accumulation of protein 8b when the protein was over-expressed in cells (Fig. 7.1, second panel).

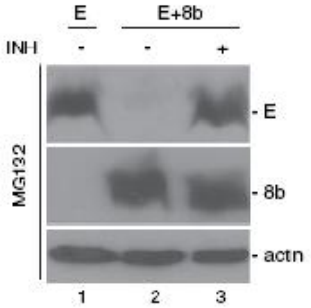

Fig. 7.1: Inhibition of protein 8b-mediated rapid degradation of the SARS-CoV E protein by the proteasome inhibitor, MG132. 293T cells expressing the SARS-CoV E alone (lane 1) or co-expressing with 8b (lanes 2 and 3) were incubated with 50 μM MG132 (lane 3), and harvested at 18 h post-transfection. Total cell lysates were separated on 17.5% SDS-PAGE gels and analyzed by western blot with appropriate antibodies.

7.2 Knockout of lysine residues on 8b does not prevent its polyubiquitination and ability to down-regulate E

In a previous study, 8b was shown to undergo both monoubiquitination and polyubiquitination (Le et al., 2007). The host ubiquitin-proteasome pathway is a commonly exploited pathway by viruses for their own protein level regulation (Banks et al., 2003) and the role of an E3 ligase is to catalyze the transfer of an activated ubiquitin from an E2 to the lysine residue of the target protein (Banks et al., 2003; Ciechanover and Ben-Saadon, 2004; Hershko and Ciechanover, 1998; Wilkinson, 2000). To explore the possibility of 8b acting as an E3 ligase, a lysine knockout mutant of 8b, 8b(K4,26,81R), was generated by substituting of the three lysine residues in 8b with arginine residues. As shown in Fig. 7.2A, both 8b and 8b(K4,26,81R) underwent monoubiquitination and polyubiquitination (Fig. 7.2A, lanes 2 and 3). The monoubiquitinated product of 8b-myc was detected at ~17 kDa while the polyubiquitinated products of 8b-myc appear as a ladder. However, the monoubiquitinated 8b was somewhat reduced in the lysine knockout mutant (Fig. 7.2A, lane 3). Thus, a novel mechanism might be involved in the polyubiquitination of 8b while the lysine residues contribute partially to the monoubiquitination of 8b.

In addition, 8b(K4,26,81R) down-regulated the expression of E as well as 8b (Fig. 7.2B, lane 2 and 3). Since the polyubiquitination of 8b cannot be abolished by lysine knockout, it cannot be ascertain if the polyubiquitination of 8b is important for the 8b-mediated down-regulation of E. However, the monoubiquitination of 8b is not essential for the 8b-mediated down-regulation of E.

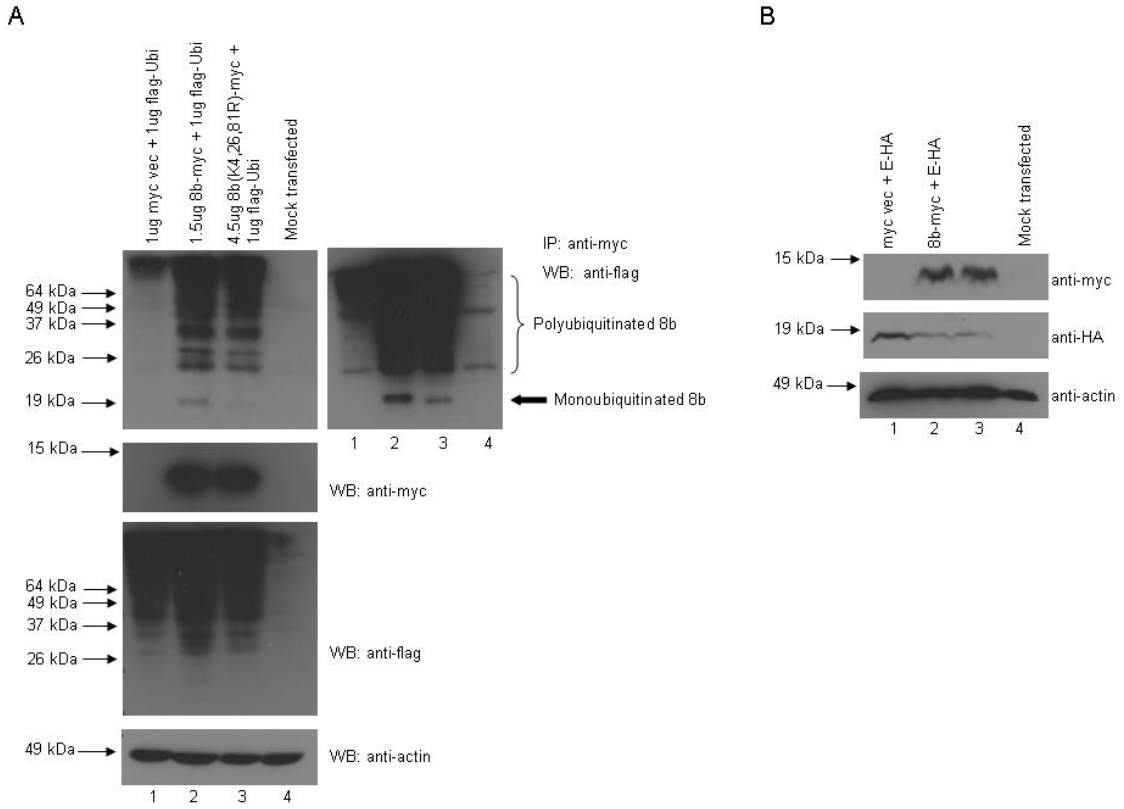

Fig. 7.2: Lysine knockout mutant of 8b undergoes polyubiquitination and down-regulates E. (A) 293T cells were transfected with cDNA constructs for expressing flag-ubiquitin (flag-Ubi) and 8b-myc or 8b(K4,26,81R)-myc. The cells were harvested at 16 h post-transfection, lysed and subjected to immunoprecipitation (IP) with anti-myc mouse monoclonal antibody and protein-A beads. The amounts of polyubiquitinated 8b-myc or 8b(K4,26,81R)-myc were determined by Western blot (WB) analysis with an anti-flag rabbit polyclonal antibody (1st panel, lanes 1-4). A darker film exposure was included (1st panel, lanes 5-8). The amounts of myc-tagged and flag-tagged proteins in the lysates before IP were determined by Western blot analysis (2nd and 3rd panels). Anti-actin monoclonal antibody was used to verify that equal amount of lysates were used in each lane (4th panel). (B) 293T cells were transfected with cDNA constructs for expressing E-HA, 8b-myc and 8b(K4,26,81R)-myc. The expressions of 8b and E were determined by Western blot analysis using anti-myc antibody (1st panel) and anti-HA antibody (2nd panel) respectively. Anti-actin monoclonal antibody was used to verify that equal amount of lysates were used in each lane (3rd panel).

7.3 Substitution of K64 to R on E increases the protein stability by reducing the polyubiquitination of E

To investigate the importance of the lysine residues on E and its polyubiquitination, three substitution mutants E(K54R), E(K64R) and E(K54,64R), were generated. As shown in Fig. 6.10A, the amounts of E protein were increased in both the E(K64R) and E(K54,64R) transfected cells when compared to wild-type E transfected cells (Fig. 7.3A, lane 1, 3 and 4). On the other hand, the expression of E(K54R) was the same as wild-type E. This result suggests that the K64R substitution can increase the protein stability of E.

A pulse-chase labeling experiment was performed in a similar manner as reported by Nal et al. (Nal et al., 2005). Consistently, the results showed that E(K64R) and E(K54,64R) decayed at slower rates than wild-type E while E(K54R) has a similar decay rate (Fig. 7.3B). The intensities of specific bands in the autoradiographs were quantified using an imaging densitometer and the percentages of remaining proteins after different times of decay were plotted. As shown in Fig. 7.3C, the half-lives of E(K64R) and E(K54,64R) are greater than 3 h while that of wild-type E and E(K54R) are less than 1 h.

Next, ubiquitination assay was performed to investigate the effects of K54R and K64R substitutions on the polyubiquitination of E. 293T cells were co-transfected with plasmids expressing flag-ubiquitin and E, E(K54R), E(K64R) or E(K54,64R), and an immunoprecipitation experiment was performed to pull-down proteins associated with the flag-tagged ubiquitin. The results showed that the K54R substitution does not affect the polyubiquitination of E(K54R) (Fig. 7.3D, lanes 2 and 3) but K64R substitution reduces the polyubiquitination of E(K64R) and E(K54,64R) (Fig. 7.3D, lanes 4 and 5).

Hence, the increase in the stabilities of E(K64R) and E(K54,64R) is correlated with a decrease in their polyubiquitination.

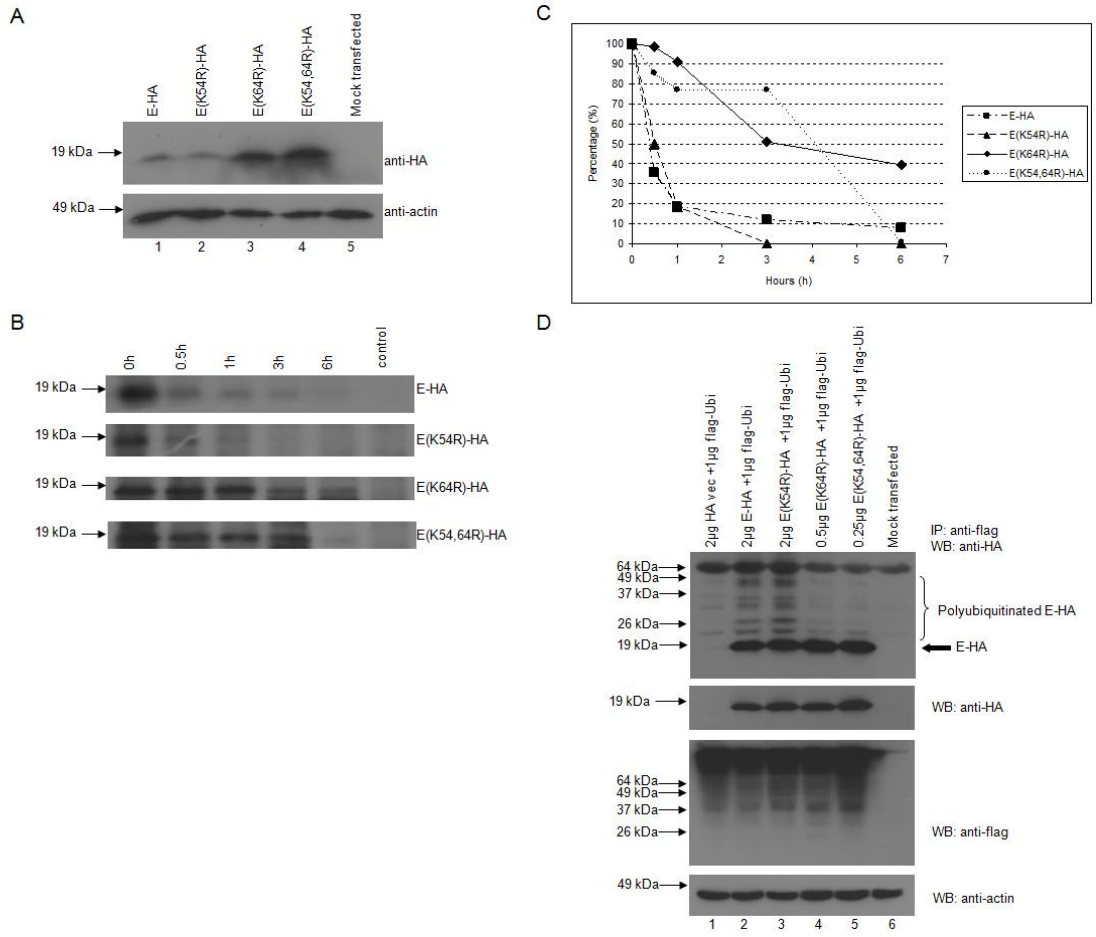

Fig. 7.3: Substitution of K64 to R on E increases its stability by reducing its polyubiquitination. (A) 293T cells were transfected with 1 µg of cDNA constructs for expressing E-HA, E(K54R)-HA, E(K64R)-HA or E(K54,64R)-HA and their protein expression levels were detected using anti-HA antibody (1st panel). Anti-actin monoclonal antibody was used to verify that equal amount of lysates were used in each lane (2nd panel). (B) Transfected cells were starved at 24 h post-transfection at 37°C for 30 min in methionine- and cysteine-free medium. Cells were pulsed for 15 min with medium containing ^{35}S-labelled methionine and cysteine amino acids and chased for 0-6 h before lysis, and subjected to IP with anti-HA monoclonal antibodies and protein-A beads. (C) A graph showing the amounts of ^{35}S radio-labeled E-HA, E(K54R)-HA, E(K64R)-HA and E(K54,64R)-HA remaining at 0.5-6 h after expression. (D) 293T cells were transfected with cDNA constructs for expressing flag-ubiquitin (flag-Ubi) and E-HA, E(K54R)-HA, E(K64R)-HA or E(K54,64R)-HA. The cells were harvested at 16 h post-transfection, lysed and subjected to IP with anti-flag mouse monoclonal antibody beads. The amounts of ubiquitinated E-HA, E(K54R)-HA, E(K64R)-HA or E(K54,64R)-HA were determined by Western blot analysis with an anti-HA rabbit polyclonal antibody (1st panel). The amounts of HA-tagged and flag-tagged proteins in the lysates before IP were determined by Western blot analysis (2nd and 3rd panels). Anti-actin monoclonal antibody was used to verify that equal amount of lysates were used in each lane (4th panel).

7.4 Both lysine residues on E are important for 8b-mediated E degradation

To determine if the lysine residues on E are important for the 8b-mediated degradation pathway, the expressions of E, E(K54R), E(K64R) and E(K54,64R) were determined in the absence or presence of 8b (Figure 7.4A). The intensities of specific bands in the autoradiographs were quantified using an imaging densitometer and the percentage reduction in E expression in the presence of 8b was computed. As shown in Figure 7.4B, both E(K54R) and E(K64R) were less sensitive to 8b-mediated degradation than wild-type E, with E(K54R) being less sensitive than E(K64R). As the double substitution mutant, E(K54,64R), was the least sensitive to 8b-mediated degradation, it appears that the contributions of K54 and K64 are additive.

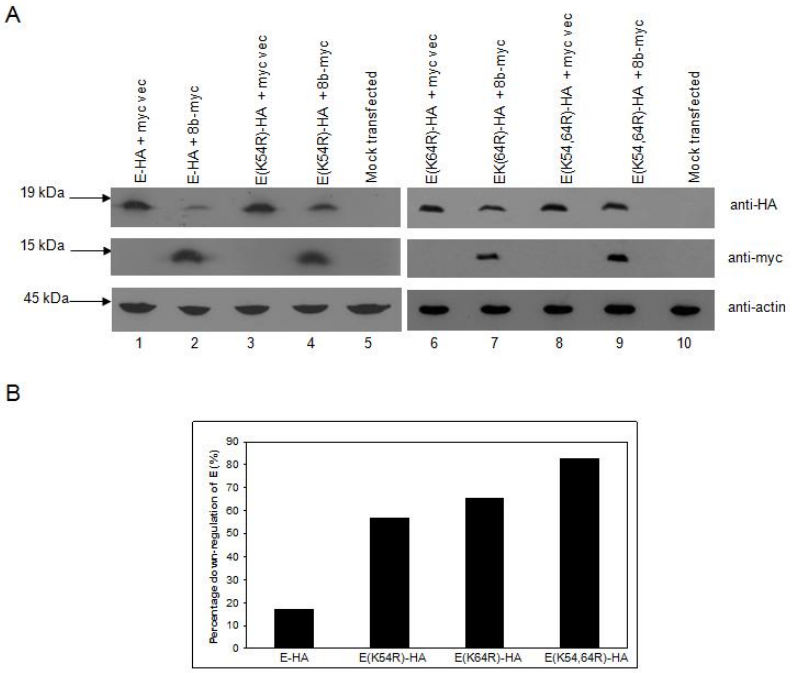

Fig. 7.4: Both lysine residues on E are involved in the 8b-mediated down-regulation of E. (A) 293T cells were transfected with cDNA constructs for expressing E-HA, E(K54R)-HA, E(K64R)-HA or E(K54,64R)-HA in the absence or presence of 8b-myc and harvested at 24 h post-transfection. The amounts of HA-tagged and myc-tagged proteins expressed were determined by Western blot analysis (1st and 2nd panels). Mock transfected cells were used as negative control (lanes 5 and 10). (B) The expression levels of E-HA, E(K54R)-HA, E(K64R)-HA and E(K54,64R)-HA were quantified with a densitometer and their expression levels in the presence of 8b relative to that in the absence of 8b are presented in the graph.

7.5 Expression of 8b increases with time in SARS-CoV infected Vero E6 cells

In chapter 6, 8b of SARS-CoV were found to be expressed in Vero E6 cells using both Western blot and immunofluorescence assays (Keng et al., 2006). However, Oostra et al. reported that they could not detect 8b in SARS-CoV infected cells at 8 h post-infection (hpi) (Oostra et al., 2007a). To address this discrepancy, the expressions of S and 8b in Vero E6 cells were analyzed at different time-points post infection (Fig. 7.5). The results showed that S was expressed early during infection and could be detected in almost all the cells at 8 hpi (Fig. 7.5, M-P). However at the 8 hpi, only a small percentage of cells have a weak expression of 8b (Fig. 7.5, F). At 24 and 32 hpi, the 8b expression increased and could be detected in a larger percentage of infected cells (Fig. 7.5, G and H, respectively). This is consistent with our previous results (Keng et al., 2006) and showed that 8b is expressed at late time-points during SARS-CoV infection.

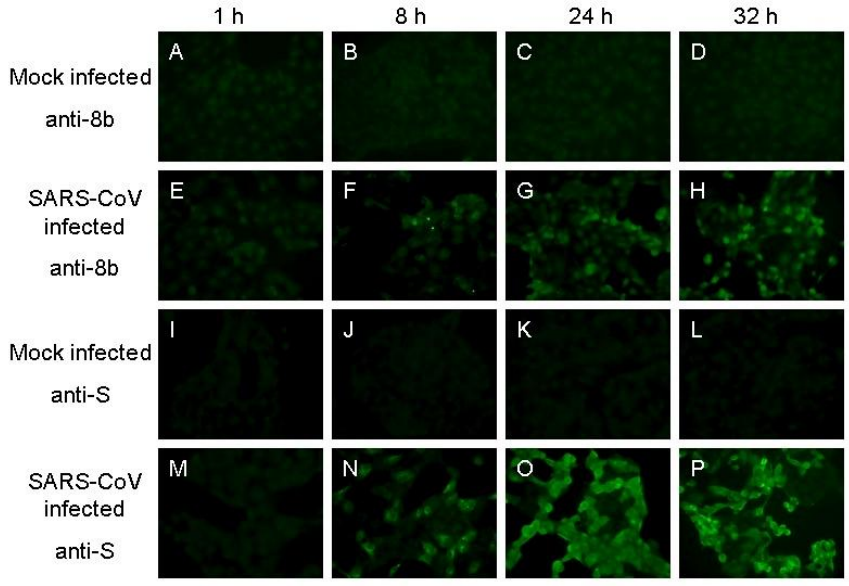

Fig. 7.5: 8b has a higher expression at late-stage infection of Vero E6 cells. Vero E6 cells were either infected with SARS-CoV (E-H, M-P) at M.O.I. of 1 or mock-infected as negative control (A-D, I-L). Cells were harvested at 1, 8, 24 and 32 hpi, fixed using 4% paraformaldehyde and permeabilized with 0.5% Triton-X 100. Expression of 8b and S were detected using anti-8b (A-H) and anti-S polyclonal antibodies (I-P), respectively.

7.6 8b is a negative modulator of SARS-CoV replication

Cells stably-expressing GFP (as control) and GFP-8b were generated to determine the effect of 8b on SARS-CoV replication. As shown by Western blot analysis (Fig. 7.6A), GFP-8b (lane 2) is expressed at a much lower expression than GFP (lane 1). To determine if the level of GFP-8b expressed in the stable cell line is sufficient to down-regulate E, the stable cell lines were transfected with the pXJ3'-E plasmid. As shown in Fig. 7.6B, the expression of E was down-regulated in GFP-8b expressing cells (lane 3) but not in the control cells expressing GFP (lane 2).

Next, the replication of SARS-CoV in these two stable cell lines was compared. The stable cell lines were infected with SARS CoV at an MOI of 0.1, and at 24 hpi, the supernatant was titrated out on a 96 well plate containing Vero E6 cells. The amount of virus was deduced by the 50 % tissue culture infective dose ($TCID_{50}$), which was calculated from the cytopathic effect (CPE) induced in cell culture by different dilutions of the harvested virus as previously described in reference (Akerstrom et al., 2005). As shown in Figure 7.6C, the amount of virus produced by the GFP-8b cells was about 10-fold lower than the GFP-expressing cells, suggesting that 8b has a negative effect on the SARS-CoV replication. The difference in viral titers is statistically significant ($p < 0.05$).

To determine if GFP-8b or GFP affects the entry of SARS-CoV into cells, a HIV pseudovirus assay that was described in chapter 4 is used (Fig. 7.6D). Luciferase readings of both stable cell lines infected with HIV pseudotyped virus bearing S (HIV-Luc-S) were similar. As would be expected, very low readings were obtained for cells infected with control pseudovirus without envelope (HIV-Luc). This suggests that the difference

in virus titers observed is not due to a change in the viral entry into cells expressing either GFP or GFP-8b.

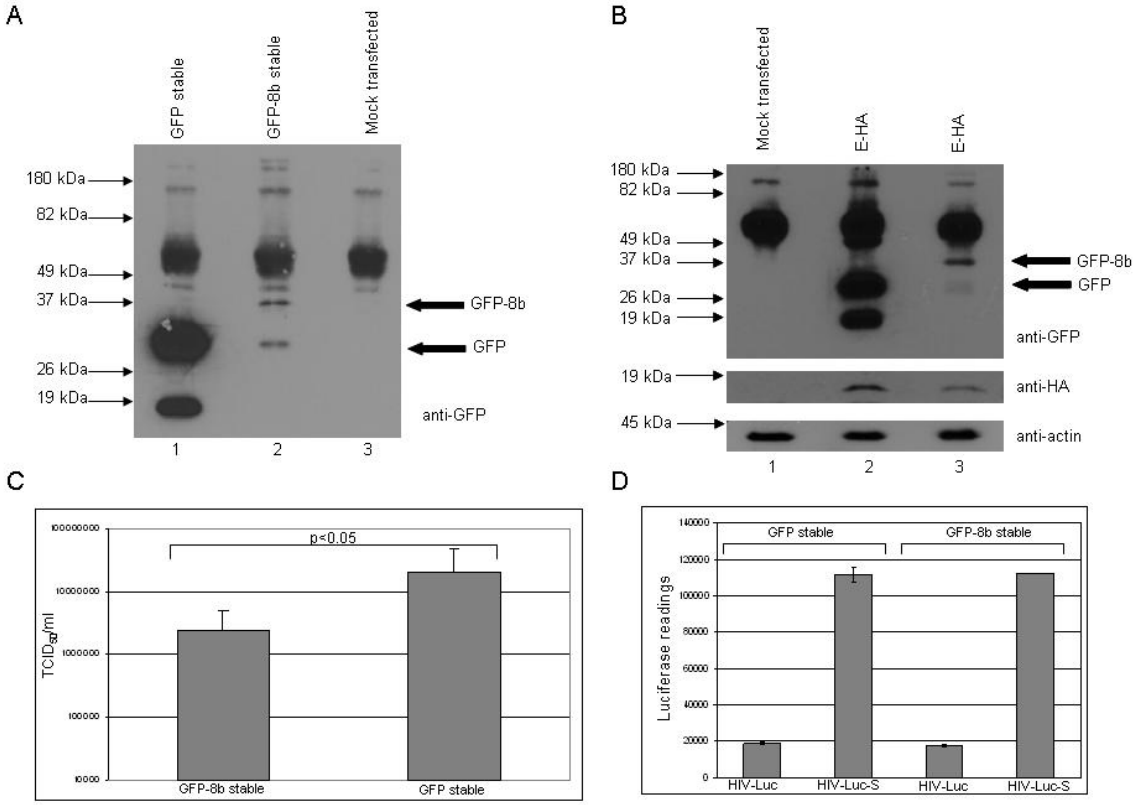

Fig. 7.6: Ectopic 8b expression reduces viral replication in Vero E6 cells. (A) Cells stably expressing GFP and GFP-8b were harvested and lysed and subjected to Western blot analysis. Expressions of GFP and GFP-8b in the stable cell lines were detected using an anti-GFP antibody. (B) GFP-8b and GFP stable cells were transfected with a cDNA construct for expressing E, harvested and lysed at 24 h post-transfection. Expressions of GFP and GFP-8b were detected using an anti-GFP antibody (1st panel). The amount of E in the cell lysates was detected using anti-E antibody (2nd panel). Anti-actin monoclonal antibody was used to verify that equal amounts of lysates were used in each lane (3rd panel). (C) A graph showing the titers of the virus produced by GFP and GFP-8b cells. The average and standard deviation of readings from 12 independent experiments are plotted. Statistical analysis was performed using Student's t test assuming unequal variance and the difference between GFP and GFP-8b cells was found to be significant ($p < 0.05$).

7.7 E is down-regulated in SARS-CoV infected GFP-8b expressing cells

To investigate the effect of 8b on the expression level of E during SARS-CoV infection, GFP-8b and GFP cells were infected with SARS-CoV at different multiplicity of infection (M.O.I.) and harvested at 18 hpi. At M.O.I of 0.1, the expression of S in the GFP-8b cells (Fig. 7.7, lane 1 and 2) was much lower than GFP cells and this is probably a result of the lower viral replication in the GFP-8b cells as observed above. At M.O.I. of 5, the expressions of S in both GFP-8b and GFP-expressing cells were similar (lanes 3 and 4). However, the expression of E was significantly lower in the GFP-8b cells compared to the GFP cells (lanes 3 and 4). This result suggests that GFP-8b down-regulates the expression of E in SARS-CoV infected cells.

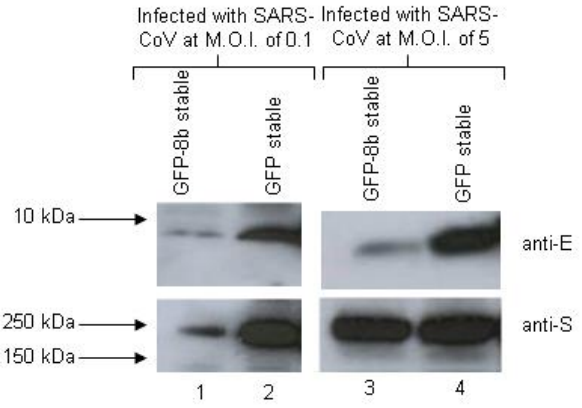

Fig. 7.7: Expression of E is down-regulated in SARS-CoV infected cells stably expressing GFP-8b. Vero E6 cells stably expressing GFP and GFP-8b were infected with SARS-CoV at M.O.I. of 0.1 (lanes 1 and 2) and M.O.I. of 5 (lanes 3 and 4). Cells were harvested and lysed at 18 hpi and the expressions of S and E in the cell lysates were detected using anti-E (1st panel) and anti-S (2nd panel) antibodies, respectively.

7.8 Effects of 8b on the transcription of host genes

To identify potential host proteins involved in the reduction of viral replication in the GFP-8b expressing cells, an oligo-nucleotide microarray analysis was performed. The host gene profiles of GFP and GFP-8b cell lines were compared to identify host genes that were increased or decreased by 8b. When compared to cells expressing GFP only, the GFP-8b cells have 78 genes down-regulated by more than 4 folds and 59 genes up-regulated by more than 4 folds (data not shown). Microarray analysis was performed for another GFP-8b stable clone, named as GFP-8b*, which has a lower expression of the GFP-8b protein (Fig. 7.8A, lanes 1 and 2). Unlike GFP-8b, the production of progeny SARS-CoV in GFP-8b* cells was found to be the same as in GFP cells (data not shown). Hence, the gene profile of GFP-8b* cells was compared to GFP-8b cells to exclude host mRNAs that are increased/decreased by GFP-8b but not involved in the regulation of viral replication. This comparison revealed that 15 host genes were down-regulated more than 2-fold in GFP-8b compared to GFP-8b* cells and 4 host genes were up-regulated more than 2-fold in GFP-8b compared to GFP-8b* cells (Table 7.1).

Next, quantitative PCR (qPCR) was performed to validate the results from the microarray analysis. For the down-regulated genes, there were no commercially available qPCR primers for 3 of them (DKFZp586D0518, DKFZp451E0119 and FLJ12280 fis genes). qPCR was performed for the other 12 genes and 7 of them were found to be down-regulated to a greater extent in GFP-8b cells than GFP-8b* cells (Fig. 7.8B). These are NTS, VDUP1, THBS1, GPM6A, KIAA1199, DTR and DAB2. As for the 4 up-regulated genes, only two of them (HLF and MYOZ1) were up-regulated a greater extent in GFP-8b cells than GFP-8b* cells (Fig. 7.8C).

Table 7.1: Host genes with different mRNA expression in GFP-8b and GFP-8b* cells as identified by microarray analysis[a]

Genes	Affymetrix ID	Ratio of mRNA expression to GFP[b]		Fold difference[c]
		GFP-8b	GFP-8b*	
Down-regulated				
NTS	206291_at	0.13	0.67	5.2
VDUP1 (TXNIP)	201010_s_at	0.01	0.04	4
THBS1	201110_s_at	0.06	0.23	3.8
DKFZp586D0518	215253_s_at	0.08	0.29	3.6
DKFZp451E0119	1566096_x_at	0.14	0.5	3.6
SNK (PLK2)	201939_at	0.2	0.67	3.4
GPM6A	209470_s_at	0.09	0.27	3
INHBA	210511_s_at	0.22	0.59	2.7
FLJ12280 fis	213909_at	0.22	0.59	2.7
DLG2 (MPP2)	206253_at	0.25	0.59	2.4
KIAA1199	212942_s_at	0.03	0.07	2.3
DSCR1 (RCAN1)	208370_s_at	0.17	0.38	2.2
BAI3	205638_at	0.19	0.38	2
DTR (HBEGF)	203821_at	0.26	0.53	2
DAB2	210757_x_at	0.25	0.5	2
Up-regulated				
HLF	204754_at	6	2.6	2.3
MYOZ (MYOZ1)	219509_at	5.3	2.5	2.1
ID2	201565_s_at	3.8	1.9	2
TSLRP (LRRC6)	206483_at	3.2	1.6	2

[a] Only genes that are up- or down-regulated in GFP-8b cells by > 2 fold than in GFP-8b* cells, are short-listed in the table.
[b] The ratio of genes transcription signals in GFP-8b or GFP-8b* cells to that in GFP control cells.
[c] The fold difference in the signal of the target genes between the GFP-8b and GFP-8b* cells. For down-regulated genes, the fold difference is GFP-8b*/GFP-8b and for upregulated genes, the fold difference is GFP-8b/GFP-8b*

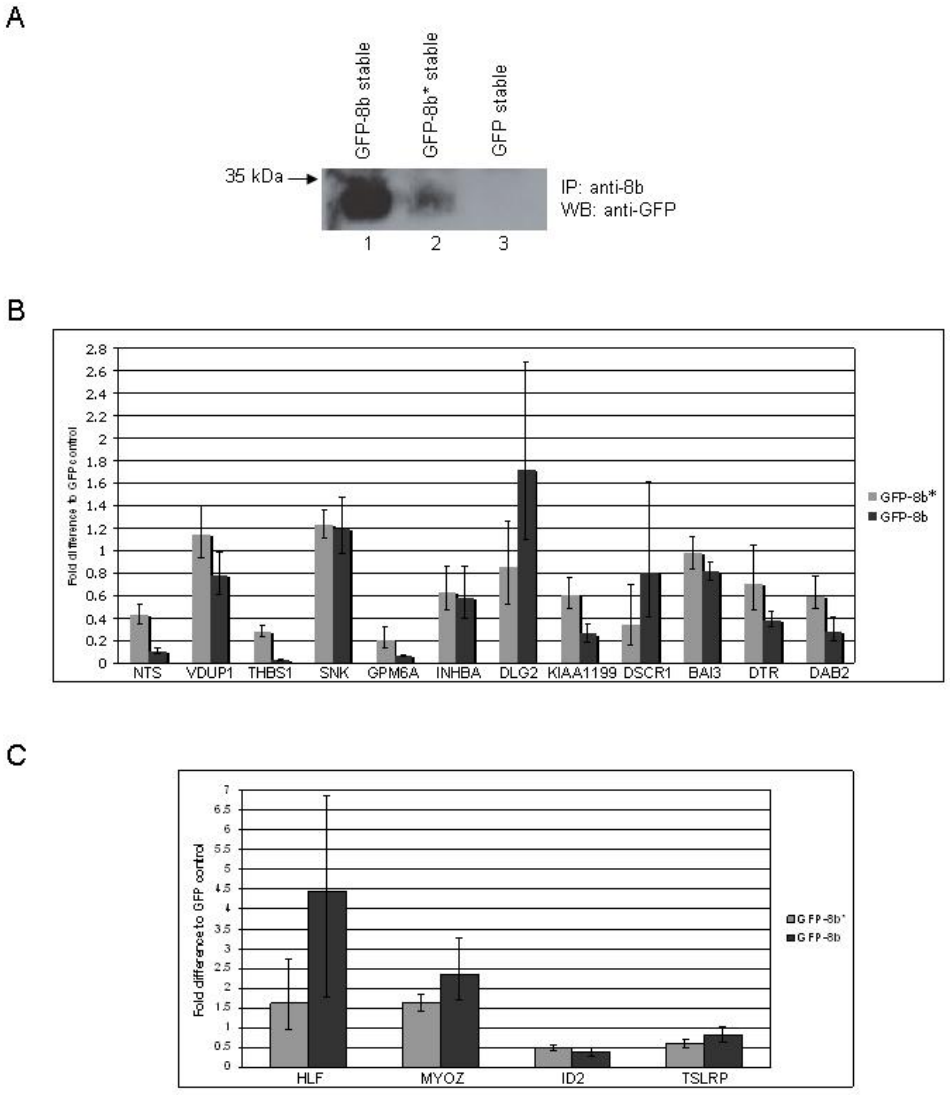

Fig. 7.8: Effects of 8b the transcriptions of host genes. (A) GFP-8b, GFP-8b* and GFP stable cells were harvested, lysed and subjected to IP with anti-8b polyclonal antibody and protein-A beads. The amounts of GFP-8b in the cell lysates of GFP-8b and GFP-8b* stable cells were detected by anti-GFP mouse monoclonal antibody. (B) Quantitative PCR was performed to validate the results from the microarray analysis (Table 1). A graph is plotted using the relative quantification (RQ) values for the down-regulated genes in GFP-8b and GFP-8b* cells, normalized to GAPDH and using GFP cells as the reference for normalization. (C) As described above, a graph is plotted for the up-regulated genes in GFP-8b and GFP-8b* cells.

7.9 Discussion

In the previous chapter, we have shown that 8b can down-regulate E in SARS-CoV infected cells (Keng et al., 2006). It was also reported that 8b can be monoubiquitinated and polyubiquitinated (Le et al., 2007). It is widely known that lysine residues are important for the binding of ubiquitin to a protein for ubiquitination (Hershko and Ciechanover, 1998). The results showed that the lysine residues in 8b are not required for its polyubiquitination or ability to down-regulate E (Figure 7.2). Furthermore, the degradation of E by 8b is dependent on both K54 and K64 in E while the half-life and polyubiquitination of E in the absence of 8b is only dependent on K64 (Figures 7.3 and 7.4). Thus, the 8b-mediated degradation of E, which can be inhibited by proteasome inhibitors (Fig. 7.1), seems to involve an ubiquitin-independent proteasome pathway. Several ubiquitin-independent proteolytic functions of the proteasome have been recently reported (Orlowski and Wilk, 2003). Although many of the ubiquitin-independent pathways have yet to be precisely defined, a recent study showed that more than 20% of cellular proteins are degraded by the proteasome via ubiquitin-independent pathways (Baugh et al., 2009).

Recently, a study using reverse genetics techniques showed that deletion of group specific genes 6, 7a, 7b, 8a, 8b and 9b from the SARS-CoV genome reduced its replication titer by 5-10 fold in human CaCo2, Huh7.5.1 and Huh-7 cells while deletion of E resulted in a 100 to 1000-fold reduction, compared to cells infected with wild-type SARS-CoV (DeDiego et al., 2007; DeDiego et al., 2008). A time-course study revealed that 8b is expressed at late time-points post infection (~32 hpi) (Figure 7.5). By comparing Vero E6 cells stably expressing GFP-8b or GFP alone, progeny virus

production was found to be significantly reduced in the presence of ectopic expression of 8b (Figure 7.6). This reduction is not due to any difference in the viral entry into the cells expressing GFP and GFP-8b. However, the expression of E in SARS-CoV infected cells is down-regulated in cells stably expressing GFP-8b when compared to GFP-expressing cells (Figure 7.7). This is consistent with our earlier observation that infected cells with high level of 8b have low level of E and suggests that 8b reduces viral replication by down-regulating the expression of E protein.

Gene profiling was used to determine the effects of 8b on host transcription. By comparing the profile of the GFP-8b stable cell-line with that of another clone, GFP-8b*, host genes that are regulated by 8b in a dose-dependent manner was shortlisted (Table 7.1). Independent validation by qPCR showed that there are 7 down-regulated genes and 2 up-regulated genes whose expressions may contribute to SARS-CoV replication (Figure 7.8). Some of these host genes have been implicated in the replication of other viruses. For example, thrombospondin-1 (THBS1) has also been shown to be down-regulated by cytomegalovirus infection (Cinatl et al., 1999) and hepatitis leukemia factor (HLF) has been shown to control hepatitis B virus transcription activity (Ishida et al., 2000). In a recent study, a reduction in the expression of the thioredoxin interacting protein (VDUP1/TXNIP) was shown to reduce the replication and secretion of hepatitis C virus (Blackham et al., 2010). Further investigations are needed to determine the roles of these proteins in regulating SARS-CoV replication.

Taken together, our results suggest that the over-expression of the SARS coronavirus 8b reduces viral replication by down-regulating E via an ubiquitin-independent proteasome pathway. In virus evolution, rapid mutation is constantly taking

place to achieve a strain which can have optimal replication titer for both efficient transmission and the ability to evade the host immune response (Bonhoeffer and Sniegowski, 2002; Vossen et al., 2002). Based on the results obtained using Vero E6 cells over-expressing 8b, it is speculated that the ability of 8b to reduce viral replication could be a mechanism to prevent the over-production of virus, after reaching an optimal viral titer, so as to reduce the pathogenesis of the host. However, future studies need to be performed to determine if 8b can modulate viral replication during natural infection. Interestingly, another SARS-CoV accessory protein, 7b, was recently shown to be an attenuating factor (Pfefferle et al., 2009a). One unanswered question is whether the replication of a SARS-CoV without 8b in the natural host will be higher than that of the wild-type virus. Previous studies have shown that the deletion of 8b and several other accessory proteins, namely 6, 7a, 7b, 8a and 9b, from the SARS-CoV genome reduced viral replication in cell cultures by 5-10 fold (DeDiego et al., 2007; DeDiego et al., 2008). Thus, it is possible that the weak down-regulation of viral replication by 8b can be counter-balanced by other accessory proteins. For example, Chen et al. have shown that the 8a protein can increase viral replication (Chen et al., 2007b). Thus, the SARS-CoV could have acquired the 8a and 8b proteins to fine-tune its replication in the human host.

CHAPTER 8: FINAL CONCLUSION AND FUTURE DIRECTIONS

Several studies have reported the importance of the SARS-CoV viral-viral protein interactions in replication complex assembly as well as viral assembly. It was demonstrated that the interaction between M and N or M and E is essential for viral assembly (Ho et al., 2004; Huang et al., 2004b). Critical viral-host interactions leading to viral entry, suppression of host immune response and host apoptosis have also been reported. The interaction of S with host ACE2 has been shown to be important for SARS-CoV entry (Li et al., 2004a; Simmons et al., 2004). The research efforts described in this thesis attempt to gain a better understanding of the viral-viral and viral-host interactions that contribute to the replication of the SARS-CoV. In this thesis, we focus on exploring the feasibility of disrupting a critical virus-host interaction, of S with ACE2, as a strategy to prevent the SARS-CoV entry and delineating the importance of the viral-viral interaction of the ORF8 proteins for the virus replication. Results of our studies are summarized below:

a) It was demonstrated that one of the five polyclonal antibodies generated against the various regions in the ectodomain of SARS-CoV S exhibits a strong neutralizing activity against SARS-CoV infection *in vitro*. This polyclonal antibody, rabbit αSΔ10, specifically targets the domain within the amino acid residues 1055 to 1192 of S.

b) Monoclonal antibodies generated against the S fragment encoding aa 1055 to 1192 were found to have SARS-CoV neutralizing activities and target either the N-terminal of HR2 domain or the region immediately upstream of the HR2 domain.

c) Two of these mAbs, mAb 1A9 and mAb 1G10, were both found to have cross-neutralizing activities against civet SARS-CoV (SZ3 strain) and bats SL-CoV (Rp3 and Rf1 strains).

d) Using escape viruses generated with mAb 1A9, two amino acids, N1056 and D1128, located near and within the binding sites of mAb 1A9 were identified to be important for its neutralizing activity.

e) It was shown that a reduction in the palmitoylation of S was one of the mechanisms employed by NO for the inhibition of SARS-CoV replication.

f) The cellular localization and interactions of the ORF8 proteins, 8a, 8b and 8ab, with other SARS-CoV proteins were shown to be different from each other.

g) The SARS-CoV 8b was demonstrated to down-regulate the small envelope E protein in both the infected and transfected cells via a post-translational pathway.

h) The mechanism of down-regulation of E by 8b was shown to be via an ubiquitin-independent proteasome pathway.

i) Viral replication was shown to be decrease by 10-fold more in cells stably expressing the GFP-8b protein compared to control cells expressing GFP alone.

j) Vero E6 ells stably expressing the 8b protein had 7 genes that were up-regulated and 2 genes that were down-regulated by more than 2 fold, when compared to normal cells. These genes may be involved in the 8b-mediated reduction of viral replication via the down-regulation of E.

In the first part of this study, we have generated and used monoclonal and polyclonal antibodies to characterize novel neutralizing epitopes within the highly conserved S2 domain of the SARS-CoV S protein (Keng et al., 2005; Lip et al., 2006). Two representative mAbs were shown to have cross-neutralizing activities against civet SARS-CoV as well as bat SL-CoV. Overall, our results have significant implications for the development of vaccine and antiviral therapeutics in the event of a re-emergence of SARS-CoV or another pathogenic coronavirus from bat reservoirs. Further work is required to humanize the mAbs and determine their efficacies in an *in vivo* infection model. In addition, mutation at two residues (N1056 and D1128) in S seems to allow the virus to escape neutralization by the mAb 1A9. As these residues have not been previously documented to play a role in viral fusion, it will be very interesting to employ biophysical or structural methods to examine the precise mechanisms by which they contribute to the fusion between viral and host membranes. The fitness of the escape viruses also needs to be examined in vitro and in vivo.

In the second part of this study, we have compared the expression, cellular localization and viral-viral interaction profile of the accessory proteins encoded by ORF8 of SARS-CoV (Keng et al., 2006). Interestingly, we observed that the 8a, 8b and 8ab proteins seem to participate in different viral-viral interactions and 8b can down-regulate the expression of E during infection via an ubiquitin-independent proteasome pathway (Keng et al., 2011). The ectopic expression of 8b also reduced viral replication in Vero E6 cells and perturbed the transcriptional level of several host proteins. The contribution of these host proteins to SARS-CoV replication remains to be determined so does the

mechanism for their regulation by 8b and/or 8ab. Our studies provide interesting insights into the potential involvement of these poorly characterized accessory proteins in viral-viral and viral-host interactions, and suggest that 8b may have evolved to act as a negative modulator of SARS-CoV replication. Further studies that use reverse genetics techniques and an appropriate animal model will be required to compare the viral replication and pathogenesis of SARS-CoV bearing either the 8ab or the 8a and 8b proteins.

REFERENCES

Akerstrom, S., Gunalan, V., Keng, C.T., Tan, Y.J., and Mirazimi, A. (2009). Dual effect of nitric oxide on SARS-CoV replication: viral RNA production and palmitoylation of the S protein are affected. Virology *395*, 1-9.

Akerstrom, S., Mirazimi, A., and Tan, Y.J. (2007). Inhibition of SARS-CoV replication cycle by small interference RNAs silencing specific SARS proteins, 7a/7b, 3a/3b and S. Antiviral Res *73*, 219-227.

Akerstrom, S., Mousavi-Jazi, M., Klingstrom, J., Leijon, M., Lundkvist, A., and Mirazimi, A. (2005). Nitric oxide inhibits the replication cycle of severe acute respiratory syndrome coronavirus. J Virol *79*, 1966-1969.

Almazan, F., Dediego, M.L., Galan, C., Escors, D., Alvarez, E., Ortego, J., Sola, I., Zuniga, S., Alonso, S., Moreno, J.L., *et al.* (2006). Construction of a severe acute respiratory syndrome coronavirus infectious cDNA clone and a replicon to study coronavirus RNA synthesis. J Virol *80*, 10900-10906.

Alvarez, E., DeDiego, M.L., Nieto-Torres, J.L., Jimenez-Guardeno, J.M., Marcos-Villar, L., and Enjuanes, L. (2010). The envelope protein of severe acute respiratory syndrome coronavirus interacts with the non-structural protein 3 and is ubiquitinated. Virology *402*, 281-291.

Anand, K., Ziebuhr, J., Wadhwani, P., Mesters, J.R., and Hilgenfeld, R. (2003). Coronavirus main proteinase (3CLpro) structure: basis for design of anti-SARS drugs. Science *300*, 1763-1767.

Arbely, E., Granot, Z., Kass, I., Orly, J., and Arkin, I.T. (2006). A trimerizing GxxxG motif is uniquely inserted in the severe acute respiratory syndrome (SARS) coronavirus spike protein transmembrane domain. Biochemistry *45*, 11349-11356.

Arbely, E., Khattari, Z., Brotons, G., Akkawi, M., Salditt, T., and Arkin, I.T. (2004). A highly unusual palindromic transmembrane helical hairpin formed by SARS coronavirus E protein. J Mol Biol *341*, 769-779.

Azzi, A., and Lin, S.X. (2004). Human SARS-coronavirus RNA-dependent RNA polymerase: activity determinants and nucleoside analogue inhibitors. Proteins *57*, 12-14.

Babcock, G.J., Esshaki, D.J., Thomas, W.D., Jr., and Ambrosino, D.M. (2004). Amino acids 270 to 510 of the severe acute respiratory syndrome coronavirus spike protein are required for interaction with receptor. J Virol *78*, 4552-4560.

Banks, L., Pim, D., and Thomas, M. (2003). Viruses and the 26S proteasome: hacking into destruction. Trends Biochem Sci *28*, 452-459.

Baranov, P.V., Henderson, C.M., Anderson, C.B., Gesteland, R.F., Atkins, J.F., and Howard, M.T. (2005). Programmed ribosomal frameshifting in decoding the SARS-CoV genome. Virology *332*, 498-510.

Barretto, N., Jukneliene, D., Ratia, K., Chen, Z., Mesecar, A.D., and Baker, S.C. (2005). The papain-like protease of severe acute respiratory syndrome coronavirus has deubiquitinating activity. J Virol *79*, 15189-15198.

Barrila, J., Bacha, U., and Freire, E. (2006). Long-range cooperative interactions modulate dimerization in SARS 3CLpro. Biochemistry *45*, 14908-14916.

Barrila, J., Gabelli, S.B., Bacha, U., Amzel, L.M., and Freire, E. (2010). Mutation of Asn28 disrupts the dimerization and enzymatic activity of SARS 3CL(pro). Biochemistry *49*, 4308-4317.

Baugh, J.M., Viktorova, E.G., and Pilipenko, E.V. (2009). Proteasomes can degrade a significant proportion of cellular proteins independent of ubiquitination. J Mol Biol *386*, 814-827.

Bell, D.M. (2004). Public health interventions and SARS spread, 2003. Emerg Infect Dis *10*, 1900-1906.

Belouzard, S., Chu, V.C., and Whittaker, G.R. (2009). Activation of the SARS coronavirus spike protein via sequential proteolytic cleavage at two distinct sites. Proc Natl Acad Sci U S A *106*, 5871-5876.

Belouzard, S., Madu, I., and Whittaker, G.R. (2010). Elastase-mediated activation of the severe acute respiratory syndrome coronavirus spike protein at discrete sites within the S2 domain. J Biol Chem *285*, 22758-22763.

Beniac, D.R., Andonov, A., Grudeski, E., and Booth, T.F. (2006). Architecture of the SARS coronavirus prefusion spike. Nat Struct Mol Biol *13*, 751-752.

Bergeron, E., Vincent, M.J., Wickham, L., Hamelin, J., Basak, A., Nichol, S.T., Chretien, M., and Seidah, N.G. (2005). Implication of proprotein convertases in the processing and spread of severe acute respiratory syndrome coronavirus. Biochem Biophys Res Commun *326*, 554-563.

Bhardwaj, K., Guarino, L., and Kao, C.C. (2004). The severe acute respiratory syndrome coronavirus Nsp15 protein is an endoribonuclease that prefers manganese as a cofactor. J Virol *78*, 12218-12224.

Bhardwaj, K., Palaninathan, S., Alcantara, J.M., Yi, L.L., Guarino, L., Sacchettini, J.C., and Kao, C.C. (2008). Structural and functional analyses of the severe acute respiratory syndrome coronavirus endoribonuclease Nsp15. J Biol Chem *283*, 3655-3664.

Bhardwaj, K., Sun, J., Holzenburg, A., Guarino, L.A., and Kao, C.C. (2006). RNA recognition and cleavage by the SARS coronavirus endoribonuclease. J Mol Biol *361*, 243-256.

Bisht, H., Roberts, A., Vogel, L., Bukreyev, A., Collins, P.L., Murphy, B.R., Subbarao, K., and Moss, B. (2004). Severe acute respiratory syndrome coronavirus spike protein expressed by attenuated vaccinia virus protectively immunizes mice. Proc Natl Acad Sci U S A *101*, 6641-6646.

Bizzozero, O.A., Bixler, H., Parkhani, J., and Pastuszyn, A. (2001). Nitric oxide reduces the palmitoylation of rat myelin proteolipid protein by an indirect mechanism. Neurochem Res *26*, 1127-1137.

Black, R.A., Rauch, C.T., Kozlosky, C.J., Peschon, J.J., Slack, J.L., Wolfson, M.F., Castner, B.J., Stocking, K.L., Reddy, P., Srinivasan, S., *et al.* (1997). A metalloproteinase disintegrin that releases tumour-necrosis factor-alpha from cells. Nature *385*, 729-733.

Blackham, S., Baillie, A., Al-Hababi, F., Remlinger, K., You, S., Hamatake, R., and McGarvey, M.J. (2010). Gene expression profiling indicates the roles of host oxidative stress, apoptosis, lipid metabolism, and intracellular transport genes in the replication of hepatitis C virus. J Virol *84*, 5404-5414.

Bonhoeffer, S., and Sniegowski, P. (2002). Virus evolution: the importance of being erroneous. Nature *420*, 367, 369.

Bosch, B.J., Bartelink, W., and Rottier, P.J. (2008b). Cathepsin L functionally cleaves the severe acute respiratory syndrome coronavirus class I fusion protein upstream of rather than adjacent to the fusion peptide. J Virol *82*, 8887-8890.

Bosch, B.J., Martina, B.E., Van Der Zee, R., Lepault, J., Haijema, B.J., Versluis, C., Heck, A.J., De Groot, R., Osterhaus, A.D., and Rottier, P.J. (2004). Severe acute respiratory syndrome coronavirus (SARS-CoV) infection inhibition using spike protein heptad repeat-derived peptides. Proc Natl Acad Sci U S A *101*, 8455-8460.

Bosch, B.J., Rossen, J.W., Bartelink, W., Zuurveen, S.J., de Haan, C.A., Duquerroy, S., Boucher, C.A., and Rottier, P.J. (2008a). Coronavirus escape from heptad repeat 2 (HR2)-derived peptide entry inhibition as a result of mutations in the HR1 domain of the spike fusion protein. J Virol *82*, 2580-2585.

Bosch, B.J., van der Zee, R., de Haan, C.A., and Rottier, P.J. (2003). The coronavirus spike protein is a class I virus fusion protein: structural and functional characterization of the fusion core complex. J Virol *77*, 8801-8811.

Bouvet, M., Debarnot, C., Imbert, I., Selisko, B., Snijder, E.J., Canard, B., and Decroly, E. (2010). In vitro reconstitution of SARS-coronavirus mRNA cap methylation. PLoS Pathog *6*, e1000863.

Bradburne, A.F. (1970). Antigenic relationships amongst coronaviruses. Arch Gesamte Virusforsch *31*, 352-364.

Brierley, I., Digard, P., and Inglis, S.C. (1989). Characterization of an efficient coronavirus ribosomal frameshifting signal: requirement for an RNA pseudoknot. Cell *57*, 537-547.

Broer, R., Boson, B., Spaan, W., Cosset, F.L., and Corver, J. (2006). Important role for the transmembrane domain of severe acute respiratory syndrome coronavirus spike protein during entry. J Virol *80*, 1302-1310.

Brown, E.G., Liu, H., Kit, L.C., Baird, S., and Nesrallah, M. (2001). Pattern of mutation in the genome of influenza A virus on adaptation to increased virulence in the mouse lung: identification of functional themes. Proc Natl Acad Sci U S A *98*, 6883-6888.

Buchholz, U.J., Bukreyev, A., Yang, L., Lamirande, E.W., Murphy, B.R., Subbarao, K., and Collins, P.L. (2004). Contributions of the structural proteins of severe acute respiratory syndrome coronavirus to protective immunity. Proc Natl Acad Sci U S A *101*, 9804-9809.

Bukreyev, A., Lamirande, E.W., Buchholz, U.J., Vogel, L.N., Elkins, W.R., St Claire, M., Murphy, B.R., Subbarao, K., and Collins, P.L. (2004). Mucosal immunisation of African green monkeys (Cercopithecus aethiops) with an attenuated parainfluenza virus expressing the SARS coronavirus spike protein for the prevention of SARS. Lancet *363*, 2122-2127.

Cai, Q.C., Jiang, Q.W., Zhao, G.M., Guo, Q., Cao, G.W., and Chen, T. (2003). Putative caveolin-binding sites in SARS-CoV proteins. Acta Pharmacol Sin *24*, 1051-1059.

Castilla, J., Sola, I., and Enjuanes, L. (1997). Interference of coronavirus infection by expression of immunoglobulin G (IgG) or IgA virus-neutralizing antibodies. J Virol *71*, 5251-5258.

Caulford, P. (2003). SARS: aftermath of an outbreak. Lancet *362 Suppl*, s2-3.

Chakraborti, S., Prabakaran, P., Xiao, X., and Dimitrov, D.S. (2005). The SARS coronavirus S glycoprotein receptor binding domain: fine mapping and functional characterization. Virol J *2*, 73.

Chan, C.M., Ma, C.W., Chan, W.Y., and Chan, H.Y. (2007). The SARS-Coronavirus Membrane protein induces apoptosis through modulating the Akt survival pathway. Arch Biochem Biophys *459*, 197-207.

Chan, C.M., Tsoi, H., Chan, W.M., Zhai, S., Wong, C.O., Yao, X., Chan, W.Y., Tsui, S.K., and Chan, H.Y. (2009). The ion channel activity of the SARS-coronavirus 3a protein is linked to its pro-apoptotic function. Int J Biochem Cell Biol *41*, 2232-2239.

Chan, C.P., Siu, K.L., Chin, K.T., Yuen, K.Y., Zheng, B., and Jin, D.Y. (2006a). Modulation of the unfolded protein response by the severe acute respiratory syndrome coronavirus spike protein. J Virol *80*, 9279-9287.

Chan, W.E., Chuang, C.K., Yeh, S.H., Chang, M.S., and Chen, S.S. (2006b). Functional characterization of heptad repeat 1 and 2 mutants of the spike protein of severe acute respiratory syndrome coronavirus. J Virol *80*, 3225-3237.

Chan, W.S., Wu, C., Chow, S.C., Cheung, T., To, K.F., Leung, W.K., Chan, P.K., Lee, K.C., Ng, H.K., Au, D.M., *et al.* (2005). Coronaviral hypothetical and structural proteins were found in the intestinal surface enterocytes and pneumocytes of severe acute respiratory syndrome (SARS). Mod Pathol *18*, 1432-1439.

Chang, C.K., Sue, S.C., Yu, T.H., Hsieh, C.M., Tsai, C.K., Chiang, Y.C., Lee, S.J., Hsiao, H.H., Wu, W.J., Chang, W.L., *et al.* (2006). Modular organization of SARS coronavirus nucleocapsid protein. J Biomed Sci *13*, 59-72.

Chau, T.N., Lee, K.C., Yao, H., Tsang, T.Y., Chow, T.C., Yeung, Y.C., Choi, K.W., Tso, Y.K., Lau, T., Lai, S.T., *et al.* (2004). SARS-associated viral hepatitis caused by a novel coronavirus: report of three cases. Hepatology *39*, 302-310.

Chen, C.Y., Chang, C.K., Chang, Y.W., Sue, S.C., Bai, H.I., Riang, L., Hsiao, C.D., and Huang, T.H. (2007a). Structure of the SARS coronavirus nucleocapsid protein RNA-binding dimerization domain suggests a mechanism for helical packaging of viral RNA. J Mol Biol *368*, 1075-1086.

Chen, C.Y., Ping, Y.H., Lee, H.C., Chen, K.H., Lee, Y.M., Chan, Y.J., Lien, T.C., Jap, T.S., Lin, C.H., Kao, L.S., *et al.* (2007b). Open reading frame 8a of the human severe acute respiratory syndrome coronavirus not only promotes viral replication but also induces apoptosis. J Infect Dis *196*, 405-415.

Chen, H., Wei, P., Huang, C., Tan, L., Liu, Y., and Lai, L. (2006). Only one protomer is active in the dimer of SARS 3C-like proteinase. J Biol Chem *281*, 13894-13898.

Chen, I.Y., Chang, S.C., Wu, H.Y., Yu, T.C., Wei, W.C., Lin, S., Chien, C.L., and Chang, M.F. (2010). Upregulation of the chemokine (C-C motif) ligand 2 via a severe acute respiratory syndrome coronavirus spike-ACE2 signaling pathway. J Virol *84*, 7703-7712.

Chen, J.Y., Chen, W.N., Poon, K.M., Zheng, B.J., Lin, X., Wang, Y.X., and Wen, Y.M. (2009a). Interaction between SARS-CoV helicase and a multifunctional cellular protein (Ddx5) revealed by yeast and mammalian cell two-hybrid systems. Arch Virol *154*, 507-512.

Chen, L., Liu, P., Gao, H., Sun, B., Chao, D., Wang, F., Zhu, Y., Hedenstierna, G., and Wang, C.G. (2004b). Inhalation of nitric oxide in the treatment of severe acute respiratory syndrome: a rescue trial in Beijing. Clin Infect Dis *39*, 1531-1535.

Chen, P., Jiang, M., Hu, T., Liu, Q., Chen, X.S., and Guo, D. (2007c). Biochemical characterization of exoribonuclease encoded by SARS coronavirus. J Biochem Mol Biol *40*, 649-655.

Chen, S., Chen, L., Tan, J., Chen, J., Du, L., Sun, T., Shen, J., Chen, K., Jiang, H., and Shen, X. (2005b). Severe acute respiratory syndrome coronavirus 3C-like proteinase N terminus is indispensable for proteolytic activity but not for enzyme dimerization. Biochemical and thermodynamic investigation in conjunction with molecular dynamics simulations. J Biol Chem *280*, 164-173.

Chen, S., Zhang, J., Hu, T., Chen, K., Jiang, H., and Shen, X. (2008). Residues on the dimer interface of SARS coronavirus 3C-like protease: dimer stability characterization and enzyme catalytic activity analysis. J Biochem *143*, 525-536.

Chen, S.C., Lo, S.Y., Ma, H.C., and Li, H.C. (2009b). Expression and membrane integration of SARS-CoV E protein and its interaction with M protein. Virus Genes *38*, 365-371.

Chen, Y., Cai, H., Pan, J., Xiang, N., Tien, P., Ahola, T., and Guo, D. (2009c). Functional screen reveals SARS coronavirus nonstructural protein nsp14 as a novel cap N7 methyltransferase. Proc Natl Acad Sci U S A *106*, 3484-3489.

Chen, Y.Y., Shuang, B., Tan, Y.X., Meng, M.J., Han, P., Mo, X.N., Song, Q.S., Qiu, X.Y., Luo, X., Gan, Q.N., *et al.* (2005c). The protein X4 of severe acute respiratory syndrome-associated coronavirus is expressed on both virus-infected cells and lung tissue of severe acute respiratory syndrome patients and inhibits growth of Balb/c 3T3 cell line. Chin Med J (Engl) *118*, 267-274.

Chen, Z., Mi, L., Xu, J., Yu, J., Wang, X., Jiang, J., Xing, J., Shang, P., Qian, A., Li, Y., *et al.* (2005d). Function of HAb18G/CD147 in invasion of host cells by severe acute respiratory syndrome coronavirus. J Infect Dis *191*, 755-760.

Cheng, A., Zhang, W., Xie, Y., Jiang, W., Arnold, E., Sarafianos, S.G., and Ding, J. (2005). Expression, purification, and characterization of SARS coronavirus RNA polymerase. Virology *335*, 165-176.

Cheng, V.C., Lau, S.K., Woo, P.C., and Yuen, K.Y. (2007). Severe acute respiratory syndrome coronavirus as an agent of emerging and reemerging infection. Clin Microbiol Rev *20*, 660-694.

Chiu, R.W., Chim, S.S., Tong, Y.K., Fung, K.S., Chan, P.K., Zhao, G.P., and Lo, Y.M. (2005). Tracing SARS-coronavirus variant with large genomic deletion. Emerg Infect Dis *11*, 168-170.

Chou, C.F., Loh, C.B., Foo, Y.K., Shen, S., Fielding, B.C., Tan, T.H., Khan, S., Wang, Y., Lim, S.G., Hong, W., *et al.* (2006). ACE2 orthologues in non-mammalian vertebrates (Danio, Gallus, Fugu, Tetraodon and Xenopus). Gene *377*, 46-55.

Chou, C.Y., Chang, H.C., Hsu, W.C., Lin, T.Z., Lin, C.H., and Chang, G.G. (2004). Quaternary structure of the severe acute respiratory syndrome (SARS) coronavirus main protease. Biochemistry *43*, 14958-14970.

Chou, T.H., Wang, S., Sakhatskyy, P.V., Mboudjeka, I., Lawrence, J.M., Huang, S., Coley, S., Yang, B., Li, J., Zhu, Q., *et al.* (2005). Epitope mapping and biological function analysis of antibodies produced by immunization of mice with an inactivated Chinese isolate of severe acute respiratory syndrome-associated coronavirus (SARS-CoV). Virology *334*, 134-143.

Chow, K.Y., Yeung, Y.S., Hon, C.C., Zeng, F., Law, K.M., and Leung, F.C. (2005). Adenovirus-mediated expression of the C-terminal domain of SARS-CoV spike protein is sufficient to induce apoptosis in Vero E6 cells. FEBS Lett *579*, 6699-6704.

Chu, D.K., Peiris, J.S., Chen, H., Guan, Y., and Poon, L.L. (2008a). Genomic characterizations of bat coronaviruses (1A, 1B and HKU8) and evidence for co-infections in Miniopterus bats. J Gen Virol *89*, 1282-1287.

Chu, L.H., Chan, S.H., Tsai, S.N., Wang, Y., Cheng, C.H., Wong, K.B., Waye, M.M., and Ngai, S.M. (2008b). Fusion core structure of the severe acute respiratory syndrome coronavirus (SARS-CoV): in search of potent SARS-CoV entry inhibitors. J Cell Biochem *104*, 2335-2347.

Ciechanover, A., and Ben-Saadon, R. (2004). N-terminal ubiquitination: more protein substrates join in. Trends Cell Biol *14*, 103-106.

Cinatl, J., Jr., Kotchetkov, R., Scholz, M., Cinatl, J., Vogel, J.U., Driever, P.H., and Doerr, H.W. (1999). Human cytomegalovirus infection decreases expression of thrombospondin-1 independent of the tumor suppressor protein p53. Am J Pathol *155*, 285-292.

Cinatl, J., Morgenstern, B., Bauer, G., Chandra, P., Rabenau, H., and Doerr, H.W. (2003a). Glycyrrhizin, an active component of liquorice roots, and replication of SARS-associated coronavirus. Lancet *361*, 2045-2046.

Connor, R.F., and Roper, R.L. (2007). Unique SARS-CoV protein nsp1: bioinformatics, biochemistry and potential effects on virulence. Trends Microbiol *15*, 51-53.

Connor, R.I., Chen, B.K., Choe, S., and Landau, N.R. (1995). Vpr is required for efficient replication of human immunodeficiency virus type-1 in mononuclear phagocytes. Virology *206*, 935-944.

Cornillez-Ty, C.T., Liao, L., Yates, J.R., 3rd, Kuhn, P., and Buchmeier, M.J. (2009). Severe acute respiratory syndrome coronavirus nonstructural protein 2 interacts with a host protein complex involved in mitochondrial biogenesis and intracellular signaling. J Virol *83*, 10314-10318.

Corver, J., Broer, R., van Kasteren, P., and Spaan, W. (2007). GxxxG motif of severe acute respiratory syndrome coronavirus spike glycoprotein transmembrane domain is not involved in trimerization and is not important for entry. J Virol *81*, 8352-8355.

Corver, J., Broer, R., van Kasteren, P., and Spaan, W. (2009). Mutagenesis of the transmembrane domain of the SARS coronavirus spike glycoprotein: refinement of the requirements for SARS coronavirus cell entry. Virol J *6*, 230.

CSMEC (2004). Molecular evolution of the SARS coronavirus during the course of the SARS epidemic in China. Science *303*, 1666-1669.

Curtis, K.M., Yount, B., and Baric, R.S. (2002). Heterologous gene expression from transmissible gastroenteritis virus replicon particles. J Virol *76*, 1422-1434.

de Haan, C.A., Masters, P.S., Shen, X., Weiss, S., and Rottier, P.J. (2002). The group-specific murine coronavirus genes are not essential, but their deletion, by reverse genetics, is attenuating in the natural host. Virology *296*, 177-189.

Decroly, E., Imbert, I., Coutard, B., Bouvet, M., Selisko, B., Alvarez, K., Gorbalenya, A.E., Snijder, E.J., and Canard, B. (2008). Coronavirus nonstructural protein 16 is a cap-0 binding enzyme possessing (nucleoside-2'O)-methyltransferase activity. J Virol *82*, 8071-8084.

DeDiego, M.L., Alvarez, E., Almazan, F., Rejas, M.T., Lamirande, E., Roberts, A., Shieh, W.J., Zaki, S.R., Subbarao, K., and Enjuanes, L. (2007). A severe acute respiratory syndrome coronavirus that lacks the E gene is attenuated in vitro and in vivo. J Virol *81*, 1701-1713.

DeDiego, M.L., Pewe, L., Alvarez, E., Rejas, M.T., Perlman, S., and Enjuanes, L. (2008). Pathogenicity of severe acute respiratory coronavirus deletion mutants in hACE-2 transgenic mice. Virology *376*, 379-389.

Deng, Y., Liu, J., Zheng, Q., Yong, W., and Lu, M. (2006). Structures and polymorphic interactions of two heptad-repeat regions of the SARS virus S2 protein. Structure *14*, 889-899.

Devaraj, S.G., Wang, N., Chen, Z., Tseng, M., Barretto, N., Lin, R., Peters, C.J., Tseng, C.T., Baker, S.C., and Li, K. (2007). Regulation of IRF-3-dependent innate immunity by the papain-like protease domain of the severe acute respiratory syndrome coronavirus. J Biol Chem *282*, 32208-32221.

Ding, L., Zhang, X.X., Wei, P., Fan, K., and Lai, L. (2005). The interaction between severe acute respiratory syndrome coronavirus 3C-like proteinase and a dimeric inhibitor by capillary electrophoresis. Anal Biochem *343*, 159-165.

Domingo, E., Escarmis, C., Sevilla, N., Moya, A., Elena, S.F., Quer, J., Novella, I.S., and Holland, J.J. (1996). Basic concepts in RNA virus evolution. FASEB J *10*, 859-864.

Dominguez, S.R., O'Shea, T.J., Oko, L.M., and Holmes, K.V. (2007). Detection of group 1 coronaviruses in bats in North America. Emerg Infect Dis *13*, 1295-1300.

Dos Ramos, F., Carrasco, M., Doyle, T., and Brierley, I. (2004). Programmed -1 ribosomal frameshifting in the SARS coronavirus. Biochem Soc Trans *32*, 1081-1083.

Drosten, C., Gunther, S., Preiser, W., van der Werf, S., Brodt, H.R., Becker, S., Rabenau, H., Panning, M., Kolesnikova, L., Fouchier, R.A., *et al.* (2003). Identification of a novel coronavirus in patients with severe acute respiratory syndrome. N Engl J Med *348*, 1967-1976.

Du, L., Kao, R.Y., Zhou, Y., He, Y., Zhao, G., Wong, C., Jiang, S., Yuen, K.Y., Jin, D.Y., and Zheng, B.J. (2007). Cleavage of spike protein of SARS coronavirus by protease factor Xa is associated with viral infectivity. Biochem Biophys Res Commun *359*, 174-179.

Duquerroy, S., Vigouroux, A., Rottier, P.J., Rey, F.A., and Bosch, B.J. (2005). Central ions and lateral asparagine/glutamine zippers stabilize the post-fusion hairpin conformation of the SARS coronavirus spike glycoprotein. Virology *335*, 276-285.

Eckerle, L.D., Becker, M.M., Halpin, R.A., Li, K., Venter, E., Lu, X., Scherbakova, S., Graham, R.L., Baric, R.S., Stockwell, T.B., *et al.* (2010). Infidelity of SARS-CoV Nsp14-exonuclease mutant virus replication is revealed by complete genome sequencing. PLoS Pathog *6*, e1000896.

Egloff, M.P., Ferron, F., Campanacci, V., Longhi, S., Rancurel, C., Dutartre, H., Snijder, E.J., Gorbalenya, A.E., Cambillau, C., and Canard, B. (2004). The severe acute respiratory syndrome-coronavirus replicative protein nsp9 is a single-stranded RNA-binding subunit unique in the RNA virus world. Proc Natl Acad Sci U S A *101*, 3792-3796.

Fan, K., Wei, P., Feng, Q., Chen, S., Huang, C., Ma, L., Lai, B., Pei, J., Liu, Y., Chen, J., *et al.* (2004). Biosynthesis, purification, and substrate specificity of severe acute respiratory syndrome coronavirus 3C-like proteinase. J Biol Chem *279*, 1637-1642.

Fan, Z., Zhuo, Y., Tan, X., Zhou, Z., Yuan, J., Qiang, B., Yan, J., Peng, X., and Gao, G.F. (2006). SARS-CoV nucleocapsid protein binds to hUbc9, a ubiquitin conjugating enzyme of the sumoylation system. J Med Virol *78*, 1365-1373.

Fang, X., Gao, J., Zheng, H., Li, B., Kong, L., Zhang, Y., Wang, W., Zeng, Y., and Ye, L. (2007). The membrane protein of SARS-CoV suppresses NF-kappaB activation. J Med Virol *79*, 1431-1439.

Fang, X., Ye, L., Timani, K.A., Li, S., Zen, Y., Zhao, M., Zheng, H., and Wu, Z. (2005). Peptide domain involved in the interaction between membrane protein and nucleocapsid protein of SARS-associated coronavirus. J Biochem Mol Biol *38*, 381-385.

Fielding, B.C., Gunalan, V., Tan, T.H., Chou, C.F., Shen, S., Khan, S., Lim, S.G., Hong, W., and Tan, Y.J. (2006). Severe acute respiratory syndrome coronavirus protein 7a interacts with hSGT. Biochem Biophys Res Commun *343*, 1201-1208.

Fielding, B.C., Tan, Y.J., Shuo, S., Tan, T.H., Ooi, E.E., Lim, S.G., Hong, W., and Goh, P.Y. (2004). Characterization of a unique group-specific protein (U122) of the severe acute respiratory syndrome coronavirus. J Virol *78*, 7311-7318.

Follis, K.E., York, J., and Nunberg, J.H. (2005). Serine-scanning mutagenesis studies of the C-terminal heptad repeats in the SARS coronavirus S glycoprotein highlight the important role of the short helical region. Virology *341*, 122-129.

Follis, K.E., York, J., and Nunberg, J.H. (2006). Furin cleavage of the SARS coronavirus spike glycoprotein enhances cell-cell fusion but does not affect virion entry. Virology *350*, 358-369.

Fouchier, R.A., Kuiken, T., Schutten, M., van Amerongen, G., van Doornum, G.J., van den Hoogen, B.G., Peiris, M., Lim, W., Stohr, K., and Osterhaus, A.D. (2003). Aetiology: Koch's postulates fulfilled for SARS virus. Nature *423*, 240.

Freundt, E.C., Yu, L., Goldsmith, C.S., Welsh, S., Cheng, A., Yount, B., Liu, W., Frieman, M.B., Buchholz, U.J., Screaton, G.R., *et al.* (2010). The open reading frame 3a protein of severe acute respiratory syndrome-associated coronavirus promotes membrane rearrangement and cell death. J Virol *84*, 1097-1109.

Frieman, M., Heise, M., and Baric, R. (2008). SARS coronavirus and innate immunity. Virus Res *133*, 101-112.

Frieman, M., Ratia, K., Johnston, R.E., Mesecar, A.D., and Baric, R.S. (2009). Severe acute respiratory syndrome coronavirus papain-like protease ubiquitin-like domain and catalytic domain regulate antagonism of IRF3 and NF-kappaB signaling. J Virol *83*, 6689-6705.

Frieman, M., Yount, B., Heise, M., Kopecky-Bromberg, S.A., Palese, P., and Baric, R.S. (2007). Severe acute respiratory syndrome coronavirus ORF6 antagonizes STAT1 function by sequestering nuclear import factors on the rough endoplasmic reticulum/Golgi membrane. J Virol *81*, 9812-9824.

Gallagher, T.M., and Buchmeier, M.J. (2001). Coronavirus spike proteins in viral entry and pathogenesis. Virology *279*, 371-374.

Gamble, T.R., Vajdos, F.F., Yoo, S., Worthylake, D.K., Houseweart, M., Sundquist, W.I., and Hill, C.P. (1996). Crystal structure of human cyclophilin A bound to the amino-terminal domain of HIV-1 capsid. Cell *87*, 1285-1294.

Geng, H., Liu, Y.M., Chan, W.S., Lo, A.W., Au, D.M., Waye, M.M., and Ho, Y.Y. (2005). The putative protein 6 of the severe acute respiratory syndrome-associated coronavirus: expression and functional characterization. FEBS Lett *579*, 6763-6768.

Godet, M., L'Haridon, R., Vautherot, J.F., and Laude, H. (1992). TGEV corona virus ORF4 encodes a membrane protein that is incorporated into virions. Virology *188*, 666-675.

Graham, R.L., and Baric, R.S. (2010). Recombination, reservoirs, and the modular spike: mechanisms of coronavirus cross-species transmission. J Virol *84*, 3134-3146.

Graham, R.L., Sims, A.C., Brockway, S.M., Baric, R.S., and Denison, M.R. (2005). The nsp2 replicase proteins of murine hepatitis virus and severe acute respiratory syndrome coronavirus are dispensable for viral replication. J Virol *79*, 13399-13411.

Gramberg, T., Hofmann, H., Moller, P., Lalor, P.F., Marzi, A., Geier, M., Krumbiegel, M., Winkler, T., Kirchhoff, F., Adams, D.H., *et al.* (2005). LSECtin interacts with filovirus glycoproteins and the spike protein of SARS coronavirus. Virology *340*, 224-236.

Graziano, V., McGrath, W.J., Yang, L., and Mangel, W.F. (2006). SARS CoV main proteinase: The monomer-dimer equilibrium dissociation constant. Biochemistry *45*, 14632-14641.

Guan, Y., Zheng, B.J., He, Y.Q., Liu, X.L., Zhuang, Z.X., Cheung, C.L., Luo, S.W., Li, P.H., Zhang, L.J., Guan, Y.J., *et al.* (2003). Isolation and characterization of viruses related to the SARS coronavirus from animals in southern China. Science *302*, 276-278.

Guarino, L.A., Bhardwaj, K., Dong, W., Sun, J., Holzenburg, A., and Kao, C. (2005). Mutational analysis of the SARS virus Nsp15 endoribonuclease: identification of residues affecting hexamer formation. J Mol Biol *353*, 1106-1117.

Guillen, J., de Almeida, R.F., Prieto, M., and Villalain, J. (2008a). Structural and dynamic characterization of the interaction of the putative fusion peptide of the S2 SARS-CoV virus protein with lipid membranes. J Phys Chem B *112*, 6997-7007.

Guillen, J., De Almeida, R.F., Prieto, M., and Villalain, J. (2009). Interaction of a peptide corresponding to the loop domain of the S2 SARS-CoV virus protein with model membranes. Mol Membr Biol *26*, 236-248.

Guillen, J., Kinnunen, P.K., and Villalain, J. (2008c). Membrane insertion of the three main membranotropic sequences from SARS-CoV S2 glycoprotein. Biochim Biophys Acta *1778*, 2765-2774.

Guillen, J., Moreno, M.R., Perez-Berna, A.J., Bernabeu, A., and Villalain, J. (2007). Interaction of a peptide from the pre-transmembrane domain of the severe acute respiratory syndrome coronavirus spike protein with phospholipid membranes. J Phys Chem B *111*, 13714-13725.

Guillen, J., Perez-Berna, A.J., Moreno, M.R., and Villalain, J. (2005). Identification of the membrane-active regions of the severe acute respiratory syndrome coronavirus spike

membrane glycoprotein using a 16/18-mer peptide scan: implications for the viral fusion mechanism. J Virol *79*, 1743-1752.

Guillen, J., Perez-Berna, A.J., Moreno, M.R., and Villalain, J. (2008b). A second SARS-CoV S2 glycoprotein internal membrane-active peptide. Biophysical characterization and membrane interaction. Biochemistry *47*, 8214-8224.

Guo, J.P., Petric, M., Campbell, W., and McGeer, P.L. (2004). SARS corona virus peptides recognized by antibodies in the sera of convalescent cases. Virology *324*, 251-256.

Haga, S., Yamamoto, N., Nakai-Murakami, C., Osawa, Y., Tokunaga, K., Sata, T., Sasazuki, T., and Ishizaka, Y. (2008). Modulation of TNF-alpha-converting enzyme by the spike protein of SARS-CoV and ACE2 induces TNF-alpha production and facilitates viral entry. Proc Natl Acad Sci U S A *105*, 7809-7814.

Haijema, B.J., Volders, H., and Rottier, P.J. (2004). Live, attenuated coronavirus vaccines through the directed deletion of group-specific genes provide protection against feline infectious peritonitis. J Virol *78*, 3863-3871.

Hakansson-McReynolds, S., Jiang, S., Rong, L., and Caffrey, M. (2006). Solution structure of the severe acute respiratory syndrome-coronavirus heptad repeat 2 domain in the prefusion state. J Biol Chem *281*, 11965-11971.

Hanel, K., Stangler, T., Stoldt, M., and Willbold, D. (2006). Solution structure of the X4 protein coded by the SARS related coronavirus reveals an immunoglobulin like fold and suggests a binding activity to integrin I domains. J Biomed Sci *13*, 281-293.

Harcourt, B.H., Jukneliene, D., Kanjanahaluethai, A., Bechill, J., Severson, K.M., Smith, C.M., Rota, P.A., and Baker, S.C. (2004). Identification of severe acute respiratory syndrome coronavirus replicase products and characterization of papain-like protease activity. J Virol *78*, 13600-13612.

Hatakeyama, S., Matsuoka, Y., Ueshiba, H., Komatsu, N., Itoh, K., Shichijo, S., Kanai, T., Fukushi, M., Ishida, I., Kirikae, T., *et al.* (2008). Dissection and identification of regions required to form pseudoparticles by the interaction between the nucleocapsid (N) and membrane (M) proteins of SARS coronavirus. Virology *380*, 99-108.

He, J., Choe, S., Walker, R., Di Marzio, P., Morgan, D.O., and Landau, N.R. (1995). Human immunodeficiency virus type 1 viral protein R (Vpr) arrests cells in the G2 phase of the cell cycle by inhibiting p34cdc2 activity. J Virol *69*, 6705-6711.

He, J.F., Peng, G.W., Zheng, H.Z., Luo, H.M., Liang, W.J., Li, L.H., Guo, R.N., and Deng, Z.H. (2003a). [An epidemiological study on the index cases of severe acute respiratory syndrome occurred in different cities among Guangdong province]. Zhonghua Liu Xing Bing Xue Za Zhi *24*, 347-349.

He, M.L., Zheng, B., Peng, Y., Peiris, J.S., Poon, L.L., Yuen, K.Y., Lin, M.C., Kung, H.F., and Guan, Y. (2003b). Inhibition of SARS-associated coronavirus infection and replication by RNA interference. JAMA *290*, 2665-2666.

He, R., Dobie, F., Ballantine, M., Leeson, A., Li, Y., Bastien, N., Cutts, T., Andonov, A., Cao, J., Booth, T.F., *et al.* (2004a). Analysis of multimerization of the SARS coronavirus nucleocapsid protein. Biochem Biophys Res Commun *316*, 476-483.

He, R., Leeson, A., Andonov, A., Li, Y., Bastien, N., Cao, J., Osiowy, C., Dobie, F., Cutts, T., Ballantine, M., *et al.* (2003c). Activation of AP-1 signal transduction pathway by SARS coronavirus nucleocapsid protein. Biochem Biophys Res Commun *311*, 870-876.

Hershko, A., and Ciechanover, A. (1998). The ubiquitin system. Annu Rev Biochem *67*, 425-479.

Ho, Y., Lin, P.H., Liu, C.Y., Lee, S.P., and Chao, Y.C. (2004). Assembly of human severe acute respiratory syndrome coronavirus-like particles. Biochem Biophys Res Commun *318*, 833-838.

Hofmann, H., Hattermann, K., Marzi, A., Gramberg, T., Geier, M., Krumbiegel, M., Kuate, S., Uberla, K., Niedrig, M., and Pohlmann, S. (2004a). S protein of severe acute respiratory syndrome-associated coronavirus mediates entry into hepatoma cell lines and is targeted by neutralizing antibodies in infected patients. J Virol *78*, 6134-6142.

Hon, C.C., Lam, T.Y., Shi, Z.L., Drummond, A.J., Yip, C.W., Zeng, F., Lam, P.Y., and Leung, F.C. (2008). Evidence of the recombinant origin of a bat severe acute respiratory syndrome (SARS)-like coronavirus and its implications on the direct ancestor of SARS coronavirus. J Virol *82*, 1819-1826.

Howard, M.W., Travanty, E.A., Jeffers, S.A., Smith, M.K., Wennier, S.T., Thackray, L.B., and Holmes, K.V. (2008). Aromatic amino acids in the juxtamembrane domain of severe acute respiratory syndrome coronavirus spike glycoprotein are important for receptor-dependent virus entry and cell-cell fusion. J Virol *82*, 2883-2894.

Hsieh, P.K., Chang, S.C., Huang, C.C., Lee, T.T., Hsiao, C.W., Kou, Y.H., Chen, I.Y., Chang, C.K., Huang, T.H., and Chang, M.F. (2005). Assembly of severe acute respiratory syndrome coronavirus RNA packaging signal into virus-like particles is nucleocapsid dependent. J Virol *79*, 13848-13855.

Hsieh, Y.C., Li, H.C., Chen, S.C., and Lo, S.Y. (2008). Interactions between M protein and other structural proteins of severe, acute respiratory syndrome-associated coronavirus. J Biomed Sci *15*, 707-717.

Hu, L.D., Zheng, G.Y., Jiang, H.S., Xia, Y., Zhang, Y., and Kong, X.Y. (2003). Mutation analysis of 20 SARS virus genome sequences: evidence for negative selection in replicase ORF1b and spike gene. Acta Pharmacol Sin *24*, 741-745.

Hu, W., Bai, B., Hu, Z., Chen, Z., An, X., Tang, L., Yang, J., and Wang, H. (2005). Development and evaluation of a multitarget real-time Taqman reverse transcription-PCR assay for detection of the severe acute respiratory syndrome-associated coronavirus and surveillance for an apparently related coronavirus found in masked palm civets. J Clin Microbiol *43*, 2041-2046.

Huang, C., Ito, N., Tseng, C.T., and Makino, S. (2006a). Severe acute respiratory syndrome coronavirus 7a accessory protein is a viral structural protein. J Virol *80*, 7287-7294.

Huang, C., Narayanan, K., Ito, N., Peters, C.J., and Makino, S. (2006b). Severe acute respiratory syndrome coronavirus 3a protein is released in membranous structures from 3a protein-expressing cells and infected cells. J Virol *80*, 210-217.

Huang, C., Peters, C.J., and Makino, S. (2007). Severe acute respiratory syndrome coronavirus accessory protein 6 is a virion-associated protein and is released from 6 protein-expressing cells. J Virol *81*, 5423-5426.

Huang, I.C., Bosch, B.J., Li, F., Li, W., Lee, K.H., Ghiran, S., Vasilieva, N., Dermody, T.S., Harrison, S.C., Dormitzer, P.R., *et al.* (2006c). SARS coronavirus, but not human coronavirus NL63, utilizes cathepsin L to infect ACE2-expressing cells. J Biol Chem *281*, 3198-3203.

Huang, Q., Yu, L., Petros, A.M., Gunasekera, A., Liu, Z., Xu, N., Hajduk, P., Mack, J., Fesik, S.W., and Olejniczak, E.T. (2004a). Structure of the N-terminal RNA-binding domain of the SARS CoV nucleocapsid protein. Biochemistry *43*, 6059-6063.

Huang, Y., Yang, Z.Y., Kong, W.P., and Nabel, G.J. (2004b). Generation of synthetic severe acute respiratory syndrome coronavirus pseudoparticles: implications for assembly and vaccine production. J Virol *78*, 12557-12565.

Hussain, S., Perlman, S., and Gallagher, T.M. (2008). Severe acute respiratory syndrome coronavirus protein 6 accelerates murine hepatitis virus infections by more than one mechanism. J Virol *82*, 7212-7222.

Imbert, I., Guillemot, J.C., Bourhis, J.M., Bussetta, C., Coutard, B., Egloff, M.P., Ferron, F., Gorbalenya, A.E., and Canard, B. (2006). A second, non-canonical RNA-dependent RNA polymerase in SARS coronavirus. EMBO J *25*, 4933-4942.

Imbert, I., Snijder, E.J., Dimitrova, M., Guillemot, J.C., Lecine, P., and Canard, B. (2008). The SARS-Coronavirus PLnc domain of nsp3 as a replication/transcription scaffolding protein. Virus Res *133*, 136-148.

Ingallinella, P., Bianchi, E., Finotto, M., Cantoni, G., Eckert, D.M., Supekar, V.M., Bruckmann, C., Carfi, A., and Pessi, A. (2004). Structural characterization of the fusion-active complex of severe acute respiratory syndrome (SARS) coronavirus. Proc Natl Acad Sci U S A *101*, 8709-8714.

Ishida, H., Ueda, K., Ohkawa, K., Kanazawa, Y., Hosui, A., Nakanishi, F., Mita, E., Kasahara, A., Sasaki, Y., Hori, M., *et al.* (2000). Identification of multiple transcription factors, HLF, FTF, and E4BP4, controlling hepatitis B virus enhancer II. J Virol *74*, 1241-1251.

Ito, N., Mossel, E.C., Narayanan, K., Popov, V.L., Huang, C., Inoue, T., Peters, C.J., and Makino, S. (2005). Severe acute respiratory syndrome coronavirus 3a protein is a viral structural protein. J Virol *79*, 3182-3186.

Ivanov, K.A., Hertzig, T., Rozanov, M., Bayer, S., Thiel, V., Gorbalenya, A.E., and Ziebuhr, J. (2004a). Major genetic marker of nidoviruses encodes a replicative endoribonuclease. Proc Natl Acad Sci U S A *101*, 12694-12699.

Ivanov, K.A., Thiel, V., Dobbe, J.C., van der Meer, Y., Snijder, E.J., and Ziebuhr, J. (2004b). Multiple enzymatic activities associated with severe acute respiratory syndrome coronavirus helicase. J Virol *78*, 5619-5632.

Jeffers, S.A., Tusell, S.M., Gillim-Ross, L., Hemmila, E.M., Achenbach, J.E., Babcock, G.J., Thomas, W.D., Jr., Thackray, L.B., Young, M.D., Mason, R.J., *et al.* (2004). CD209L (L-SIGN) is a receptor for severe acute respiratory syndrome coronavirus. Proc Natl Acad Sci U S A *101*, 15748-15753.

Jia, H.P., Look, D.C., Shi, L., Hickey, M., Pewe, L., Netland, J., Farzan, M., Wohlford-Lenane, C., Perlman, S., and McCray, P.B., Jr. (2005). ACE2 receptor expression and severe acute respiratory syndrome coronavirus infection depend on differentiation of human airway epithelia. J Virol *79*, 14614-14621.

Joseph, J.S., Saikatendu, K.S., Subramanian, V., Neuman, B.W., Brooun, A., Griffith, M., Moy, K., Yadav, M.K., Velasquez, J., Buchmeier, M.J., *et al.* (2006). Crystal structure of nonstructural protein 10 from the severe acute respiratory syndrome coronavirus reveals a novel fold with two zinc-binding motifs. J Virol *80*, 7894-7901.

Joseph, J.S., Saikatendu, K.S., Subramanian, V., Neuman, B.W., Buchmeier, M.J., Stevens, R.C., and Kuhn, P. (2007). Crystal structure of a monomeric form of severe acute respiratory syndrome coronavirus endonuclease nsp15 suggests a role for hexamerization as an allosteric switch. J Virol *81*, 6700-6708.

Kamitani, W., Huang, C., Narayanan, K., Lokugamage, K.G., and Makino, S. (2009). A two-pronged strategy to suppress host protein synthesis by SARS coronavirus Nsp1 protein. Nat Struct Mol Biol *16*, 1134-1140.

Kamitani, W., Narayanan, K., Huang, C., Lokugamage, K., Ikegami, T., Ito, N., Kubo, H., and Makino, S. (2006). Severe acute respiratory syndrome coronavirus nsp1 protein suppresses host gene expression by promoting host mRNA degradation. Proc Natl Acad Sci U S A *103*, 12885-12890.

Kan, B., Wang, M., Jing, H., Xu, H., Jiang, X., Yan, M., Liang, W., Zheng, H., Wan, K., Liu, Q., *et al.* (2005). Molecular evolution analysis and geographic investigation of

severe acute respiratory syndrome coronavirus-like virus in palm civets at an animal market and on farms. J Virol *79*, 11892-11900.

Kanzawa, N., Nishigaki, K., Hayashi, T., Ishii, Y., Furukawa, S., Niiro, A., Yasui, F., Kohara, M., Morita, K., Matsushima, K., *et al.* (2006). Augmentation of chemokine production by severe acute respiratory syndrome coronavirus 3a/X1 and 7a/X4 proteins through NF-kappaB activation. FEBS Lett *580*, 6807-6812.

Karjee, S., Minhas, A., Sood, V., Ponia, S.S., Banerjea, A.C., Chow, V.T., Mukherjee, S.K., and Lal, S.K. (2010). The 7a accessory protein of SARS-CoV acts as a RNA silencing suppressor. J Virol.

Keng, C.T., Akerstrom, S., Leung, C.S., Poon, L.L., Peiris, J.S., Mirazimi, A., and Tan, Y.J. (2011). SARS coronavirus 8b reduces viral replication by down-regulating E via an ubiquitin-independent proteasome pathway. Microbes Infect *13*, 179-188.

Keng, C.T., Choi, Y.W., Welkers, M.R., Chan, D.Z., Shen, S., Gee Lim, S., Hong, W., and Tan, Y.J. (2006). The human severe acute respiratory syndrome coronavirus (SARS-CoV) 8b protein is distinct from its counterpart in animal SARS-CoV and down-regulates the expression of the envelope protein in infected cells. Virology *354*, 132-142.

Keng, C.T., Zhang, A., Shen, S., Lip, K.M., Fielding, B.C., Tan, T.H., Chou, C.F., Loh, C.B., Wang, S., Fu, J., *et al.* (2005). Amino acids 1055 to 1192 in the S2 region of severe acute respiratory syndrome coronavirus S protein induce neutralizing antibodies: implications for the development of vaccines and antiviral agents. J Virol *79*, 3289-3296.

Keyaerts, E., Vijgen, L., Chen, L., Maes, P., Hedenstierna, G., and Van Ranst, M. (2004a). Inhibition of SARS-coronavirus infection in vitro by S-nitroso-N-acetylpenicillamine, a nitric oxide donor compound. Int J Infect Dis *8*, 223-226.

Khan, S., Fielding, B.C., Tan, T.H., Chou, C.F., Shen, S., Lim, S.G., Hong, W., and Tan, Y.J. (2006). Over-expression of severe acute respiratory syndrome coronavirus 3b protein induces both apoptosis and necrosis in Vero E6 cells. Virus Res *122*, 20-27.

Khan, S., Ng, M.L., and Tan, Y.J. (2007). Expression of the severe acute respiratory syndrome coronavirus 3a protein and the assembly of coronavirus-like particles in the baculovirus expression system. Methods Mol Biol *379*, 35-50.

Khattari, Z., Brotons, G., Akkawi, M., Arbely, E., Arkin, I.T., and Salditt, T. (2006). SARS coronavirus E protein in phospholipid bilayers: an x-ray study. Biophys J *90*, 2038-2050.

Knoops, K., Kikkert, M., Worm, S.H., Zevenhoven-Dobbe, J.C., van der Meer, Y., Koster, A.J., Mommaas, A.M., and Snijder, E.J. (2008). SARS-coronavirus replication is supported by a reticulovesicular network of modified endoplasmic reticulum. PLoS Biol *6*, e226.

Komar, A.A., and Hatzoglou, M. (2005). Internal ribosome entry sites in cellular mRNAs: mystery of their existence. J Biol Chem *280*, 23425-23428.

Kopecky-Bromberg, S.A., Martinez-Sobrido, L., Frieman, M., Baric, R.A., and Palese, P. (2007). Severe acute respiratory syndrome coronavirus open reading frame (ORF) 3b, ORF 6, and nucleocapsid proteins function as interferon antagonists. J Virol *81*, 548-557.

Kopecky-Bromberg, S.A., Martinez-Sobrido, L., and Palese, P. (2006). 7a protein of severe acute respiratory syndrome coronavirus inhibits cellular protein synthesis and activates p38 mitogen-activated protein kinase. J Virol *80*, 785-793.

Krokhin, O., Li, Y., Andonov, A., Feldmann, H., Flick, R., Jones, S., Stroeher, U., Bastien, N., Dasuri, K.V., Cheng, K., *et al.* (2003). Mass spectrometric characterization of proteins from the SARS virus: a preliminary report. Mol Cell Proteomics *2*, 346-356.

Ksiazek, T.G., Erdman, D., Goldsmith, C.S., Zaki, S.R., Peret, T., Emery, S., Tong, S., Urbani, C., Comer, J.A., Lim, W., *et al.* (2003). A novel coronavirus associated with severe acute respiratory syndrome. N Engl J Med *348*, 1953-1966.

Kuba, K., Imai, Y., Rao, S., Gao, H., Guo, F., Guan, B., Huan, Y., Yang, P., Zhang, Y., Deng, W., *et al.* (2005). A crucial role of angiotensin converting enzyme 2 (ACE2) in SARS coronavirus-induced lung injury. Nat Med *11*, 875-879.

Kubo, H., Takase-Yoden, S., and Taguchi, F. (1993). Neutralization and fusion inhibition activities of monoclonal antibodies specific for the S1 subunit of the spike protein of neurovirulent murine coronavirus JHMV c1-2 variant. J Gen Virol *74 (Pt 7)*, 1421-1425.

Kuiken, T., Fouchier, R.A., Schutten, M., Rimmelzwaan, G.F., van Amerongen, G., van Riel, D., Laman, J.D., de Jong, T., van Doornum, G., Lim, W., *et al.* (2003). Newly discovered coronavirus as the primary cause of severe acute respiratory syndrome. Lancet *362*, 263-270.

Kumar, P., Gunalan, V., Liu, B., Chow, V.T., Druce, J., Birch, C., Catton, M., Fielding, B.C., Tan, Y.J., and Lal, S.K. (2007). The nonstructural protein 8 (nsp8) of the SARS coronavirus interacts with its ORF6 accessory protein. Virology *366*, 293-303.

Lai, C.C., Jou, M.J., Huang, S.Y., Li, S.W., Wan, L., Tsai, F.J., and Lin, C.W. (2007). Proteomic analysis of up-regulated proteins in human promonocyte cells expressing severe acute respiratory syndrome coronavirus 3C-like protease. Proteomics *7*, 1446-1460.

Lai, C.W., Chan, Z.R., Yang, D.G., Lo, W.H., Lai, Y.K., Chang, M.D., and Hu, Y.C. (2006). Accelerated induction of apoptosis in insect cells by baculovirus-expressed SARS-CoV membrane protein. FEBS Lett *580*, 3829-3834.

Lai, M.M., and Cavanagh, D. (1997). The molecular biology of coronaviruses. Adv Virus Res *48*, 1-100.

Lam, T.T., Hon, C.C., Lam, P.Y., Yip, C.W., Zeng, F., and Leung, F.C. (2008). Comments to the predecessor of human SARS coronavirus in 2003-2004 epidemic. Vet Microbiol *126*, 390-393.

Lamirande, E.W., DeDiego, M.L., Roberts, A., Jackson, J.P., Alvarez, E., Sheahan, T., Shieh, W.J., Zaki, S.R., Baric, R., Enjuanes, L., *et al.* (2008). A live attenuated severe acute respiratory syndrome coronavirus is immunogenic and efficacious in golden Syrian hamsters. J Virol *82*, 7721-7724.

Lau, S.K., Li, K.S., Huang, Y., Shek, C.T., Tse, H., Wang, M., Choi, G.K., Xu, H., Lam, C.S., Guo, R., *et al.* (2010). Ecoepidemiology and complete genome comparison of different strains of severe acute respiratory syndrome-related Rhinolophus bat coronavirus in China reveal bats as a reservoir for acute, self-limiting infection that allows recombination events. J Virol *84*, 2808-2819.

Lau, S.K., Woo, P.C., Li, K.S., Huang, Y., Tsoi, H.W., Wong, B.H., Wong, S.S., Leung, S.Y., Chan, K.H., and Yuen, K.Y. (2005b). Severe acute respiratory syndrome coronavirus-like virus in Chinese horseshoe bats. Proc Natl Acad Sci U S A *102*, 14040-14045.

Lavillette, D., Barbouche, R., Yao, Y., Boson, B., Cosset, F.L., Jones, I.M., and Fenouillet, E. (2006). Significant redox insensitivity of the functions of the SARS-CoV spike glycoprotein: comparison with HIV envelope. J Biol Chem *281*, 9200-9204.

Law, A.H., Lee, D.C., Cheung, B.K., Yim, H.C., and Lau, A.S. (2007). Role for nonstructural protein 1 of severe acute respiratory syndrome coronavirus in chemokine dysregulation. J Virol *81*, 416-422.

Law, H.K., Cheung, C.Y., Ng, H.Y., Sia, S.F., Chan, Y.O., Luk, W., Nicholls, J.M., Peiris, J.S., and Lau, Y.L. (2005a). Chemokine up-regulation in SARS-coronavirus-infected, monocyte-derived human dendritic cells. Blood *106*, 2366-2374.

Law, P.T., Wong, C.H., Au, T.C., Chuck, C.P., Kong, S.K., Chan, P.K., To, K.F., Lo, A.W., Chan, J.Y., Suen, Y.K., *et al.* (2005b). The 3a protein of severe acute respiratory syndrome-associated coronavirus induces apoptosis in Vero E6 cells. J Gen Virol *86*, 1921-1930.

Law, P.Y., Liu, Y.M., Geng, H., Kwan, K.H., Waye, M.M., and Ho, Y.Y. (2006). Expression and functional characterization of the putative protein 8b of the severe acute respiratory syndrome-associated coronavirus. FEBS Lett *580*, 3643-3648.

Le, T.M., Wong, H.H., Tay, F.P., Fang, S., Keng, C.T., Tan, Y.J., and Liu, D.X. (2007). Expression, post-translational modification and biochemical characterization of proteins encoded by subgenomic mRNA8 of the severe acute respiratory syndrome coronavirus. FEBS J *274*, 4211-4222.

Lee, N., Hui, D., Wu, A., Chan, P., Cameron, P., Joynt, G.M., Ahuja, A., Yung, M.Y., Leung, C.B., To, K.F., *et al.* (2003). A major outbreak of severe acute respiratory syndrome in Hong Kong. N Engl J Med *348*, 1986-1994.

Li, F., Berardi, M., Li, W., Farzan, M., Dormitzer, P.R., and Harrison, S.C. (2006). Conformational states of the severe acute respiratory syndrome coronavirus spike protein ectodomain. J Virol *80*, 6794-6800.

Li, F., Li, W., Farzan, M., and Harrison, S.C. (2005a). Structure of SARS coronavirus spike receptor-binding domain complexed with receptor. Science *309*, 1864-1868.

Li, F.Q., Xiao, H., Tam, J.P., and Liu, D.X. (2005b). Sumoylation of the nucleocapsid protein of severe acute respiratory syndrome coronavirus. FEBS Lett *579*, 2387-2396.

Li, Q., Wang, L., Dong, C., Che, Y., Jiang, L., Liu, L., Zhao, H., Liao, Y., Sheng, Y., Dong, S., *et al.* (2005c). The interaction of the SARS coronavirus non-structural protein 10 with the cellular oxido-reductase system causes an extensive cytopathic effect. J Clin Virol *34*, 133-139.

Li, W., Greenough, T.C., Moore, M.J., Vasilieva, N., Somasundaran, M., Sullivan, J.L., Farzan, M., and Choe, H. (2004a). Efficient replication of severe acute respiratory syndrome coronavirus in mouse cells is limited by murine angiotensin-converting enzyme 2. J Virol *78*, 11429-11433.

Li, W., Moore, M.J., Vasilieva, N., Sui, J., Wong, S.K., Berne, M.A., Somasundaran, M., Sullivan, J.L., Luzuriaga, K., Greenough, T.C., *et al.* (2003b). Angiotensin-converting enzyme 2 is a functional receptor for the SARS coronavirus. Nature *426*, 450-454.

Li, W., Shi, Z., Yu, M., Ren, W., Smith, C., Epstein, J.H., Wang, H., Crameri, G., Hu, Z., Zhang, H., *et al.* (2005d). Bats are natural reservoirs of SARS-like coronaviruses. Science *310*, 676-679.

Liang, G., Chen, Q., Xu, J., Liu, Y., Lim, W., Peiris, J.S., Anderson, L.J., Ruan, L., Li, H., Kan, B., *et al.* (2004). Laboratory diagnosis of four recent sporadic cases of community-acquired SARS, Guangdong Province, China. Emerg Infect Dis *10*, 1774-1781.

Liao, Q.J., Ye, L.B., Timani, K.A., Zeng, Y.C., She, Y.L., Ye, L., and Wu, Z.H. (2005). Activation of NF-kappaB by the full-length nucleocapsid protein of the SARS coronavirus. Acta Biochim Biophys Sin (Shanghai) *37*, 607-612.

Liao, Y., Lescar, J., Tam, J.P., and Liu, D.X. (2004). Expression of SARS-coronavirus envelope protein in Escherichia coli cells alters membrane permeability. Biochem Biophys Res Commun *325*, 374-380.

Liao, Y., Yuan, Q., Torres, J., Tam, J.P., and Liu, D.X. (2006). Biochemical and functional characterization of the membrane association and membrane permeabilizing

activity of the severe acute respiratory syndrome coronavirus envelope protein. Virology *349*, 264-275.

Lindner, H.A., Fotouhi-Ardakani, N., Lytvyn, V., Lachance, P., Sulea, T., and Menard, R. (2005). The papain-like protease from the severe acute respiratory syndrome coronavirus is a deubiquitinating enzyme. J Virol *79*, 15199-15208.

Lip, K.M., Shen, S., Yang, X., Keng, C.T., Zhang, A., Oh, H.L., Li, Z.H., Hwang, L.A., Chou, C.F., Fielding, B.C., *et al.* (2006). Monoclonal antibodies targeting the HR2 domain and the region immediately upstream of the HR2 of the S protein neutralize in vitro infection of severe acute respiratory syndrome coronavirus. J Virol *80*, 941-950.

Liu, D.X., Cavanagh, D., Green, P., and Inglis, S.C. (1991). A polycistronic mRNA specified by the coronavirus infectious bronchitis virus. Virology *184*, 531-544.

Liu, D.X., and Inglis, S.C. (1992). Internal entry of ribosomes on a tricistronic mRNA encoded by infectious bronchitis virus. J Virol *66*, 6143-6154.

Liu, M., Gu, C., Wu, J., and Zhu, Y. (2006a). Amino acids 1 to 422 of the spike protein of SARS associated coronavirus are required for induction of cyclooxygenase-2. Virus Genes *33*, 309-317.

Liu, S., Xiao, G., Chen, Y., He, Y., Niu, J., Escalante, C.R., Xiong, H., Farmar, J., Debnath, A.K., Tien, P., *et al.* (2004). Interaction between heptad repeat 1 and 2 regions in spike protein of SARS-associated coronavirus: implications for virus fusogenic mechanism and identification of fusion inhibitors. Lancet *363*, 938-947.

Lontok, E., Corse, E., and Machamer, C.E. (2004). Intracellular targeting signals contribute to localization of coronavirus spike proteins near the virus assembly site. J Virol *78*, 5913-5922.

Lu, A., Zhang, H., Zhang, X., Wang, H., Hu, Q., Shen, L., Schaffhausen, B.S., Hou, W., and Li, L. (2004). Attenuation of SARS coronavirus by a short hairpin RNA expression plasmid targeting RNA-dependent RNA polymerase. Virology *324*, 84-89.

Lu, W., Zheng, B.J., Xu, K., Schwarz, W., Du, L., Wong, C.K., Chen, J., Duan, S., Deubel, V., and Sun, B. (2006). Severe acute respiratory syndrome-associated coronavirus 3a protein forms an ion channel and modulates virus release. Proc Natl Acad Sci U S A *103*, 12540-12545.

Lu, Y., Neo, T.L., Liu, D.X., and Tam, J.P. (2008). Importance of SARS-CoV spike protein Trp-rich region in viral infectivity. Biochem Biophys Res Commun *371*, 356-360.

Luo, C., Luo, H., Zheng, S., Gui, C., Yue, L., Yu, C., Sun, T., He, P., Chen, J., Shen, J., *et al.* (2004a). Nucleocapsid protein of SARS coronavirus tightly binds to human cyclophilin A. Biochem Biophys Res Commun *321*, 557-565.

Luo, H., Chen, Q., Chen, J., Chen, K., Shen, X., and Jiang, H. (2005b). The nucleocapsid protein of SARS coronavirus has a high binding affinity to the human cellular heterogeneous nuclear ribonucleoprotein A1. FEBS Lett *579*, 2623-2628.

Luo, H., Wu, D., Shen, C., Chen, K., Shen, X., and Jiang, H. (2006). Severe acute respiratory syndrome coronavirus membrane protein interacts with nucleocapsid protein mostly through their carboxyl termini by electrostatic attraction. Int J Biochem Cell Biol *38*, 589-599.

Luo, H., Ye, F., Chen, K., Shen, X., and Jiang, H. (2005a). SR-rich motif plays a pivotal role in recombinant SARS coronavirus nucleocapsid protein multimerization. Biochemistry *44*, 15351-15358.

Luo, H., Ye, F., Sun, T., Yue, L., Peng, S., Chen, J., Li, G., Du, Y., Xie, Y., Yang, Y., *et al.* (2004b). In vitro biochemical and thermodynamic characterization of nucleocapsid protein of SARS. Biophys Chem *112*, 15-25.

Madu, I.G., Belouzard, S., and Whittaker, G.R. (2009b). SARS-coronavirus spike S2 domain flanked by cysteine residues C822 and C833 is important for activation of membrane fusion. Virology *393*, 265-271.

Madu, I.G., Roth, S.L., Belouzard, S., and Whittaker, G.R. (2009a). Characterization of a highly conserved domain within the severe acute respiratory syndrome coronavirus spike protein S2 domain with characteristics of a viral fusion peptide. J Virol *83*, 7411-7421.

Marra, M.A., Jones, S.J., Astell, C.R., Holt, R.A., Brooks-Wilson, A., Butterfield, Y.S., Khattra, J., Asano, J.K., Barber, S.A., Chan, S.Y., *et al.* (2003). The Genome sequence of the SARS-associated coronavirus. Science *300*, 1399-1404.

Martina, B.E., Haagmans, B.L., Kuiken, T., Fouchier, R.A., Rimmelzwaan, G.F., Van Amerongen, G., Peiris, J.S., Lim, W., and Osterhaus, A.D. (2003). Virology: SARS virus infection of cats and ferrets. Nature *425*, 915.

Marzi, A., Gramberg, T., Simmons, G., Moller, P., Rennekamp, A.J., Krumbiegel, M., Geier, M., Eisemann, J., Turza, N., Saunier, B., *et al.* (2004). DC-SIGN and DC-SIGNR interact with the glycoprotein of Marburg virus and the S protein of severe acute respiratory syndrome coronavirus. J Virol *78*, 12090-12095.

Matsuyama, S., Ujike, M., Morikawa, S., Tashiro, M., and Taguchi, F. (2005). Protease-mediated enhancement of severe acute respiratory syndrome coronavirus infection. Proc Natl Acad Sci U S A *102*, 12543-12547.

McBride, C.E., Li, J., and Machamer, C.E. (2007). The cytoplasmic tail of the severe acute respiratory syndrome coronavirus spike protein contains a novel endoplasmic reticulum retrieval signal that binds COPI and promotes interaction with membrane protein. J Virol *81*, 2418-2428.

McBride, C.E., and Machamer, C.E. (2010a). A single tyrosine in the severe acute respiratory syndrome coronavirus membrane protein cytoplasmic tail is important for efficient interaction with spike protein. J Virol *84*, 1891-1901.

McBride, C.E., and Machamer, C.E. (2010b). Palmitoylation of SARS-CoV S protein is necessary for partitioning into detergent-resistant membranes and cell-cell fusion but not interaction with M protein. Virology *405*, 139-148.

McIntosh, K., Kapikian, A.Z., Hardison, K.A., Hartley, J.W., and Chanock, R.M. (1969). Antigenic relationships among the coronaviruses of man and between human and animal coronaviruses. J Immunol *102*, 1109-1118.

McReynolds, S., Jiang, S., Guo, Y., Celigoy, J., Schar, C., Rong, L., and Caffrey, M. (2008). Characterization of the prefusion and transition states of severe acute respiratory syndrome coronavirus S2-HR2. Biochemistry *47*, 6802-6808.

McReynolds, S., Jiang, S., Rong, L., and Caffrey, M. (2009). Dynamics of SARS-coronavirus HR2 domain in the prefusion and transition states. J Magn Reson *201*, 218-221.

Meier, C., Aricescu, A.R., Assenberg, R., Aplin, R.T., Gilbert, R.J., Grimes, J.M., and Stuart, D.I. (2006). The crystal structure of ORF-9b, a lipid binding protein from the SARS coronavirus. Structure *14*, 1157-1165.

Miknis, Z.J., Donaldson, E.F., Umland, T.C., Rimmer, R.A., Baric, R.S., and Schultz, L.W. (2009). Severe acute respiratory syndrome coronavirus nsp9 dimerization is essential for efficient viral growth. J Virol *83*, 3007-3018.

Minakshi, R., Padhan, K., Rani, M., Khan, N., Ahmad, F., and Jameel, S. (2009). The SARS Coronavirus 3a protein causes endoplasmic reticulum stress and induces ligand-independent downregulation of the type 1 interferon receptor. PLoS One *4*, e8342.

Minskaia, E., Hertzig, T., Gorbalenya, A.E., Campanacci, V., Cambillau, C., Canard, B., and Ziebuhr, J. (2006). Discovery of an RNA virus 3'->5' exoribonuclease that is critically involved in coronavirus RNA synthesis. Proc Natl Acad Sci U S A *103*, 5108-5113.

Mortola, E., and Roy, P. (2004). Efficient assembly and release of SARS coronavirus-like particles by a heterologous expression system. FEBS Lett *576*, 174-178.

Moser, M.J., Holley, W.R., Chatterjee, A., and Mian, I.S. (1997). The proofreading domain of Escherichia coli DNA polymerase I and other DNA and/or RNA exonuclease domains. Nucleic Acids Res *25*, 5110-5118.

Moshynskyy, I., Viswanathan, S., Vasilenko, N., Lobanov, V., Petric, M., Babiuk, L.A., and Zakhartchouk, A.N. (2007). Intracellular localization of the SARS coronavirus protein 9b: evidence of active export from the nucleus. Virus Res *127*, 116-121.

Nal, B., Chan, C., Kien, F., Siu, L., Tse, J., Chu, K., Kam, J., Staropoli, I., Crescenzo-Chaigne, B., Escriou, N., *et al.* (2005). Differential maturation and subcellular localization of severe acute respiratory syndrome coronavirus surface proteins S, M and E. J Gen Virol *86*, 1423-1434.

Narayanan, K., Huang, C., Lokugamage, K., Kamitani, W., Ikegami, T., Tseng, C.T., and Makino, S. (2008a). Severe acute respiratory syndrome coronavirus nsp1 suppresses host gene expression, including that of type I interferon, in infected cells. J Virol *82*, 4471-4479.

Narayanan, K., Huang, C., and Makino, S. (2008b). SARS coronavirus accessory proteins. Virus Res *133*, 113-121.

Nelson, C.A., Pekosz, A., Lee, C.A., Diamond, M.S., and Fremont, D.H. (2005). Structure and intracellular targeting of the SARS-coronavirus Orf7a accessory protein. Structure *13*, 75-85.

Netland, J., Ferraro, D., Pewe, L., Olivares, H., Gallagher, T., and Perlman, S. (2007). Enhancement of murine coronavirus replication by severe acute respiratory syndrome coronavirus protein 6 requires the N-terminal hydrophobic region but not C-terminal sorting motifs. J Virol *81*, 11520-11525.

Neuman, B.W., Joseph, J.S., Saikatendu, K.S., Serrano, P., Chatterjee, A., Johnson, M.A., Liao, L., Klaus, J.P., Yates, J.R., 3rd, Wuthrich, K., *et al.* (2008). Proteomics analysis unravels the functional repertoire of coronavirus nonstructural protein 3. J Virol *82*, 5279-5294.

Ni, L., Zhu, J., Zhang, J., Yan, M., Gao, G.F., and Tien, P. (2005). Design of recombinant protein-based SARS-CoV entry inhibitors targeting the heptad-repeat regions of the spike protein S2 domain. Biochem Biophys Res Commun *330*, 39-45.

Nicholls, J.M., Butany, J., Poon, L.L., Chan, K.H., Beh, S.L., Poutanen, S., Peiris, J.S., and Wong, M. (2006). Time course and cellular localization of SARS-CoV nucleoprotein and RNA in lungs from fatal cases of SARS. PLoS Med *3*, e27.

Obitsu, S., Ahmed, N., Nishitsuji, H., Hasegawa, A., Nakahama, K., Morita, I., Nishigaki, K., Hayashi, T., Masuda, T., and Kannagi, M. (2009). Potential enhancement of osteoclastogenesis by severe acute respiratory syndrome coronavirus 3a/X1 protein. Arch Virol *154*, 1457-1464.

Oostra, M., de Haan, C.A., de Groot, R.J., and Rottier, P.J. (2006). Glycosylation of the severe acute respiratory syndrome coronavirus triple-spanning membrane proteins 3a and M. J Virol *80*, 2326-2336.

Oostra, M., de Haan, C.A., and Rottier, P.J. (2007a). The 29-nucleotide deletion present in human but not in animal severe acute respiratory syndrome coronaviruses disrupts the functional expression of open reading frame 8. J Virol *81*, 13876-13888.

Oostra, M., te Lintelo, E.G., Deijs, M., Verheije, M.H., Rottier, P.J., and de Haan, C.A. (2007b). Localization and membrane topology of coronavirus nonstructural protein 4: involvement of the early secretory pathway in replication. J Virol *81*, 12323-12336.

Orlowski, M., and Wilk, S. (2003). Ubiquitin-independent proteolytic functions of the proteasome. Arch Biochem Biophys *415*, 1-5.

Padhan, K., Minakshi, R., Towheed, M.A., and Jameel, S. (2008). Severe acute respiratory syndrome coronavirus 3a protein activates the mitochondrial death pathway through p38 MAP kinase activation. J Gen Virol *89*, 1960-1969.

Padhan, K., Tanwar, C., Hussain, A., Hui, P.Y., Lee, M.Y., Cheung, C.Y., Peiris, J.S., and Jameel, S. (2007). Severe acute respiratory syndrome coronavirus Orf3a protein interacts with caveolin. J Gen Virol *88*, 3067-3077.

Pan, J., Peng, X., Gao, Y., Li, Z., Lu, X., Chen, Y., Ishaq, M., Liu, D., Dediego, M.L., Enjuanes, L., *et al.* (2008). Genome-wide analysis of protein-protein interactions and involvement of viral proteins in SARS-CoV replication. PLoS One *3*, e3299.

Parthasarathy, K., Ng, L., Lin, X., Liu, D.X., Pervushin, K., Gong, X., and Torres, J. (2008). Structural flexibility of the pentameric SARS coronavirus envelope protein ion channel. Biophys J *95*, L39-41.

Peiris, J.S., Guan, Y., and Yuen, K.Y. (2004). Severe acute respiratory syndrome. Nat Med *10*, S88-97.

Peiris, J.S., Lai, S.T., Poon, L.L., Guan, Y., Yam, L.Y., Lim, W., Nicholls, J., Yee, W.K., Yan, W.W., Cheung, M.T., *et al.* (2003b). Coronavirus as a possible cause of severe acute respiratory syndrome. Lancet *361*, 1319-1325.

Pervushin, K., Tan, E., Parthasarathy, K., Lin, X., Jiang, F.L., Yu, D., Vararattanavech, A., Soong, T.W., Liu, D.X., and Torres, J. (2009). Structure and inhibition of the SARS coronavirus envelope protein ion channel. PLoS Pathog *5*, e1000511.

Peti, W., Johnson, M.A., Herrmann, T., Neuman, B.W., Buchmeier, M.J., Nelson, M., Joseph, J., Page, R., Stevens, R.C., Kuhn, P., *et al.* (2005). Structural genomics of the severe acute respiratory syndrome coronavirus: nuclear magnetic resonance structure of the protein nsP7. J Virol *79*, 12905-12913.

Petit, C.M., Chouljenko, V.N., Iyer, A., Colgrove, R., Farzan, M., Knipe, D.M., and Kousoulas, K.G. (2007). Palmitoylation of the cysteine-rich endodomain of the SARS-coronavirus spike glycoprotein is important for spike-mediated cell fusion. Virology *360*, 264-274.

Petit, C.M., Melancon, J.M., Chouljenko, V.N., Colgrove, R., Farzan, M., Knipe, D.M., and Kousoulas, K.G. (2005). Genetic analysis of the SARS-coronavirus spike glycoprotein functional domains involved in cell-surface expression and cell-to-cell fusion. Virology *341*, 215-230.

Pewe, L., Zhou, H., Netland, J., Tangudu, C., Olivares, H., Shi, L., Look, D., Gallagher, T., and Perlman, S. (2005). A severe acute respiratory syndrome-associated coronavirus-specific protein enhances virulence of an attenuated murine coronavirus. J Virol *79*, 11335-11342.

Pfefferle, S., Krahling, V., Ditt, V., Grywna, K., Muhlberger, E., and Drosten, C. (2009a). Reverse genetic characterization of the natural genomic deletion in SARS-Coronavirus strain Frankfurt-1 open reading frame 7b reveals an attenuating function of the 7b protein in-vitro and in-vivo. Virol J *6*, 131.

Pfefferle, S., Oppong, S., Drexler, J.F., Gloza-Rausch, F., Ipsen, A., Seebens, A., Muller, M.A., Annan, A., Vallo, P., Adu-Sarkodie, Y., *et al.* (2009b). Distant relatives of severe acute respiratory syndrome coronavirus and close relatives of human coronavirus 229E in bats, Ghana. Emerg Infect Dis *15*, 1377-1384.

Plant, E.P., and Dinman, J.D. (2008). The role of programmed-1 ribosomal frameshifting in coronavirus propagation. Front Biosci *13*, 4873-4881.

Poon, L.L., Chu, D.K., Chan, K.H., Wong, O.K., Ellis, T.M., Leung, Y.H., Lau, S.K., Woo, P.C., Suen, K.Y., Yuen, K.Y., *et al.* (2005). Identification of a novel coronavirus in bats. J Virol *79*, 2001-2009.

Prentice, E., McAuliffe, J., Lu, X., Subbarao, K., and Denison, M.R. (2004). Identification and characterization of severe acute respiratory syndrome coronavirus replicase proteins. J Virol *78*, 9977-9986.

Putics, A., Filipowicz, W., Hall, J., Gorbalenya, A.E., and Ziebuhr, J. (2005). ADP-ribose-1"-monophosphatase: a conserved coronavirus enzyme that is dispensable for viral replication in tissue culture. J Virol *79*, 12721-12731.

Qiu, M., Shi, Y., Guo, Z., Chen, Z., He, R., Chen, R., Zhou, D., Dai, E., Wang, X., Si, B., *et al.* (2005). Antibody responses to individual proteins of SARS coronavirus and their neutralization activities. Microbes Infect *7*, 882-889.

Rasschaert, D., Duarte, M., and Laude, H. (1990). Porcine respiratory coronavirus differs from transmissible gastroenteritis virus by a few genomic deletions. J Gen Virol *71 (Pt 11)*, 2599-2607.

Ratia, K., Saikatendu, K.S., Santarsiero, B.D., Barretto, N., Baker, S.C., Stevens, R.C., and Mesecar, A.D. (2006). Severe acute respiratory syndrome coronavirus papain-like protease: structure of a viral deubiquitinating enzyme. Proc Natl Acad Sci U S A *103*, 5717-5722.

Reed, L., and Muench, H. (1938). A simple method of estimating fifty percent endpoints. Am J Hyg *27*, 493-497.

Reed, M.L., Dove, B.K., Jackson, R.M., Collins, R., Brooks, G., and Hiscox, J.A. (2006). Delineation and modelling of a nucleolar retention signal in the coronavirus nucleocapsid protein. Traffic *7*, 833-848.

Ren, W., Li, W., Yu, M., Hao, P., Zhang, Y., Zhou, P., Zhang, S., Zhao, G., Zhong, Y., Wang, S., *et al.* (2006). Full-length genome sequences of two SARS-like coronaviruses in horseshoe bats and genetic variation analysis. J Gen Virol *87*, 3355-3359.

Ren, W., Qu, X., Li, W., Han, Z., Yu, M., Zhou, P., Zhang, S.Y., Wang, L.F., Deng, H., and Shi, Z. (2008). Difference in receptor usage between severe acute respiratory syndrome (SARS) coronavirus and SARS-like coronavirus of bat origin. J Virol *82*, 1899-1907.

Ricagno, S., Egloff, M.P., Ulferts, R., Coutard, B., Nurizzo, D., Campanacci, V., Cambillau, C., Ziebuhr, J., and Canard, B. (2006). Crystal structure and mechanistic determinants of SARS coronavirus nonstructural protein 15 define an endoribonuclease family. Proc Natl Acad Sci U S A *103*, 11892-11897.

Ritchie, G., Harvey, D.J., Feldmann, F., Stroeher, U., Feldmann, H., Royle, L., Dwek, R.A., and Rudd, P.M. (2010). Identification of N-linked carbohydrates from severe acute respiratory syndrome (SARS) spike glycoprotein. Virology *399*, 257-269.

Roberts, A., Vogel, L., Guarner, J., Hayes, N., Murphy, B., Zaki, S., and Subbarao, K. (2005). Severe acute respiratory syndrome coronavirus infection of golden Syrian hamsters. J Virol *79*, 503-511.

Rockx, B., Corti, D., Donaldson, E., Sheahan, T., Stadler, K., Lanzavecchia, A., and Baric, R. (2008). Structural basis for potent cross-neutralizing human monoclonal antibody protection against lethal human and zoonotic severe acute respiratory syndrome coronavirus challenge. J Virol *82*, 3220-3235.

Rota, P.A., Oberste, M.S., Monroe, S.S., Nix, W.A., Campagnoli, R., Icenogle, J.P., Penaranda, S., Bankamp, B., Maher, K., Chen, M.H., *et al.* (2003). Characterization of a novel coronavirus associated with severe acute respiratory syndrome. Science *300*, 1394-1399.

Rowe, T., Gao, G., Hogan, R.J., Crystal, R.G., Voss, T.G., Grant, R.L., Bell, P., Kobinger, G.P., Wivel, N.A., and Wilson, J.M. (2004). Macaque model for severe acute respiratory syndrome. J Virol *78*, 11401-11404.

Rowland, R.R., Chauhan, V., Fang, Y., Pekosz, A., Kerrigan, M., and Burton, M.D. (2005). Intracellular localization of the severe acute respiratory syndrome coronavirus nucleocapsid protein: absence of nucleolar accumulation during infection and after expression as a recombinant protein in vero cells. J Virol *79*, 11507-11512.

Ruan, Y.J., Wei, C.L., Ee, A.L., Vega, V.B., Thoreau, H., Su, S.T., Chia, J.M., Ng, P., Chiu, K.P., Lim, L., *et al.* (2003). Comparative full-length genome sequence analysis of

14 SARS coronavirus isolates and common mutations associated with putative origins of infection. Lancet *361*, 1779-1785.

Saikatendu, K.S., Joseph, J.S., Subramanian, V., Clayton, T., Griffith, M., Moy, K., Velasquez, J., Neuman, B.W., Buchmeier, M.J., Stevens, R.C., *et al.* (2005). Structural basis of severe acute respiratory syndrome coronavirus ADP-ribose-1"-phosphate dephosphorylation by a conserved domain of nsP3. Structure *13*, 1665-1675.

Saikatendu, K.S., Joseph, J.S., Subramanian, V., Neuman, B.W., Buchmeier, M.J., Stevens, R.C., and Kuhn, P. (2007). Ribonucleocapsid formation of severe acute respiratory syndrome coronavirus through molecular action of the N-terminal domain of N protein. J Virol *81*, 3913-3921.

Sainz, B., Jr., Rausch, J.M., Gallaher, W.R., Garry, R.F., and Wimley, W.C. (2005a). Identification and characterization of the putative fusion peptide of the severe acute respiratory syndrome-associated coronavirus spike protein. J Virol *79*, 7195-7206.

Sainz, B., Jr., Rausch, J.M., Gallaher, W.R., Garry, R.F., and Wimley, W.C. (2005b). The aromatic domain of the coronavirus class I viral fusion protein induces membrane permeabilization: putative role during viral entry. Biochemistry *44*, 947-958.

Sawicki, S.G., and Sawicki, D.L. (2005a). Coronavirus transcription: a perspective. Curr Top Microbiol Immunol *287*, 31-55.

Sawicki, S.G., Sawicki, D.L., and Siddell, S.G. (2007). A contemporary view of coronavirus transcription. J Virol *81*, 20-29.

Sawicki, S.G., Sawicki, D.L., Younker, D., Meyer, Y., Thiel, V., Stokes, H., and Siddell, S.G. (2005b). Functional and genetic analysis of coronavirus replicase-transcriptase proteins. PLoS Pathog *1*, e39.

Schaecher, S.R., Diamond, M.S., and Pekosz, A. (2008b). The transmembrane domain of the severe acute respiratory syndrome coronavirus ORF7b protein is necessary and sufficient for its retention in the Golgi complex. J Virol *82*, 9477-9491.

Schaecher, S.R., Mackenzie, J.M., and Pekosz, A. (2007b). The ORF7b protein of severe acute respiratory syndrome coronavirus (SARS-CoV) is expressed in virus-infected cells and incorporated into SARS-CoV particles. J Virol *81*, 718-731.

Schaecher, S.R., Stabenow, J., Oberle, C., Schriewer, J., Buller, R.M., Sagartz, J.E., and Pekosz, A. (2008a). An immunosuppressed Syrian golden hamster model for SARS-CoV infection. Virology *380*, 312-321.

Schaecher, S.R., Touchette, E., Schriewer, J., Buller, R.M., and Pekosz, A. (2007a). Severe acute respiratory syndrome coronavirus gene 7 products contribute to virus-induced apoptosis. J Virol *81*, 11054-11068.

Senanayake, S.D., and Brian, D.A. (1997). Bovine coronavirus I protein synthesis follows ribosomal scanning on the bicistronic N mRNA. Virus Res *48*, 101-105.

Seo, S.H., Hoffmann, E., and Webster, R.G. (2002). Lethal H5N1 influenza viruses escape host anti-viral cytokine responses. Nat Med *8*, 950-954.

Serrano, P., Johnson, M.A., Almeida, M.S., Horst, R., Herrmann, T., Joseph, J.S., Neuman, B.W., Subramanian, V., Saikatendu, K.S., Buchmeier, M.J., *et al.* (2007). Nuclear magnetic resonance structure of the N-terminal domain of nonstructural protein 3 from the severe acute respiratory syndrome coronavirus. J Virol *81*, 12049-12060.

Sharma, K., Surjit, M., Satija, N., Liu, B., Chow, V.T., and Lal, S.K. (2007). The 3a accessory protein of SARS coronavirus specifically interacts with the 5'UTR of its genomic RNA, Using a unique 75 amino acid interaction domain. Biochemistry *46*, 6488-6499.

Shen, S., Lin, P.S., Chao, Y.C., Zhang, A., Yang, X., Lim, S.G., Hong, W., and Tan, Y.J. (2005). The severe acute respiratory syndrome coronavirus 3a is a novel structural protein. Biochem Biophys Res Commun *330*, 286-292.

Shen, X., Xue, J.H., Yu, C.Y., Luo, H.B., Qin, L., Yu, X.J., Chen, J., Chen, L.L., Xiong, B., Yue, L.D., *et al.* (2003). Small envelope protein E of SARS: cloning, expression, purification, CD determination, and bioinformatics analysis. Acta Pharmacol Sin *24*, 505-511.

Shi, J., Sivaraman, J., and Song, J. (2008a). Mechanism for controlling the dimer-monomer switch and coupling dimerization to catalysis of the severe acute respiratory syndrome coronavirus 3C-like protease. J Virol *82*, 4620-4629.

Shi, Y., Wan, Z., Li, L., Li, P., Li, C., Ma, Q., and Cao, C. (2004). Antibody responses against SARS-coronavirus and its nucleocaspid in SARS patients. J Clin Virol *31*, 66-68.

Shi, Z., and Hu, Z. (2008b). A review of studies on animal reservoirs of the SARS coronavirus. Virus Res *133*, 74-87.

Shih, Y.P., Chen, C.Y., Liu, S.J., Chen, K.H., Lee, Y.M., Chao, Y.C., and Chen, Y.M. (2006). Identifying epitopes responsible for neutralizing antibody and DC-SIGN binding on the spike glycoprotein of the severe acute respiratory syndrome coronavirus. J Virol *80*, 10315-10324.

Simmons, G., Gosalia, D.N., Rennekamp, A.J., Reeves, J.D., Diamond, S.L., and Bates, P. (2005). Inhibitors of cathepsin L prevent severe acute respiratory syndrome coronavirus entry. Proc Natl Acad Sci U S A *102*, 11876-11881.

Simmons, G., Reeves, J.D., Rennekamp, A.J., Amberg, S.M., Piefer, A.J., and Bates, P. (2004). Characterization of severe acute respiratory syndrome-associated coronavirus (SARS-CoV) spike glycoprotein-mediated viral entry. Proc Natl Acad Sci U S A *101*, 4240-4245.

Sims, A.C., Baric, R.S., Yount, B., Burkett, S.E., Collins, P.L., and Pickles, R.J. (2005). Severe acute respiratory syndrome coronavirus infection of human ciliated airway epithelia: role of ciliated cells in viral spread in the conducting airways of the lungs. J Virol *79*, 15511-15524.

Siu, K.L., Kok, K.H., Ng, M.H., Poon, V.K., Yuen, K.Y., Zheng, B.J., and Jin, D.Y. (2009). Severe acute respiratory syndrome coronavirus M protein inhibits type I interferon production by impeding the formation of TRAF3.TANK.TBK1/IKKepsilon complex. J Biol Chem *284*, 16202-16209.

Siu, Y.L., Teoh, K.T., Lo, J., Chan, C.M., Kien, F., Escriou, N., Tsao, S.W., Nicholls, J.M., Altmeyer, R., Peiris, J.S., *et al.* (2008). The M, E, and N structural proteins of the severe acute respiratory syndrome coronavirus are required for efficient assembly, trafficking, and release of virus-like particles. J Virol *82*, 11318-11330.

Snijder, E.J., Bredenbeek, P.J., Dobbe, J.C., Thiel, V., Ziebuhr, J., Poon, L.L., Guan, Y., Rozanov, M., Spaan, W.J., and Gorbalenya, A.E. (2003). Unique and conserved features of genome and proteome of SARS-coronavirus, an early split-off from the coronavirus group 2 lineage. J Mol Biol *331*, 991-1004.

Song, H.C., Seo, M.Y., Stadler, K., Yoo, B.J., Choo, Q.L., Coates, S.R., Uematsu, Y., Harada, T., Greer, C.E., Polo, J.M., *et al.* (2004). Synthesis and characterization of a native, oligomeric form of recombinant severe acute respiratory syndrome coronavirus spike glycoprotein. J Virol *78*, 10328-10335.

Song, H.D., Tu, C.C., Zhang, G.W., Wang, S.Y., Zheng, K., Lei, L.C., Chen, Q.X., Gao, Y.W., Zhou, H.Q., Xiang, H., *et al.* (2005). Cross-host evolution of severe acute respiratory syndrome coronavirus in palm civet and human. Proc Natl Acad Sci U S A *102*, 2430-2435.

Spiegel, M., Pichlmair, A., Martinez-Sobrido, L., Cros, J., Garcia-Sastre, A., Haller, O., and Weber, F. (2005). Inhibition of Beta interferon induction by severe acute respiratory syndrome coronavirus suggests a two-step model for activation of interferon regulatory factor 3. J Virol *79*, 2079-2086.

Stertz, S., Reichelt, M., Spiegel, M., Kuri, T., Martinez-Sobrido, L., Garcia-Sastre, A., Weber, F., and Kochs, G. (2007). The intracellular sites of early replication and budding of SARS-coronavirus. Virology *361*, 304-315.

Stoneley, M., and Willis, A.E. (2004). Cellular internal ribosome entry segments: structures, trans-acting factors and regulation of gene expression. Oncogene *23*, 3200-3207.

Su, D., Lou, Z., Sun, F., Zhai, Y., Yang, H., Zhang, R., Joachimiak, A., Zhang, X.C., Bartlam, M., and Rao, Z. (2006). Dodecamer structure of severe acute respiratory syndrome coronavirus nonstructural protein nsp10. J Virol *80*, 7902-7908.

Subbarao, K., McAuliffe, J., Vogel, L., Fahle, G., Fischer, S., Tatti, K., Packard, M., Shieh, W.J., Zaki, S., and Murphy, B. (2004). Prior infection and passive transfer of neutralizing antibody prevent replication of severe acute respiratory syndrome coronavirus in the respiratory tract of mice. J Virol *78*, 3572-3577.

Sui, J., Hwang, W.C., Perez, S., Wei, G., Aird, D., Chen, L.M., Santelli, E., Stec, B., Cadwell, G., Ali, M., *et al.* (2009). Structural and functional bases for broad-spectrum neutralization of avian and human influenza A viruses. Nat Struct Mol Biol *16*, 265-273.

Sui, J., Li, W., Murakami, A., Tamin, A., Matthews, L.J., Wong, S.K., Moore, M.J., Tallarico, A.S., Olurinde, M., Choe, H., *et al.* (2004). Potent neutralization of severe acute respiratory syndrome (SARS) coronavirus by a human mAb to S1 protein that blocks receptor association. Proc Natl Acad Sci U S A *101*, 2536-2541.

Sui, J., Li, W., Roberts, A., Matthews, L.J., Murakami, A., Vogel, L., Wong, S.K., Subbarao, K., Farzan, M., and Marasco, W.A. (2005). Evaluation of human monoclonal antibody 80R for immunoprophylaxis of severe acute respiratory syndrome by an animal study, epitope mapping, and analysis of spike variants. J Virol *79*, 5900-5906.

Sulea, T., Lindner, H.A., Purisima, E.O., and Menard, R. (2005). Deubiquitination, a new function of the severe acute respiratory syndrome coronavirus papain-like protease? J Virol *79*, 4550-4551.

Sulkin, S.E., and Allen, R. (1974). Virus infections in bats. Monogr Virol *8*, 1-103.

Sung, S.C., Chao, C.Y., Jeng, K.S., Yang, J.Y., and Lai, M.M. (2009). The 8ab protein of SARS-CoV is a luminal ER membrane-associated protein and induces the activation of ATF6. Virology *387*, 402-413.

Supekar, V.M., Bruckmann, C., Ingallinella, P., Bianchi, E., Pessi, A., and Carfi, A. (2004). Structure of a proteolytically resistant core from the severe acute respiratory syndrome coronavirus S2 fusion protein. Proc Natl Acad Sci U S A *101*, 17958-17963.

Surjit, M., Kumar, R., Mishra, R.N., Reddy, M.K., Chow, V.T., and Lal, S.K. (2005). The severe acute respiratory syndrome coronavirus nucleocapsid protein is phosphorylated and localizes in the cytoplasm by 14-3-3-mediated translocation. J Virol *79*, 11476-11486.

Surjit, M., and Lal, S.K. (2008). The SARS-CoV nucleocapsid protein: a protein with multifarious activities. Infect Genet Evol *8*, 397-405.

Surjit, M., Liu, B., Chow, V.T., and Lal, S.K. (2006). The nucleocapsid protein of severe acute respiratory syndrome-coronavirus inhibits the activity of cyclin-cyclin-dependent kinase complex and blocks S phase progression in mammalian cells. J Biol Chem *281*, 10669-10681.

Surjit, M., Liu, B., Jameel, S., Chow, V.T., and Lal, S.K. (2004b). The SARS coronavirus nucleocapsid protein induces actin reorganization and apoptosis in COS-1 cells in the absence of growth factors. Biochem J *383*, 13-18.

Surjit, M., Liu, B., Kumar, P., Chow, V.T., and Lal, S.K. (2004a). The nucleocapsid protein of the SARS coronavirus is capable of self-association through a C-terminal 209 amino acid interaction domain. Biochem Biophys Res Commun *317*, 1030-1036.

Sutton, G., Fry, E., Carter, L., Sainsbury, S., Walter, T., Nettleship, J., Berrow, N., Owens, R., Gilbert, R., Davidson, A., *et al.* (2004). The nsp9 replicase protein of SARS-coronavirus, structure and functional insights. Structure *12*, 341-353.

Taguchi, F., and Shimazaki, Y.K. (2000). Functional analysis of an epitope in the S2 subunit of the murine coronavirus spike protein: involvement in fusion activity. J Gen Virol *81*, 2867-2871.

Tan, J., Kusov, Y., Mutschall, D., Tech, S., Nagarajan, K., Hilgenfeld, R., and Schmidt, C.L. (2007c). The "SARS-unique domain" (SUD) of SARS coronavirus is an oligo(G)-binding protein. Biochem Biophys Res Commun *364*, 877-882.

Tan, J., Vonrhein, C., Smart, O.S., Bricogne, G., Bollati, M., Kusov, Y., Hansen, G., Mesters, J.R., Schmidt, C.L., and Hilgenfeld, R. (2009). The SARS-unique domain (SUD) of SARS coronavirus contains two macrodomains that bind G-quadruplexes. PLoS Pathog *5*, e1000428.

Tan, T.H., Barkham, T., Fielding, B.C., Chou, C.F., Shen, S., Lim, S.G., Hong, W., and Tan, Y.J. (2005c). Genetic lesions within the 3a gene of SARS-CoV. Virol J *2*, 51.

Tan, Y.J., Fielding, B.C., Goh, P.Y., Shen, S., Tan, T.H., Lim, S.G., and Hong, W. (2004b). Overexpression of 7a, a protein specifically encoded by the severe acute respiratory syndrome coronavirus, induces apoptosis via a caspase-dependent pathway. J Virol *78*, 14043-14047.

Tan, Y.J., Teng, E., Shen, S., Tan, T.H., Goh, P.Y., Fielding, B.C., Ooi, E.E., Tan, H.C., Lim, S.G., and Hong, W. (2004a). A novel severe acute respiratory syndrome coronavirus protein, U274, is transported to the cell surface and undergoes endocytosis. J Virol *78*, 6723-6734.

Tan, Y.J., Tham, P.Y., Chan, D.Z., Chou, C.F., Shen, S., Fielding, B.C., Tan, T.H., Lim, S.G., and Hong, W. (2005b). The severe acute respiratory syndrome coronavirus 3a protein up-regulates expression of fibrinogen in lung epithelial cells. J Virol *79*, 10083-10087.

Tan, Y.X., Tan, T.H., Lee, M.J., Tham, P.Y., Gunalan, V., Druce, J., Birch, C., Catton, M., Fu, N.Y., Yu, V.C., *et al.* (2007b). Induction of apoptosis by the severe acute respiratory syndrome coronavirus 7a protein is dependent on its interaction with the Bcl-XL protein. J Virol *81*, 6346-6355.

Tang, X.C., Zhang, J.X., Zhang, S.Y., Wang, P., Fan, X.H., Li, L.F., Li, G., Dong, B.Q., Liu, W., Cheung, C.L., *et al.* (2006). Prevalence and genetic diversity of coronaviruses in bats from China. J Virol *80*, 7481-7490.

Tangudu, C., Olivares, H., Netland, J., Perlman, S., and Gallagher, T. (2007). Severe acute respiratory syndrome coronavirus protein 6 accelerates murine coronavirus infections. J Virol *81*, 1220-1229.

Tanner, J.A., Watt, R.M., Chai, Y.B., Lu, L.Y., Lin, M.C., Peiris, J.S., Poon, L.L., Kung, H.F., and Huang, J.D. (2003). The severe acute respiratory syndrome (SARS) coronavirus NTPase/helicase belongs to a distinct class of 5' to 3' viral helicases. J Biol Chem *278*, 39578-39582.

te Velthuis, A.J., Arnold, J.J., Cameron, C.E., van den Worm, S.H., and Snijder, E.J. (2010). The RNA polymerase activity of SARS-coronavirus nsp12 is primer dependent. Nucleic Acids Res *38*, 203-214.

ter Meulen, J., Bakker, A.B., van den Brink, E.N., Weverling, G.J., Martina, B.E., Haagmans, B.L., Kuiken, T., de Kruif, J., Preiser, W., Spaan, W., *et al.* (2004). Human monoclonal antibody as prophylaxis for SARS coronavirus infection in ferrets. Lancet *363*, 2139-2141.

Thiel, V., Ivanov, K.A., Putics, A., Hertzig, T., Schelle, B., Bayer, S., Weissbrich, B., Snijder, E.J., Rabenau, H., Doerr, H.W., *et al.* (2003). Mechanisms and enzymes involved in SARS coronavirus genome expression. J Gen Virol *84*, 2305-2315.

Thiel, V., and Siddell, S.G. (1994). Internal ribosome entry in the coding region of murine hepatitis virus mRNA 5. J Gen Virol *75 (Pt 11)*, 3041-3046.

Timani, K.A., Liao, Q., Ye, L., Zeng, Y., Liu, J., Zheng, Y., Yang, X., Lingbao, K., Gao, J., and Zhu, Y. (2005). Nuclear/nucleolar localization properties of C-terminal nucleocapsid protein of SARS coronavirus. Virus Res *114*, 23-34.

Torres, J., Maheswari, U., Parthasarathy, K., Ng, L., Liu, D.X., and Gong, X. (2007). Conductance and amantadine binding of a pore formed by a lysine-flanked transmembrane domain of SARS coronavirus envelope protein. Protein Sci *16*, 2065-2071.

Torres, J., Parthasarathy, K., Lin, X., Saravanan, R., Kukol, A., and Liu, D.X. (2006). Model of a putative pore: the pentameric alpha-helical bundle of SARS coronavirus E protein in lipid bilayers. Biophys J *91*, 938-947.

Tripet, B., Howard, M.W., Jobling, M., Holmes, R.K., Holmes, K.V., and Hodges, R.S. (2004). Structural characterization of the SARS-coronavirus spike S fusion protein core. J Biol Chem *279*, 20836-20849.

Tseng, Y.T., Wang, S.M., Huang, K.J., Lee, A.I., Chiang, C.C., and Wang, C.T. (2010). Self-assembly of severe acute respiratory syndrome coronavirus membrane protein. J Biol Chem *285*, 12862-12872.

Tu, C., Crameri, G., Kong, X., Chen, J., Sun, Y., Yu, M., Xiang, H., Xia, X., Liu, S., Ren, T., *et al.* (2004). Antibodies to SARS coronavirus in civets. Emerg Infect Dis *10*, 2244-2248.

Ujike, M., Nishikawa, H., Otaka, A., Yamamoto, N., Matsuoka, M., Kodama, E., Fujii, N., and Taguchi, F. (2008). Heptad repeat-derived peptides block protease-mediated direct entry from the cell surface of severe acute respiratory syndrome coronavirus but not entry via the endosomal pathway. J Virol *82*, 588-592.

van Hemert, M.J., van den Worm, S.H., Knoops, K., Mommaas, A.M., Gorbalenya, A.E., and Snijder, E.J. (2008). SARS-coronavirus replication/transcription complexes are membrane-protected and need a host factor for activity in vitro. PLoS Pathog *4*, e1000054.

Vega, V.B., Ruan, Y., Liu, J., Lee, W.H., Wei, C.L., Se-Thoe, S.Y., Tang, K.F., Zhang, T., Kolatkar, P.R., Ooi, E.E., *et al.* (2004). Mutational dynamics of the SARS coronavirus in cell culture and human populations isolated in 2003. BMC Infect Dis *4*, 32.

Vijaykrishna, D., Smith, G.J., Zhang, J.X., Peiris, J.S., Chen, H., and Guan, Y. (2007). Evolutionary insights into the ecology of coronaviruses. J Virol *81*, 4012-4020.

von Grotthuss, M., Wyrwicz, L.S., and Rychlewski, L. (2003). mRNA cap-1 methyltransferase in the SARS genome. Cell *113*, 701-702.

Voss, D., Kern, A., Traggiai, E., Eickmann, M., Stadler, K., Lanzavecchia, A., and Becker, S. (2006). Characterization of severe acute respiratory syndrome coronavirus membrane protein. FEBS Lett *580*, 968-973.

Voss, D., Pfefferle, S., Drosten, C., Stevermann, L., Traggiai, E., Lanzavecchia, A., and Becker, S. (2009). Studies on membrane topology, N-glycosylation and functionality of SARS-CoV membrane protein. Virol J *6*, 79.

Vossen, M.T., Westerhout, E.M., Soderberg-Naucler, C., and Wiertz, E.J. (2002). Viral immune evasion: a masterpiece of evolution. Immunogenetics *54*, 527-542.

Wang, J.M., Wang, L.F., and Shi, Z.L. (2008a). Construction of a non-infectious SARS coronavirus replicon for application in drug screening and analysis of viral protein function. Biochem Biophys Res Commun *374*, 138-142.

Wang, M., Jing, H.Q., Xu, H.F., Jiang, X.G., Kan, B., Liu, Q.Y., Wan, K.L., Cui, B.Y., Zheng, H., Cui, Z.G., *et al.* (2005b). [Surveillance on severe acute respiratory syndrome associated coronavirus in animals at a live animal market of Guangzhou in 2004]. Zhonghua Liu Xing Bing Xue Za Zhi *26*, 84-87.

Wang, M., Yan, M., Xu, H., Liang, W., Kan, B., Zheng, B., Chen, H., Zheng, H., Xu, Y., Zhang, E., *et al.* (2005a). SARS-CoV infection in a restaurant from palm civet. Emerg Infect Dis *11*, 1860-1865.

Wang, S., Guo, F., Liu, K., Wang, H., Rao, S., Yang, P., and Jiang, C. (2008b). Endocytosis of the receptor-binding domain of SARS-CoV spike protein together with virus receptor ACE2. Virus Res *136*, 8-15.

Watanabe, R., Matsuyama, S., Shirato, K., Maejima, M., Fukushi, S., Morikawa, S., and Taguchi, F. (2008). Entry from the cell surface of severe acute respiratory syndrome coronavirus with cleaved S protein as revealed by pseudotype virus bearing cleaved S protein. J Virol *82*, 11985-11991.

Wathelet, M.G., Orr, M., Frieman, M.B., and Baric, R.S. (2007). Severe acute respiratory syndrome coronavirus evades antiviral signaling: role of nsp1 and rational design of an attenuated strain. J Virol *81*, 11620-11633.

Wei, P., Fan, K., Chen, H., Ma, L., Huang, C., Tan, L., Xi, D., Li, C., Liu, Y., Cao, A., *et al.* (2006). The N-terminal octapeptide acts as a dimerization inhibitor of SARS coronavirus 3C-like proteinase. Biochem Biophys Res Commun *339*, 865-872.

WHO (2004). Summary of probable SARS cases with onset of illness from 1 November 2002 to 31 July 2003.

Wilkinson, K.D. (2000). Ubiquitination and deubiquitination: targeting of proteins for degradation by the proteasome. Semin Cell Dev Biol *11*, 141-148.

Wilson, L., McKinlay, C., Gage, P., and Ewart, G. (2004). SARS coronavirus E protein forms cation-selective ion channels. Virology *330*, 322-331.

Wong, S.K., Li, W., Moore, M.J., Choe, H., and Farzan, M. (2004). A 193-amino acid fragment of the SARS coronavirus S protein efficiently binds angiotensin-converting enzyme 2. J Biol Chem *279*, 3197-3201.

Woo, P.C., Lau, S.K., Huang, Y., and Yuen, K.Y. (2009). Coronavirus diversity, phylogeny and interspecies jumping. Exp Biol Med (Maywood) *234*, 1117-1127.

Woo, P.C., Lau, S.K., Li, K.S., Poon, R.W., Wong, B.H., Tsoi, H.W., Yip, B.C., Huang, Y., Chan, K.H., and Yuen, K.Y. (2006). Molecular diversity of coronaviruses in bats. Virology *351*, 180-187.

Wu, D., Tu, C., Xin, C., Xuan, H., Meng, Q., Liu, Y., Yu, Y., Guan, Y., Jiang, Y., Yin, X., *et al.* (2005). Civets are equally susceptible to experimental infection by two different severe acute respiratory syndrome coronavirus isolates. J Virol *79*, 2620-2625.

Wu, X.D., Shang, B., Yang, R.F., Yu, H., Ma, Z.H., Shen, X., Ji, Y.Y., Lin, Y., Wu, Y.D., Lin, G.M., *et al.* (2004a). The spike protein of severe acute respiratory syndrome (SARS) is cleaved in virus infected Vero-E6 cells. Cell Res *14*, 400-406.

Xiao, X., Chakraborti, S., Dimitrov, A.S., Gramatikoff, K., and Dimitrov, D.S. (2003). The SARS-CoV S glycoprotein: expression and functional characterization. Biochem Biophys Res Commun *312*, 1159-1164.

Xiao, X., Feng, Y., Chakraborti, S., and Dimitrov, D.S. (2004). Oligomerization of the SARS-CoV S glycoprotein: dimerization of the N-terminus and trimerization of the ectodomain. Biochem Biophys Res Commun *322*, 93-99.

Xu, H.F., Wang, M., Zhang, Z.B., Zou, X.Z., Gao, Y., Liu, X.N., Lu, E.J., Pan, B.Y., Wu, S.J., and Yu, S.Y. (2004d). [An epidemiologic investigation on infection with severe acute respiratory syndrome coronavirus in wild animals traders in Guangzhou]. Zhonghua Yu Fang Yi Xue Za Zhi *38*, 81-83.

Xu, K., Zheng, B.J., Zeng, R., Lu, W., Lin, Y.P., Xue, L., Li, L., Yang, L.L., Xu, C., Dai, J., *et al.* (2009). Severe acute respiratory syndrome coronavirus accessory protein 9b is a virion-associated protein. Virology *388*, 279-285.

Xu, X., Liu, Y., Weiss, S., Arnold, E., Sarafianos, S.G., and Ding, J. (2003). Molecular model of SARS coronavirus polymerase: implications for biochemical functions and drug design. Nucleic Acids Res *31*, 7117-7130.

Xu, Y., Liu, Y., Lou, Z., Qin, L., Li, X., Bai, Z., Pang, H., Tien, P., Gao, G.F., and Rao, Z. (2004b). Structural basis for coronavirus-mediated membrane fusion. Crystal structure of mouse hepatitis virus spike protein fusion core. J Biol Chem *279*, 30514-30522.

Xu, Y., Su, N., Qin, L., Bai, Z., Gao, G.F., and Rao, Z. (2004a). Crystallization and preliminary crystallographic analysis of the heptad-repeat complex of SARS coronavirus spike protein. Acta Crystallogr D Biol Crystallogr *60*, 2377-2379.

Xu, Y., Zhu, J., Liu, Y., Lou, Z., Yuan, F., Cole, D.K., Ni, L., Su, N., Qin, L., Li, X., *et al.* (2004c). Characterization of the heptad repeat regions, HR1 and HR2, and design of a fusion core structure model of the spike protein from severe acute respiratory syndrome (SARS) coronavirus. Biochemistry *43*, 14064-14071.

Yan, X., Hao, Q., Mu, Y., Timani, K.A., Ye, L., Zhu, Y., and Wu, J. (2006a). Nucleocapsid protein of SARS-CoV activates the expression of cyclooxygenase-2 by binding directly to regulatory elements for nuclear factor-kappa B and CCAAT/enhancer binding protein. Int J Biochem Cell Biol *38*, 1417-1428.

Yan, Z., Tripet, B., and Hodges, R.S. (2006b). Biophysical characterization of HRC peptide analogs interaction with heptad repeat regions of the SARS-coronavirus Spike fusion protein core. J Struct Biol *155*, 162-175.

Yang, Y., Xiong, Z., Zhang, S., Yan, Y., Nguyen, J., Ng, B., Lu, H., Brendese, J., Yang, F., Wang, H., *et al.* (2005b). Bcl-xL inhibits T-cell apoptosis induced by expression of SARS coronavirus E protein in the absence of growth factors. Biochem J *392*, 135-143.

Yang, Z.Y., Huang, Y., Ganesh, L., Leung, K., Kong, W.P., Schwartz, O., Subbarao, K., and Nabel, G.J. (2004a). pH-dependent entry of severe acute respiratory syndrome coronavirus is mediated by the spike glycoprotein and enhanced by dendritic cell transfer through DC-SIGN. J Virol *78*, 5642-5650.

Yao, Y.X., Ren, J., Heinen, P., Zambon, M., and Jones, I.M. (2004). Cleavage and serum reactivity of the severe acute respiratory syndrome coronavirus spike protein. J Infect Dis *190*, 91-98.

Ye, Z., Wong, C.K., Li, P., and Xie, Y. (2008). A SARS-CoV protein, ORF-6, induces caspase-3 mediated, ER stress and JNK-dependent apoptosis. Biochim Biophys Acta *1780*, 1383-1387.

Yi, C.E., Ba, L., Zhang, L., Ho, D.D., and Chen, Z. (2005). Single amino acid substitutions in the severe acute respiratory syndrome coronavirus spike glycoprotein determine viral entry and immunogenicity of a major neutralizing domain. J Virol *79*, 11638-11646.

You, J., Dove, B.K., Enjuanes, L., DeDiego, M.L., Alvarez, E., Howell, G., Heinen, P., Zambon, M., and Hiscox, J.A. (2005). Subcellular localization of the severe acute respiratory syndrome coronavirus nucleocapsid protein. J Gen Virol *86*, 3303-3310.

Yount, B., Roberts, R.S., Sims, A.C., Deming, D., Frieman, M.B., Sparks, J., Denison, M.R., Davis, N., and Baric, R.S. (2005). Severe acute respiratory syndrome coronavirus group-specific open reading frames encode nonessential functions for replication in cell cultures and mice. J Virol *79*, 14909-14922.

Yu, D., MD., Li, H., Xu, R., MPH, He, J., Lin, J., Li, L., Li, W., Xu, H., *et al.* (2003). Prevalence of IgG antibody to SARS-associated coronavirus in animal traders--Guangdong Province, China, 2003. MMWR Morb Mortal Wkly Rep *52*, 986-987.

Yu, I.M., Gustafson, C.L., Diao, J., Burgner, J.W., 2nd, Li, Z., Zhang, J., and Chen, J. (2005). Recombinant severe acute respiratory syndrome (SARS) coronavirus nucleocapsid protein forms a dimer through its C-terminal domain. J Biol Chem *280*, 23280-23286.

Yu, I.M., Oldham, M.L., Zhang, J., and Chen, J. (2006). Crystal structure of the severe acute respiratory syndrome (SARS) coronavirus nucleocapsid protein dimerization domain reveals evolutionary linkage between corona- and arteriviridae. J Biol Chem *281*, 17134-17139.

Yuan, K., Yi, L., Chen, J., Qu, X., Qing, T., Rao, X., Jiang, P., Hu, J., Xiong, Z., Nie, Y., *et al.* (2004). Suppression of SARS-CoV entry by peptides corresponding to heptad regions on spike glycoprotein. Biochem Biophys Res Commun *319*, 746-752.

Yuan, Q., Liao, Y., Torres, J., Tam, J.P., and Liu, D.X. (2006c). Biochemical evidence for the presence of mixed membrane topologies of the severe acute respiratory syndrome coronavirus envelope protein expressed in mammalian cells. FEBS Lett *580*, 3192-3200.

Yuan, X., Li, J., Shan, Y., Yang, Z., Zhao, Z., Chen, B., Yao, Z., Dong, B., Wang, S., Chen, J., *et al.* (2005a). Subcellular localization and membrane association of SARS-CoV 3a protein. Virus Res *109*, 191-202.

Yuan, X., Shan, Y., Zhao, Z., Chen, J., and Cong, Y. (2005b). G0/G1 arrest and apoptosis induced by SARS-CoV 3b protein in transfected cells. Virol J *2*, 66.

Yuan, X., Wu, J., Shan, Y., Yao, Z., Dong, B., Chen, B., Zhao, Z., Wang, S., Chen, J., and Cong, Y. (2006b). SARS coronavirus 7a protein blocks cell cycle progression at G0/G1 phase via the cyclin D3/pRb pathway. Virology *346*, 74-85.

Yuan, X., Yao, Z., Wu, J., Zhou, Y., Shan, Y., Dong, B., Zhao, Z., Hua, P., Chen, J., and Cong, Y. (2007). G1 phase cell cycle arrest induced by SARS-CoV 3a protein via the cyclin D3/pRb pathway. Am J Respir Cell Mol Biol *37*, 9-19.

Zakhartchouk, A.N., Viswanathan, S., Mahony, J.B., Gauldie, J., and Babiuk, L.A. (2005). Severe acute respiratory syndrome coronavirus nucleocapsid protein expressed by an adenovirus vector is phosphorylated and immunogenic in mice. J Gen Virol *86*, 211-215.

Zeng, R., Yang, R.F., Shi, M.D., Jiang, M.R., Xie, Y.H., Ruan, H.Q., Jiang, X.S., Shi, L., Zhou, H., Zhang, L., *et al.* (2004). Characterization of the 3a protein of SARS-associated coronavirus in infected vero E6 cells and SARS patients. J Mol Biol *341*, 271-279.

Zhai, Y., Sun, F., Li, X., Pang, H., Xu, X., Bartlam, M., and Rao, Z. (2005). Insights into SARS-CoV transcription and replication from the structure of the nsp7-nsp8 hexadecamer. Nat Struct Mol Biol *12*, 980-986.

Zhang, L., Wei, L., Jiang, D., Wang, J., Cong, X., and Fei, R. (2007a). SARS-CoV nucleocapsid protein induced apoptosis of COS-1 mediated by the mitochondrial pathway. Artif Cells Blood Substit Immobil Biotechnol *35*, 237-253.

Zhang, Q.L., Ding, Y.Q., He, L., Wang, W., Zhang, J.H., Wang, H.J., Cai, J.J., Geng, J., Lu, Y.D., and Luo, Y.L. (2003a). [Detection of cell apoptosis in the pathological tissues of patients with SARS and its significance]. Di Yi Jun Yi Da Xue Xue Bao *23*, 770-773.

Zhang, X., Wu, K., Wang, D., Yue, X., Song, D., Zhu, Y., and Wu, J. (2007b). Nucleocapsid protein of SARS-CoV activates interleukin-6 expression through cellular transcription factor NF-kappaB. Virology *365*, 324-335.

Zhao, J., Falcon, A., Zhou, H., Netland, J., Enjuanes, L., Perez Brena, P., and Perlman, S. (2009). Severe acute respiratory syndrome coronavirus protein 6 is required for optimal replication. J Virol *83*, 2368-2373.

Zhao, X., Nicholls, J.M., and Chen, Y.G. (2008). Severe acute respiratory syndrome-associated coronavirus nucleocapsid protein interacts with Smad3 and modulates transforming growth factor-beta signaling. J Biol Chem *283*, 3272-3280.

Zhao, Z., Li, H., Wu, X., Zhong, Y., Zhang, K., Zhang, Y.P., Boerwinkle, E., and Fu, Y.X. (2004). Moderate mutation rate in the SARS coronavirus genome and its implications. BMC Evol Biol *4*, 21.

Zheng, K., Ma, G., Zhou, J., Zen, M., Zhao, W., Jiang, Y., Yu, Q., and Feng, J. (2007). Insight into the activity of SARS main protease: Molecular dynamics study of dimeric and monomeric form of enzyme. Proteins *66*, 467-479.

Zhong, N., Zhang, S., Zou, P., Chen, J., Kang, X., Li, Z., Liang, C., Jin, C., and Xia, B. (2008). Without its N-finger, the main protease of severe acute respiratory syndrome coronavirus can form a novel dimer through its C-terminal domain. J Virol *82*, 4227-4234.

Zhong, N.S., Zheng, B.J., Li, Y.M., Poon, Xie, Z.H., Chan, K.H., Li, P.H., Tan, S.Y., Chang, Q., Xie, J.P., *et al.* (2003). Epidemiology and cause of severe acute respiratory syndrome (SARS) in Guangdong, People's Republic of China, in February, 2003. Lancet *362*, 1353-1358.

Zhou, B., Liu, J., Wang, Q., Liu, X., Li, X., Li, P., Ma, Q., and Cao, C. (2008). The nucleocapsid protein of severe acute respiratory syndrome coronavirus inhibits cell cytokinesis and proliferation by interacting with translation elongation factor 1alpha. J Virol *82*, 6962-6971.

Zhou, Y., Lu, K., Pfefferle, S., Bertram, S., Glowacka, I., Drosten, C., Pohlmann, S., and Simmons, G. (2010). A single asparagine-linked glycosylation site of the severe acute respiratory syndrome coronavirus spike glycoprotein facilitates inhibition by mannose-binding lectin through multiple mechanisms. J Virol *84*, 8753-8764.

Zhu, J., Xiao, G., Xu, Y., Yuan, F., Zheng, C., Liu, Y., Yan, H., Cole, D.K., Bell, J.I., Rao, Z., *et al.* (2004). Following the rule: formation of the 6-helix bundle of the fusion core from severe acute respiratory syndrome coronavirus spike protein and identification of potent peptide inhibitors. Biochem Biophys Res Commun *319*, 283-288.

Ziebuhr, J., Snijder, E.J., and Gorbalenya, A.E. (2000). Virus-encoded proteinases and proteolytic processing in the Nidovirales. J Gen Virol *81*, 853-879.

Zuniga, S., Sola, I., Moreno, J.L., Sabella, P., Plana-Duran, J., and Enjuanes, L. (2007). Coronavirus nucleocapsid protein is an RNA chaperone. Virology *357*, 215-227.

Zwick, M.B., Jensen, R., Church, S., Wang, M., Stiegler, G., Kunert, R., Katinger, H., and Burton, D.R. (2005). Anti-human immunodeficiency virus type 1 (HIV-1) antibodies 2F5 and 4E10 require surprisingly few crucial residues in the membrane-proximal external region of glycoprotein gp41 to neutralize HIV-1. J Virol *79*, 1252-1261.

APPENDICES

Appendix 1: Primers for constructions of plasmids for expression of S and S mutants

Primer	Sequence	Application
SS03-56	5'-ACGGATCCACCATGTTTATTTTCTTATTA-3'	Cloning full-length S
SS03-57	3'-GTAGGCCTATGTGTAATGTAATTTGAC-5'	Cloning full-length S
SS03-62	5'-AAGGATCCAGATCAGACACTCTTTATTT-3'	Cloning SΔ1
SS03-63	3'-AAAATCTCGAGTTGTAGAGCACAGAG-5'	Cloning SΔ1
SS03-60	5'- CAGGATCCTCAACCTTTAAGTGCTATG-3'	Cloning SΔ2
SS03-61	3'- CTATCTCGAGTCAGGTAATATTTGTGAAA-5'	Cloning SΔ2
SS03-68	5'- CTGGATCCTTTTCGCTTGATGTTTC-3'	Cloning SΔ3
SS03-69	3'- TATTACTCGAGGGAGAAAGGCACATT-5'	Cloning SΔ3
SS03-101	5'- CTGGATCCTCTTTTATTGAGGACTTGC-3'	Cloning SΔ9
SS03-102	3'- TGAACTCGAGCTCCTGGGATGGCACAT-5'	Cloning SΔ9
SS03-103	5'- AGGGATCCCACCTTATGTCCTTCC-3'	Cloning SΔ10
SS03-104	3'- AAACCTCGAGAGGCCATTTAATATATTGC-5'	Cloning SΔ10
SS03-111	3'- CAGGATCCTTAACAAGAGCATGCACCCT-5'	Cloning SΔ11
SS03-112	3'- CCGGATCCTTAATACCAAGGCCATTTAATA-5'	Cloning SΔ12
SS03-113	3'- GAGGATCCTTAGCCTGAAATGTCGCCAA-5'	Cloning SΔ13
SS03-114	3'- TGGGATCCTTATGTAATTAACCTGTCAATT-5'	Cloning SΔ14
SS03-115	3'- AGGGATCCTTAGGTAACTCCAATGCCATT-5'	Cloning SΔ15
SS03-116	3'- TCGGATCCTTACCTCTTAGTTGGCTTTAG-5'	Cloning SΔ16
SS04-100	3'-TGGGATGGGTAGCCCTTTCCACAAA-5'	Cloning SΔ50
SS04-101	5'-AGGGCTACCCATCCCAGGAGAGGA-3'	Cloning SΔ50
SS04-102	3'-CGAGGGAACACATACGTGACATGTAG-5'	Cloning SΔ51
SS04-103	5'-CGTATGTGTTCCCTCGTGAAGGTGT-3'	Cloning SΔ51
SS04-104	3'-GAAAAGAAGTATGCTTTGCCTTCATG-5'	Cloning SΔ52
SS04-105	5'-AAGCATACTTCTTTTCTCCACAAATAATT-3'	Cloning SΔ52
SS04-106	3'-TTAGCGACGTCGCCAAGATCAACATC-5'	Cloning SΔ53
SS04-107	5'-TTGGCGACGTCGCTAAAAATTTAAATGAA-3'	Cloning SΔ53
SS04-108	3'-GGCCATTTCTCATTGAGGCGGTCAAT-5'	Cloning SΔ54
SS04-109	5'-TCAATGAGAAATGGCCTTGGTATGTTT-3'	Cloning SΔ54
SS04-94	3'-CGAACGGATTGTTGAAATGGTTGAAATG-5'	Cloning SΔ55
SS04-95	5'-TTCAACAATCCGTTCGAGATCCTAAA-3'	Cloning SΔ55
SS04-96	3'-ATGTCTAAATCAGTGAAATCAGAAACAT-5'	Cloning SΔ56
SS04-97	5'-TCACTGATTTAGACATTTCACCTTGCT-3'	Cloning SΔ56
SS04-98	3'-GATGTTTTAACATCACGGCCAAATTG-5'	Cloning SΔ57
SS04-99	5'-GTGATGTTAAAACATCTGAAATATTAGAC-3'	Cloning SΔ57
SS04-77	3'-CAGAGCTCTTATGTGTAATGTAATTTGACAC-5'	Cloning (SΔ50-57)
CT08-14	5'-GAGTATGTCGACACTTCTTAT-3'	Cloning S(H641Y)
CT08-15	3'-ATAAGAAGTGTCGACATACTC-5'	Cloning S(H641Y)
CT08-16	5'-ACTATAGAAGTAATGCCTGTT-3'	Cloning S(T706I)
CT08-17	3'-AACAGGCATTACTTCTATAGT-5'	Cloning S(T706I)
CT08-18	5'-TGGATTGACATTTGGTG-3'	Cloning S(W869L)
CT08-19	3'-CACCAAATGTCAATCCA-5'	Cloning S(W869L)
CT08-20	5'-CCAGGAGAGGAAATTCA-3'	Cloning S(N1056K)
CT08-21	3'-TGAATTTCCTCTCCTGG-5'	Cloning S(N1056K)
CT08-22	5'-TGCCTCATTCAAAGAAGA-3'	Cloning S(D1128A)
CT08-23	3'-TCTTCTTTGAATGAGGCA-5'	Cloning S(D1128A)

Appendix 2: Primers for constructions of plasmids for expression of ORF8 proteins and mutants

Primer	Sequence	Application
8a_forward	5'-CGGGATCCACCATGGGAATGAAACTTCTC-3'	Cloning 8a and 8ab
8a_reverse	3'-CCGCTCGAGCTAGTGTTGTACC-5'	Cloning 8a
8b_forward	5'-CGGGATCCACCATGGGAATGTGCTTGAAG-3'	Cloning 8b
8b_reverse	3'-CCGCTCGAGCCATTTGTTCGTTTATT-5'	Cloning 8b and 8ab
8a_delN15F	5'-CGGGATCCACCATGGGAATGAAACTTCTC-3'	Cloning 8aΔN15
8b_delN26F	5'-CGGGATCCACCATGGGAGTTTTACCTTT-3'	Cloning 8bΔN26
CT07-11	5'-CGGGATCCATGTGCTTGAGGAT-3'	Cloning 8b(K4R)
CT07-07	5'-AGGTAAAACCCTTCCTAG-3'	Cloning 8b(K26R)
CT07-08	3'-CTAGGAAGGGTTTTACCT-5'	Cloning 8b(K26R)
CT07-10	3'-CCGCTCGAGCCAATTTGTTCGTCTATT-5'	Cloning 8b(K81R)

Appendix 3: Primers for constructions of plasmids for expression of E protein and mutants

Primer	Sequence	Application
SS03-42	5'-AGGGATCCACCATGTACTCATTCGTTTC-3'	Cloning E
SS03-48	3'-TAGTTCTCGAGGACCAGAAGATCAGGAA-5'	Cloning E
CT06-01	5'-TTAGTAAGACCAACGGTTT-3'	Cloning E(K54R)
CT06-02	3'-AAACCGTTGGTCTTACTAA-5'	Cloning E(K54R)
CT06-03	5'-CGTGTTAGAAATCTGAACT-3'	Cloning E(K64R)
CT06-04	3'-AGTTCAGATTTCTAACACG-5'	Cloning E(K64R)